U.PORTO

DOUTORAMENTO

BIOLOGIA BÁSICA E APLICADA

Post-transcriptional gene regulation during synaptic plasticity

Mariana Miranda Fontes

D

2018

U.PORTO

Mariana Miranda Fontes. Post-transcriptional gene regulation during synaptic plasticity

D.ICBAS **2018**

Post-transcriptional gene regulation during synaptic plasticity

Mariana Miranda Fontes

INSTITUTO DE CIÊNCIAS BIOMÉDICAS ABEL SALAZAR

MARIANA MIRANDA FONTES

POST-TRANSCRIPTIONAL GENE REGULATION DURING SYNAPTIC PLASTICITY

Tese de Candidatura ao grau de Doutor em
Biologia Básica e Aplicada submetida ao Instituto de
Ciências Biomédicas Abel Salazar da Universidade do
Porto

Orientadora – Kelsey C. Martin
Categoria – Professor, Department of Biological Chemistry;
Dean, David Geffen School of Medicine
Afiliação – University of California, Los Angeles

Co-orientadora – Alexandra Moreira
Categoria – Investigadora Principal
Afiliação – Instituto de Ciências Biomédicas Abel
Salazar da Universidade do Porto

This thesis is dedicated to my parents and grandmother

This work was supported by Fundação para a Ciência e Tecnologia (FCT) by means of a Ph.D. fellowship SFRH/BD/ 51289/2010 awarded to Mariana Miranda Fontes through the Graduate Program in Areas of Basic and Applied Biology (GABBA), Universidade do Porto, Portugal. The National Institutes of Health (NIH) also supported the research.

Acknowledgments

First of all, I would like to thank my mentor Kelsey Martin, who believed in me and gave me the opportunity to join her lab. Kelsey received me with open arms in her family home when I first landed in LA and her warmth and support continued throughout all these years. My PhD has been a long and challenging journey, but in Kelsey's office (and skype calls) I could always find perspective, focus, and calm. Kelsey has been a true inspiration to me. She is a scientist, but also a dedicated mother and wife, and a passionate advocate for science and social justice. She is kind, assertive and fair; and focuses on people over outcomes, and good science over publications. She supported my development as an independent scientist, and my pursuit to learn new skills and gain new experiences in entrepreneurship and business. I am truly fortunate to have you as my mentor. Thank you.

A particular thank you to the GABBA program directors over the years, Prof. Dr. Alexandre do Carmo and Prof. Dr. António Amorim, and to Professor Maria de Sousa and Catarina Carona, without whom none of it would be possible. Thank you for fighting to keep the program running without compromising the foundation values – of diversity, collaboration, openness and excellence - that make GABBA an incredibly unique and special program. As an All Time GABBA, I can only hope that one day I will be able to give back and support young scientists. I thank (Prof. Dr.) Alexandra Moreira, for being my mentor, making sure I keep on track and responding to all my last-minute requests within a few minutes always with a caring and supportive "voice". The GABBA program gave me not only a platform to develop my doctoral studies but also a new family. I would like to thank my colleagues from GABBA 14th: Inezita, Cachorro, Andre, Ferreirinha, Netinho, Rena, Milene, McLindo, Bruno, Daniel and Catarina for all the overly passionate, dramatic and oversharing moments and debates we had for 6 months; for the Casa Conceicao that became a new home in Porto; for all the great travels, dances and sunsets over Porto wine; and for always being there with words of encouragement to help me deal with frustrations and decisions, and to celebrate successes. It's wonderful to know that "we will always have Porto".

My PhD was a truly collaborative effort. I couldn't have overcome the daily research challenges of my projects without the help of my colleagues at the Martin lab, the Tian lab, the Coppola lab and the O'Dell lab. I would like to thank all the members of the Martin lab for giving feedback on my project, helping me with technical issues and

taking me out to Tsujita on a regular basis. I am specially thankful to Victoria who performed preliminary experiments that paved the way to the work presented in chapter II; to Ji-Ann who gave me the opportunity to work with him in the project presented in chapter III; to Patrick for the long discussions about Science, his constructive criticism about my project and his delightful supply of candy and Japanese movie suggestions; to Elliott for his pranks that kept my laughing in lab and for putting up with my early skype calls with my mom in Portuguese; to Shivan for his motivational morning talks/songs in the car; and to Martina for being my indistinguishable twin sister in the department and a best friend for life. At the Tian lab, I would like to thank Aysegul and Professor Bin Tian who were delightful to collaborate with and that worked incredibly hard to continue moving the project forward and publish our studies 2 years after I left the lab. Although we have never met in person, I truly feel like you are some of the most reliable, friendly and insightful colleagues I have ever had. To the Coppola lab, specially to Alden, Riki and Giovanni, thank you for all your help with bioinformatic analysis since the very first beginning of our project. And a very heart felt thank you to Professor Tom O'Dell and his team for always making me feel welcome in the lab, for the sarcastic comments that always made me laugh and for all the weekend and last-minute support with experiments that were critical to the project.

I also want to thank my closest friends that encouraged me to push forward and aim high during my PhD. Together with Gianmarco, Nadia and Martina were my main support pillars at UCLA - they first introduced me to women in science events that shaped my vision and ambition for women in society, and they brought an incredible joy to my life by taking me to trips to the desert, the beach, the mountains, the opera and to many brunch and cheese outings. Gianmarco is without a doubt the most feminist man I know. He was relentlessly supportive and keen to see me thrive – our start trek evenings had a critical role in the outcome of these studies. Being so far away from home meant I missed several unmissable events. I am thankful that even across continents, my best friends Joana and Joao, Ines and Ana assured we continued to share our lives over skype and poorly planned trips and continued to be as close as 14 or 25 years ago. Talking to you always felt like being in the home I missed.

Finally, the people I must thank the most are my parents, for always being by my side. For being my loudest critics and my most passionate supporters. From taking calls in the middle of the night, shipping areias and presunto 5000 miles away, saving hundreds of backup thesis drafts, and asking "how is the paper/thesis going" every day for the past 6 years. Your support and example meant the world to me. Muito obrigada.

TABLE OF CONTENTS

Abstract

Neurons are highly polarized cells that communicate with one another at points of contact known as synapses. The ability to regulate the number and strength of synapses in an experience-dependent manner is called synaptic plasticity and has been shown to underlie learning and memory. Long-lasting forms of synaptic plasticity require tight control of gene expression in the nucleus and at synapses. In this study, we used two approaches to investigate the post-transcriptional mechanisms of gene expression regulation in neurons that, when impaired, contribute to neurological diseases.

The first part of my thesis focused on alternative cleavage and polyadenylation (APA), which contributes to the diversity of the transcriptomic pool by producing mRNA isoforms with distinct 3' untranslated regions (3'UTRs) and/or coding sequences. Alternative 3'UTRs and coding sequences can affect the expression, localization, and interactions of transcripts and their cognate proteins therefore impacting neuronal proteins function. Here, we investigated whether and how long-lasting phases of synaptic plasticity are coupled to changes in the 3'end processing of transcripts though APA. We used 3' region extraction and deep sequencing (3'READS), a specialized method for identifying APA isoforms, to examine APA regulation by neuronal activity in acute hippocampal slices. We observed a significant and global increase in the usage of proximal and intronic polyadenylation sites (PAS) 3 hours after long-term potentiation (LTP) induction, consistent with LTP triggering a shortening of 3'UTRs and a shortening of the overall length of transcripts. In contrast, global APA regulation was undetectable 1 hour post-LTP induction suggesting that APA is temporally regulated. RNA-sequencing (RNA-seq) of the mouse hippocampal transcriptome addressed whether the change in PAS usage in response to LTP affected mRNA abundance. We found that LTP induced significant changes in gene expression patterns 3 hours post-LTP induction, primarily by increasing the abundance of a subset of transcripts. Further analysis of individual transcripts at a large scale revealed that APA is mostly uncoupled from mRNA abundance regulation, raising the question of how the observed trend in APA regulation impacts neuronal function during LTP. Taken together, our results reveal that neuronal activity induces significant changes in APA that alter 3'UTR length and overall transcripts size, contributing to the intricate program of gene expression regulation underlying long-lasting, learning-related hippocampal plasticity.

The second part of my thesis research focuses on RNA-binding proteins, which play a critical role in controlling the localization, abundance and function of neuronal

mRNAs. We studied RbFox1, a neuronal RNA-binding protein previously identified as a hub gene for autism-related genes in human genetic studies. RbFox1 binds to a well-defined RNA sequence, (U)GCAUG, and is alternatively spliced into nuclear and cytoplasmic forms. In the nucleus, Rbfox1 functions as a regulator of RNA splicing; however, its role in the cytoplasm remained largely unknown. In this study we set out to dissect the cytoplasmic functions of RbFox1 in neurons. Previously, our group profiled the transcriptome of mouse hippocampal cultures in which RbFox1 and its homologue RbFox3 were knocked down. Most of the differentially regulated transcripts that have RbFox1 binding sites in their 3'-untranslated regions (3'UTR) were downregulated in the absence of RbFox1 and Rbfox3, suggesting that RbFox proteins increase mRNA expression levels in neurons. In this study, a subset of these transcripts was validated by RNA-seq of neuronal cultures lacking RbFox1 and their expression was rescued upon AAV-RbFox1 cytoplasmic isoform transduction. To identify the direct targets of each of the RbFox1 isoforms we performed individual-nucleotide cross-linking and immunoprecipitation followed by sequencing (iCLIP-seq) for the nucleoplasmic and cytoplasmic neuronal fractions separately. We identified that cytoplasmic RbFox1 binds predominantly to the 3'UTR of transcripts causing an increase in stability and translation of its targets and these targets are enriched in cortical development and autism genes. We characterized in more detail the RbFox1 regulation of two proteins essential for plasticity: Camk2α and Camta1. We cloned the 3'UTR of these genes into a luciferase reporter and showed that cytoplasmic RbFox1 can increase the luciferase activities and mRNA levels of these reporters in an RbFox1 site dependent manner. The (U)GCAUG sequence is one of the most conserved elements in the 3'-UTRs of human genes and we found that these sequences overlap significantly with or locate close to microRNA (miRNA)-target sites. Amongst other potential mechanisms, we postulate that RbFox1 binds to the 3'-UTR of target transcripts and increases their stability by competing with miRNAs. The results of this project provide additional insights to advance the understanding of the molecular interactions that underlie neural circuit dysfunction in autism-spectrum disorders.

Above all, these two approaches highlight the intricacy of gene expression regulation in the brain and open new avenues to future studies.

Resumo

Os neurónios são células altamente polarizadas que comunicam entre si através de pontos de contacto conhecidos por sinapses. A capacidade de regular o número e a força das sinapses de uma forma dependente de experiências foi denominada plasticidade sináptica, e constitui a base molecular da formação de memórias e aprendizagem. Formas duradouras de plasticidade sináptica exigem um controlo rígido da expressão génica ao nível nuclear e das sinapses. Neste estudo foram utilizadas duas abordagens para investigar os mecanismos pós-transcricionais de regulação da expressão génica em neurónios que, quando debilitados, contribuem para o desenvolvimento de doenças neurológicas.

A primeira parte da tese foca-se no processo de clivagem e poliadenilação alternativa (APA) que contribui para a diversidade do pool transcriptomico através da produção de isoformas de mRNA com regiões 3' não traduzidas (3'UTRs) e/ou sequências codificantes diferentes. 3'UTRs e sequências codificantes alternativas podem afetar a expressão, localização e interações de mRNAs e suas correspondentes proteínas, levando a uma potencial alteração da função de proteínas neuronais. Neste estudo, investigámos de que forma a plasticidade sináptica de longa duração está acoplada a mudanças no processamento final dos transcritos via APA. Para examinar os efeitos da atividade neuronal na regulação de APA em secções de hipocampo, utilizámos um método especializado para a identificação de isoformas de APA chamado extração de regiões 3' e sequenciamento profundo (3'READS). Observámos um aumento significativo e global no uso de locais de poliadenilação (PAS) proximais e intronicos 3 horas após a indução de potenciação de longa duração (LTP), consistente com a LTP resultar num encurtamento de 3'UTRs e uma redução global do comprimento de transcritos. Em contraste, a regulação da APA a níveis globais foi indetectável 1 hora após a indução de LTP, sugerindo que o mecanismo de APA é temporalmente regulado. O sequenciamento de RNA (RNA-seq) do transcriptoma hipocampal do ratinho permitiu-nos investigar se a mudança no uso de PAS em resposta à indução de LTP resulta numa alteração da concentração de mRNAs. Descobrimos que a LTP induziu mudanças significativas nos padrões de expressão génica 3 horas após a indução da LTP, principalmente pelo aumento da abundância de uma subpopulação de transcritos. Uma análise mais aprofundada de alguns transcritos em larga escala revelou que a APA é na maioria dos casos desacoplada da regulação da abundância de mRNA, levantando questões relativas ao impacto da regulação da APA na função neuronal durante a LTP. Conjuntamente, os nossos resultados revelam que a atividade neuronal induz alterações significativas na

APA que alteram o comprimento das 3'UTRs e o tamanho geral dos transcritos, contribuindo para o complexo programa de regulação da expressão génica associado à plasticidade do hipocampo que fundamenta a aprendizagem de longa duração.

A segunda parte da tese centra-se na investigação de proteínas de ligação ao RNA, que desempenham um papel crítico no controlo da localização, abundância e função dos mRNAs neuronais. Estudámos a RbFox1, uma proteína neuronal de ligação ao RNA previamente identificada como elemento central de genes associados ao autismo em estudos genéticos humanos. A RbFox1 liga-se a uma sequência de RNA bem definida, (U)GCAUG, e é alternativamente spliced em formas nucleares e citoplasmáticas. No núcleo, a Rbfox1 funciona como um regulador do splicing de RNA; no entanto, o seu papel no citoplasma permaneceu em grande parte desconhecido. Neste estudo, dissecámos as funções citoplasmáticas da RbFox1 em neurónios. Anteriormente, o nosso grupo começou por estudar o perfil transcriptomico de culturas de hipocampo de ratinhos em que RbFox1 e a sua proteína homóloga RbFox3 estavam ausentes. Foi descoberto que a maioria dos transcritos diferencialmente regulados que possuem sítios de ligação RbFox1 em 3'UTRs são reprimidos na ausência de RbFox1 e Rbfox3, sugerindo que as proteínas RbFox aumentam os níveis de expressão de mRNA em neurónios. Neste estudo, um subconjunto desses transcritos foi validado por RNA-seq de culturas neuronais sem RbFox1 e a sua expressão foi resgatada após a transdução da isoforma citoplasmática AAV-RbFox1. Para identificar os alvos diretos de cada uma das isoformas de RbFox1, realizámos a reticulação de nucleotídeos individuais e a imunoprecipitação seguida de sequenciamento (iCLIP-seq) para as fracções neuroplasmáticas e citoplasmáticas separadamente. Verificámos que a RbFox1 citoplasmática se liga predominantemente ás 3'UTRs de transcritos causando um aumento na estabilidade e tradução dos seus alvos, e que estes alvos estão enriquecidos em genes de desenvolvimento cortical e autismo. Caraterizámos com mais detalhe a regulação mediada por RbFox1 de duas proteínas essenciais para a plasticidade: Camk2α e Camta1. Clonámos a 3'UTR desses genes num repórter da luciferase e mostrámos que a RbFox1 citoplasmática pode aumentar as atividades da luciferase e os níveis de mRNA desses repórteres de maneira dependente do local de ligação da RbFox1. A sequência GCAUG(U) é um dos elementos mais conservados nas 3'UTRs dos genes humanos. Descobrimos que essas sequências se sobrepõem significativamente ou se localizam próximas de locais de ligação para microRNAs (miRNA). Entre outros mecanismos potenciais, postulamos que a RbFox1 se liga à 3'UTR de transcriptos alvo e aumenta a sua estabilidade competindo com miRNAs. Os resultados deste projeto contribuem deste modo para o

avanço do nosso entendimento sobre as interações moleculares associadas às disfunções do circuito neural em perturbações do espectro do autismo.

Concluindo, estas duas abordagens destacam a complexidade da regulação da expressão génica no cérebro e abrem novos caminhos para futuros estudos.

List of Abbreviations

LTP – Long-term potentiation
E-LTP - Early-phase of LTP
L-LTP – Late-phase of LTP
LTD – Long-term depression
APA – alternative cleavage and polyadenylation
mRNA – messenger ribonucleic acid
miRNA - microRNA
UTR – untranslated region
3´-UTR – 3’ untranslated region
5´-UTR – 5’ untranslated region
DE – differentially expressed
Poly(A) – polyadenosine
PAS – polyadenylation site
RNA Seq – sequencing
3´READS - 3’ region extraction and deep sequencing
PAS-Seq - Poly(A) Site Sequencing
CAMKII - Ca2+/calmodulin-dependent protein kinase II
AMPAR - alpha-amino-3-hydroxy-5-methyl-4-isoxazolepropionic acid
cAMP - cyclic adenosine monophosphate
RBP – RNA-binding protein
RBFOX1 – RNA binding protein Fox-1 Homolog 1
FMRP – Fragile X Mental Retardation Protein
MBNL – Muscleblind-like splicing regulator
C/P - cleavage and polyadenylation
RNAPII - RNA polymerase II

1. Chapter I – General introduction

1. CHAPTER I – GENERAL INTRODUCTION

1.1 From synaptic plasticity to memory formation

For many centuries philosophers, psychologists and scientists have been fascinated with the function of the human brain and have engaged in relentless attempts to uncover the basis of complex abilities such as perception, memory and cognition (Berlucchi and Buchtel, 2009). In the late 1800s, William James introduced the concept of plasticity in the brain and theorized that the behavioral habits observed in living beings relied on changes in nervous system pathways (James, 1890)1. The neuroanatomist Santiago Ramon y Cajal used Golgi staining to provide the first concrete evidence that the brain was composed of individual cells (neurons) that harbored distinct and extensive processes. Cajal highlighted that neuronal networks were not in cytoplasmic continuity but instead individual neurons communicated with one another through specialized junctions, later called synapses by Sherrington (Cajal, 1894). Eugenio Tanzi identified these points of contact between adjacent neurons as potential sites for neuronal plasticity. Tanzi also anticipated that repeated activity could lead to changes in the resistance of neuronal connections and linked those changes to the formation of associative memories and practice-dependent motor skills (Tanzi, 1893). Advances in technology, including the use of intracellular microelectrodes to record neuronal activity and electron microscopy to visualize the ultrastructure of synapses, opened new avenues to understanding brain biology and memory formation. Donald Hebb hypothesized that learning and long-term memory resulted from the strengthening of synaptic connections caused by repetitive and associative firing of adjacent neurons – a theory popularized by the iconic statement “neurons that wire together, fire together”(Hebb, 1949).

The first compiling evidence implicating the hippocampus in the formation of new memories originated from the study of epileptic patient Henry Gustav Molaison, widely known as patient H.M., in the late 1950s. H.M. underwent bilateral removal of the hippocampus and neighboring regions in the medial temporal lobe as treatment for severe seizures. As a result of the surgery, the patient developed both anterograde amnesia (inability to form new memories) and partial retrograde amnesia (inability to recall old memories), while his working memory (short-term memory) remained intact (Scoville and Milner, 1957; Squire and Wixted, 2011). Additional studies of patients with long-term memory deficits caused by hippocampal lesions corroborated these early findings and established the hippocampus as a critical brain region for memory formation.

The hippocampus receives information from the nearby entorhinal cortex and projects back to the cortex and the subiculum through pyramidal neurons of the CA1 (Figure 1). The cortical inputs reach the CA1 region through both direct and indirect excitatory pathways, together called the perforant pathway. In the direct pathway, axons from the entorhinal cortex project directly into the dendrites of the CA1 neurons. The indirect pathway comprises a trisynaptic pathway journey spanning from the perforant pathway, in which axons from the entorhinal cortex form synapses with dendrites from the granule cells of the dentate gyrus, to the mossy fiber pathway, in which axons from the dentate granule cells project into neurons of the CA3 region, to the Schaffer collateral pathway, where CA3 axons excite pyramidal neurons of the CA1 region of the hippocampus. The well-defined layered architecture of the hippocampus allowed for early studies of electrophysiology to start uncovering the physiological mechanisms that underlie learning and memory.

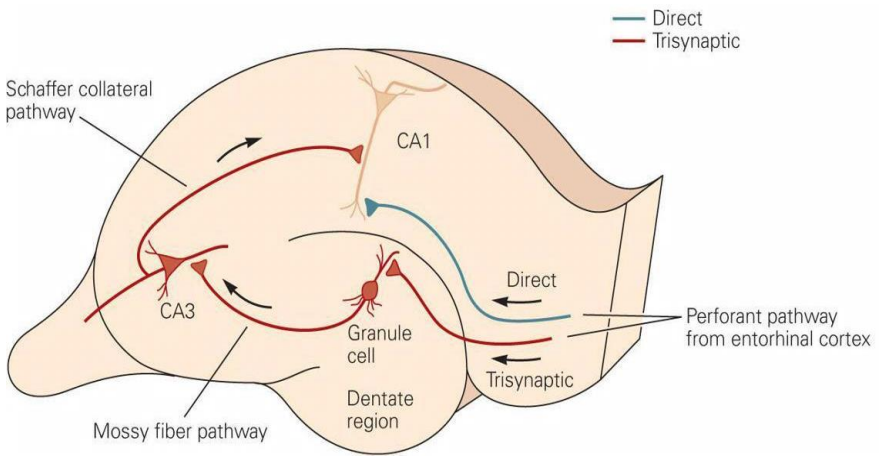

Figure 1 – The hippocampal synaptic circuitry (Kandel et al., 2013)

In 1973, Timothy Bliss and Terje Lomo discovered that electrical stimulation of the perforant pathway of anesthetized rabbits led to long-lasting and activity-dependent changes in synaptic strength in the hippocampus. They found that the delivery of brief trains of high frequency stimuli to the perforant pathway resulted in an increase in synaptic transmission, as measured by the amplitude of excitatory postsynaptic potentials (EPSPs), which could last hours. This phenomenon was then named long-term potentiation (LTP). Long-term depression (LTD) describes a persistent weakening of synaptic strength in response to specific patterns of neuronal firing or activity. Both LTP and LTD are forms of synaptic plasticity, defined by the ability of neurons to modify the strength of synaptic connections in an experience-dependent manner (Bliss and Collingridge, 1993; Silva et al., 1992).

In the 1960s and 1970s, the Eric Kandel and colleagues provided the first convincing evidence linking molecular mechanisms to long-lasting changes in synaptic strength that in turn resulted in specific learning behaviors. The group pioneered the use *Aplysia californica* as a model system for studying learning-related synaptic plasticity. *Aplysia* are marine molluscs with a central nervous system of approximately 20,000 large and stereotyped nerve cells that can perform simple learning behaviors such as developing long-term sensitization of the gill-withdrawal reflex following repeated tail shocks. This learning paradigm was recapitulated in *Aplysia* sensory-motor culture systems, allowing to study behavior at a resolution of single neuron cells and individual synapses (Martin et al., 1997a).

LTP exhibits two distinct forms based on temporal and molecular features: a transient early-phase (E-LTP) that lasts for minutes to a few hours, and a late-phase (L-LTP) that lasts several hours to days (Figure 2). One train of electrical stimulation (1s at 100Hz) produces short lasting plasticity and four or more trains at 10min intervals are required to elicit L-LTP.

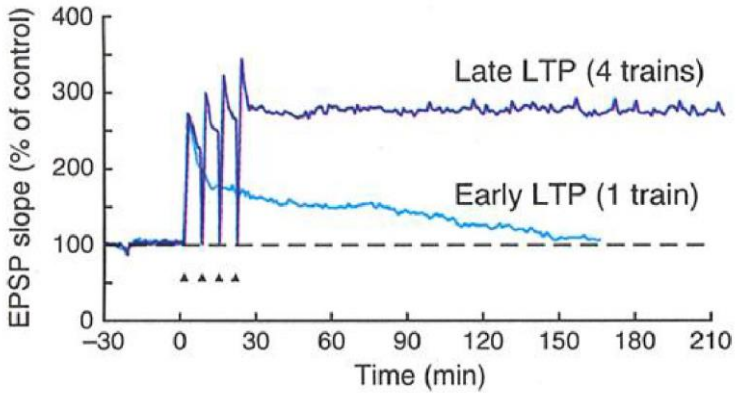

Figure 2 - Early and late-phases of LTP in the Schaffer collateral pathway
(Kandel, 2001)

Studies using transcriptional and translational inhibitors revealed that the E-LTP is independent of new gene expression whereas L-LTP requires *de novo* transcription and translation (Frey et al., 1988; Ho et al., 2011; Kandel, 2001; Nguyen et al., 1994). Mansuy and Winder tested long-term memory tasks in mutant mice lacking calcineurin (a phosphatase critical for LTP) and showed that E-LTP correlates with short-term memory and L-LTP with long-term memory (Mansuy et al., 1998; Winder et al., 1998). Consistently, short-term memory is independent of new protein production while long-term memory integrity relies on new protein synthesis (Flexner et al., 1963; Kandel, 2001). In the early phase of LTP, postsynaptic depolarization of the membrane

activates N-methyl-D-aspartate (NMDA) receptors by reliving their Mg2+ blockage. Activated NMDAR channels trigger calcium influx and promote the activation of several protein kinases, including the Ca2+/calmodulin-dependent protein kinase II (CAMKII), which phosphorylates alpha-amino-3-hydroxy-5-methyl-4-isoxazolepropionic acid (AMPA) receptors (AMPARs) and initiates a signaling cascade that triggers AMPAR trafficking to the postsynaptic membrane (Figure 3). The increased number of phosphorylated AMPARs at the synapse is thought necessary and sufficient to increase synaptic efficacy and drive LTP. The persistence of long-lasting increases in synaptic connectively (L-LTP) are characterized by the activation of adenylyl cyclase that produces cyclic adenosine monophosphate (cAMP) and require the translocation of protein kinase isoform A (PKA) and mitogen-activated protein kinase (MAPK) from stimulated synaptic spines to the nucleus to activate the transcription factor cAMP response element binding protein-1 (CREB) via phosphorylation at serine 133 (Lonze and Ginty, 2002; Martin et al., 1997b; Mayford et al., 2012; Shaywitz and Greenberg, 1999). CREB-mediated *de novo* gene expression is crucial for L-LTP and required for memory formation (Silva et al., 1998).

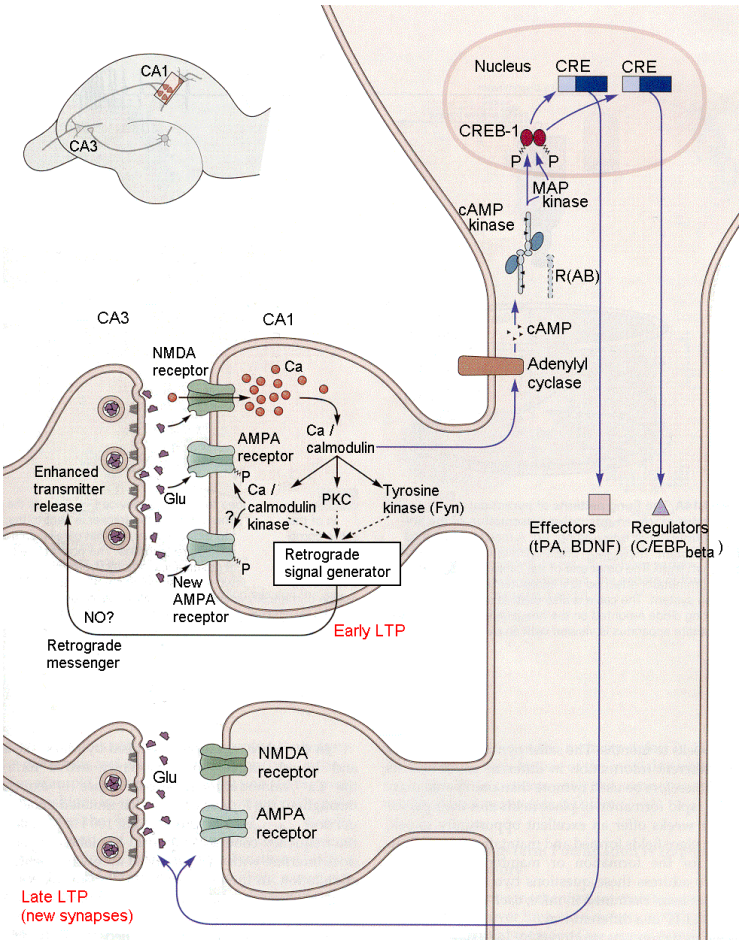

Figure 3 - Diagram of early and late phase LTP

(Kandel et al., 2013)

To gain insight into the program of gene expression underlying long-term memory, previous studies used microarrays, high-throughput RNA sequencing, and mass spectrometry to identify global changes in gene expression that occur during L-LTP (Chang et al., 2006; Gu et al., 2015; Håvik et al., 2007; Maag et al., 2015; McNair et al., 2006; Ryan et al., 2012). More recently, Patrick Chen and colleagues profiled the temporal gene expression changes of excitatory neurons in hippocampal slices undergoing L-LTP and identified a comprehensive list of transcripts differentially loaded into ribosomes as a result of LTP induction (Chen et al., 2017b).

1.2. Co-and post-transcriptional mechanisms of gene expression regulation in the brain

1.2.1. RNA-binding proteins

RNA-binding proteins (RBPs) play critical roles during neuronal development and plasticity by impacting several co- and post-transcriptional steps of gene expression (Figure 4). RBPs control the abundance and localization of transcripts to different sub-compartments of the cell, regulating RNA metabolism processes such as transcription, splicing, cleavage and polyadenylation, miRNA targeting, translation, trafficking, and degradation of transcripts. The importance of RBPs at a physiological scale is highlighted by the discovery of several neurological diseases associated with mutations in RBP-coding genes (Gao and Taylor, 2014; Liu-Yesucevitz et al., 2011; Wang et al., 2016). For example, loss of function of the fragile-X mental retardation protein (FMRP), an RBP involved in mRNA localization and translation, causes fragile-X mental retardation, which is the most common monogenic cause of autism spectrum disorders (Lukong et al., 2008).

The RbFox family of proteins includes the RNA-binding protein 1 (RbFox1, also called A2BP1), RbFox2 (RBM9) and Rbfox3 (NeuN) and constitutes an exquisite example of RBPs that participate in multiple mRNA regulatory functions in the brain. The interest in RbFox1 was initially driven by its interaction with Ataxin-2 (an RBP involved in mRNA translation and linked to spinocerebellar ataxia type 2 (SCA2) and amyotrophic lateral sclerosis (ALS) neurodegenerative disorders) and the discovery of Rbfox1 mutations linked to epilepsy and autism spectrum disorders (Bhalla et al., 2004; Martin et al., 2007; Sebat et al., 2007). In mice, CNS-specific depletion of RbFox1 results in spontaneous seizures indicating a role in neuronal excitability (Gehman et al., 2011). Analysis of post-mortem autistic and normal brains validated the early clinical correlation studies and identified RbFox1 as a major regulation hub for autism-related

genes (Voineagu et al., 2011). The sequencing of mRNAs bound to RbFox proteins (through crosslinking and immunoprecipitation followed by high-throughput sequencing HITS-CLIP) uncovered RbFox targets important for brain development and autism (Weyn-Vanhentenryck et al., 2014).

RBPs recognize RNA motifs located most often in the 3'-UTR or 5´-UTR of transcripts. In contrast with most RBPs, the RbFox family recognize a unique and highly conserved RNA binding sequence in the 3'-UTR – (U)GCAUG – which greatly simplifies molecular studies (Jin et al., 2003). Rbfox1 is alternatively spliced into a nuclear and a cytoplasmic isoform that exhibit different functions within the cell: the nuclear isoform is an alternative splicing regulator and the cytoplasmic isoform promotes mRNA stability (Lee et al., 2009; Ray et al., 2013). The exact mechanisms by which RbFox1 increases the stability of its target transcripts remains still largely unknown and it forms the subject of the study presented in chapter II.

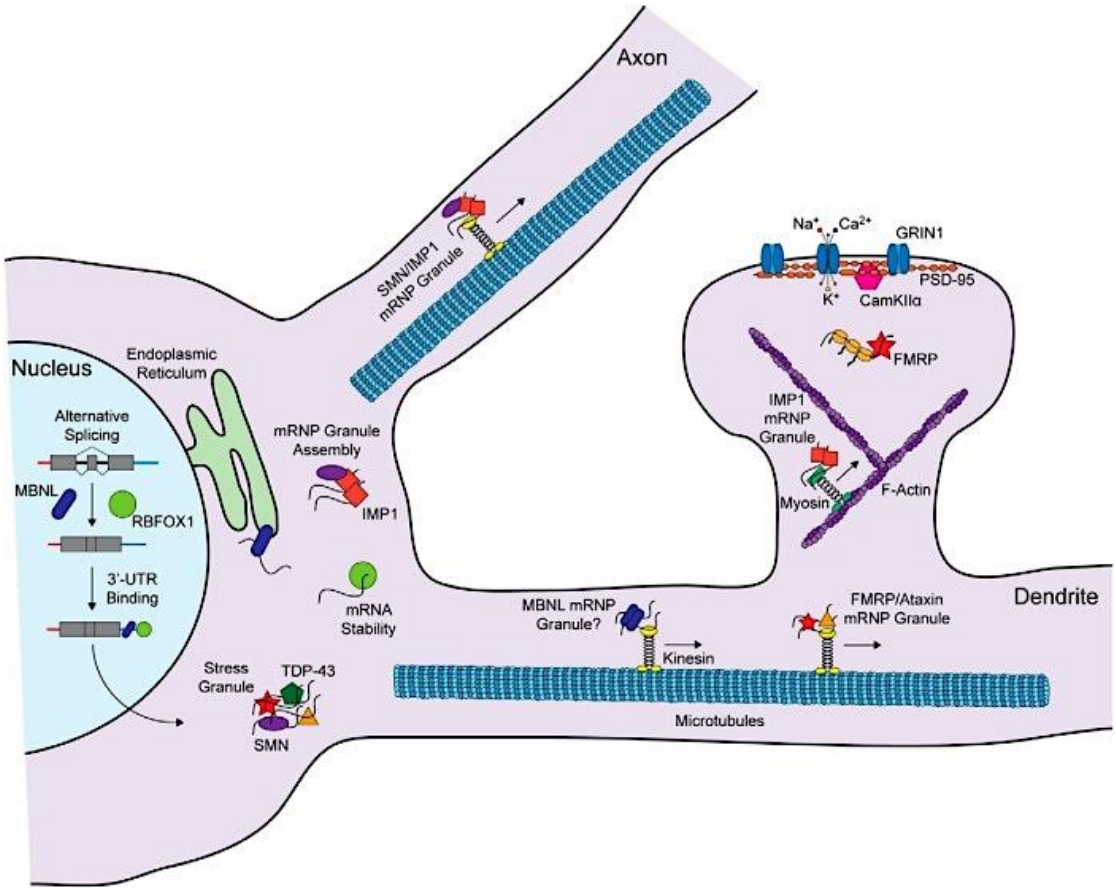

Figure 4 – Spatiotemporal regulation of RNA processing and local translation in neurons by RNA-binding proteins *(Wang et al., 2016)*

1.2.1.1. RBP-mediated localization of mRNAs

RNA localization to specific subcellular compartments is an evolutionary conserved mechanism that enables the spatial and temporal control of protein expression. In neurons and other asymmetric cells, trans-acting RBPs recognize and bind specific cis-acting elements in mRNAs to form messenger ribonucleoproteins (mRNPs), which are packed into RNA transport granules for delivery to the required subcellular locations in a translationally repressed state via motor proteins (Kiebler and Bassell, 2006; Martin and Ephrussi, 2009).

The tight regulation of translation is particularly key in highly polarized cells such as neurons, which possess long axons and dendrites and require rapid and efficient protein synthesis within distal compartments in response to extracellular stimuli (Arimura et al., 2007; Martin KC et al., 2009). Local translation provides a means whereby changes in synaptic strength can quickly occur in a synapse-specific manner, thereby increasing the specificity of the gene expression mechanisms underlying memory formation (Martin KC et al., 2000).

The first evidence for the existence of translation in distal neuronal compartments came from the detection of polyribosomes in dendrites by Steward and Levy (Steward and Levy, 1982). Key components of the protein translational machinery were later identified in neuronal processes, including translation factors (Tang et al., 2002). While most transcripts are restricted to the soma or expressed in both axonal and dendritic subcompartments, a few transcripts show remarkable specificity in their pattern of localization. In-situ hybridizations and high-throughput sequencing studies revealed that a large population of transcripts localizes to dendrites and/or axons (Cajigas et al., 2012; Eberwine et al., 2002; Poon et al., 2006; Taliaferro et al., 2016). The mRNA encoding Tau, a protein implicated in neurodegenerative diseases such as Alzheimer's disease, is selectively delivered to axons in developing neurons while CAMK2A and microtubule-associated protein 2 (MAP2) are highly enriched in the dendrites of mature neurons (Litman et al., 1993; Mayford et al., 1996).

An increasing number of studies quickly demonstrated that not only can local protein translation occur but that it also is integral to plasticity, including to the formation of new synapses. For example, hippocampal slices with the soma isolated from the dendrites and axons were still found capable of displaying a long-lasting type of potentiation or depression when stimulated via BDNF or metabotropic glutamate receptors, respectively (Huber et al., 2000; Kang and Schuman, 1996). Consistently with the role of local translation in plasticity, polyribosomes were found translocated to synapses in an activity-dependent manner and L-LTP dependent on the translation activation via MAPK signaling pathways (Bourne et al., 2007; Kelleher et al., 2004;

Ostroff et al., 2002). Additional metabolic labeling experiments, protein-synthesis inhibitor assays and functional studies on localized mRNAs important for L-LTP, unequivocally demonstrated the critical role of local protein synthesis to synaptic plasticity and the storage of information in the brain (Glock et al., 2017; Martin and Zukin, 2006; Sutton and Schuman, 2006; Tan et al., 2013; Wang et al., 2009). The dendritically localized Camk2A protein illustrates the importance of this mechanism to memory formation. Mice with a targeted mutation of the 3'UTR cis-elements responsible for the trafficking of Camk2a mRNA to dendrites displayed a large reduction of Camk2a protein levels at synapses and developed impairments in late-phase LTP and long-term memory (Miller et al., 2002).

1.2.2. Alternative cleavage and polyadenylation

The cleavage and polyadenylation (C/P) of RNA polymerase II (RNAPII) products is a nearly universal 3' end processing phenomenon in eukaryotes that is critical for the maturation of transcripts and triggered by RBPs (Colgan and Manley, 1997). C/P is a two-step mechanism consisting of the endonucleolytic cleavage of pre-mRNAs followed by the polymerization of a polyadenosine (poly(A)) tail that is involved in many aspects of mRNA metabolism, including nuclear export, stability and translation (Figure 5). The C/P reaction is coupled to transcription termination and is mediated by approximately 20 core trans-acting factors and auxiliary proteins in the nucleus. Some of the C/P machinery components form subcomplexes - including the Cleavage and Polyadenylation Specific Factor (CPSF), the Cleavage stimulation Factor (CstF), the Cleavage Factor I(CFI) and the Cleavage Factor II(CFII) – and others act as single proteins – including Symplekin, poly(A) polymerase (PAP), nuclear poly(A) binding protein (PABPN) and the RNAPII. First, CPSF catalyzes the cleavage of the pre-mRNA, 10–30 nucleotides downstream of its binding site, in the polyA site (PAS), which is defined by upstream and downstream *cis* regulatory elements. Upstream elements include the canonical polyadenylation signal A[A/U]UAAA or its close variants, UGA elements and U-rich sequences, while U- and GU-rich elements are found downstream of the cleavage site(Di Giammartino et al., 2011; Elkon et al., 2013; Tian and Graber, 2012)**.** CstF and CFI add specificity to the binding of CPSF to the RNA. Once the cleavage is completed, PAP starts building the poly(A) tail by adding adenine monophosphates to the pre-mRNA 3'end, with the support of PAB2, until the length of the tail causes the loss of interaction between PAP and CPSF. The poly(A) tail has a restricted length and varies widely between species, ranging between 250 and 500 adenines per poly(A) tail in humans. Regulating the size of the poly(A) tail

adds an additional layer of complexity to gene regulation whereby transcripts with very short tails are preferentially degraded or translationally inhibited.

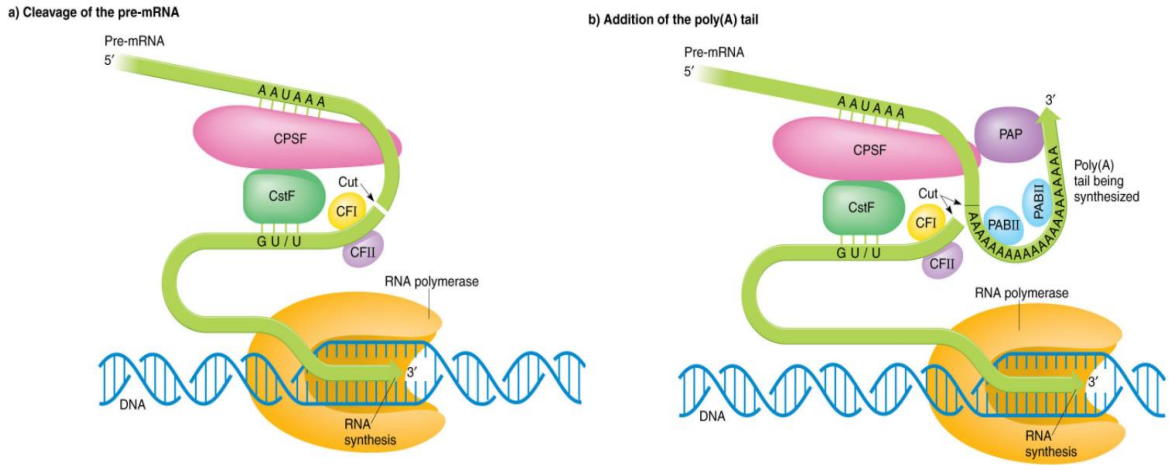

Figure 5 – 3'end processing of mRNAs - cleavage and polyadenylation

(Peter J Russel, 2009)

Most mammalian genes contain several PASs and display alternative cleavage and polyadenylation (APA) that yields multiple mRNA isoforms with alternative terminal exons (ATE) and/or 3'UTRs with variable length(Tian et al., 2005). High throughput sequencing of the 3' end of transcripts has revealed that ~79% of mRNAs and ~66% of long non-coding RNAs in mouse tissues have APA isoforms(Hoque et al., 2013). Although APA can increase protein diversity when ATE are coupled with coding sequence (CDS) changes, the majority of APA events occur within the terminal exons and alter 3'UTR length without affecting the CDS(Hoque et al., 2013).

Genome-wide analyses have begun to uncover the broad set of biological processes modulated by extensive APA. Global trends of 3'UTR shortening were found in cell proliferation (Sandberg et al., 2008) and cancer cells (Mayr and Bartel, 2009), while 3' UTR lengthening was been associated with cell differentiation and embryonic development (Ji et al., 2009; Shepard et al., 2011). Unique patterns of APA regulation have also been detected in several tissues (Lianoglou et al., 2013; Wang et al., 2008; Zhang et al., 2005b)**,** including enhanced utilization of distal PAS that produce longer alternative 3'UTRs (aUTRs) in the brain (Hilgers et al., 2011; Miura et al., 2013, 2014; Smibert et al., 2012; Zhang et al., 2005b).

Elements within the 3'UTR contain binding sites for RNA-binding proteins and miRNAs that regulate many aspects of mRNA metabolism, including mRNA localization, stability, translation, and protein localization (Elkon et al., 2013; Lutz and Moreira, 2011; Mayr, 2016; Tian and Manley, 2013). Hence, controlling the length and

composition of the 3'UTR serves as a critical node of post-transcriptional regulation. Regulation of the 3'UTR plays a particularly important role in compartmentalized gene expression in neurons through the above-mentioned localization and regulated translation of mRNAs within dendrites and at synapses (Job and Eberwine, 2001; Martin et al., 1997a; Martin and Ephrussi, 2009; Sutton and Schuman, 2006; Wang et al., 2010a). In fact, RNA sequencing of the synaptic neuropil in mouse hippocampus identified over 2,000 axonally and dendritically localized mRNAs (Cajigas et al., 2012), and the localization of these mRNAs often depends on cis-acting elements within the 3'UTR (Martin and Ephrussi, 2009).

The wide range of 3'UTR profiles observed in the brain raises the question of how and to what extent does plasticity-inducing stimuli affect the global regulation of APA in neurons. In one early genome-wide analysis, Flavell et al. (2008) used microarray analysis to identify global changes in APA induced by potassium chloride membrane depolarization of rat neuronal hippocampal cultures. The authors observed a switch in pA usage after stimulation that favored the production of truncated mRNAs, accompanied in some cases by the production of truncated proteins (Flavell et al., 2008). This study began to uncover the APA changes involved in neuronal potentiation and motivated the project described in chapter II.

Studies on individual transcripts provide insights into the impact of alternative 3'UTR usage on neuronal function. For example, activity-dependent APA of brain-derived neurotrophic factor (*Bdnf*) mRNA controls the subcellular localization and translation of *Bdnf* mRNA in a manner that regulates dendritic spine enlargement and LTP(An et al., 2008; Lau et al., 2010; Pattabiraman et al., 2005). As another example of 3'UTR-dependent translational regulation, miR-483-5p binds to sequences in the long but not the short 3'UTR isoform of the epigenetic factor methyl CpG-binding protein 2 (MeCP2)(Han et al., 2013) to downregulate MeCP2 protein concentrations in human fetal brain, and this downregulation is critical to normal brain development (Chahrour and Zoghbi, 2007; Han et al., 2013).

1.2.3. Regulation by microRNAs

MicroRNAs (miRNAs) are highly conserved small (18-22 nucleotides) non-coding molecules that regulate gene expression, mainly via sequence-specific binding within the 3'UTR region of mRNAs. miRNAs module mRNA levels by triggering the destabilization or translation repression of transcripts loaded selectively into RNA-induced silencing complexes (RISC). To achieve specificity, each miRNA contains a sequence in the 2-7 position from their 5'end, named seed sequence, that allows the

recognition and binding to specific mRNAs via complementary base-pairing (Huntzinger and Izaurralde, 2011). The dynamic nature of miRNAs regulation – where a miRNA can target several hundred transcripts and each transcript can be targeted by many miRNAs – is especially suitable to post-transcriptionally fine-tune gene expression in complex networks, such as neuronal circuitry (Bartel, 2009). Indeed, early studies found that 60-80% of all miRNAs are expressed in brain and identified populations of miRNAs with brain-specific or brain-enriched patterns of expression, suggesting that miRNAs play important functions in the central nervous system (Lagos-Quintana et al., 2002; Landgraf et al., 2007; McNeill and Van Vactor, 2012; Sempere et al., 2004). miRNA gene expression profiling of individual brain regions revealed that miRNAs display heterogeneous patterns of expression between adjacent neuroanatomic regions, raising the need to investigate specific brain regions and neuronal types (He et al., 2012).

Several studies showed the importance and mechanism of action of miRNAs in hippocampal development and function. In hippocampal neuronal cultures, the constitutive depletion of an RNase III enzyme that is central to the production of mature miRNAs called Dicer, led to widespread cell death highlighting the involvement of miRNAs in neuronal survival (Hebert et al., 2010). *In vivo* studies characterizing conditional knockout mice that lacked Dicer in excitatory neurons of the forebrain reported dramatic effects in the hippocampal tissue morphogenesis, including aberrant hippocampal patterning and neuronal organization (Davis et al., 2008). Interestingly, mice subject to inducible disruption of Dicer in excitatory neurons of the adult forebrain displayed improved performance in cognitive tests (Konopka et al., 2010). Although Dicer plays additional cellular roles in the brain that are unrelated to the biogenesis of miRNAs (Rybak-Wolf et al., 2014), this observation suggested miRNAs are involved in learning and memory. Deciphering the miRNA:mRNA target interactions at a genome-wide level is a crucial step to understand miRNA regulation in the hippocampus. Several studies performed high-throughput sequencing of miRNAs and targeted mRNAs bound to structural proteins of the RISC complex (mostly Ago2) revealing the miRNA-mediated networks held in the human and mouse brain (Boudreau et al., 2014; Chi et al., 2009; Tan et al., 2013), and more specifically in hippocampal neurons (Malmevik et al., 2015). Consistent with the importance of miRNA regulation in neural circuit formation and function, miRNAs and key components of the miRNA processing machinery have been detected in dendrites and at synapses (Ashraf et al., 2006; Banerjee et al., 2009; Kye et al., 2007; Lugli et al., 2008; Siegel et al., 2009). Furthermore, several studies identified hippocampal miRNAs changing their

abundance or localization within the cell in an activity-dependent manner associated with important consequences for synaptic plasticity (Eacker et al., 2011).

miR-132 expression was shown to be induced by the transcription factor CREB and to mediate neuronal outgrowth (Vo et al., 2005; Wayman et al., 2008). Subsequent *in vivo* studies overexpressing miR-132 in forebrain neurons resulted in mice with significant impairments in novel object recognition memory and showed the role of miR-132 in the modulation of dendritic spine density and volume (Hansen et al., 2010). Other brain-enriched miRNAs, such as miR-134, miR-138 and miR-125b were also identified as major regulators of dendritic spine morphogenesis, which importantly correlates with synaptic strength (Fiore et al., 2009; Holtmaat and Svoboda, 2009; Schratt et al., 2006; Siegel et al., 2009). In another study, the brain-specific and highly abundant miR-124 was found to inhibit long-term plasticity through negative regulation of the transcription factor CREB (Rajasethupathy et al., 2009).

The molecular pathways that underlie the orchestrated regulation of synaptic plasticity by miRNAs are still only partially understood. It has been postulated that under basal conditions, a pool of miRNAs represses the translation of pre-existing localized mRNAs. Induced by neuronal activity, the ubiquitin-proteosome system re-localizes to spines and triggers the degradation of critical components of the RNA–induced silencing complex (RISC), which allows the release of miRNAs and protein synthesis to take place (Ashraf et al., 2006; Banerjee et al., 2009; Ehlers, 2003). Another mechanism proposed to explain the activity-dependent function of miRNAs proposes that dendritic P-body-like structures store miRNAs and their translationally repressed target mRNAs during unstimulated conditions, and, can release them following synaptic activity (Cougot N et al., 2008).

1.3. Experimental models of hippocampal plasticity

There are several widely accepted *in vivo* and *in vitro* models to study hippocampal plasticity. The most commonly used to address molecular questions are hippocampal primary cell cultures and hippocampal slice preparations. Neuronal cell cultures have the advantage of being relatively easy to prepare, surviving for several weeks and allowing the visualization and manipulation of individual neurons and neuronal connections which are critical to uncover the cellular and intracellular mechanisms of neurobiology. In the study described in chapter III, we used cell cultures to be able to specifically express different isoforms of our protein of interest, RbFox1. Unlike primary cell cultures, hippocampal slice preparations maintain largely the cytoarchitecture and synaptic circuits of the intact hippocampus and thus provide a

more relevant system to study neurophysiology. Acute hippocampal slice preparations are usually obtained from the adult rodent brain and experiments are performed within a day. In contrast, hippocampal slice cultures are most often derived from embryonic or P0 rodent brains and can be maintained in vitro for weeks to months. There are several validated protocols to induce long-lasting forms of LTP in hippocampal slices, both using electrical and chemical stimulation. In the study presented in chapter II, we chose to use a chemical LTP induction paradigm (cLTP) to induce L-LTP in the Shaffer collateral pathway of acute hippocampal slices as this model not only preserves the physiological connections of the rodent hippocampus but also activates a larger number of synapses than the localized electrical stimulation.

cLTP induction recapitulates physiological hippocampal plasticity by requiring bursting of CA3 neurons and producing a long-lasting NMDAR-dependent plasticity that needs *de novo* transcription and translation (Chotiner et al., 2003; Makhinson et al., 1999). First forskolin activates the cAMP signaling pathway to allow a persistent increase in the levels of CAMKIIA required for LTP induction and maintenance. Then, elevated levels of potassium lead to a global depolarization where both ligand-gated and voltage-gated ion channels are activated to allow the influx of calcium and activation of calcium signaling pathways. Depolarization triggers glutamate release and NMDA receptors activation that is necessary for LTP induction in CA3-CA1 synapses. The activation of a larger number of synapses results in a higher sensitivity and higher signal to noise, which is particularly important for RNA-Seq and 3'READS experiments that rely on relatively large yields of high quality RNA.

2. Chapter II - Activity-dependent regulation of alternative cleavage and polyadenylation during LTP

The "Chapter II – Activity-dependent regulation of alternative cleavage and polyadenylation during LTP" consists of a co-first authorship publication and complementary insights. Here is clarified the contribution of each of the authors to the article:

2.1. Publication:

Mariana M. Fontes[1,2,#], Aysegul Guvenek[3,#], Riki Kawaguchi[4], Dinghai Zheng[3], Alden Huang[4], Victoria M. Ho[1,5], Patrick B. Chen[1,5], Xiaochuan Liu[3], Thomas J. O'Dell[6], Giovanni Coppola[4], *Bin Tian[3] & *Kelsey C. Martin[1,4]. Activity-Dependent Regulation of Alternative Cleavage and Polyadenylation During Hippocampal Long-Term Potentiation, *Scientific Reports* 2017 Dec 12;7(1):17377, doi: 10.1038/s41598-017-17407-w

[1]Department of Biological Chemistry, David Geffen School of Medicine, University of California, Los Angeles, Los Angeles, CA;
[2]Graduate Program in Areas of Basic and Applied Biology, University of Porto, Porto, Portugal; [3]Department of Microbiology, Biochemistry and Molecular Genetics, Rutgers New Jersey Medical School, Newark, NJ;
[4]Department of Psychiatry and Biobehavioral Sciences, Semel Institute for Neuroscience, David Geffen School of Medicine, University of California, Los Angeles, Los Angeles, CA;
[5]Interdepartmental Graduate Program in Neuroscience, University of California, Los Angeles, Los Angeles, CA;
[6]Department of Physiology, David Geffen School of Medicine, University of California, Los Angeles, Los Angeles, CA

[#]These authors contributed equally to this work.

*Corresponding Authors:

Kelsey C. Martin E-MAIL: kcmartin@mednet.ucla.edu; TEL: (310) 825-5687
Bin Tian E-MAIL: btian@rutgers.edu; TEL: (973) 972-3615

Mariana Miranda Fontes, the candidate for the PhD degree at the University of Porto, contributed to the paper by defining the main question of the project, designing the experiments, performing the chemical stimulation of hippocampal slices, preparing and validating by qPCR the RNA samples for PAS-Seq, RNA-Seq and miR-seq and writing the paper.

The contribution of each author to the publication is clarified in the section "Authors contribution" with the following text:

"Authors contribution: MF, BT, and KCM conceived of and designed the experiments. MMF, DZ, AH, VMH, and PBC performed the experiments. AG, RK, XL, GC, and BT analyzed the data. TJO contributed reagents and materials. MMF, AG, BT, and KCM wrote the paper."

Activity-Dependent Regulation of Alternative Cleavage and Polyadenylation During Hippocampal Long-Term Potentiation

Keywords: Alternative cleavage and polyadenylation, hippocampus, long-term potentiation, memory, gene expression, synaptic plasticity

2.1.1.ABSTRACT

Long-lasting forms of synaptic plasticity that underlie learning and memory require new transcription and translation for their persistence. The remarkable polarity and compartmentalization of neurons raises questions about the spatial and temporal regulation of gene expression within neurons. Alternative cleavage and polyadenylation (APA) generates mRNA isoforms with different 3' untranslated regions (3'UTRs) and/or coding sequences. Changes in the 3'UTR composition of mRNAs can alter gene expression by regulating transcript localization, stability and/or translation, while changes in the coding sequences lead to mRNAs encoding distinct proteins. Using specialized 3' end deep sequencing methods, we undertook a comprehensive analysis of APA following induction of long-term potentiation (LTP) of mouse hippocampal CA3-CA1 synapses. We identified extensive LTP-induced APA changes, including a general trend of 3'UTR shortening and activation of intronic APA isoforms. Comparison with transcriptome profiling indicated that most APA regulatory events were uncoupled from changes in transcript abundance. We further show that specific APA regulatory events can impact expression of two molecules with known functions during LTP, including 3'UTR APA of *Notch1* and intronic APA of *Creb1*. Together, our results reveal that activity-dependent APA provides an important layer of gene regulation during learning and memory.

2.1.2. INTRODUCTION

Long-term potentiation (LTP) is a form of synaptic plasticity that corresponds to a long-lasting increase in synaptic transmission in response to specific patterns of neuronal firing or activity, and underlies learning and memory (Bliss and Collingridge, 1993; Silva et al., 1992). The early-phase of LTP (E-LTP) is independent of new gene expression while the late-phase of LTP (L-LTP), which lasts several hours to days, requires new transcription and translation (Frey et al., 1988; Ho et al., 2011; Kandel, 2001; Nguyen et al., 1994).

Pre-mRNA cleavage and polyadenylation (C/P) is a nearly universal 3' end processing mechanism for protein-coding genes in eukaryotes, and is coupled to transcription termination (Colgan and Manley, 1997). C/P consists of an endonucleolytic

cleavage of pre-mRNAs followed by the synthesis of a polyadenosine tail, and is carried out by the C/P complex, which contains over 20 factors and many associated factors (Shi et al., 2009). The site for C/P, known as polyA site (PAS), is defined by upstream and downstream cis regulatory elements, the most prominent of which is the A[A/U]UAAA element located upstream of the PAS (Di Giammartino et al., 2011; Elkon et al., 2013; Tian and Graber, 2012).

Most mammalian genes contain multiple PASs that yield multiple mRNA isoforms (Derti et al., 2012; Hoque et al., 2013; Tian et al., 2005). While the majority of alternative PASs are located within the 3'-most exon and lead to changes in 3'UTR lengths, a sizable fraction of PASs are located in introns and control the selection of alternative terminal exons, affecting both coding sequences (CDSs) and 3'UTRs (Hoque et al., 2013). A growing number of mechanisms have been found to regulate APA, including core C/P factors (Li et al., 2015; Shi and Manley, 2015), splicing factors (Berg et al., 2012; Li et al., 2015), and RNA-binding proteins that interact with sequence motifs near the PAS (Zheng and Tian, 2014).

Several tissues exhibit unique patterns of APA regulation (Lianoglou et al., 2013; Wang et al., 2008; Zhang et al., 2005b). For example, distal PASs tend to be selected in the brain, leading to preferential expression of mRNAs with long 3'UTRs (Hilgers et al., 2011; Miura et al., 2013, 2014; Smibert et al., 2012; Zhang et al., 2005a). Since the 3'UTR contains binding motifs for RNA-binding proteins and miRNA target sites, alteration of 3'UTR length offers an effective means to modulate gene expression by controlling aspects of mRNA metabolism, such as stability and translation (Elkon et al., 2013; Lutz and Moreira, 2011; Mayr, 2016; Tian and Manley, 2017).

In keeping with the preferential expression of distal PAS isoforms in neurons, 3'UTRs play a particularly important role in compartmentalized gene expression by directing the localization and regulated translation of mRNAs within dendrites and axons and at synapses (Job and Eberwine, 2001; Martin et al., 1997a; Sutton and Schuman, 2006; Wang et al., 2010b). RNA sequencing of the synaptic neuropil in mouse hippocampus identified over 2,000 axonally and dendritically localized mRNAs (Cajigas et al., 2012). Localization of mRNAs in neurons often depends on specific cis-acting elements within the 3'UTR (Holt and Schuman, 2013; Martin and Ephrussi, 2009). Interestingly, Taliaferro et al. found that transcripts using distal alternative last exons tended to be localized to neurites (Taliaferro et al., 2016). In addition, several studies have reported APA regulation following neuronal activation. An early microarray analysis found that a set of genes expressed truncated mRNAs through APA in cultured rat neuronal hippocampal cells following chronic potassium chloride depolarization (Flavell et al., 2008). It was suggested that the APA events may couple with transcriptional regulation through MEF2 (Flavell et al., 2008). Using Rat PC12

and mouse MN-1 neurons, Berg et al. showed that activity-induced APA changes were recapitulated by functional inhibition of U1 snRNP (Berg et al., 2012), a complex that is involved not only in 5' splice site recognition but also in the inhibition of premature usage of PAS (Berg et al., 2012; Li et al., 2015; Luo et al., 2013). The authors suggested that shortage of U1 snRNP during transcriptional upregulation following neuronal activation may lead to activation of proximal PAS.

Here, using deep sequencing of 3' ends of transcripts, we systematically characterized APA regulation following LTP induction in acute mouse hippocampal slices. We examined both 3'UTR APA and intronic APA events at different time points post LTP, and analyzed the interplay between APA and gene expression regulation. Our study reveals global shortening of 3'UTR and activation of intronic APA, in line with previous reports. However, APA events are largely uncoupled from gene expression changes, and constitute a distinct layer of gene regulation during LTP.

2.1.3. RESULTS

We were interested in understanding whether and how APA, a widespread pre-mRNA processing mechanism, plays a role in LTP. To this end, we perfused acute hippocampal mini-slices with forskolin and high concentrations of calcium and potassium to induce chemical LTP (cLTP). This form of LTP depends on bursting of CA3 neurons and produces a long-lasting, NMDAR-dependent plasticity that requires new transcription and translation (Chotiner et al., 2003; Makhinson et al., 1999). We extracted RNA from hippocampal mini-slices 1 (1 hr) and 3 hours (3 hr) post LTP induction (Fig. 1a), collecting time-matched controls from the same animals (Fig. 1a, see Materials and Methods (Chotiner et al., 2003; Makhinson et al., 1999). Reverse transcription-quantitative PCR (RT-qPCR) analysis of the immediate early gene Arc as well as the short and long intronic APA homer1 isoforms confirmed their regulation after LTP induction, as previously reported (Chen et al., 2017b; Sala et al., 2003).

To determine APA profiles after LTP induction, we subjected RNA samples to 3'READS, a method we previously developed to specifically study the 3' end of transcripts (Zheng et al., 2016) (see Materials and Methods). After exclusion of outlier samples (Fig. S1), we obtained >10 million (M) PAS-containing reads per sample and identified 24,908 PASs in 13,445 genes, including 294 non-coding RNA genes. About 55% of identified PASs were associated with AAUAAA, 17% with AUUAAA, 20% with other close variants, and ~8% with no identifiable A[A/U]UAAA or their close variants in the -40 to -1 nt region of the PAS (Fig. 1b). These values were comparable at 1 hr and 3 hr, for both control and LTP samples. We note that a higher percentage of PASs were associated with the AAUAAA hexamer in

our RNA samples than the 42% previously reported in the mouse genome (Hoque et al., 2013), presumably because APA transcripts in brain preferentially use distal PASs (Hilgers et al., 2011; Ho et al., 2011; Miura et al., 2013; Smibert et al., 2012; Zhang et al., 2005a), which are more frequently associated with AAUAAA than proximal PASs (Tian et al., 2005).

Approximately half of all detected protein-coding genes used 2 or more PASs, with no significant difference in the number of PASs per gene between control and LTP samples (Fig. 1c). As shown in Fig. 1e, most PASs (>85%) were found in the 3'UTR of the 3'-most exon, with less than 15% of PASs located in introns. Notably, we observed a small but significant (3,432 vs. 2,911, $P = 5.3 \times 10^{-16}$, Binomial test) global increase in the number of detected intronic PASs 3 hr post LTP, suggesting upregulation of intronic PAS usage following LTP induction (see below for more analysis). By contrast, no significant difference was detected 1 hr post LTP.

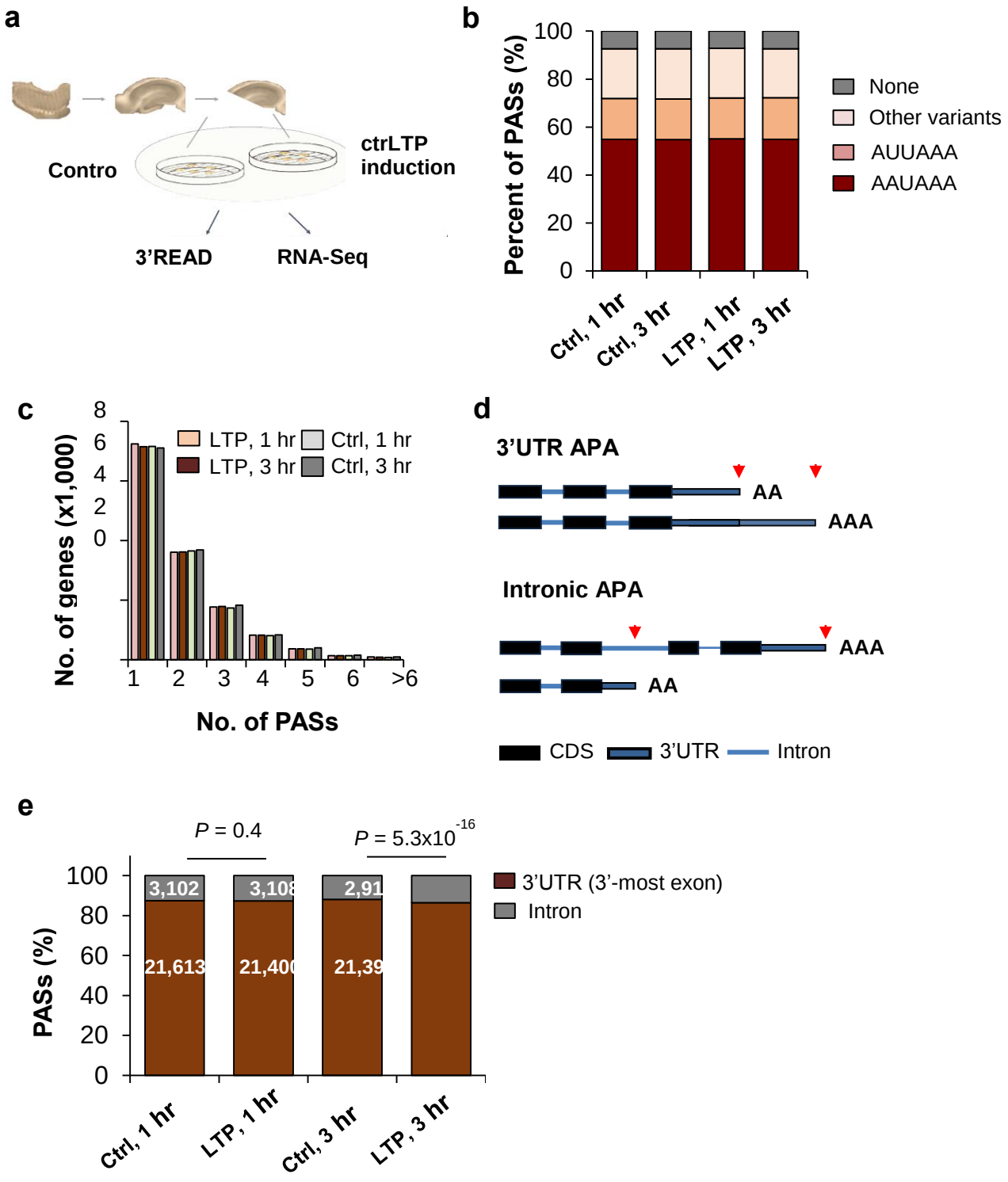

Figure 1. Analysis of APA in LTP. (a) Experimental design. RNAs from chemical LTP (cLTP)-induced and time-matched control hippocampal slices was subjected to 3'READS+ analysis to examine APA, or RNA-seq for gene expression. (b) Distribution of the A[A/U]UAA element in identified poly(A) sites (PASs). Percentage of PASs associated with either AAUAAA, AUUAAA, other variants of A[A/U]UAAA, or not associated with any A[A/U]UAAA element are shown for each sample group. (c) Number of PASs identified per gene. Genes with only one PAS have the highest frequency and the majority of genes displayed APA in the hippocampal samples analyzed. (d) Diagram showing 3'UTR APA (top) and intronic APA (bottom). 3'UTR APA isoforms have alternative 3' UTRs resulting from the choice of different

PASs in the 3'UTR. Two PASs are shown, i.e., proximal PAS and distal PAS. Intronic APA isoforms have different 3'UTRs as well as coding sequences (CDS). (e) Distribution of PASs in different regions of the mRNA: 3'UTR (in 3'-most exon only) vs. upstream intron. Change of PAS distribution during LTP is observed 3 hr post LTP induction. Number of PAS in each region is specified in each bar. P-values (Binomial test) indicate difference in fractions of 3'UTR PASs and intronic PASs in LTP vs. control samples.

LTP induces global shortening of 3'UTRs

We next focused on 3'UTR APA events and asked whether there was a global change in 3'UTR length after LTP induction. To simplify our analysis, we focused on the two most abundant 3'UTR APA isoforms, named proximal and distal PASs based on their relative positions in the 3'UTR (Fig. 2a), and compared their relative expression changes in LTP-induced vs. control samples. While similar numbers of genes displayed 3'UTR shortening and lengthening after 1 hr of LTP induction (72 vs. 88, Fig. 2b), a bias toward 3'UTR shortening was detected 3 hr post LTP induction (203 vs. 77, Fig. 2c). Notably, the genes that displayed 3'UTR changes 3 hr after LTP induction were largely distinct from those with 3'UTR changes 1 hr after LTP induction (Fig. 2d).

To measure the extent of 3'UTR length change elicited by LTP, we divided genes into groups with lengthened 3'UTRs, unchanged 3'UTRs or shortened 3'UTRs, and calculated their average difference in 3'UTR length. At 1 hr, both lengthened and shortened 3'UTR genes underwent mild changes in 3'UTR length (median = 64 nucleotides (nt) and 55 nt, respectively, Fig. 2e). By contrast, at 3 hr, while genes with lengthened 3'UTRs displayed a mild change of 3'UTR length (median = 43 nt), genes with shortened 3'UTRs showed a more pronounced 3'UTR length change (median = 81 nt) (Fig. 2f).

3'UTR length changes have previously been shown to alter miRNA targeting (Mayr and Bartel, 2009; Sandberg et al., 2008). We next set out to globally identify miRNA target sites that would be affected by 3' UTR shortening 3 hr after LTP induction. Of the 164 genes that displayed both 3'UTR shortening and contained miRNA target sites (based on the TargetScan database), 117 had their miRNA target sites (882 sites in total) removed by 3'UTR shortening (Fig. 2g). Thus, 3'UTR shortening could potentially play an important role in modulating miRNA regulation following LTP induction. An example gene, *Notch1,* is shown in Fig. 2h, displayed significant 3'UTR shortening in the 3 hr samples (P= 4 X 10^{-4}, Fig. 2e), but not in the 1 hr samples. The Notch1 protein has been reported to be critical for hippocampal synaptic plasticity and memory formation (Alberi et al., 2011; Brai et al., 2015). Interestingly, we found a target site for miR-384-5p between the proximal and distal PASs of *Notch1* (Fig. 2h), a miRNA whose downregulation was shown to be required for the maintenance of LTP (Gu et al., 2015). Thus, shortening of *Notch1* 3'UTR after LTP induction could help de-repress *Notch1* expression by miR-384-5P, contributing to LTP maintenance.

RT-qPCR analysis using primer sets targeting a common coding region and a region that exists only in the long 3'UTR isoform confirmed increased *Notch1* gene expression and relatively higher expression of short 3'UTR isoform compared to long 3'UTR isoform (Fig. 2j).

Previous studies in other systems have indicated that the distance between two 3'UTR PASs, also known as alternative 3'UTR (aUTR) size (Fig. 2a), often correlates with the extent of 3'UTR APA (Li et al., 2015), a phenomenon likely attributable to competition between the two adjacent PASs for usage. We thus divided genes with 3'UTR-APA regulation at 1 hr or 3 hr post-LTP into five groups based on their aUTR sizes (aUTR bins 1-5) and asked whether the difference in the relative expression of two APA isoforms between LTP and control samples (relative expression difference, RED) was a function of aUTR size. The mean RED values shown in Fig. 2i revealed that genes with longer aUTRs underwent significantly greater 3'UTR shortening 3 hr post-LTP as compared to 1 hr (gene bin 1 vs gene bin 5 comparison at 3 hr: p-value=2.2×10^{-11}, Wilcoxon rank sum test). Together, these results indicate that LTP drives a general shortening of 3'UTR 3 hr post LTP induction, especially in transcripts with long aUTRs.

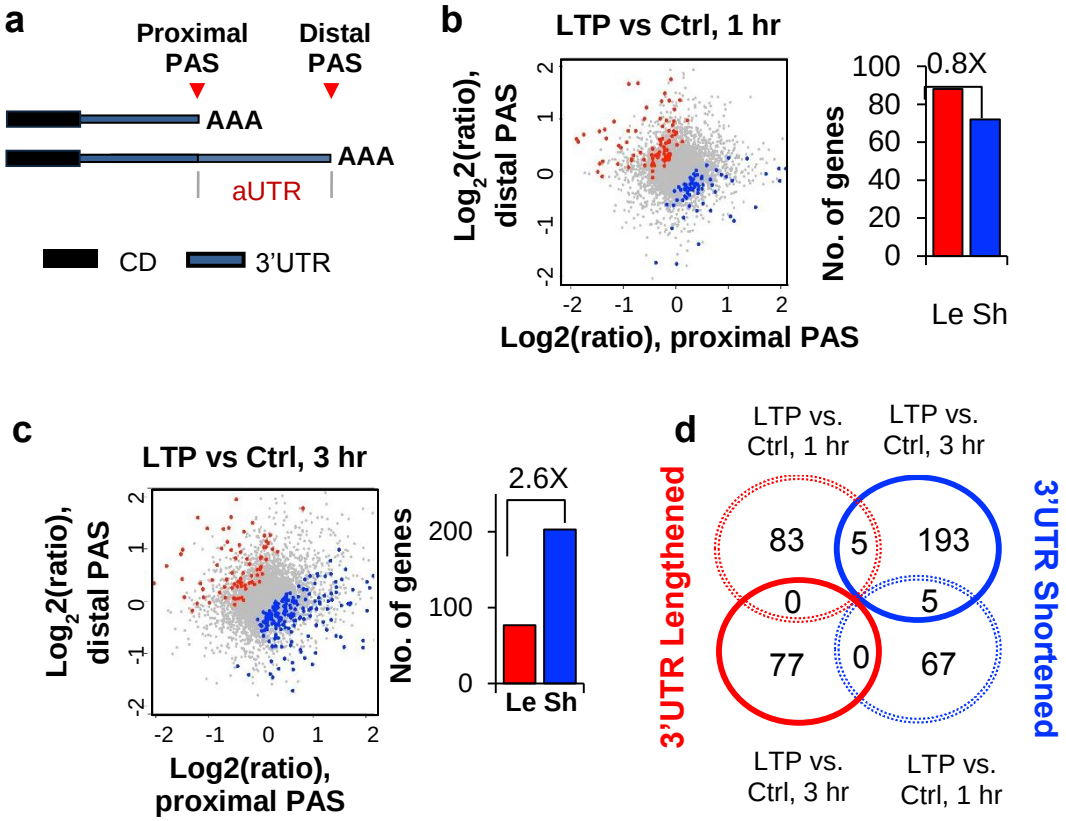

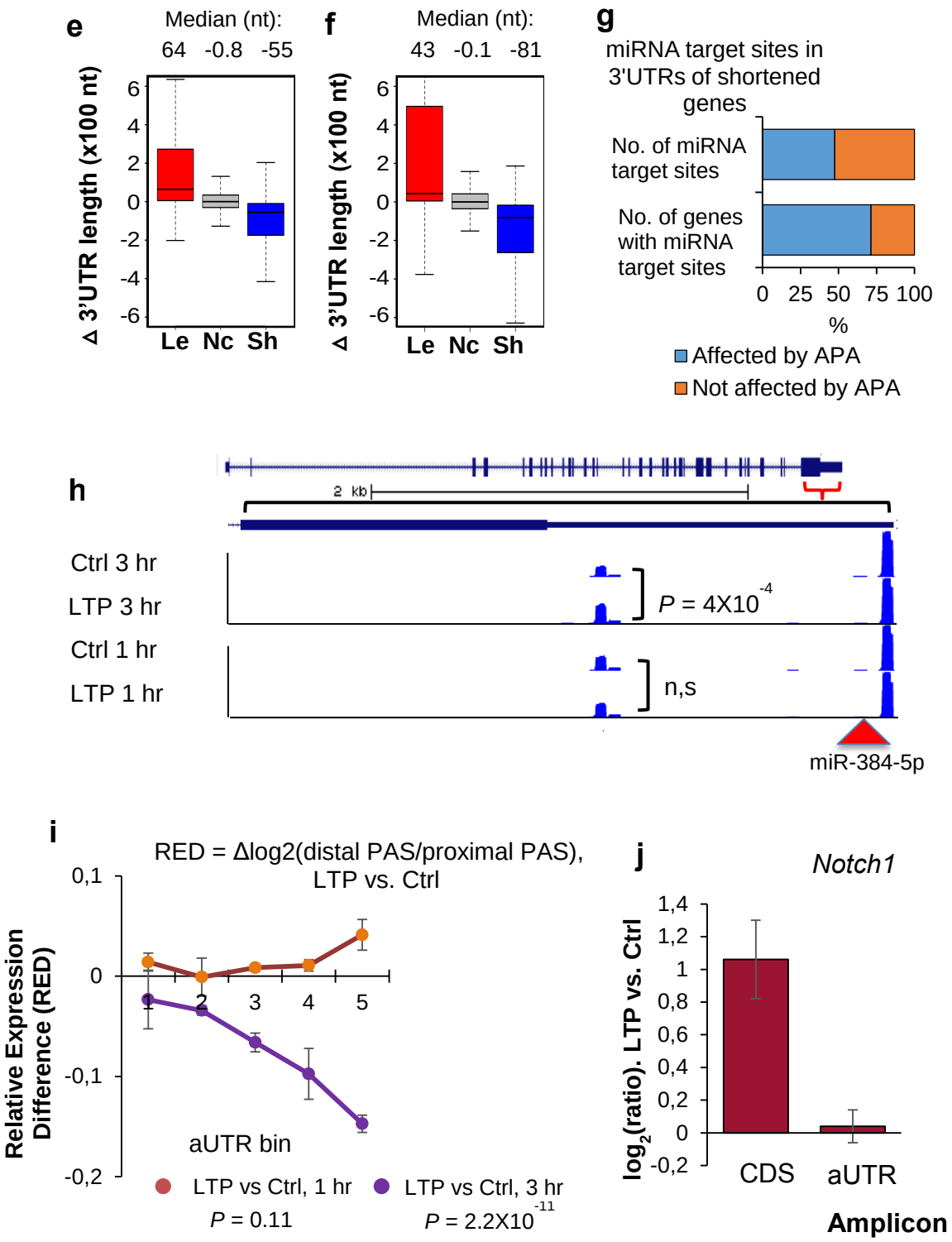

Figure 2. Regulation of 3'UTR APA after LTP induction. (a) Schematic of 3'UTR APA. (b) 3'UTR APA regulation after 1 hr LTP induction. Left, Scatterplot comparing expression changes of proximal and distal PASs after 1 hr LTP induction. Genes that significantly switched to proximal PAS usage are in blue and those that switched to distal PAS usage are in red (P < 0.05, DEXSeq, and relative abundance change >5%). Grey dots are genes without significant APA regulation. Right, bar graph comparing the number of genes with lengthened or shortened 3'UTRs (Le and Sh, respectively). (c) As in (b), 3 hr post LTP induction. (d) Venn diagram comparing genes with significant 3'UTR regulation 1 hr post LTP

induction and 3 hr post LTP induction. (e) 3'UTR length change in 1 hr post LTP induction. Genes with 3'UTRs significantly shortened (blue), lengthened (red), or unchanged (grey) are shown. 3'UTR size was based on weighted mean of all 3'UTR isoforms. Median values are indicated on the top. (f) As in (e), except that data are based on 3 hr post LTP induction. (g) Effect of 3'UTR shortening on miRNA targeting. Number of miRNA target sites that are removed (882) or not removed (972) by 3'UTR shortening is indicated in the upper bar, and number of genes that contain removed (117) or not removed (47) miRNA target sites by 3'UTR shortening are indicated in lower bar. (h) An example gene *Notch1*, which displayed 3'UTR shortening after LTP. USCS genome browser tracks of 3'READS data are shown. Gene structure and 3'UTR sequence are indicated on top. Peaks from two polyA sites indicate reads for corresponding APA isoforms. miR-384-5p target site is indicated. Reads are based on combined samples. (i) Relationship between aUTR size and 3'UTR-APA regulation at 1 hr or 3 hr post LTP induction. Relative expression difference (RED) was calculated for all genes with APA sites. The formula of RED is indicated above the graph. Genes were divided into five groups (aUTR bins, listed on the right) based on aUTR size, with approximately equal number of genes in each bin. For each bin, mean RED was calculated. Error bars are standard error of mean (SEM). P-value (Wilcoxon rank sum test) indicates the difference between bin 1 and bin 5. (j) RT-qPCR validation of *Notch1* APA regulation. Two different primer sets were used to detect the expression of a common coding region (right bar) and a region in the alternative 3'UTR (left bar). Error bars are SEM of 4 replicates.

3'UTR regulation and changes in transcript abundance

Gene ontology analysis of genes with 3'UTR shortening indicated that genes with diverse functions are affected by this mechanism (Table S3). We next asked whether there was any correlation between LTP-induced 3'UTR changes and LTP-induced changes in transcript abundance. To obtain high-resolution gene expression data, we performed RNA-seq from a separate set of acute mouse hippocampal mini-slices 1 hr or 3 hr after LTP induction, with time-matched controls from the same animals. To prevent 3'UTR changes from influencing gene expression analysis, we used only RNA-seq reads mapping to the coding region of genes (see Materials and Methods for details). We identified 79 and 1,029 genes that were significantly differentially expressed at 1 hr and 3 hr time points (fold change > 1.2, FDR < 0.1, DEseq) (Fig. 3a and 3b). At both time points, upregulated genes outnumbered downregulated ones (77 vs. 2 at 1 hr; 907 vs. 122 at 3 hr, Fig. 3c), indicating that LTP primarily elicits activation of gene expression (Chen et al., 2017b). Notably, most genes regulated at 1 hr were also regulated at 3 hr (Fig. 3d), indicating continuous activation of expression. The top differentially expressed (DE) genes we identified are consistent with previous studies (Hermey et al., 2013; Leach et al., 2012; Majdan and Shatz, 2006), including upregulation of Gadd45g, Egr2, c-Fos, Arc and Npas4 (Table 1). Notably, gene expression changes based on RNA-seq were well correlated with those based on 3'READS ($r = 0.81$ and $r = 0.78$ for significantly regulated genes at 1 hr and 3 hr, respectively, Figure S2), attesting to the quality of our sequencing data.

GO analysis of DE genes after LTP induction revealed several common terms at 1 hr and 3 hr, including those related to signaling (“signal transduction” and “single organism signaling”), metabolic process (“positive regulation of metabolic process” and “negative regulation of macromolecule metabolic process”, “nucleic acid metabolic process”), and nucleus (“nucleus”, Table 2). Additionally, DE genes at 1 hr were enriched in “tissue development” and “transcription factor complex” (Table 2). At 3 hr, DE genes were also enriched in “neuron projection development” and “excitatory synapse” (Table 2). Thus, GO terms do not appear to overlap with those associated with genes showing 3’UTR shortening (Table S3). In addition, Ingenuity Pathway Analysis (IPA) identified a set of transcription factors (TFs) that are predicted to regulate genes with expression changes post LTP (Fig. 3e), including CREM, CREB1, and HDAC4, which is consistent with the notion that CREB proteins plays key roles in memory and synaptic plasticity, and facilitates the late phase of LTP (Barco et al., 2002; Benito and Barco, 2010; Silva et al., 1998). By contrast, no significant TFs were predicted to be associated with genes showing 3’UTR shortening (data not shown). Taken together, both GO and IPA analysis results indicate that transcriptional regulation and APA may target different sets of genes.

To specially address the interplay between 3’UTR-APA change and gene expression regulation, we analyzed the mRNA expression fold change of genes with significantly shortened and lengthened 3’UTR isoforms ($P < 0.05$, DEXSeq and relative abundance change of APA isoform >5%). There was no discernable correlation between gene expression change and 3’UTR-APA regulation at 1 hr post LTP (Fig. 3f). At 3 hr post LTP, while genes with lengthened 3’UTRs appeared to be modestly downregulated as compared to genes with shortened or unchanged 3’UTRs ($P = 0.03$ or $P= 0.08$, respectively, Wilcoxon test, Fig. 3g), there was no discernable difference between genes without 3’UTR APA changes and those with shortened 3’UTRs ($P = 0.12$, Wilcoxon test, Fig. 3g). Therefore, alteration of 3’UTR length is largely uncoupled from gene expression changes.

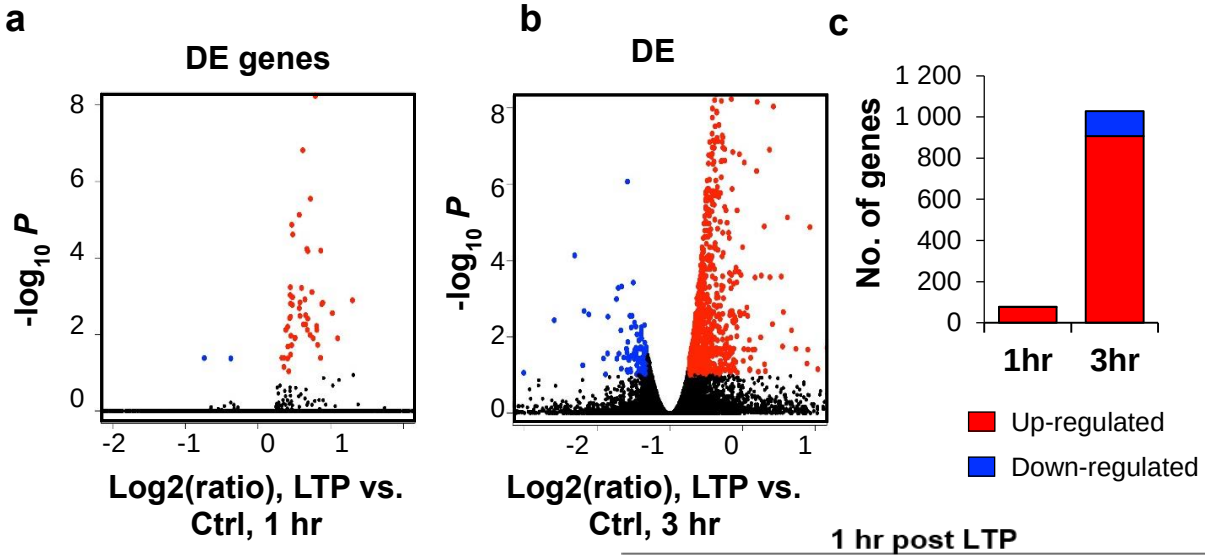

d

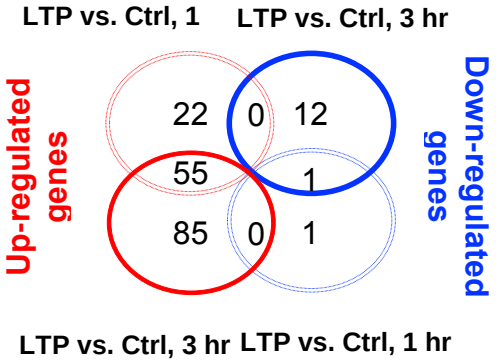

e

1 hr post LTP

Upstream Regulator	Molecule Type	Predicted Activation	p-value of overlap
CREM	TF	Activated	1.7E-35
CREB1	TF	Activated	1.3E-34
SRF	TF		6.6E-13

3 hr post LTP

Upstream Regulator	Molecule Type	Predicted Activation	p-value of overlap
CREB1	TF	Activated	1.4E-13
HDAC4	TF		2.9E-09
CREM	TF	Activated	3.1E-09

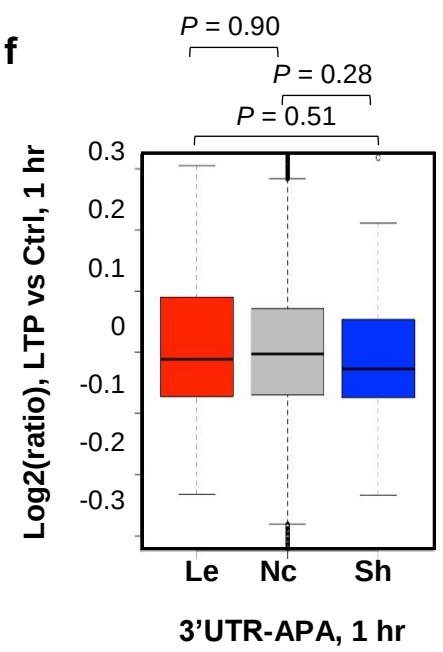

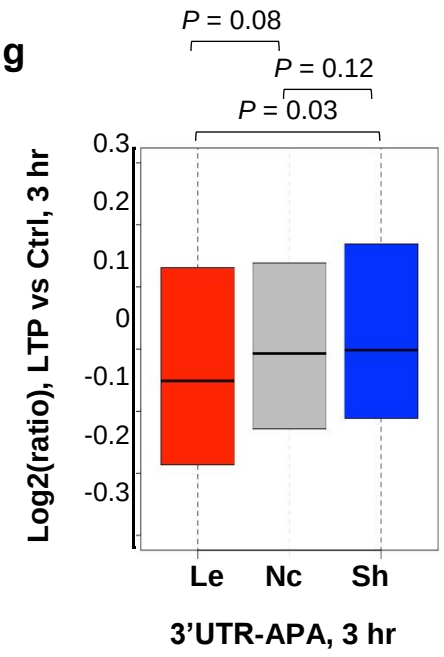

Figure 3. Regulation of gene expression after LTP induction. Differentially expressed (DE) genes 1 hr (a) or 3 hr (b) post LTP induction, as determined by RNA-seq. X-axis, log2(ratio) of gene expression (LTP vs Control); Y- axis, $-\log_{10}P$ (DESeq). DE genes were selected based on expression change >20% and FDR < 0.1. Genes with upregulated expression are highlighted in red and those with downregulated expression in blue. Grey dots are genes without significant regulation. (c) Bar graph summarizing DE genes shown in (a) and (b). (d) Venn diagram comparing DE genes at 1 hr LTP and 3 hr LTP. (e) IPA upstream regulator analysis for significantly regulated genes. This data is generated through the use of Ingenuity Pathways Analysis, a web-delivered application (www.Ingenuity.com). (f) and (g) Gene expression regulation vs. LTP-induced 3'UTR-APA regulation. Box plots showing the log2(ratio) of gene expression, LTP vs. Ctrl, for genes with 3'UTR lengthened (Le), shortened (Sh) or no change (Nc) at 1 hr (f) or 3 hr (g) post LTP induction. Only genes with significant 3'UTR APA regulation (those from Fig. 2) were included. P-values (Wilcoxon rank sum test) indicate difference between comparing gene groups.

Widespread activation of intronic APA during LTP

About 12% of APA sites identified in our samples were located in introns (Fig. 1e), which can impact coding sequence usage. We next tested the significance of the LTP-induced regulation of intronic APA usage. We combined all isoforms using PASs in RefSeq-supported introns and compared their expression with all transcripts using PASs in the 3'-most exon (Fig. 4a). We detected a modest difference at 1 hr between genes with activated intronic APA and genes with repressed intronic APA (33 vs. 28, Fig. 4b). However, at 3 hr post LTP, genes with activated intronic APA significantly outnumbered those with repressed intronic PAS by 2.8-fold (78 vs. 27, Fig. 4c). These data indicate that LTP induces not only a general shortening of 3'UTR but also triggers an overall transcript truncation through increased usage of intronic PASs. In addition, the genes with intronic APA regulation at 1 hr differed from those with intronic APA regulation at 3 hr (Fig. 4d).

We then asked whether intronic APA is related to gene expression level changes. At the 1 hr post LTP time-point, gene expression changes appeared to be unrelated to intronic APA regulation (Fig. 4e). By contrast, at 3 hr post LTP, genes with repressed intronic APA tended to be upregulated relative to genes without APA regulation or with activated intronic APA ($P = 0.04$ or 0.02, respectively, Wilcoxon rank sum test, Fig. 4f). However, genes with activated intronic APA, which accounted for most of the APA events, did not show significant difference in expression compared to genes without intronic APA changes ($P = 0.35$, Wilcoxon rank sum test). Therefore, intronic activation of APA is not coupled with activation of gene expression. GO analysis did not reveal any terms highly significantly enriched for genes with activated intronic APA (Table S4), indicating that intronic APA regulation, unlike transcriptional control, is not specific for genes with certain functions.

We next examined how intronic APA was related to 3'UTR-APA. Using the 3 hr post-LTP data, we identified 107 genes with both shortened 3'UTRs and activated intronic APA, a number greater than genes with shortened 3'UTRs and repressed intronic APA (48),

lengthened 3'UTRs and activated intronic APA (77) or lengthened 3'UTRs and repressed intronic APA (45) (Fig. 4g). This result indicates that, for a group of genes, 3'UTR shortening is coupled with activation of intronic APA. Presumably, for those genes, proximal PASs are generally preferred regardless of the location, in the 3'-most exon or in an intron.

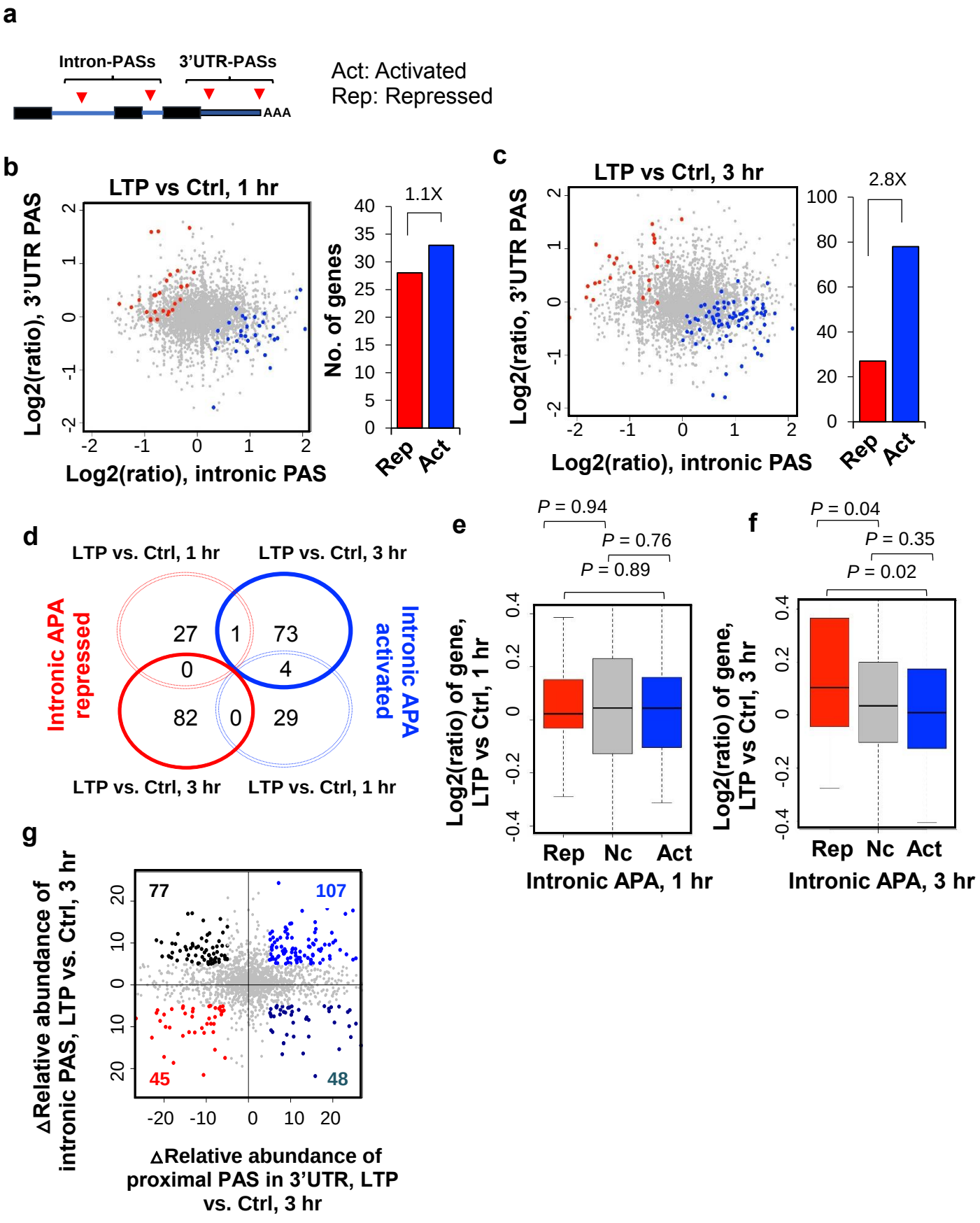
a
Intron-PASs
3'UTR-PASs
AAA
Act: Activated
Rep: Repressed
b
LTP vs Ctrl, 1 hr
Log2(ratio), 3'UTR PAS
Log2(ratio), intronic PAS
No. of genes
1.1X
Rep
Act
c
LTP vs Ctrl, 3 hr
Log2(ratio, 3'UTR PAS
Log2(ratio), intronic PAS
2.8X
Rep
Act
d
LTP vs. Ctrl, 1 hr
LTP vs. Ctrl, 3 hr
Intronic APA repressed
Intronic APA activated
27
1
73
0
4
82
0
29
LTP vs. Ctrl, 3 hr
LTP vs. Ctrl, 1 hr
e
P = 0.94
P = 0.76
P = 0.89
Log2(ratio) of gene, LTP vs Ctrl, 1 hr
Rep
Nc
Act
Intronic APA, 1 hr
f
P = 0.04
P = 0.35
P = 0.02
Log2(ratio) of gene, LTP vs Ctrl, 3 hr
Rep
Nc
Act
Intronic APA, 3 hr
g
ΔRelative abundance of intronic PAS, LTP vs. Ctrl, 3 hr
77
107
45
48
ΔRelative abundance of proximal PAS in 3'UTR, LTP vs. Ctrl, 3 hr

Figure 4. Regulation of intronic APA after LTP induction. (a) Schematic of intronic APA analysis. Intronic PASs were compared with 3'UTR-PASs. (b) and (c) Left, scatterplot comparing expression change (LTP vs. control) of intronic PASs (x-axis) and 3'UTR PASs (y-axis). Genes with significantly activated intronic PAS usage are shown in blue (Act) and those with significantly repressed intronic PAS usage in red (Rep) ($p < 0.05$, DEXSeq and relative abundance change > 5%). Grey dots represent genes without significant regulation (Nc). Right, bar graph showing the number of genes with activated or repressed intronic APA. (d) Venn diagram comparing genes with CDS-APA regulation at 1 hr post LTP and 3 hr post LTP. Genes correspond to those in (b) and (c). (e) and (f), Box plot showing the $\log_2$ratio (LTP/Ctrl) of genes with intronic PAS activation or intronic PAS repression, 1 hr (e) or 3 hr (f) post LTP induction. Genes with significant intronic APA regulation are those from (a) or (b). P-values (Wilcoxon rank sum test) indicate the difference between comparing groups. (g) Scatterplot comparing 3'UTR APA regulation (x-axis) and intronic APA regulation (y-axis) at 3 hr post LTP induction. Δ relative abundance for 3'UTR APA is based on the two 3'UTR PASs with most reads, as in Fig. 2, and Δ relative abundance for intronic APA is based on all intronic PAS reads vs. all 3'UTR PAS reads. Genes with intronic APA and/or 3'UTR APA change (>5% relative abundance) are highlighted with different colors based on the type of change.

Previous studies have shown that intronic APA events regulated by certain factors, such as U1 snRNP (U1) (Berg et al., 2012) and RNA polymerase II associated factor (PAF) complex (Yang et al., 2016), display a 5' to 3' polarity, i.e., more regulation at the 5' end than the 3' end. By dividing intronic PAS isoforms into 5 groups based on the intron locations of their PASs, i.e., first intron (+1), second (+2), last (-1), second to last (-2), and middle (between +2 and -2 introns), we found that PASs located in the 5'-most intron (+1) indeed had the highest increase in usage as compared to those in the 3'-most intron 3 hr post LTP ($P = 0.008$, Wilcoxon rank sum test). By contrast, no such trend was discernable with the 1 hr APA events (Fig. 5a). This result suggests that a regulatory mechanism similar to U1 and PAF complex, which specifically impacts 5' intronic PASs, takes place 3 hr post LTP (see Discussion).

To further explore the consequences of intronic APA activation following LTP induction, we examined protein domains that could be removed or truncated through shortening of coding regions. Of the 147 genes that showed significant intronic PAS activation and contained Pfam-annotated domains, 109 could lose their protein domains (258 domains in total) as a result of intronic APA activation (Fig. 5b). One of the most significantly regulated genes by intronic APA was *Creb1*, whose intronic PAS increased both 1 hr and 3 hr post LTP inductions (Fig. 5c). The regulated intronic PAS is located at the 5' end of the first intron (Fig. 5c), usage of which could remove much of the protein sequence of *Creb1*, including two key domains—the phosphorylated kinase-inducible-domain (pKID) and basic leucine zipper domain (bZIP) (Fig. 5c). Since *Creb1* plays a central role in transcriptional activation of many genes during LTP, as previously shown (Alberini, 2009; Lonze and Ginty, 2002) and predicted by our IPA analysis in this study (Fig. 3e), we hypothesized that activation of its intronic APA may function to inhibit *Creb1* expression, blunting its role in

transcriptional activation. Indeed, using the RNA-seq data, we found that while *Creb1* mRNA appeared unchanged 1 hr post LTP, it was slightly downregulated 3 hr post LTP (Fig. 5d). Importantly, downregulation of *Creb1* mRNA mainly occurred to exons downstream of the intronic PAS but not to the first exon (Fig. 5e), suggesting that downregulation of *Creb1* mRNA level occurred through the usage of intronic PAS. Consistent with repressed *Creb1* expression, upregulation of *Creb1* target genes was decreased 3 hr post LTP as compared to 1 hr post LTP ($P = 1.6x10^{-5}$, Fig. 5f). Notably, the intronic PAS of *Creb1* is conserved in human and rat based on PolyA_DB {Wang R, 2018 #3001}, highlighting its functional importance. Taken together, intronic APA of *Creb1* may play an important role in downregulation of its gene expression, controlling the extent and/or timing of the Creb1-mediated gene expression program.

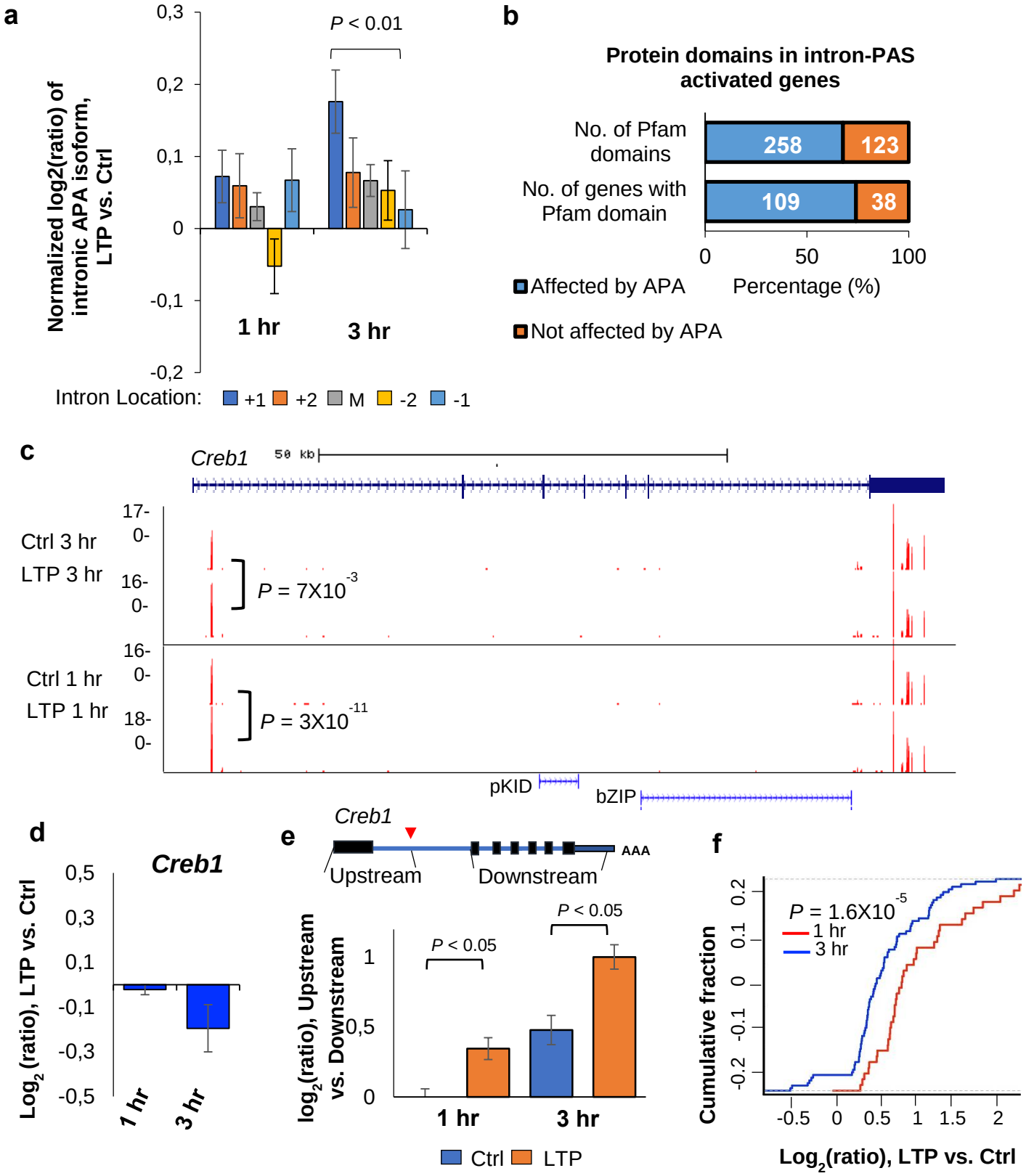
a
Normalized log2(ratio) of intronic APA isoform, LTP vs. Ctrl
P < 0.01
1 hr
3 hr
Intron Location: +1 +2 M -2 -1
b
Protein domains in intron-PAS activated genes
No. of Pfam domains
No. of genes with Pfam domain
258
123
109
38
Affected by APA
Not affected by APA
Percentage (%)
c
Creb1
50 kb
Ctrl 3 hr
LTP 3 hr
P = 7X10-3
Ctrl 1 hr
LTP 1 hr
P = 3X10-11
pKID
bZIP
d
Creb1
Log2 (ratio), LTP vs. Ctrl
1 hr
3 hr
e
Creb1
AAA
Upstream
Downstream
log2(ratio), Upstream vs. Downstream
P < 0.05
P < 0.05
1 hr
3 hr
Ctrl
LTP
f
Cumulative fraction
P = 1.6X10-5
1 hr
3 hr
Log2(ratio), LTP vs. Ctrl

Figure 5. Characteristics of intronic APA after LTP induction. (a) Normalized expression changes of intronic PAS isoforms. Intronic PAS isoforms were divided into five groups based on the intron location where PAS resides, i.e., first (+1), second (+2), last (-1), second to last (-2), and middle (between +2 and -2 introns). Expression changes are expressed as log2(ratio), LTP vs. Ctrl. Only genes with ≥4 introns and only PAS isoforms with ≥2 reads were used for analysis. Values for five intron groups were normalized by mean-centering. Error bars are standard error of mean. P-value (Wilcoxon rank sum test) indicating difference between first and last intron values is shown. (b) Protein domains that can potentially be removed or truncated by intronic PAS activation. Number of pfam domains that can be removed or not removed by intronic APA is indicated in the upper bar, and number of genes that contain domains removed or not removed by intronic PAS activation is indicated in the lower bar. (c) An example gene *Creb1*, which displayed significant intronic PAS activation. Gene structure is shown on top and peaks for PASs are shown in USCS genome browser tracks. P-values based on comparison of intronic PAS and 3'UTR PAS (DEXSeq) are indicated. Pfam domains are indicated. Reads are acquired by combined samples. (d) Gene expression change of *Creb1* after LTP. (e) Expression changes based on RNA-seq reads mapped to different regions of *Creb1*. Schematic of *Creb1* is shown on the top, and log2(ratio) from indicated region is shown in a bar plot. Two regions were analyzed, including the region from transcription start site to the intronic PAS, and the region from the second to the last exons. (f) $Log_{2(}$ratio), Gene expression changes (LTP vs. Ctrl) of CREB1 target genes obtained from the IPA database. The blue curve corresponds to 81 target genes in the 3 hr post LTP samples, whereas the red corresponds to 37 target genes in the 1 hr post LTP samples.

2.1.4. DISCUSSION

Regulation of transcription and protein synthesis is critical during L-LTP (Chang et al., 2006; Gu et al., 2015; Håvik et al., 2007; Maag et al., 2015; McNair et al., 2006; Ryan et al., 2012), and post-transcriptional gene regulation is key to the development and function of neural circuits (Buxbaum et al., 2015; Holt and Schuman, 2013; Raj and Blencowe, 2015). mRNA isoform changes through APA represent a widespread, although poorly understood, mechanism in eukaryotes. APA may play a special regulatory role in the neural system, because neuronal transcripts generally have long 3'UTRs (Miura et al., 2013; Zhang et al., 2005b) and sequence motifs in 3'UTRs contribute to both spatial and temporal control of gene expression during neuronal plasticity (Martin and Ephrussi, 2009). Inspired by studies indicating activity-dependent regulation of APA in neurons (Berg et al., 2012; Flavell et al., 2008), we undertook a genome-wide approach to systematically examine activity-dependent APA regulation following LTP induction in mouse hippocampal slices. With a specialized 3' end-based sequencing method, 3'READS, we uncovered a global trend of 3'UTR shortening and activation of intronic APA 3 hr post LTP, a time point that also involves substantial transcriptional changes. By contrast, the global APA regulation was not discernable 1hr post LTP, when only a small number of genes have expression changes. Thus, it is possible that regulation of PAS usage, a co-transcriptional process, is globally coupled with transcriptional regulation. On the other hand, for individual genes, we did not observe coupling between 3'UTR shortening or activation of intronic PASs with regulation of gene expression.

Comparison with previous studies. The APA regulation following LTP induction detected in our study is consistent with a previous microarray study done in cultured rat hippocampal neurons that reported significant transcript truncation following KCl depolarization (Flavell et al., 2008). Of note, our stimulation protocol induced Hebbian synaptic plasticity (Chotiner et al., 2003), while the 1 hr or 6 hr of continuous KCl depolarization in cultured neurons likely produced homeostatic plasticity (O'Leary et al., 2010). Despite this difference, 10 of the 29 genes undergoing APA regulation (34.5%, 30 predicted-only genes from Flavell et al., 2008 were excluded) following KCl depolarization also underwent APA regulation after LTP induction in hippocampal slices, suggesting a common mechanism of APA regulation during homeostatic and Hebbian plasticity. Our high-resolution genome-wide approach provides additional insights into APA regulation during plasticity by expanding the catalog of genes with activity-dependent APA changes from a total of 59 in Flavell et al. (2008) to over 1,100 genes (Fig. 1f). Our study further provides a comprehensive characterization of the two different types of APA regulation, 3'UTR APA and intronic APA, which could not be dissected using microarrays or traditional RNA-seq. Notably, we also performed the same experiments using PAS-Seq, another 3' end-based sequencing method (Shepard et al., 2011). However, due to high variance of read counts across samples and within genes, we could not identify significantly regulated APA isoforms following LTP induction (data not shown), attesting to the technical advantage of using 3'READS in analysis of APA.

Potential mechanisms. The molecular mechanism(s) underlying activity-dependent APA regulation during LTP remain largely unclear. Global shortening of 3'UTRs and activation of intronic APA sites have been observed in proliferating cells compared to quiescent ones (Sandberg et al., 2008). Cancer cells, undifferentiated cells and cells at early developmental stages display similar patterns (Ji et al., 2009; Mayr and Bartel, 2009; Shepard et al., 2011). The mechanisms underlying proliferation-based APA are largely unknown, although higher expression levels of C/P factors and thus increased general C/P activity have been suggested to be responsible for more efficient 3' end processing at proximal PASs (Ji et al., 2009; Ji and Tian, 2009). While we did not observe increased expression of C/P factors at the RNA level post LTP (Fig. S3a), the C/P factor gene *Wdr33*, did appear to be regulated by APA (Fig. S3b), raising the possibility that regulation of certain C/P factors may lead to the global APA changes observed in this study. In addition, we cannot rule out the possibility that some of the C/P factors might be regulated post-translationally and have altered activities post LTP.

The Dreyfuss lab reported that a shortage of U1 snRNP (U1) relative to the pre-mRNA abundance caused subdued inhibition of cleavage/polyadenylation by U1(Berg et al., 2012) and, consequently, activation of proximal PASs in introns and 3'UTRs. Indeed, using our previous 3'READS data from mouse C2C12 myoblast cells (Li et al., 2015), we found that the expression of intronic APA isoform of *Creb1* increased by 3.7-fold when U1 was functionally inhibited by an antisense oligo to U1 snRNA (Fig. S5a). Global activation of proximal PASs in 3'UTRs and introns has also been reported in cells with reduced expression of the PAF complex (Yang et al., 2016), which plays a role in promoter-proximal pausing and transcriptional elongation(Chen et al., 2017a),(Fischl et al., 2017). We also re-analyzed our previous data of knockdown of Paf1, one of the subunits of PAF complex, in C2C12 cells. Interestingly, intronic APA of *Creb1* increased by 7.8-fold when Paf1 was knocked down (Fig. S5b). Although we did not detect a global correlation in intronic APA regulation between U1 inhibition or Paf1 knockdown and LTP activation, there were modest correlations between these conditions for PAS regulation in the first intron (r = 0.21 and 0.31 for Paf1 knockdown vs. LTP and for U1 inhibition vs. LTP, respectively, Pearson correlation, Fig. S5d and Fig. S5e). This result suggests that PASs in the first intron, as in the case of *Creb1*, might be regulated by U1 and/or PAF mechanisms in cells activated for LTP. Future studies need to determine mechanistic details concerning these potential connections.

Intriguingly, we also found from our previous data that knockdown of PABPN1 in C2C12 cells substantially upregulated the expression of the intronic APA isoform of *Creb1* by 16-fold in C2C12 cells[15]. Because of PABPN1's role in nuclear RNA surveillance [15],(Bresson and Conrad, 2013), it is possible that the intronic PAS isoform of *Creb1* is rapidly degraded after usage. This further supports the model that intronic polyadenylation of *Creb1* serves to inhibit the expression of full-length isoform. Moreover, similar to U1 inhibition and Paf1 knockdown, regulation of PASs in the first introns of genes by LTP was modestly correlated with those by siPABN1 (r = 0.34, Pearson correlation, Fig. S5f), suggesting a general pattern similar to that of the intronic PAS of *Creb1*.

Functional implications. APA generates mRNA isoforms with different 3'UTR lengths and/or coding sequences. mRNA isoforms resulting from LTP induction may localize to distinct subcellular compartments, and produce different protein levels (Cohen et al., 2014; Mayr, 2016; Miura et al., 2014). The functional consequences of 3'UTR-APA events emerge from differences in cis-regulatory elements contained within the alternative 3'UTRs, including motifs recognized by miRNAs and RBPs. Shorter 3'UTR isoforms can escape miRNA-mediated destabilization and translation repression through the loss of miRNA binding sites, a strategy that is used to achieve both cell type specificity and correct developmental timing (Boutet et al., 2012; Han et al., 2013; Nam et al., 2014). Indeed, we found that genes with

lengthened 3'UTRs tended to be downregulated, implying a role for 3'UTR in gene regulation during hippocampal plasticity. A case in point is the *Notch1* gene, which plays important roles in LTP and whose 3'UTR shortening removes a target site of miR-384-5-p, an important miRNA for LTP maintenance (Alberi et al., 2011; Brai et al., 2015; Gu et al., 2015) . Future studies are needed to examine the detailed mechanisms and consequences behind APA of *Notch1* and explore other similar cases.

Intronic APA events can impact protein functions by generating alternative C-termini. For example, intronic APA was previously shown to affect the molecular functions of *Homer1*, a gene that undergoes differential APA 3 hr post LTP induction. Our data is consistent with this finding (Fig. S5). The shorter *Homer1* CDS isoform that is inducible by neuronal activity acts in dominant negative fashion to inhibit the function of the full-length *Homer1* isoform (Sala et al., 2003) by preventing dimerization. Here we revealed significant regulation of intronic APA in *Creb1*, which plays a key role in LTP (Frank and Greenberg, 1994). Activation of intronic PAS of *Creb1* leads to a significantly truncated transcript that is likely to be rapidly degraded (see above). This mechanism may function to limit *Creb1*'s function in gene activation during LTP. Notably, activation of PAS in the first intron, as in the case of *Creb1*, is a widespread phenomenon during LTP. Further proteomic studies will provide insights into whether there is a surge of short peptides during LTP induction as a result of intronic APA activation, and, if so, whether they play functional roles in learning and memory.

2.1.5. METHODS

Preparation of hippocampal acute slices. Hippocampal slices were prepared from isoflurane-anesthetized 2-3 month old male C57BL/6 mice (Charles River, Wilmington, MA, USA). Hippocampi were quickly isolated on ice, and 400-micron thick transverse slices were cut using a manual tissue chopper. The dentate gyrus was trimmed with a single incision, and the slices were placed in interface chambers at 30^{o}C to recover for 2 hr with continuous ACSF perfusion. From a single animal we collected ~10 hippocampal slices. Half of the mini-slices were used for cLTP induction and the remaining treated with a DMSO vehicle solution as time-matched controls. cLTP was induced by perfusing ACSF containing 50 uM forskolin for 5 min followed by 5 min of 50 uM forskolin, 30 mM KCl and 10 mM Ca2+ ACSF. Control slices were treated in parallel with ACSF containing 0.2% DMSO for 10 min. Slices were collected 1 hr or 3 hr post stimulation by freezing in dry ice. Use of mice in this study followed the recommendations of and protocol approved by the UCLA Institutional Animal Care and Use Committee. To validate successful LTP induction, we monitored expression of candidate transcripts by qPCR, and prepared sequencing libraries from samples that exhibited LTP-

induced upregulation of *Arc* mRNA and increases in *Homer1* short isoform and unaltered concentrations of *Homer1* long isoform and *Hprt*. We obtained triplicates for all controls and cLTP samples for 3'READS+, RNA-seq and PAS-seq experiments.

RNA extraction and RT-qPCR. To extract RNA, frozen slices were homogenized using a pestle in Trizol for 5 min. 200 uL of chloroform per 1mL of TRIZOL were added to the homogenate and after centrifugation the top aqueous phase was collected. To precipitate and elute total RNA containing both mRNA and small RNAs we then used the Qiagen microRNeasy kit. We obtained ~2.5 ug of total RNA from 5 hippocampal slices. For RT-qPCRs we used 200 ng of total RNA and performed reverse transcription with random hexamers and SuperScript III in a total volume of 20 uL. The cDNA was then quantified by qPCR using SYBR green (primer sequences available upon request). The mRNA levels of *Hprt* were used as internal controls since its expression is activity-independent (Santos and Duarte, 2008).

RNA-seq and Differential Expression Analysis. Three biological replicates of each condition (control and LTP-induced) at two different time-points (1 hr and 3 hr) after LTP were collected. For each replicate, hippocampal slices from the same animal were used to generate both LTP-induced samples and matched controls. The minimum RIN of all samples was 7.5, as determined by the 4200 Tapestation Instrument (Agilent). All RNA-seq libraries were prepared using the TruSeq Stranded Total RNA sample prep kit with Ribo-Zero according to manufacturer's specified protocol (Illumina). Samples were multiplexed and sequenced across multiple HiSeq 2500 high-output lanes using 100 bp paired-end reads to achieve a minimum depth of ~75 M reads per sample. Transcriptome alignment was performed using STAR v. 2.4.1c (Dobin et al., 2013) with default settings, and GRCm38/mm10 (Data statistics, Table S2). Raw counts were quantified using R GenomicFeatures and GenomicAlignments and RSamtools packages (Lawrence et al., 2013). Differential expression analysis was performed for each time-point separately in DESeq (Anders and Huber, 2010). We excluded outlier samples, as determined by sample clustering (Fig. S1b). We applied an FDR cutoff of <0.1 and fold change >1.2 as the threshold for significance. GO analysis was carried out based on Fisher's exact test.

3'READS+ and analysis. The 3' region extraction and deep sequencing (3'READS+) method was previously described in (Zheng et al., 2016). Briefly, 1 µg of input RNA was used for each sample, and poly(A)+ RNA was selected using oligo d(T)25 magnetic beads (NEB), followed by on-bead fragmentation using RNase III (NEB). Poly(A)+ RNA fragments were then selected using a chimeric oligo containing 15 regular dTs and five locked nucleic acid

dTs conjugated on streptavidin beads, followed by RNase H (NEB) digestion. Eluted RNA fragments were ligated with 5' and 3' adapters, followed by RT and PCR (15x) to obtain cDNA libraries for sequencing on the Illumina platform. Processing of 3'READS+ data was carried out as previously described (Hoque et al., 2013). Briefly, reads were mapped to the mouse genome using bowtie 2 (Langmead and Salzberg, 2012). Reads with ≥ 2 unaligned Ts at the 5' end were used to identify PASs. PASs located within 24 nt from each other were clustered together (Table S1).

APA analysis. Differential expression of APA isoforms are carried out with DEXSeq (Anders et al., 2012). Significant events were those with $p< 0.05$ and relative abundance difference >5%. Outlier samples were excluded as determined by sample clustering (Fig. S1a). Relative expression (RE) of two most abundant 3'UTR APA isoforms, e.g., proximal and distal PASs, was calculated by log2 (idstal PAS/proximal PAS). Relative Expression Difference (RED) of two isoforms in two samples was based on difference in RE between the two isoforms in the two samples. For intronic APA analysis, RE was based on comparison of all intronic APA isoforms combined (intronic PAS set) with all 3'UTR PAS isoforms combined (3'UTR PAS set), and RED was also based on the two sets. The weighted mean of 3'UTR size for each gene was based on 3'UTR sizes of all APA isoforms, weighted by the expression level of each isoform based on the number of PASS reads.

Analysis of introns. The intron location was based on the RefSeq database, considering all RefSeq-supported splicing isoforms. Introns were divided into five groups; first, second, last, second last and middle (contains all the introns between +2 and -2). Only genes with at least four introns were analyzed. Relative expression was calculated by intronic PAS read number divided by that of 3'UTR PASs of the same gene.

Data access. The sequencing data from this study has been submitted to the NCBI Gene Expression Omnibus under SuperSeries accession number GSE84644 (RNA-seq, GSE84503; 3'READS+, GSE84643). RNA-seq and 3' READS data can also be accessed through a web based expression browser at https://coppolalab.ucla.edu/gclabapps/3readsbrowser/home. Reviewerlink: https://www.ncbi.nlm.nih.gov/geo/query/acc.cgi?token=efmjesqabfetlef&acc=GSE84644

ACKNOWLEDGMENTS

We thank S. L. Zipursky for comments on the manuscript, members of BT and KCM labs for helpful discussions, and S. Deverasetty for development of the 3'READS+ and RNA-seq web browser. We thank Q. Wang for assistance with PAS-Seq library preparation and protocol optimization. This work was supported by NIH R01GM084089 (to BT), NIH R01NS045324 (to KCM), NIH R01MH060919 (to TJO), Graduate Program in Areas of Basic and Applied Biology and Fundação para a Ciência e a Tecnologia SFRH / BD / 51289 / 2010 (to MMF). We acknowledge the support of the NINDS Informatics Center for Neurogenetics and Neurogenomics (P30 NS062691).

COMPETING FINANCIAL INTERESTS

None.

AUTHOR CONTRIBUTIONS

MMF, BT, and KCM conceived of and designed the experiments. MMF, DZ, AH, VMH, and PBC performed the experiments. AG, RK, XL, GC, and BT analyzed the data. TJO contributed reagents and materials. MMF, AG, BT, and KCM wrote the paper.

TABLES

Table 1. Top 25 differentially expressed (DE) genes at 1 hr and 3 hr post LTP induction.

DE genes 1 hr post LTP			DE genes 3 hr post LTP		
Gene	**Log2(ratio)**	**FDR**	**Gene**	**Log2(ratio)**	**FDR**
Btg2	2.4	2.5E-99	*Rasl11a*	2.0	2.7E-86
Egr2	2.3	2.1E-80	*Fos*	1.5	2.4E-64
Fos	1.9	3.5E-70	*Tinf2*	1.6	1.1E-51
Nr4a1	1.6	8.8E-66	*Arc*	1.2	2.1E-42
Arc	1.8	1.3E-47	*Cyr61*	1.8	1.4E-41
Dusp6	1.0	3.9E-27	*Txndc11*	1.1	2.9E-32
Gadd45g	1.3	1.4E-26	*Sik1*	1.3	7.7E-32
Npas4	2.6	2.7E-22	*Thbs1*	1.8	2.3E-31
Dusp1	1.3	3.3E-19	*Gem*	1.1	4.9E-26
Trib1	1.3	2.2E-18	*Btg2*	1.2	3.7E-25
Ppp1r15a	1.0	1.0E-17	*Pax6*	1.1	1.3E-22
Errfi1	0.8	2.6E-17	*Gadd45g*	1.0	1.3E-21
Egr1	1.3	7.7E-16	*Il6*	1.2	8.1E-20
Nr4a2	0.9	1.0E-15	*Kmt2d*	0.8	2.0E-19
Arl4d	1.1	4.3E-15	*Trh*	2.1	3.4E-19
Sik1	1.0	3.9E-14	*Rtl1*	0.8	1.6E-17
Fosb	1.4	1.0E-13	*Ppp1r3g*	1.4	7.7E-16
Rgs4	0.7	1.8E-13	*Grin2b*	0.7	1.3E-15
Egr4	2.1	7.8E-13	*Rnf217*	0.9	6.2E-14
Ciart	0.9	3.4E-12	*Ccnl1*	0.7	7.1E-13
Cyr61	0.8	4.3E-10	*Nfkb1*	0.7	1.1E-12
Csrnp1	0.7	4.3E-10	*Nfil3*	0.8	1.1E-12
Thbs1	0.9	7.7E-10	*Sipa1l3*	0.9	2.2E-12
Junb	1.7	9.0E-10	*Nr4a2*	1.0	8.0E-12
Ptgs2	0.9	1.7E-09	*Iqsec2*	0.7	8.0E-12

Log_2(ratio) and FDR (DESeq). FDR was based on multiple testing adjustment using the Benjamini-Hochberg method.

Table 2. GO terms enriched for upregulated and downregulated genes 1 hr or 3 hr post LTP induction.

GO term	Category	$-\text{Log}_{10} P$
Enriched for DE genes, 1 hr post LTP		
positive regulation of metabolic process	BP	16.3
negative regulation of macromolecule metabolic process	BP	12.1
tissue development	BP	10.6
signal transduction	BP	8.8
nucleic acid metabolic process	BP	8.6
nucleus	CC	8.4
transcription factor complex	CC	4.0
protein phosphatase type 1 complex	CC	3.0
Enriched for DE genes, 3 hr post LTP		
neuron projection development	BP	7.5
single organism signaling	BP	7.3
regulation of nucleic acid-templated transcription	BP	5.9
negative regulation of macromolecule metabolic process	BP	5.5
positive regulation of metabolic process	BP	5.5
neuron part	CC	8.6
excitatory synapse	CC	4.6
nucleus	CC	3.9

BP, biological process; CC, cellular component. *P* is based on the Fisher's exact test.

2.1.6. SUPPLEMENTAL FIGURES

Figure S1

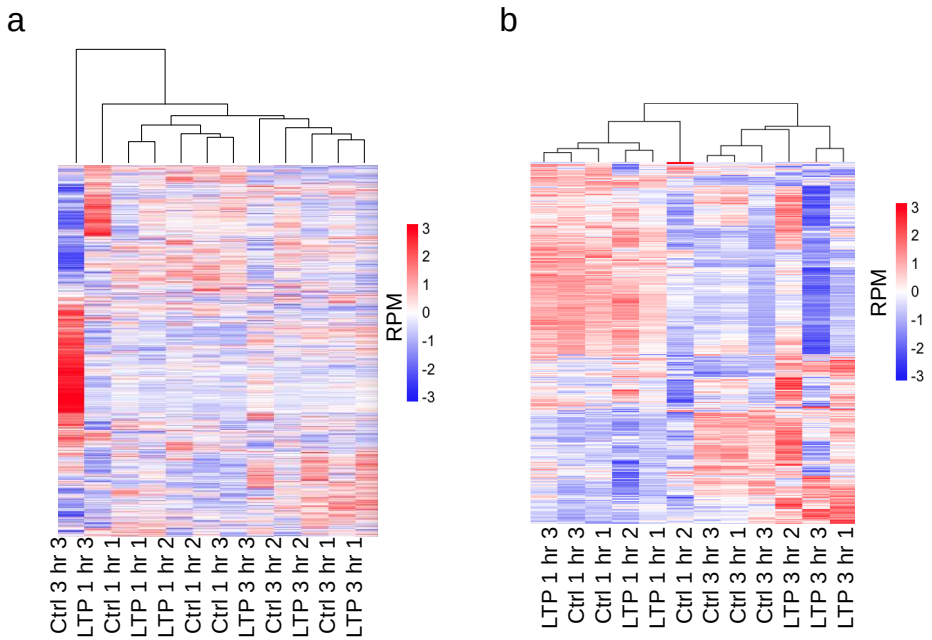

Figure S1. Clustering analysis of LTP and control samples. (a) RPM values (log2) of top 10,000 PASs were used. Control 3 hr sample #3 was identified as an outlier. (b) RPM values (log2) of top 2,000 genes were used. Control 1 hr sample #2 was identified as outliers.

Figure S2

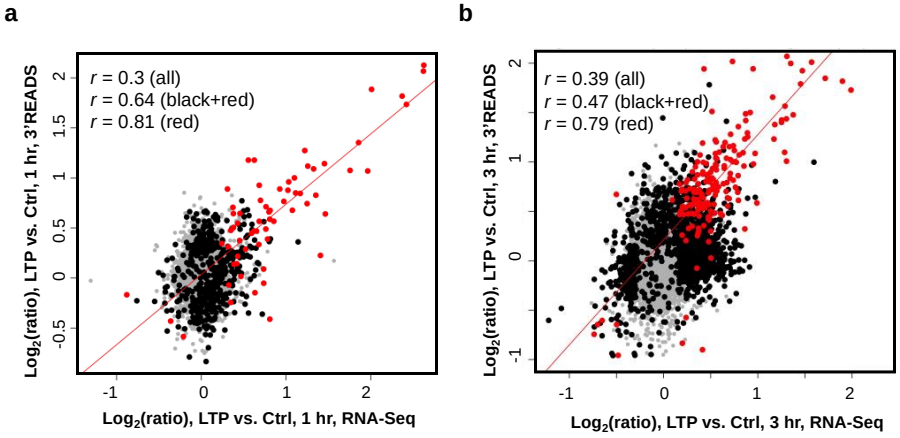

Figure S2. Correlation of gene expression between RNA-Seq and 3'READS in 1 hr (a) and 3 hr (b) samples. Number of genes analyzed is 9,746 or 9,998 for 1 hr or 3 hr sample, respectively. Each dot is a gene and red dots are genes that are commonly regulated in both datasets, black dots are genes that are significantly regulated in one of the datasets, and gray dots are genes not regulated in either dataset.

Figure S3

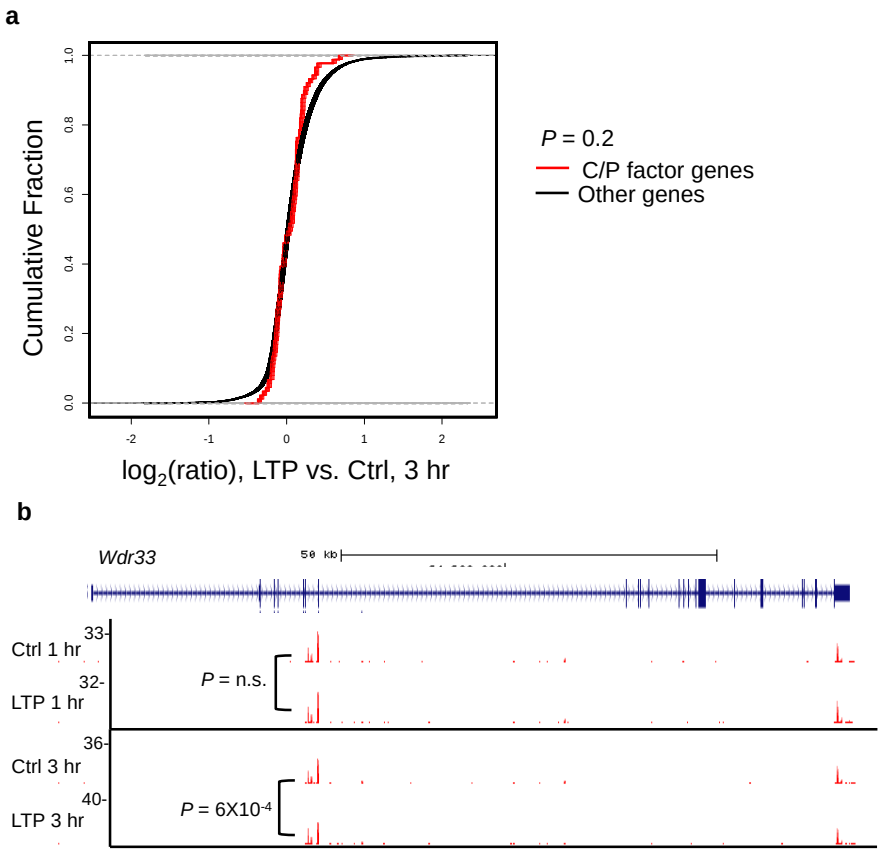

Figure S3. Regulation of C/P factors genes. (a) Log_2(ratio)(LTP vs. Ctrl) of C/P factor genes and other genes, red curve is 89 C/P factor genes in 3 hr post LTP sample and black curve is other genes in 3 hr post LTP. (b) Intronic APA regulation of *Wdr33*. *P*-values were based on DEXSeq, and read numbers are indicated. See Figure 2h for details about the figure format.

Figure S4

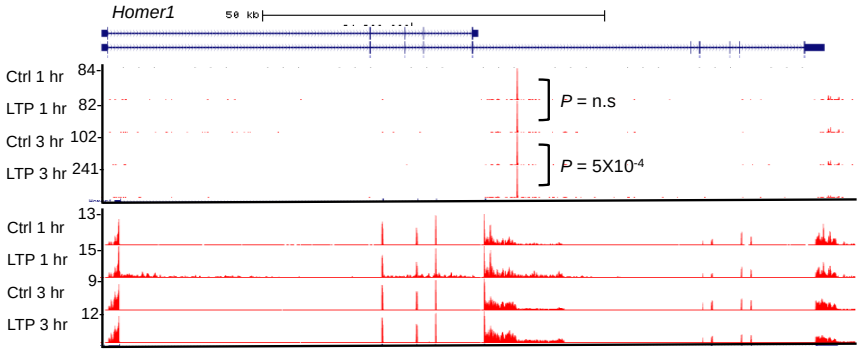

Figure S4. UCSC genome browser view of *Homer1*. *Homer1* is a gene with activated intronic PAS. Gene structure is on top and PAS peaks are shown in tracks. The top four tracks are 3'READS data and the bottom four are RNA-Seq data. *P-values* by DEXSeq are indicated for intronic PAS. Reads are based on combined samples.

Figure S5

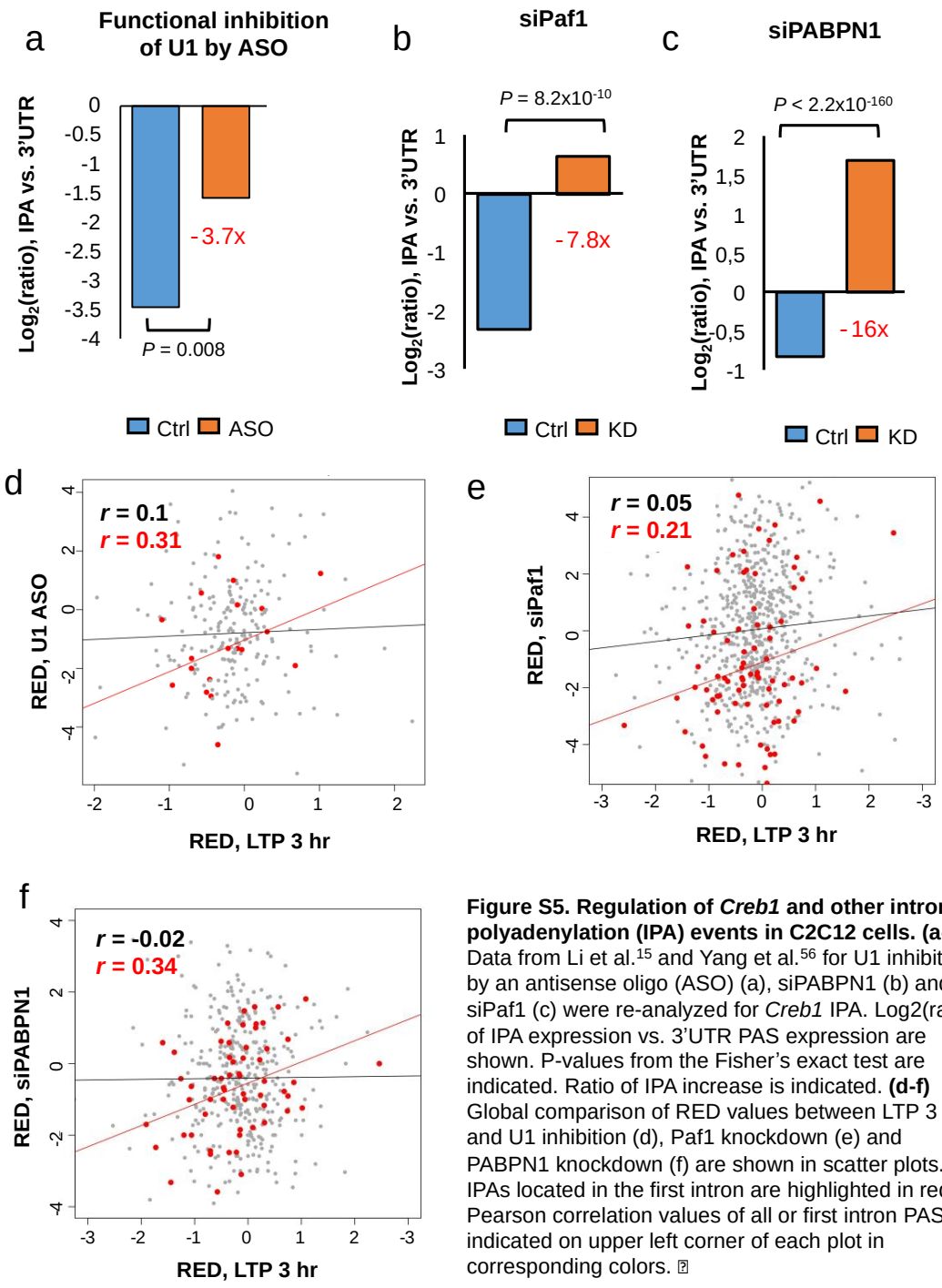

Figure S5. Regulation of *Creb1* and other intronic polyadenylation (IPA) events in C2C12 cells. (a-c) Data from Li et al.[15] and Yang et al.[56] for U1 inhibition by an antisense oligo (ASO) (a), siPABPN1 (b) and siPaf1 (c) were re-analyzed for *Creb1* IPA. Log2(ratio) of IPA expression vs. 3'UTR PAS expression are shown. P-values from the Fisher's exact test are indicated. Ratio of IPA increase is indicated. **(d-f)** Global comparison of RED values between LTP 3 hr and U1 inhibition (d), Paf1 knockdown (e) and PABPN1 knockdown (f) are shown in scatter plots. IPAs located in the first intron are highlighted in red. Pearson correlation values of all or first intron PAS are indicated on upper left corner of each plot in corresponding colors.

2.1.7. SUPPLEMENTAL TABLES

Table S1. Statistics of 3'READS data.

Treatment	Time	Replicate	Total Reads	Mapped Reads	PASS	PASS %	Genic Reads read #>2, relative abundance>= 5%	Genic # of PAS	# of mRNA Genes	# of lncRNA Genes
Ctrl	1 hr	1	34,848,574	27,725,785	16,160,999	58.29	13,296,101	26,172	13,825	312
Ctrl	1 hr	2	37,893,332	28,830,344	15,754,344	54.65	12,954,097	25,885	13,731	313
Ctrl	1 hr	3	35,724,383	27,301,906	14,910,311	54.61	12,127,640	25,585	13,660	316
Ctrl	3 hr	1	34,336,951	27,021,000	14,533,107	53.78	11,978,476	25,760	13,705	300
Ctrl	3 hr	2	30,955,479	24,040,417	13,025,963	54.18	10,777,384	24,984	13,481	294
Ctrl	3 hr	3	24,257,204	20,137,227	13,329,374	66.19	10,713,874	26,684	13,863	330
LTP	1 hr	1	34,415,120	26,444,088	15,056,295	56.94	12,431,953	26,083	13,737	304
LTP	1 hr	2	35,384,159	27,504,487	15,041,935	54.69	12,353,179	25,844	13,727	314
LTP	1 hr	3	33,241470	23,641,517	12,027,623	50.88	9,792,437	24,908	13,445	306
LTP	3 hr	1	35,690,878	28,110,280	15,491,954	55.11	12,627,502	26,508	13,886	299
LTP	3 hr	2	32,684,202	25,946,636	14,309,010	55.15	11,822,957	25,807	13,656	304
LTP	3 hr	3	34,750,310	27,646,273	16,144,649	58.40	13,103,896	26,916	13,886	308

Poly(A) site-supporting (PASS) reads are those containing at least 2 non-genomic As at the 3'end.

Table S2. Statistics of RNA-seq data.

Treatment	Time	Replicate	Total Reads	Uniquely mapped Reads	Mapped reads %
Ctrl	1 hr	1	74,798,155	62,727,464	83.8
Ctrl	1 hr	2	102,624,047	84,770,513	82.6
Ctrl	1 hr	3	79,008,105	66,650,143	84.3
Ctrl	3 hr	1	88,073,394	74,098,617	84.1
Ctrl	3 hr	2	90,060,999	75,888,083	84.2
Ctrl	3 hr	3	102,083,620	83,818,708	82.1
LTP	1 hr	1	83,145,392	69,797,724	83.9
LTP	1 hr	2	77,250,609	64,010,343	82.8
LTP	1 hr	3	81,487,345	68,440,528	83.9
LTP	3 hr	1	89,125,216	75,920,310	85.1
LTP	3 hr	2	86,950,262	72,304,399	83.1
LTP	3 hr	3	94,701,352	77,544,850	81.8

Table S3. GO terms enriched for genes with shortened or lengthened 3'UTRs 3 hr post LTP.

GO Term	Category	$-\log_{10} P$
Enriched for 3'UTR shortened Genes, 3 hr post LTP		
ossification	BP	5.4
negative regulation of photoreceptor cell differentiation	BP	4.7
regulation of gliogenesis	BP	4.4
positive regulation of smooth muscle cell proliferation	BP	4.4
hair follicle maturation	BP	4.3
nuclear lumen	CC	5.6
nuclear body	CC	3.3
Enriched for 3'UTR lengthened Genes, 3 hr post LTP		
negative regulation of lipid catabolic process	BP	2.4
cellular response to extracellular stimulus	BP	2.4
establishment of mitotic spindle localization	BP	2.3
response to activity	BP	2.3
energy homeostasis	BP	2.1
membrane-bounded organelle	CC	2.2
nuclear periphery	CC	2.0

BP, biological process; CC, cellular component. *P* is based on the Fisher's exact test.

Table S4. GO terms enriched for genes with activated or repressed intronic PAS 3 hr post LTP.

GO term	Category	$-\log_{10} P$
Enriched for genes with activated intronic PAS, 3 hr post LTP		
chaperone cofactor-dependent protein refolding	BP	3.6
neurotrophin signaling pathway	BP	3.2
lung saccule development	BP	3.0
cellular response to hepatocyte growth factor stimulus	BP	2.7
transcription initiation from RNA polymerase II promoter	BP	2.7
intracellular non-membrane-bounded organelle	CC	3.4
nucleoplasm	CC	2.8
Enriched for genes with repressed intronic PAS, 3 hr post LTP		
negative regulation of inflammatory response to antigenic stimulus	BP	3.6
ephrin receptor signaling pathway	BP	2.8
myeloid leukocyte differentiation	BP	2.7
cell-substrate junction assembly	BP	2.3
protein targeting	BP	2.1
signal recognition particle receptor complex	CC	2.5
laminin-3 complex	CC	2.3

BP, biological process; CC, cellular component. *P* is based on the Fisher's exact test.

2.1.8. REFERENCES

Alberi, L., Liu, S., Wang, Y., Badie, R., Smith-Hicks, C., Wu, J., et al. (2011). Activity-Induced Notch Signaling in Neurons Requires Arc/Arg3.1 and Is Essential for Synaptic Plasticity in Hippocampal Networks. *Neuron* 69, 437–444. doi:10.1016/j.neuron.2011.01.004.

Alberini, C. M. (2009). Transcription Factors in Long-Term Memory and Synaptic Plasticity. *Physiol. Rev*, 121–145. doi:10.1152/physrev.00017.2008.

Allen, N. J., and Eroglu, C. (2017). Cell Biology of Astrocyte-Synapse Interactions. *Neuron* 96, 697–708. doi:10.1016/j.neuron.2017.09.056.

An, J. J., Gharami, K., Liao, G.-Y., Woo, N. H., Lau, A. G., Vanevski, F., et al. (2008). Distinct Role of Long 3′ UTR BDNF mRNA in Spine Morphology and Synaptic Plasticity in Hippocampal Neurons. *Cell* 134, 175–187. doi:10.1016/j.cell.2008.05.045.

Anders, S., and Huber, W. (2010). Differential expression analysis for sequence count data. *Genome Biol.* 11, R106. doi:10.1186/gb-2010-11-10-r106.

Anders, S., Reyes, A., and Huber, W. (2012). Detecting differential usage of exons from RNA-seq data. *Genome Res.* 22, 2008–2017. doi:10.1101/gr.133744.111.

Ashraf, S. I., McLoon, A. L., Sclarsic, S. M., and Kunes, S. (2006). Synaptic protein synthesis associated with memory is regulated by the RISC pathway in Drosophila. *Cell* 124, 191–205. doi:10.1016/j.cell.2005.12.017.

Banerjee, S., Neveu, P., and Kosik, K. S. (2009). A Coordinated Local Translational Control Point at the Synapse Involving Relief from Silencing and MOV10 Degradation. *Neuron* 64, 871–884. doi:10.1016/j.neuron.2009.11.023.

Barco, A., Alarcon, J. M., and Kandel, E. R. (2002). Expression of constitutively active CREB protein facilitates the late phase of long-term potentiation by

enhancing synaptic capture. *Cell* 108, 689–703. doi:10.1016/S0092-8674(02)00657-8.

Bartel, D. P. (2009). MicroRNAs: Target Recognition and Regulatory Functions. *Cell* 136, 215–233. doi:10.1016/j.cell.2009.01.002.

Benito, E., and Barco, A. (2010). CREB's control of intrinsic and synaptic plasticity: implications for CREB-dependent memory models. *Trends Neurosci.* 33, 230–240. doi:10.1016/j.tins.2010.02.001.

Berg, M. G., Singh, L. N., Younis, I., Liu, Q., Pinto, A. M., Kaida, D., et al. (2012). U1 snRNP determines mRNA length and regulates isoform expression. *Cell* 150, 53–64. doi:10.1016/j.cell.2012.05.029.

Berlucchi, G., and Buchtel, H. A. (2009). Neuronal plasticity: Historical roots and evolution of meaning. *Exp. Brain Res.* 192, 307–319. doi:10.1007/s00221-008-1611-6.

Bhalla, K., Phillips, H., Crawford, J., McKenzie, O. D., Mulley, J., Eyre, H., et al. (2004). The de novo chromosome 16 translocations of two patients with abnormal phenotypes (mental retardation and epilepsy) disrupt the A2BP1 gene. *J. Hum. Genet.* 49. doi:10.1007/s10038-004-0145-4.

Bliss, T. V, and Collingridge, G. L. (1993). A synaptic model of memory: long-term potentiation in the hippocampus. *Nature* 361, 31–39. doi:10.1038/361031a0.

Boudreau, R. L., Jiang, P., Gilmore, B. L., Spengler, R. M., Tirabassi, R., Nelson, J. A., et al. (2014). Transcriptome-wide discovery of microRNA binding sites in Human Brain. *Neuron* 81, 294–305. doi:10.1016/j.neuron.2013.10.062.

Bourne, J. N., Sorra, K. E., Hurlburt, J., and Harris, K. M. (2007). Polyribosomes are increased in spines of CA1 dendrites 2 h after the induction of LTP in mature rat hippocampal slices. *Hippocampus* 17, 1–4. doi:10.1002/hipo.20238.

Boutet, S. C., Cheung, T. H., Quach, N. L., Liu, L., Prescott, S. L., Edalati, A., et al.

(2012). Alternative polyadenylation mediates microRNA regulation of muscle stem cell function. *Cell Stem Cell* 10, 327–336. doi:10.1016/j.stem.2012.01.017.

Brai, E., Marathe, S., Astori, S., Fredj, N. Ben, Perry, E., Lamy, C., et al. (2015). Notch1 Regulates Hippocampal Plasticity Through Interaction with the Reelin Pathway, Glutamatergic Transmission and CREB Signaling. *Front. Cell. Neurosci.* 9. doi:10.3389/fncel.2015.00447.

Bresson, S. M., and Conrad, N. K. (2013). The Human Nuclear Poly(A)-Binding Protein Promotes RNA Hyperadenylation and Decay. *PLoS Genet.* 9. doi:10.1371/journal.pgen.1003893.

Buxbaum, A. R., Yoon, Y. J., Singer, R. H., and Park, H. Y. (2015). Single-molecule insights into mRNA dynamics in neurons. *Trends Cell Biol.* 25, 468–475. doi:10.1016/j.tcb.2015.05.005.

Cajal, S. R. Y. (1894). The Croonian Lecture: La Fine Structure des Centres Nerveux. *Proc. R. Soc. London* 55, 444–468. doi:10.1098/rspl.1894.0063.

Cajigas, I. J., Tushev, G., Will, T. J., Tom Dieck, S., Fuerst, N., and Schuman, E. M. (2012). The Local Transcriptome in the Synaptic Neuropil Revealed by Deep Sequencing and High-Resolution Imaging. *Neuron* 74, 453–466. doi:10.1016/j.neuron.2012.02.036.

Chahrour, M., and Zoghbi, H. Y. (2007). The Story of Rett Syndrome: From Clinic to Neurobiology. *Neuron* 56, 422–437. doi:10.1016/j.neuron.2007.10.001.

Chang, S. P., Gong, R., Stuart, J., and Tang, S. J. (2006). Molecular network and chromosomal clustering of genes involved in synaptic plasticity in the hippocampus. *J. Biol. Chem.* 281, 30195–30211. doi:10.1074/jbc.M605876200.

Chen, F. X., Xie, P., Collings, C. K., Cao, K., Aoi, Y., Marshall, S. A., et al. (2017a). PAF1 regulation of promoter-proximal pause release via enhancer activation. *Science (80-.).*, eaan3269. doi:10.1126/science.aan3269.

Chen, P. B., Kawaguchi, R., Blum, C., Achiro, J. M., Coppola, G., O'Dell, T. J., et al. (2017b). Mapping Gene Expression in Excitatory Neurons during Hippocampal Late-Phase Long-Term Potentiation. *Front. Mol. Neurosci.* 10, 1–16. doi:10.3389/fnmol.2017.00039.

Chi, S. W., Zang, J. B., Mele, A., and Darnell, R. B. (2009). Argonaute HITS-CLIP decodes microRNA-mRNA interaction maps. *Nature* 460, 479–86. doi:10.1038/nature08170.

Chotiner, J. K., Khorasani, H., Nairn, A. C., O'Dell, T. J., and Watson, J. B. (2003). Adenylyl cyclase-dependent form of chemical long-term potentiation triggers translational regulation at the elongation step. *Neuroscience* 116, 743–752. doi:10.1016/S0306-4522(02)00797-2.

Cohen, J. E., Lee, P. R., and Fields, R. D. (2014). Systematic identification of 3'-UTR regulatory elements in activity-dependent mRNA stability in hippocampal neurons. *Philos. Trans. R. Soc. B Biol. Sci.* 369, 20130509–20130509. doi:10.1098/rstb.2013.0509.

Colgan, D. F., and Manley, J. L. (1997). Mechanism and regulation of mRNA polyadenylation. *Genes Dev.* 11, 2755–2766. doi:10.1101/gad.11.21.2755.

Davis, T. H., Cuellar, T. L., Koch, S. M., Barker, A. J., Harfe, B. D., McManus, M. T., et al. (2008). Conditional loss of Dicer disrupts cellular and tissue morphogenesis in the cortex and hippocampus. *J. Neurosci.* 28, 4322–4330. doi:10.1523/JNEUROSCI.4815-07.2008.

Derti, A., Garrett-Engele, P., MacIsaac, K. D., Stevens, R. C., Sriram, S., Chen, R., et al. (2012). A quantitative atlas of polyadenylation in five mammals. *Genome Res.* 22, 1173–1183. doi:10.1101/gr.132563.111.

Di Giammartino, D. C., Nishida, K., and Manley, J. L. (2011). Mechanisms and Consequences of Alternative Polyadenylation. *Mol. Cell* 43, 853–866.

doi:10.1016/j.molcel.2011.08.017.

Dobin, A., Davis, C. A., Schlesinger, F., Drenkow, J., Zaleski, C., Jha, S., et al. (2013). STAR: Ultrafast universal RNA-seq aligner. *Bioinformatics* 29, 15–21. doi:10.1093/bioinformatics/bts635.

Eacker, S. M., Keuss, M. J., Berezikov, E., Dawson, V. L., and Dawson, T. M. (2011). Neuronal activity regulates hippocampal miRNA expression. *PLoS One* 6. doi:10.1371/journal.pone.0025068.

Eberwine, J., Belt, B., Kacharmina, J. E., and Miyashiro, K. (2002). Analysis of subcellularly localized mRNAs using in situ hybridization, mRNA amplification, and expression profiling. *Neurochem. Res.* 27, 1065–1077. doi:10.1023/A:1020956805307.

Ehlers, M. D. (2003). Activity level controls postsynaptic composition and signaling via the ubiquitin-proteasome system. *Nat. Neurosci.* 6, 231–242. doi:10.1038/nn1013.

Elkon, R., Ugalde, A. P., and Agami, R. (2013). Alternative cleavage and polyadenylation: extent, regulation and function. *Nat. Rev. Genet.* 14, 496–506. doi:10.1038/nrg3482.

Fiore, R., Khudayberdiev, S., Christensen, M., Siegel, G., Flavell, S. W., Kim, T. K., et al. (2009). Mef2-mediated transcription of the miR379-410 cluster regulates activity-dependent dendritogenesis by fine-tuning Pumilio2 protein levels. *Embo J* 28, 697–710. doi:10.1038/emboj.2009.10.

Fischl, H., Howe, F. S., Furger, A., and Mellor, J. (2017). Paf1 Has Distinct Roles in Transcription Elongation and Differential Transcript Fate. *Mol. Cell* 65, 685–698.e8. doi:10.1016/j.molcel.2017.01.006.

Flavell, S. W., Kim, T., Gray, J. M., Harmin, D. A., Hemberg, M., Hong, E. J., et al. (2008). Genome-Wide Analysis of MEF2 Transcriptional Program Reveals

Synaptic Target Genes and Neuronal Activity-Dependent Polyadenylation Site Selection. *Neuron* 60, 1022–1038. doi:10.1016/j.neuron.2008.11.029.

Flexner, J. B., Flexner, L. B., and Stellar, E. (1963). Memory in Mice as Affected by Intracerebral Puromycin. *Science (80-.).* 141, 57–59. doi:10.1126/science.141.3575.57.

Frey, U., Krug, M., Reymann, K. G., and Matthies, H. (1988). Anisomycin, an inhibitor of protein synthesis, blocks late phases of LTP phenomena in the hippocampal CA1 region in vitro. *Brain Res.* 452, 57–65. doi:10.1016/0006-8993(88)90008-X.

Gao, F.-B., and Taylor, J. P. (2014). RNA metabolism in neurological disease. *Brain Res.* 1584, 1–2. doi:10.1016/j.brainres.2014.09.011.

Gehman, L. T., Stoilov, P., Maguire, J., Damianov, A., Lin, C. H., Shiue, L., et al. (2011). The splicing regulator Rbfox1 (A2BP1) controls neuronal excitation in the mammalian brain. in *Nature Genetics*, 706–711. doi:10.1038/ng.841.

Glock, C., Heumüller, M., and Schuman, E. M. (2017). mRNA transport & local translation in neurons. *Curr. Opin. Neurobiol.* 45, 169–177. doi:10.1016/j.conb.2017.05.005.

Gu, Q.-H., Yu, D., Hu, Z., Liu, X., Yang, Y., Luo, Y., et al. (2015). miR-26a and miR-384-5p are required for LTP maintenance and spine enlargement. *Nat. Commun.* 6, 6789. doi:10.1038/ncomms7789.

Han, K., Gennarino, V. A., Lee, Y., Pang, K., Hashimoto-Torii, K., Choufani, S., et al. (2013). Human-specific regulation of MeCP2 levels in fetal brains by microRNA miR-483-5p. *Genes Dev.* 27, 485–490. doi:10.1101/gad.207456.112.

Hansen, K. F., Sakamoto, K., Wayman, G. A., Impey, S., and Obrietan, K. (2010). Transgenic miR132 alters neuronal spine density and impairs novel object recognition memory. *PLoS One* 5. doi:10.1371/journal.pone.0015497.

Håvik, B., Røkke, H., Dagyte, G., Stavrum, A. K., Bramham, C. R., and Steen, V. M.

(2007). Synaptic activity-induced global gene expression patterns in the dentate gyrus of adult behaving rats: Induction of immunity-linked genes. *Neuroscience* 148, 925–936. doi:10.1016/j.neuroscience.2007.07.024.

He, M., Liu, Y., Wang, X., Zhang, M. Q., Hannon, G. J., and Huang, Z. J. (2012). Cell-type-based analysis of microRNA profiles in the mouse brain. *Neuron* 73, 35–48. doi:10.1016/j.neuron.2011.11.010.

Hebb, D. O. (1949). *The Organization of Behavior*.

Hebert, S. S., Papadopoulou, A. S., Smith, P., Galas, M. C., Planel, E., Silahtaroglu, A. N., et al. (2010). Genetic ablation of dicer in adult forebrain neurons results in abnormal tau hyperphosphorylation and neurodegeneration. *Hum. Mol. Genet.* 19, 3959–3969. doi:10.1093/hmg/ddq311.

Hermey, G., Mahlke, C., Gutzmann, J. J., Schreiber, J., Blüthgen, N., and Kuhl, D. (2013). Genome-Wide Profiling of the Activity-Dependent Hippocampal Transcriptome. *PLoS One* 8. doi:10.1371/journal.pone.0076903.

Hilgers, V., Perry, M. W., Hendrix, D., Stark, A., Levine, M., and Haley, B. (2011). Neural-specific elongation of 3' UTRs during Drosophila development. *Proc. Natl. Acad. Sci. U. S. A.* 108, 15864–9. doi:10.1073/pnas.1112672108.

Ho, V. M., Lee, J.-A., and Martin, K. C. (2011). The cell biology of synaptic plasticity. *Science* 334, 623–8. doi:10.1126/science.1209236.

Holt, C. E., and Schuman, E. M. (2013). The central dogma decentralized: New perspectives on RNA function and local translation in neurons. *Neuron* 80, 648–657. doi:10.1016/j.neuron.2013.10.036.

Holtmaat, A., and Svoboda, K. (2009). Experience-dependent structural synaptic plasticity in the mammalian brain. *Nat. Rev. Neurosci.* 10, 647–658. doi:10.1038/nrn2699.

Hoque, M., Ji, Z., Zheng, D., Luo, W., Li, W., You, B., et al. (2013). Analysis of

alternative cleavage and polyadenylation by 3' region extraction and deep sequencing. *Nat. Methods* 10, 133–9. doi:10.1038/nmeth.2288.

Hrvatin, S., Hochbaum, D. R., Nagy, M. A., Cicconet, M., Robertson, K., Cheadle, L., et al. (2018). Single-cell analysis of experience-dependent transcriptomic states in the mouse visual cortex. *Nat. Neurosci.* 21, 120–129. doi:10.1038/s41593-017-0029-5.

Huber, K. M., Kayser, M. S., and Bear, M. F. (2000). Role for rapid dendritic protein synthesis in hippocampal mGluR- dependent long-term depression. *Science (80-.).* 288, 1254–1256. doi:10.1126/science.288.5469.1254.

Huntzinger, E., and Izaurralde, E. (2011). Gene silencing by microRNAs: contributions of translational repression and mRNA decay. *Nat. Rev. Genet.* 12, 99–110. doi:10.1038/nrg2936.

James, W. (1890). *The principles of psychology (Vols. 1 & 2)*. doi:10.1037/10538-000.

Ji, Z., Lee, J. Y., Pan, Z., Jiang, B., and Tian, B. (2009). Progressive lengthening of 3' untranslated regions of mRNAs by alternative polyadenylation during mouse embryonic development. *Proc. Natl. Acad. Sci. U. S. A.* 106, 7028–33. doi:10.1073/pnas.0900028106.

Ji, Z., and Tian, B. (2009). Reprogramming of 3' untranslated regions of mRNAs by alternative polyadenylation in generation of pluripotent stem cells from different cell types. *PLoS One* 4, e8419. doi:10.1371/journal.pone.0008419.

Jin, Y., Suzuki, H., Maegawa, S., Endo, H., Sugano, S., Hashimoto, K., et al. (2003). A vertebrate RNA-binding protein Fox-1 regulates tissue-specific splicing via the pentanucleotide GCAUG. *EMBO J.* 22, 905–912. doi:10.1093/emboj/cdg089.

Job, C., and Eberwine, J. (2001). Localization and translation of mRNA in dendrites and axons. *Nat. Rev. Neurosci.* 2, 889–898. doi:10.1038/35104069.

Kandel, E. R. (2001). The Molecular Biology of Memory Storage: A Dialogue between Genes and Synapses. *Science (80-.).* 294, 1030–1038. doi:10.1126/science.1067020.

Kandel, E. R., Schwartz, J. H., and Jessell, T. M. (2013). *Principles of Neural Science*. doi:10.1036/0838577016.

Kang, H., and Schuman, E. M. (1996). A Requirement for Local Protein Synthesis in Neurotrophin-Induced Hippocampal Synaptic Plasticity. *Science (80-.).* 273, 1402–1406. doi:10.1126/science.273.5280.1402.

Kelleher, R. J., Govindarajan, A., Jung, H.-Y., Kang, H., and Tonegawa, S. (2004). Translational Control by MAPK Signaling in Long-Term Synaptic Plasticity and Memory. *Cell* 116, 467–479. doi:10.1016/S0092-8674(04)00115-1.

Kiebler, M. A., and Bassell, G. J. (2006). Neuronal RNA Granules: Movers and Makers. *Neuron* 51, 685–690. doi:10.1016/j.neuron.2006.08.021.

Konopka, W., Kiryk, A., Novak, M., Herwerth, M., Parkitna, J. R., Wawrzyniak, M., et al. (2010). MicroRNA loss enhances learning and memory in mice. *J. Neurosci.* 30, 14835–42. doi:10.1523/JNEUROSCI.3030-10.2010.

Kye, M.-J., Liu, T., Levy, S. F., Xu, N. L., Groves, B. B., Bonneau, R., et al. (2007). Somatodendritic microRNAs identified by laser capture and multiplex RT-PCR. *RNA* 13, 1224–1234. doi:10.1261/rna.480407.

Lagos-Quintana, M., Rauhut, R., Yalcin, A., Meyer, J., Lendeckel, W., and Tuschl, T. (2002). Identification of tissue-specific MicroRNAs from mouse. *Curr. Biol.* 12, 735–739. doi:10.1016/S0960-9822(02)00809-6.

Landgraf, P., Rusu, M., Sheridan, R., Sewer, A., Iovino, N., Aravin, A., et al. (2007). A Mammalian microRNA Expression Atlas Based on Small RNA Library Sequencing. *Cell* 129, 1401–1414. doi:10.1016/j.cell.2007.04.040.

Langmead, B., and Salzberg, S. L. (2012). Fast gapped-read alignment with Bowtie

2. *Nat Methods* 9, 357–359. doi:10.1038/nmeth.1923.

Lau, A. G., Irier, H. a, Gu, J., Tian, D., Ku, L., Liu, G., et al. (2010). Distinct 3'UTRs differentially regulate activity-dependent translation of brain-derived neurotrophic factor (BDNF). *Proc. Natl. Acad. Sci. U. S. A.* 107, 15945–50. doi:10.1073/pnas.1002929107.

Lawrence, M., Huber, W., Pagès, H., Aboyoun, P., Carlson, M., Gentleman, R., et al. (2013). Software for Computing and Annotating Genomic Ranges. *PLoS Comput. Biol.* 9. doi:10.1371/journal.pcbi.1003118.

Leach, P. T., Poplawski, S. G., Kenney, J. W., Hoffman, B., Liebermann, D. a, Abel, T., et al. (2012). Gadd45b knockout mice exhibit selective deficits in hippocampus-dependent long-term memory. *Learn. Mem.* 19, 319–24. doi:10.1101/lm.024984.111.

Lee, J. A., Tang, Z. Z., and Black, D. L. (2009). An inducible change in Fox-1/A2BP1 splicing modulates the alternative splicing of downstream neuronal target exons. *Genes Dev.* 23, 2284–2293. doi:10.1101/gad.1837009.

Li, W., You, B., Hoque, M., Zheng, D., Luo, W., Ji, Z., et al. (2015). Systematic profiling of poly(a)+ transcripts modulated by core 3' end processing and splicing factors reveals regulatory rules of alternative cleavage and polyadenylation. *PLoS Genet.* 11, e1005166. doi:10.1371/journal.pgen.1005166.

Lianoglou, S., Garg, V., Yang, J. L., Leslie, C. S., and Mayr, C. (2013). Ubiquitously transcribed genes use alternative polyadenylation to achieve tissue-specific expression. *Genes Dev.* 27, 2380–2396. doi:10.1101/gad.229328.113.

Litman, P., Barg, J., Rindzoonski, L., and Ginzburg, I. (1993). Subcellular localization of tau mRNA in differentiating neuronal cell culture: Implications for neuronal polarity. *Neuron* 10, 627–638. doi:10.1016/0896-6273(93)90165-N.

Liu-Yesucevitz, L., Bassell, G. J., Gitler, A. D., Hart, A. C., Klann, E., Richter, J. D., et al. (2011). Local RNA Translation at the Synapse and in Disease. *J. Neurosci.* 31, 16086–16093. doi:10.1523/JNEUROSCI.4105-11.2011.

Lonze, B. E., and Ginty, D. D. (2002). Function and Regulation of CREB Family Transcription Factors in the Nervous System CREB and its close relatives are now widely accepted. *Neuron* 35, 605–623. doi:10.1016/S0896-6273(02)00828-0.

Love, M. I., Huber, W., and Anders, S. (2014). Moderated estimation of fold change and dispersion for RNA-seq data with DESeq2. *Genome Biol.* 15, 1–34. doi:Artn 550\rDoi 10.1186/S13059-014-0550-8.

Lugli, G., Torvik, V. I., Larson, J., and Smalheiser, N. R. (2008). Expression of microRNAs and their precursors in synaptic fractions of adult mouse forebrain. *J. Neurochem.* 106, 650–661. doi:10.1111/j.1471-4159.2008.05413.x.

Lukong, K. E., Chang, K. wei, Khandjian, E. W., and Richard, S. (2008). RNA-binding proteins in human genetic disease. *Trends Genet.* 24, 416–425. doi:10.1016/j.tig.2008.05.004.

Luo, W., Ji, Z., Pan, Z., You, B., Hoque, M., Li, W., et al. (2013). The Conserved Intronic Cleavage and Polyadenylation Site of CstF-77 Gene Imparts Control of 3′ End Processing Activity through Feedback Autoregulation and by U1 snRNP. *PLoS Genet.* 9. doi:10.1371/journal.pgen.1003613.

Lutz, C. S., and Moreira, A. (2011). Alternative mRNA polyadenylation in eukaryotes: An effective regulator of gene expression. *Wiley Interdiscip. Rev. RNA* 2, 22–31. doi:10.1002/wrna.47.

Maag, J. L. V, Panja, D., Sporild, I., Patil, S., Kaczorowski, D. C., Bramham, C. R., et al. (2015). Dynamic expression of long noncoding RNAs and repeat elements in synaptic plasticity. *Front. Neurosci.* 9, 1–16. doi:10.3389/fnins.2015.00351.

Majdan, M., and Shatz, C. J. (2006). Effects of visual experience on activity-dependent gene regulation in cortex. *Nat. Neurosci.* 9, 650–9. doi:10.1038/nn1674.

Makhinson, M., Chotiner, J. K., Watson, J. B., and O'Dell, T. J. (1999). Adenylyl cyclase activation modulates activity-dependent changes in synaptic strength and Ca2+/calmodulin-dependent kinase II autophosphorylation. *J. Neurosci.* 19, 2500–2510.

Malmevik, J., Petri, R., Klussendorf, T., Knauff, P., Åkerblom, M., Johansson, J., et al. (2015). Identification of the miRNA targetome in hippocampal neurons using RIP-seq. *Nat. Publ. Gr.* 5, 12609. doi:10.1038/srep12609.

Mansuy, I. M., Mayford, M., Jacob, B., Kandel, E. R., and Bach, M. E. (1998). Restricted and regulated overexpression reveals calcineurin as a key component in the transition from short-term to long-term memory. *Cell* 92, 39–49. doi:10.1016/S0092-8674(00)80897-1.

Martin, C. L., Duvall, J. A., Ilkin, Y., Simon, J. S., Arreaza, M. G., Wilkes, K., et al. (2007). Cytogenetic and molecular characterization of A2BP1/FOX1 as a candidate gene for autism. *Am. J. Med. Genet. Part B Neuropsychiatr. Genet.* 144, 869–876. doi:10.1002/ajmg.b.30530.

Martin, K. C., Casadio, A., Zhu, H., Yaping, E., Rose, J. C., Chen, M., et al. (1997a). Synapse-specific, long-term facilitation of aplysia sensory to motor synapses: A function for local protein synthesis in memory storage. *Cell* 91, 927–938. doi:10.1016/S0092-8674(00)80484-5.

Martin, K. C., and Ephrussi, A. (2009). mRNA Localization: Gene Expression in the Spatial Dimension. *Cell* 136, 719–730. doi:10.1016/j.cell.2009.01.044.

Martin, K. C., Michael, D., Rose, J. C., Barad, M., Casadio, A., Zhu, H., et al. (1997b). MAP kinase translocates into the nucleus of the presynaptic cell and is

required for long-term facilitation in Aplysia. *Neuron* 18, 899–912. doi:10.1016/S0896-6273(00)80330-X.

Martin, K. C., and Zukin, R. S. (2006). RNA Trafficking and Local Protein Synthesis in Dendrites: An Overview. *J. Neurosci.* 26, 7131–7134. doi:10.1523/JNEUROSCI.1801-06.2006.

Mayford, M., Baranes, D., Podsypanina, K., and Kandel, E. R. (1996). The 3'-untranslated region of CaMKII is a cis-acting signal for the localization and translation of mRNA in dendrites. *Proc. Natl. Acad. Sci.* 93, 13250–13255. doi:10.1073/pnas.93.23.13250.

Mayford, M., Siegelbaum, S. A., and Kandel, E. R. (2012). Synapses and memory storage. *Cold Spring Harb. Perspect. Biol.* 4, 1–18. doi:10.1101/cshperspect.a005751.

Mayr, C. (2016). Evolution and Biological Roles of Alternative 3'UTRs. *Trends Cell Biol.*, 227–37. doi:10.1016/j.tcb.2015.10.012.

Mayr, C., and Bartel, D. P. (2009). Widespread shortening of 3'UTRs by alternative cleavage and polyadenylation activates oncogenes in cancer cells. *Cell* 138, 673–84. doi:10.1016/j.cell.2009.06.016.

McNair, K., Davies, C. H., and Cobb, S. R. (2006). Plasticity-related regulation of the hippocampal proteome. *Eur. J. Neurosci.* 23, 575–580. doi:10.1111/j.1460-9568.2005.04542.x.

McNeill, E., and Van Vactor, D. (2012). MicroRNAs Shape the Neuronal Landscape. *Neuron* 75, 363–379. doi:10.1016/j.neuron.2012.07.005.

Miller, S., Yasuda, M., Coats, J. K., Jones, Y., Martone, M. E., and Mayford, M. (2002). Disruption of dendritic translation of CaMKIIα impairs stabilization of synaptic plasticity and memory consolidation. *Neuron* 36, 507–519. doi:10.1016/S0896-6273(02)00978-9.

Miura, P., Sanfilippo, P., Shenker, S., and Lai, E. C. (2014). Alternative polyadenylation in the nervous system: To what lengths will 3' UTR extensions take us? *BioEssays* 36, 766–777. doi:10.1002/bies.201300174.

Miura, P., Shenker, S., Andreu-agullo, C., Miura, P., Shenker, S., Andreu-agullo, C., et al. (2013). Widespread and extensive lengthening of 3 ′ UTRs in the mammalian brain. *Genome Res.*, 812–825. doi:10.1101/gr.146886.112.

Nam, J. W., Rissland, O. S., Koppstein, D., Abreu-Goodger, C., Jan, C., Agarwal, V., et al. (2014). Global analyses of the effect of different cellular contexts on microRNA targeting. *Mol. Cell* 53, 1031–1043. doi:10.1016/j.molcel.2014.02.013.

Nguyen, P. V, Abel, T., and Kandel, E. R. (1994). Requirement of a critical period of transcription for induction of a late phase of LTP. *Science* 265, 1104–7. doi:10.1126/science.8066450.

O'Leary, T., van Rossum, M. C. W., and Wyllie, D. J. A. (2010). Homeostasis of intrinsic excitability in hippocampal neurones: dynamics and mechanism of the response to chronic depolarization. *J. Physiol.* 588, 157–70. doi:10.1113/jphysiol.2009.181024.

Ostroff, L. E., Fiala, J. C., Allwardt, B., and Harris, K. M. (2002). Polyribosomes redistribute from dendritic shafts into spines with enlarged synapses during LTP in developing rat hippocampal slices. *Neuron* 35, 535–545. doi:10.1016/S0896-6273(02)00785-7.

Pattabiraman, P. P., Tropea, D., Chiaruttini, C., Tongiorgi, E., Cattaneo, A., and Domenici, L. (2005). Neuronal activity regulates the developmental expression and subcellular localization of cortical BDNF mRNA isoforms in vivo. *Mol. Cell. Neurosci.* 28, 556–70. doi:10.1016/j.mcn.2004.11.010.

Peter J Russel (2009). *iGenetics: A molecular approach*. 3rd ed. Pearson.

Poon, M. M., Choi, S.-H., Jamieson, C. a M., Geschwind, D. H., and Martin, K. C. (2006). Identification of process-localized mRNAs from cultured rodent hippocampal neurons. *J. Neurosci.* 26, 13390–9. doi:10.1523/JNEUROSCI.3432-06.2006.

Prieto, G. A., Snigdha, S., Baglietto-Vargas, D., Smith, E. D., Berchtold, N. C., Tong, L., et al. (2015). Synapse-specific IL-1 receptor subunit reconfiguration augments vulnerability to IL-1β in the aged hippocampus. *Proc. Natl. Acad. Sci.* 112, E5078–E5087. doi:10.1073/pnas.1514486112.

Raj, B., and Blencowe, B. J. (2015). Alternative Splicing in the Mammalian Nervous System: Recent Insights into Mechanisms and Functional Roles. *Neuron* 87, 14–27. doi:10.1016/j.neuron.2015.05.004.

Rajasethupathy, P., Fiumara, F., Sheridan, R., Betel, D., Puthanveettil, S. V, Russo, J. J., et al. (2009). Characterization of small RNAs in Aplysia reveals a role for miR-124 in constraining synaptic plasticity through CREB. *Neuron* 63, 803–17. doi:10.1016/j.neuron.2009.05.029.

Ray, D., Kazan, H., Cook, K. B., Weirauch, M. T., Najafabadi, H. S., Li, X., et al. (2013). A compendium of RNA-binding motifs for decoding gene regulation. *Nature* 499, 172–7. doi:10.1038/nature12311.

Ryan, M. M., Ryan, B., Kyrke-Smith, M., Logan, B., Tate, W. P., Abraham, W. C., et al. (2012). Temporal profiling of gene networks associated with the late phase of long-term potentiation in vivo. *PLoS One* 7, 1–14. doi:10.1371/journal.pone.0040538.

Rybak-Wolf, A., Jens, M., Murakawa, Y., Herzog, M., Landthaler, M., and Rajewsky, N. (2014). A variety of dicer substrates in human and C. elegans. *Cell* 159, 1153–1167. doi:10.1016/j.cell.2014.10.040.

Sala, C., Futai, K., Yamamoto, K., Worley, P. F., Hayashi, Y., and Sheng, M. (2003).

Inhibition of dendritic spine morphogenesis and synaptic transmission by activity-inducible protein Homer1a. *J. Neurosci.* 23, 6327–37. doi:23/15/6327 [pii].

Sandberg, R., Neilson, J. R., Sarma, A., Sharp, P. A., and Burge, C. B. (2008). Proliferating Cells Express mRNAs with shortened 3' untranslated regions and fewer microRNA target sites. *Science (80-.).* 320, 1643–1648. Available at: http://science.sciencemag.org/content/320/5883/1643.full-text.pdf+html.

Santos, A. R. A., and Duarte, C. B. (2008). Validation of internal control genes for expression studies: Effects of the neurotrophin BDNF on hippocampal neurons. *J. Neurosci. Res.* 86, 3684–3692. doi:10.1002/jnr.21796.

Sanz, E., Yang, L., Su, T., Morris, D. R., McKnight, G. S., and Amieux, P. S. (2009). Cell-type-specific isolation of ribosome-associated mRNA from complex tissues. *Proc. Natl. Acad. Sci. U. S. A.* 106, 13939–44. doi:10.1073/pnas.0907143106.

Schratt, G. M., Tuebing, F., Nigh, E. a, Kane, C. G., Sabatini, M. E., Kiebler, M., et al. (2006). A brain-specific microRNA regulates dendritic spine development. *Nature* 439, 283–9. doi:10.1038/nature04367.

Scoville, W. B., and Milner, B. (1957). LOSS OF RECENT MEMORY AFTER BILATERAL HIPPOCAMPAL LESIONS. *J. Neurol. Neurosurg. Psychiatry* 20, 11–21. doi:10.1136/jnnp.20.1.11.

Sebat, J., Lakshmi, B., Malhotra, D., Troge, J., Lese-Martin, C., Walsh, T., et al. (2007). Strong association of de novo copy number mutations with autism. *Science (80-.).* 316, 445–449. doi:10.1126/science.1138659.

Sempere, L. F., Freemantle, S., Pitha-Rowe, I., Moss, E., Dmitrovsky, E., and Ambros, V. (2004). Expression profiling of mammalian microRNAs uncovers a subset of brain-expressed microRNAs with possible roles in murine and human neuronal differentiation. *Genome Biol.* 5, R13. doi:10.1186/gb-2004-5-3-r13.

Shaywitz, A. J., and Greenberg, M. E. (1999). CREB: A Stimulus-Induced Transcription Factor Activated by A Diverse Array of Extracellular Signals. *Annu. Rev. Biochem.* 68, 821–861. doi:10.1146/annurev.biochem.68.1.821.

Shepard, P. J., Choi, E.-A., Lu, J., Flanagan, L. a, Hertel, K. J., and Shi, Y. (2011). Complex and dynamic landscape of RNA polyadenylation revealed by PAS-Seq. *RNA* 17, 761–772. doi:10.1261/rna.2581711.

Shi, Y., Di Giammartino, D. C., Taylor, D., Sarkeshik, A., Rice, W. J., Yates, J. R., et al. (2009). Molecular Architecture of the Human Pre-mRNA 3′ Processing Complex. *Mol. Cell* 33, 365–376. doi:10.1016/j.molcel.2008.12.028.

Shi, Y., and Manley, J. L. (2015). The end of the message: Multiple protein:RNA interactions define the mRNA polyadenylation site. *Genes Dev.* 29, 889–897. doi:10.1101/gad.261974.115.

Siegel, G., Obernosterer, G., Fiore, R., Oehmen, M., Bicker, S., Christensen, M., et al. (2009). A functional screen implicates microRNA-138-dependent regulation of the depalmitoylation enzyme APT1 in dendritic spine morphogenesis. *Nat. Cell Biol.* 11, 705–16. doi:10.1038/ncb1876.

Silva, A. J., Kogan, J. H., Frankland, P. W., and Kida, S. (1998). CREB AND MEMORY. *Annu. Rev. Neurosci.* 21, 127–148. doi:10.1146/annurev.neuro.21.1.127.

Silva, a J., Paylor, R., Wehner, J. M., and Tonegawa, S. (1992). Impaired spatial learning in alpha-calcium-calmodulin kinase II mutant mice. *Science* 257, 206–211. doi:10.1126/science.1321493.

Smibert, P., Miura, P., Westholm, J. O., Shenker, S., May, G., Duff, M. O., et al. (2012). Global patterns of tissue-specific alternative polyadenylation in Drosophila. *Cell Rep.* 1, 277–289. doi:10.1016/j.celrep.2012.01.001.Global.

Squire, L., and Wixted, J. T. (2011). The Cognitive Neuroscience of Human Memory

Since H.M. *Annu. Rev. Neurosci.* 34, 259–88. doi:10.1146/annurev-neuro-061010-113720.

Steward, O., and Levy, W. B. (1982). Preferential localization of polyribosomes under the base of dendritic spines in granule cells of the dentate gyrus. *J Neurosci* 2, 284–291. doi:0270-6474/82/0203-0284.

Sutton, M. A., and Schuman, E. M. (2006). Dendritic Protein Synthesis, Synaptic Plasticity, and Memory. *Cell* 127, 49–58. doi:10.1016/j.cell.2006.09.014.

Taliaferro, J. M., Vidaki, M., Oliveira, R., Gertler, F. B., Swanson, M. S., Burge, C. B., et al. (2016). Distal Alternative Last Exons Localize mRNAs to Neural Projections. *Mol. Cell*, 1–13. doi:10.1016/j.molcel.2016.01.020.

Tan, C. L., Plotkin, J. L., Venø, M. T., von Schimmelmann, M., Feinberg, P., Mann, S., et al. (2013). MicroRNA-128 governs neuronal excitability and motor behavior in mice. *Science* 342, 1254–8. doi:10.1126/science.1244193.

Tang, S. J., Reis, G., Kang, H., Gingras, A.-C., Sonenberg, N., and Schuman, E. M. (2002). A rapamycin-sensitive signaling pathway contributes to long-term synaptic plasticity in the hippocampus. *Proc. Natl. Acad. Sci. U. S. A.* 99, 467–72. doi:10.1073/pnas.012605299.

Tanzi, E. (1893). I fatti e le induzioni dell'odierna istologia del sistema nervoso. *Riv Sper Fren Med Leg*, 419–472.

Tian, B., and Graber, J. H. (2012). Signals for pre-mRNA cleavage and polyadenylation. *Wiley Interdiscip. Rev. RNA* 3, 385–396. doi:10.1002/wrna.116.

Tian, B., Hu, J., Zhang, H., and Lutz, C. S. (2005). A large-scale analysis of mRNA polyadenylation of human and mouse genes. *Nucleic Acids Res.* 33, 201–212. doi:10.1093/nar/gki158.

Tian, B., and Manley, J. L. (2013). Alternative cleavage and polyadenylation: The long and short of it. *Trends Biochem. Sci.* 38, 312–320.

doi:10.1016/j.tibs.2013.03.005.

Tian, B., and Manley, J. L. (2017). Alternative polyadenylation of mRNA precursors. *Nat. Rev. Mol. Cell Biol.* 18, 18–30. doi:10.1038/nrm.2016.116.

Vo, N., Klein, M. E., Varlamova, O., Keller, D. M., Yamamoto, T., Goodman, R. H., et al. (2005). A cAMP-response element binding protein-induced microRNA regulates neuronal morphogenesis. *Proc. Natl. Acad. Sci. U. S. A.* 102, 16426–31. doi:10.1073/pnas.0508448102.

Voineagu, I., Wang, X., Johnston, P., Lowe, J. K., Tian, Y., Horvath, S., et al. (2011). Transcriptomic analysis of autistic brain reveals convergent molecular pathology. *Nature* 474, 380–386. doi:10.1038/nature10110.

Wang, D. O., Kim, S. M., Zhao, Y., Hwang, H., Miura, S. K., Sossin, W. S., et al. (2009). Synapse- and stimulus-specific local translation during long-term neuronal plasticity. *Science* 324, 1536–1540. doi:10.1126/science.1173205.

Wang, D. O., Martin, K. C., and Zukin, R. S. (2010a). Spatially restricting gene expression by local translation at synapses. *Trends Neurosci.* 33, 173–82. doi:10.1016/j.tins.2010.01.005.

Wang, E. T., Sandberg, R., Luo, S., Khrebtukova, I., Zhang, L., Mayr, C., et al. (2008). Alternative isoform regulation in human tissue transcriptomes. *Nature* 456, 470–476. doi:10.1038/nature07509.

Wang, E. T., Taliaferro, J. M., Lee, J.-A., Sudhakaran, I. P., Rossoll, W., Gross, C., et al. (2016). Dysregulation of mRNA Localization and Translation in Genetic Disease. *J. Neurosci.* 36, 11418–11426. doi:10.1523/JNEUROSCI.2352-16.2016.

Wang, W.-X., Wilfred, B. R., Hu, Y., Stromberg, A. J., and Nelson, P. T. (2010b). Anti-Argonaute RIP-Chip shows that miRNA transfections alter global patterns of mRNA recruitment to microribonucleoprotein complexes. *RNA* 16, 394–404.

doi:10.1261/rna.1905910.

Wayman, G. A., Davare, M., Ando, H., Fortin, D., Varlamova, O., Cheng, H.-Y. M., et al. (2008). An activity-regulated microRNA controls dendritic plasticity by down-regulating p250GAP. *Proc. Natl. Acad. Sci.* 105, 9093–9098. doi:10.1073/pnas.0803072105.

Weyn-Vanhentenryck, S. M., Mele, A., Yan, Q., Sun, S., Farny, N., Zhang, Z., et al. (2014). HITS-CLIP and Integrative Modeling Define the Rbfox Splicing-Regulatory Network Linked to Brain Development and Autism. *Cell Rep.* 6, 1139–1152. doi:10.1016/j.celrep.2014.02.005.

Winder, D. G., Mansuy, I. M., Osman, M., Moallem, T. M., and Kandel, E. R. (1998). Genetic and pharmacological evidence for a novel, intermediate phase of long-term potentiation suppressed by calcineurin. *Cell* 92, 25–37. doi:10.1016/S0092-8674(00)80896-X.

Yang, Y., Li, W., Hoque, M., Hou, L., Shen, S., Tian, B., et al. (2016). PAF Complex Plays Novel Subunit-Specific Roles in Alternative Cleavage and Polyadenylation. *PLoS Genet.* 12. doi:10.1371/journal.pgen.1005794.

Zeisel, a., Manchado, a. B. M., Codeluppi, S., Lonnerberg, P., La Manno, G., Jureus, a., et al. (2015). Cell types in the mouse cortex and hippocampus revealed by single-cell RNA-seq. *Science (80-.).* 347, 1138–42. doi:10.1126/science.aaa1934.

Zhang, H., Hu, J., Recce, M., and Tian, B. (2005a). PolyA_DB: A database for mammalian mRNA polyadenylation. *Nucleic Acids Res.* 33, 116–120. doi:10.1093/nar/gki055.

Zhang, H., Lee, J. Y., and Tian, B. (2005b). Biased alternative polyadenylation in human tissues. *Genome Biol* 6, R100. doi:10.1186/gb-2005-6-12-r100.

Zheng, D., Liu, X., and Tian, B. I. N. (2016). 3′ READS+ , a sensitive and accurate

method for 3′ end sequencing of polyadenylated RNA. *Rna*, 1–9. doi:10.1261/rna.057075.116.forms.

Zheng, D., and Tian, B. (2014). RNA-binding proteins in regulation of alternative cleavage and polyadenylation. *Adv. Exp. Med. Biol.* 825, 97–127. doi:10.1007/978-1-4939-1221-6_3.

Zhong, J., Zhang, T., and Bloch, L. M. (2006). Dendritic mRNAs encode diversified functionalities in hippocampal pyramidal neurons. *BMC Neurosci.* 7, 17. doi:10.1186/1471-2202-7-17.

2.2. Additional insights

2.2.1. Gene expression changes post-LTP induction

To obtain high resolution gene expression data, we performed RNA-sequencing from of acute mouse hippocampal slices 1 hr and 3 hrs after LTP induction, with time-matched controls from the same animals. We performed differential expression (DE) analysis between controls and LTP-induced samples for each time-point separately, using a paired study design in DESeq2(Love et al., 2014). At 1 hr post-stimulation, we considered the expression of approximately 15,205 genes (mean count > 24.5), and found 63 genes that showed significant DE, with all but one transcript upregulated (FDR <0.05, 0.4<log2FC<-0.4 corresponding to ~30% change, Fig. 1a, 1c). At 3 hrs, 337 genes were significantly upregulated and 31 downregulated out of a total of 14,102 tested transcripts (mean count > 46.2, FDR < 0.05, 0.4<log2FC<-0.4, Fig. 1b, 1c), suggesting that L-LTP drives global changes in the transcriptome as early as 1 hr post-induction, primarily through increases in the concentration of transcripts, with an increase in DE genes between 1 and 3 hrs after stimulation.

Importantly, the top DE genes we identified are consistent with previous studies of DE following neuronal activity(Hermey et al., 2013; Leach et al., 2012; Majdan and Shatz, 2006), including upregulation of Gadd45g and Egr2, and of immediate early genes c-Fos, Arc and Npas4. GO analysis of DE genes revealed that the top functional category at both time points the top functional category included genes that regulate transcription, with the number of genes in that group increasing from 26 at 1 hr to 77 at 3 hrs (Webgestalt, adjusted p-value<0.05, minimum 4 genes per category, using brain genes as reference, Fig. 1d, 1e). Additionally, DE genes at 1hr encoded proteins involved in cell communication,

response to stimulus and protein kinase activity, all of which are involved in synaptic responses to stimulation (Fig. 1d). At 3 hrs, DE genes were also enriched in voltage-gated channels activity and in the category of behavior (Fig. 1e).

The activity-induced temporal patterns of gene expression in Fig. 1f show that the number of DE genes was 5.8 times higher at 3 hrs than at 1 hr, and that the magnitude of change in expression of individual transcripts increased over time after cLTP induction (more intense red and blue signal at 3 hrs than 1 hr). We then asked whether the same DE genes were regulated at both 1 hr and 3 hr time-points and found that half of all DE genes at 1 hr (71 genes) were also DE at 3 hrs (no fold change cut-off applied, Fig. 1g). Our data is consistent with a model in which there is a progressive accumulation of DE genes to sustain the long-lasting effects of LTP rather than a spike of upregulation of unique transcripts at 3 hrs.

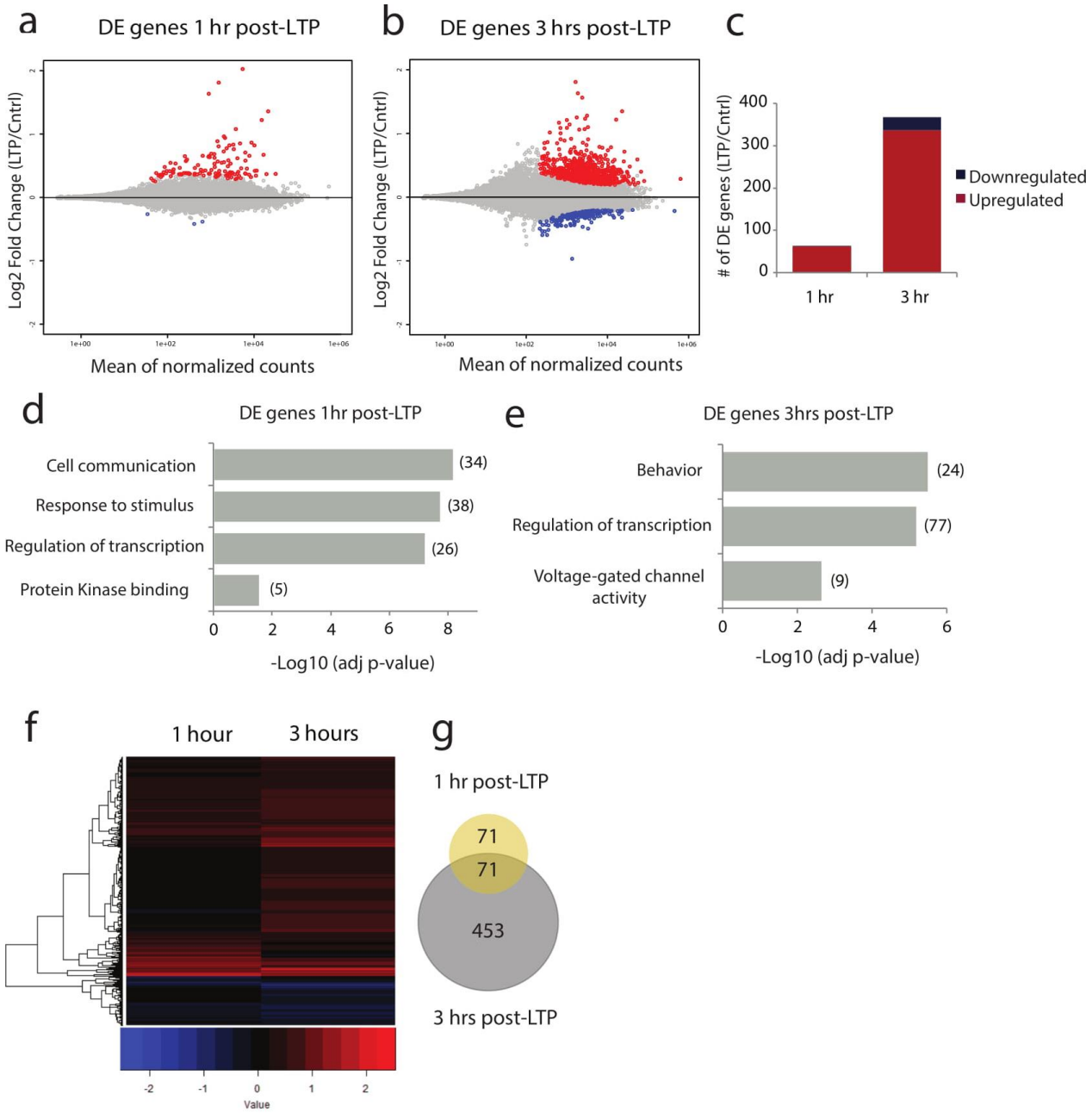

Figure 1 - Regulation of gene expression after LTP induction.

a, b - Gene expression analysis of hippocampal slices 1 hour (a) and 3 hours after LTP treatment (b). X-axis: normalized read counts; Y- axis: log2(fold change) in cLTP vs control; Genes that are upregulated during LTP are highlighted in red and genes with lower expression upon LTP are shown in blue (FDR<0.05). Grey denotes genes that do not have significant regulation.

c - Number of genes upregulated or downregulated 1 hour or 3 hours post-LTP (FDR<0.05, -0.4>log2FC>0.4).

d, e - Enrichment analysis of genes differentially expressed 1 hour (d) or 3 hours (e) post-LTP induction. Bar graphs display the top gene ontology enriched categories obtained using Webgestalt. X axis shows the statistical significance of the enrichment relative to 14,000 hippocampal-expressed genes (FDR<0.1, Benjamini–Hochberg correction, 4 genes minimum per category). Number of genes in each category is shown in parentheses.

f, g - Comparison of genes differentially expressed 1 hour and 3 hours post-LTP induction (-0.4>log2FC>0.4; FDR<0.05). Heatmap shows upregulated genes in red and downregulated genes in blue (f). Venn diagram shows the number of genes changed in each and both time-points (g).

2.2.2. Specialized methods to study 3'-UTR regulation

Our study looking at APA during LTP highlights the importance of using specialized 3'end sequencing methods to comprehensively address APA regulation, and further sheds light on the relative merits of two of these methods, 3'READS and PAS-seq. While RNA-sequencing accurately detects gene expression changes and alternative splicing events, it often leads to low sequencing coverage of the 5' and 3' ends of transcripts, compromising the data quality for APA analysis (**Fig. 2**).

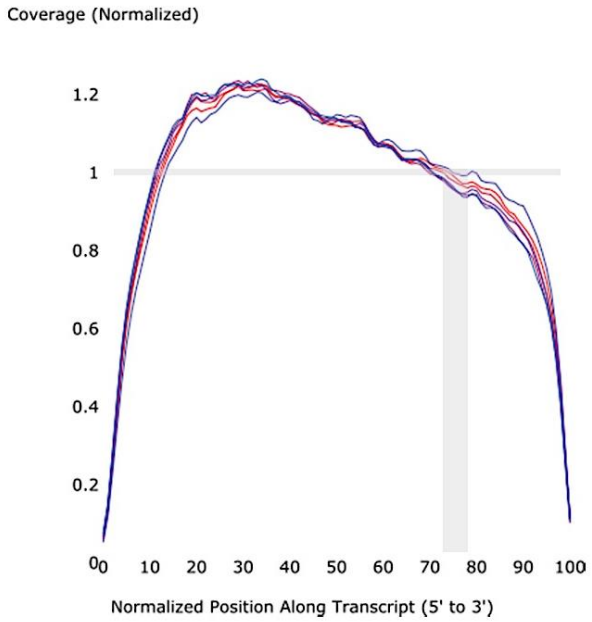

Figure 2 – Relationship between coverage of RNA-seq reads and reads position within the transcripts.
Diagram of reads coverage for all 12 samples (1 hr and 3 hrs triplicates of controls and cLTP induced samples), highlighting a drop in sequencing coverage in the 5' and 3' end of transcripts.

Several sequencing methods that enrich the coverage of the 3'end of transcripts have been developed, including 3'READS and Poly(A) Site Sequencing (PAS-Seq,(Hoque et al., 2013; Shepard et al., 2011)). We analyzed APA using both 3'READS and PAS-Seq. We performed PAS-Seq on triplicates of control and cLTP-induced slices collected 1 and 3 hrs post-stimulation to obtain a total of ~10M reads per sample. Of these, 51%-59% uniquely mapped to the mouse genome and ~18% aligned to 3'UTRs. We removed 5% of the 3'UTR reads due to internal priming and identified ~20,000 clusters of pAs. In contrast with 3'READS, PAS-Seq revealed a high data dispersion (2.2 for low abundant genes and 2.8 for middle to high abundant genes), with low consistency in mapped reads for a given gene across samples, and high frequency of false priming in transcript regions other than pAs (**Fig. 3a-d**). Due to the high variance of read counts across samples and within genes, we found no

statistically significant DE APA isoforms following LTP (FDR cutoff <0.1). In addition, we identified a smaller number of genes with proximal and distal pAs using PAS-Seq than with 3'READS (~700 vs. ~3,000 genes), and found a low cluster correlation value for 3'UTR-APA clusters (proximal and distal pAs) across the two methods (**Fig. 3e**). Therefore, we focused our analysis uniquely on the 3'READS data that showed data consistency across samples (Pearson correlation coefficients above 0.93 for all samples as shown in the pair-wise scatterplots in **Fig. 4**) and clear separation between control and experimental groups.

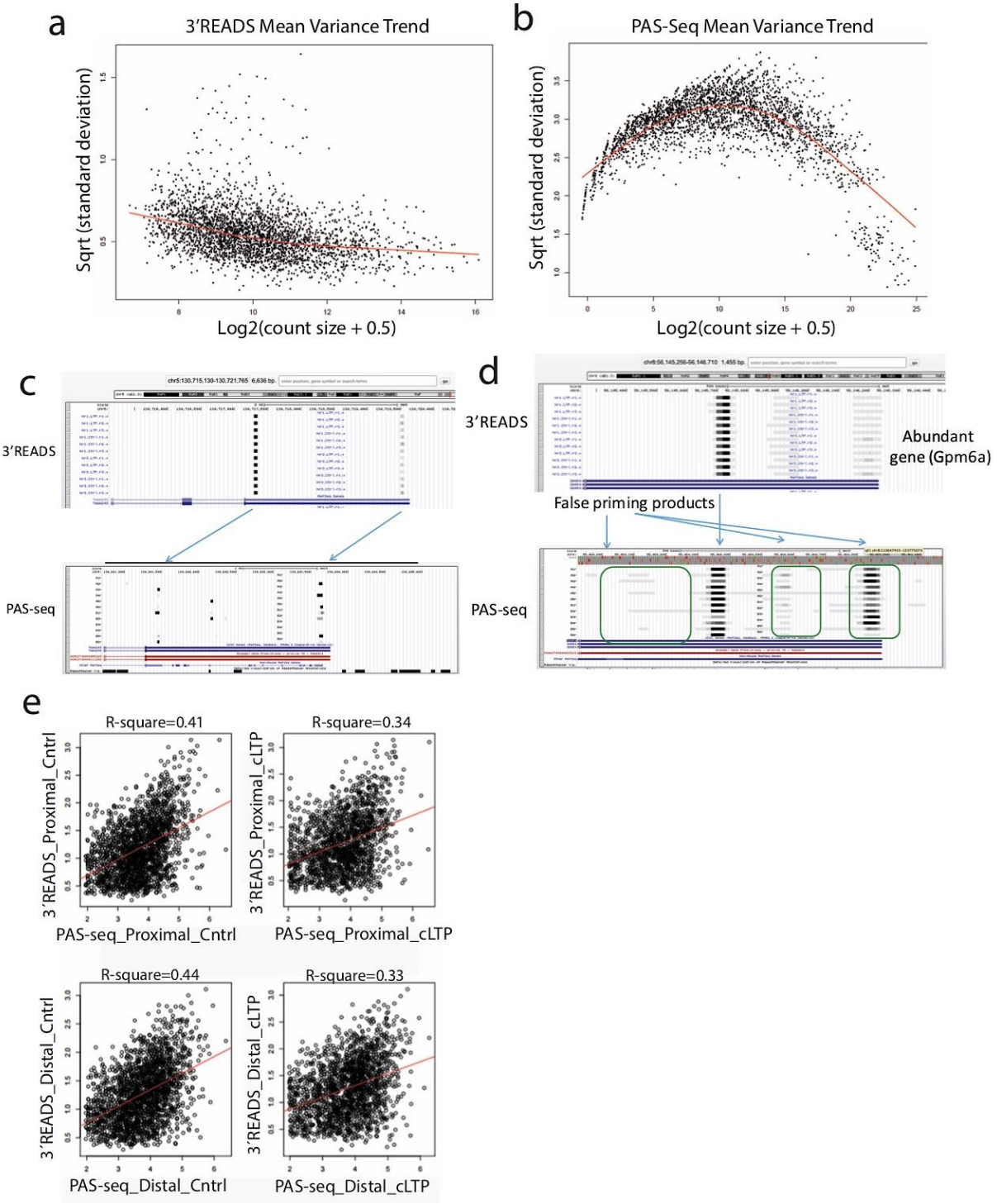

Figure 3- Comparison of 3'READS and PAS-Seq data.

a, b - Graphics show in red the mean variance trend for 3'READS (a) and PAS-seq data (b). The data dispersion is based on reads per million; X-axis is square root of standard deviation; Y-axis shows the genes abundance based on log2(reads count size + 0.5). PAS-Seq data showing a high variance between samples and a 5-6 times larger dispersion than in the 3'READS data. In PAS-Seq low abundance genes

had an average ~2.8 dispersion, while middle to high abundance transcripts had a ~2.2 dispersion.

c - Mapped reads alignment for transcript Tmem248 across samples in 3'READS (upper panel) and PAS-Seq (lower panel). Data reveals a high consistency in the reads coverage for 3'READS, in contrast with a high variance in PAS-Seq.

d - Reads alignment for Gpm6a, a highly abundant gene (with lower sequencing variance), using 3'READS (upper panel) and PAS-Seq (lower panel) in all 12 samples. Data shown in these panels is after internal priming removal (defined as 10nt out immediate 14nt downstream are As). Although there is some consistency between 3'READS and PAS-Seq in the central region of the panels, we observed a high frequency of false priming products in PAS-Seq.

e - Correlation between 3'UTR-APA clusters (proximal and distal pAs) in 3'READS and PAS-Seq. Panels show the correlation for the 3hrs time-point, including controls (left panels) and cLTP induced samples (right panels). Spearman correlation values are based on RPM values for proximal pAs (upper panels) and distal pAs (lower panels) clusters between 3'READS (y-axis) and PAS-Seq (x-axis). R2 values range between 0.33 and 0.44.

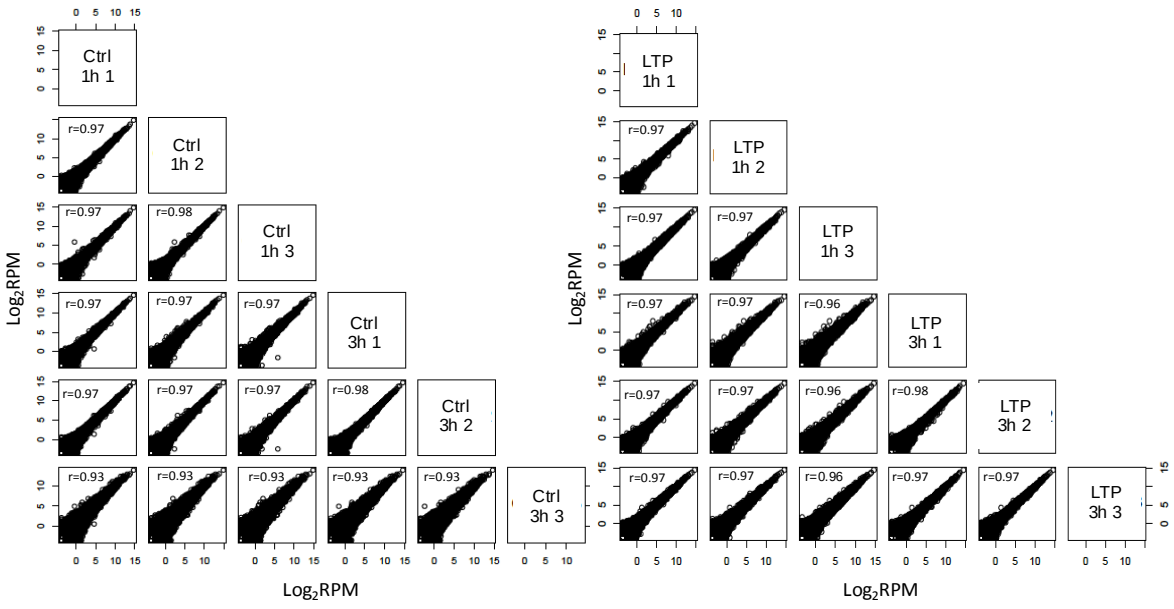

Figure 4 - Pairwise correlation of 3'READS samples. RPM values of PASs were used. Left, control samples; right, LTP samples. Pearson correlation coefficient (r) is shown for each comparison.

2.2.3. References

Hermey, G., Mahlke, C., Gutzmann, J. J., Schreiber, J., Blüthgen, N., and Kuhl, D. (2013). Genome-Wide Profiling of the Activity-Dependent Hippocampal Transcriptome. *PLoS One* 8. doi:10.1371/journal.pone.0076903.

Hoque, M., Ji, Z., Zheng, D., Luo, W., Li, W., You, B., et al. (2013). Analysis of alternative cleavage and polyadenylation by 3' region extraction and deep sequencing. *Nat. Methods* 10, 133–9. doi:10.1038/nmeth.2288.

Leach, P. T., Poplawski, S. G., Kenney, J. W., Hoffman, B., Liebermann, D. a, Abel, T., et al. (2012). Gadd45b knockout mice exhibit selective deficits in hippocampus-dependent long-term memory. *Learn. Mem.* 19, 319–24. doi:10.1101/lm.024984.111.

Love, M. I., Huber, W., and Anders, S. (2014). Moderated estimation of fold change and dispersion for RNA-seq data with DESeq2. *Genome Biol.* 15, 1–34. doi:Artn 550\rDoi 10.1186/S13059-014-0550-8.

Majdan, M., and Shatz, C. J. (2006). Effects of visual experience on activity-dependent gene regulation in cortex. *Nat. Neurosci.* 9, 650–9. doi:10.1038/nn1674.

Shepard, P. J., Choi, E.-A., Lu, J., Flanagan, L. a, Hertel, K. J., and Shi, Y. (2011). Complex and dynamic landscape of RNA polyadenylation revealed by PAS-Seq. *RNA* 17, 761–772. doi:10.1261/rna.2581711

3. Chapter III – Cytoplasmic RbFox1 regulates the expression of synaptic and autism-related genes

The "Chapter III – Cytoplasmic RbFox1 regulates the expression of synaptic and autism-related genes" consists of a co-authorship publication as 4th author. Here is clarified the contribution of each of the authors:

3.1. Publication

Ji-Ann Lee[1], Andrey Damianov[2], Chia-Ho Lin[2], **Mariana Fontes[1]**, Neelroop N. Parikshak[3], Erik S. Anderson[2], Daniel H. Geschwind[3], Douglas L. Black[2,4], and Kelsey C. Martin[1]. Cytoplasmic Rbfox1 regulates the expression of synaptic and autism-related genes, *Neuron*, 2016 Jan 6;89(1):113-28, DOI: 10.1016/j.neuron.2015.11.025

[1]Department of Biological Chemistry,

[2]Department of Microbiology, Immunology, and Molecular Genetics,

[3]Program in Neurobehavioral Genetics, Semel Institute, David Geffen School of Medicine,

[4]Howard Hughes Medical Institute,

[1,2,3,4] - University of California, Los Angeles, Los Angeles, CA90095, USA

Mariana Fontes, the candidate for the PhD degree at the University of Porto, contributed to the paper by creating AAV constructs to knockdown and rescue specific RbFox1 isoforms in RNA-seq experiments, performed luciferase assays to measure the expression of RbFox1 targets, studied by immunocytochemistry whether the loss of cytoplasmic RbFox1 affected neuronal morphology, and tested the hypothesis that RbFox1 increases the stability of transcripts by competing with miRNAs using luciferase assays in the context of specific miRNAs overexpression.

The contribution of each author to the publication is clarified in the section "Authors contribution" with the following text:

"J.A.L. and K.C.M. designed the experiments with input from D.L.B.. J.A.L. performed co-culture, RNAi, and rescue experiments for microarray and RNA sequencing experiments, and all biochemical experiments. E.S.A. prepared cDNA for microarray experiments. A.D. and J.A.L. performed iCLIP experiments. J.A.L. and M.F. performed luciferase assays. C.H.L. and J.A.L performed bioinformatic analyses. N.N.P performed gene set enrichment analyses. Figures were prepared by

J.A.L., C.H.L., and N.N.P. The manuscript was written by J.A.L and K.C.M with input from the other authors."

Cytoplasmic Rbfox1 regulates the expression of synaptic and autism-related genes

Keywords: Rbfox1, alternative splicing, autism, RNA-binding protein, miRNA

HIGHLIGHTS

1. Nuclear and cytoplasmic Rbfox1 isoforms regulate distinct neuronal mRNAs.
2. Cytoplasmic Rbfox1 regulates the stability and translation of its target mRNAs.
3. Rbfox1 and miRNA binding sites overlap significantly in target mRNA 3'UTRs.
4. Cytoplasmic Rbfox1 targets are enriched in cortical development and autism genes.

IN BRIEF

Rbfox1 regulates the splicing of many exons in the nucleus of neurons. Lee at al. demonstrate that Rbfox1 also binds to the 3' UTR of target mRNAs in the cytoplasm to upregulate the expression of synaptic and autism-related genes.

3.1.1. SUMMARY

Human genetic studies have identified the neuronal RNA binding protein, Rbfox1, as a candidate gene for autism spectrum disorders. While Rbfox1 functions as a splicing regulator in the nucleus, it is also alternatively spliced to produce cytoplasmic isoforms. To investigate the function of cytoplasmic Rbfox1, we knocked down Rbfox proteins in mouse neurons and rescued with cytoplasmic or nuclear Rbfox1. Transcriptome profiling showed that nuclear Rbfox1 rescued splicing changes, whereas cytoplasmic Rbfox1 rescued changes in mRNA levels. iCLIP-seq of subcellular fractions revealed that Rbfox1 bound predominantly to introns in nascent RNA, while cytoplasmic Rbox1 bound to 3' UTRs. Cytoplasmic Rbfox1 binding increased target mRNA stability and translation, and Rbfox1 and miRNA binding sites overlapped significantly. Cytoplasmic Rbfox1 target mRNAs were enriched in genes involved in cortical development and autism. Our results uncover a new Rbfox1 regulatory network and highlight the importance of cytoplasmic RNA metabolism to cortical development and disease.

3.1.2. INTRODUCTION

Post-transcriptional regulation of RNA within neurons provides temporal and spatial control of gene expression during brain development and plasticity. RNA binding proteins (RBPs) play central roles in regulating each step of RNA processing. Mutations in RBPs have been found to cause and/or contribute to many human neurodevelopmental and neurologic disorders (Darnell and Richter, 2012; Lukong et al., 2008). Human genetic studies have focused attention on Rbfox1, a vertebrate homolog of the *Caenorhabditis elegans Feminizing gene 1 on X* (also known as Ataxin-2 Binding Protein 1, A2BP1) by associating chromosomal translocations and copy number variations in Rbfox1 with autism-spectrum disorders (ASDs) (Martin et al., 2007; Sebat et al., 2007). A gene co-expression network analysis of post mortem cerebral cortex from individuals with ASD identified Rbfox1 as a hub gene in a module of co-expressed transcripts involved in neuronal function and down-regulated in ASD (Voineagu et al., 2011). Other studies found Rbfox1 mutations associated with human epilepsy syndromes (Bhalla et al., 2004; Lal et al., 2013a; Lal et al., 2013b; Martin et al., 2007), which is often co-morbid with ASD.

Mammals express three Rbfox paralogs: Rbfox1 expressed in neurons, heart and muscle; Rbfox2 expressed in these three tissues as well as in stem cells, hematopoietic cells, and other cells; and Rbfox3 (also known as NeuN) expressed only in neurons (Kim et al., 2009b; Kuroyanagi, 2009). All Rbfox proteins contain a single RNA recognition motif (RRM)-type RNA binding domain that binds the hexanucleotide (U)GCAUG with great specificity (Auweter et al., 2006). When this sequence is present in regulated exons or flanking introns, Rbfox functions as a splicing regulator to promote or repress exon inclusion (Kuroyanagi, 2009). Studies in knockout (KO) mice revealed a role for Rbfox1 in regulating neuronal splicing networks involved in neurodevelopmental disorders and in controlling neuronal excitability (Gehman et al., 2011). A subsequent study identified several hundred additional Rbfox1 dependent splicing changes during neuronal differentiation of human fetal primary neural progenitor cells (Fogel et al., 2012). Crosslinking-immunoprecipitation and RNAseq (CLIP-seq) identified additional Rbfox1 splicing targets in mouse brain, including many ASD related genes (Lovci et al., 2013; Weyn-Vanhentenryck et al., 2014).

Rbfox1 is itself alternatively spliced to produce nuclear and cytoplasmic isoforms, referred to as Rbfox1_N and Rbfox1_C, respectively (Lee et al., 2009; Nakahata and Kawamoto, 2005). While the function of Rbfox1_N in splicing has been well studied, the function of Rbfox1_C is largely unexplored. The conservation of Rbfox binding sites in the 3' UTRs of many neuronal transcripts suggests that Rbfox1 plays a role in regulating mRNAs in the cytoplasm (Ray et al., 2013; Xie et al., 2005). Ray et al (2013) correlated the expression of Rbfox1 in different tissues with the presence of Rbfox1 binding sites in 3' UTRs and proposed that Rbfox1 stabilizes target mRNAs. Although they confirmed this by luciferase assay for one target using Rbfox1_N, it was not clear whether this stabilization arose from Rbfox1 actions in the nucleus or the cytoplasm. Other studies identifying Rbfox1 targets using CLIP-seq were done in whole tissue and thus could not differentiate between nuclear and cytoplasmic targets of Rbfox1 (Lovci et al., 2013; Weyn-Vanhentenryck et al., 2014).

To dissect the functions of Rbfox1 in the cytoplasm and nucleus, we profiled the transcriptome of neurons expressing either Rbfox1_C or Rbfox1_N. We complemented these experiments with Rbfox1 individual-nucleotide resolution CLIP (iCLIP) from subcellular fractions of neurons to identify the specific transcripts bound by Rbfox1 in the cytoplasm. Together, these findings identify a large number of transcripts regulated by cytoplasmically localized Rbfox1, independent of its effect on splicing. Our results indicate that the cytoplasmic portion of the Rbfox1 regulatory network controls many essential neuronal functions and further shows that these cytoplasmic targets overlap extensively with regulatory modules involved in cortical development and ASD.

3.1.3. RESULTS

Rbfox1_C is expressed at significant levels in mouse brain

The Rbfox1 gene contains several promoters and alternatively spliced exons, which generate multiple protein isoforms (Damianov and Black, 2010). The skipping of mouse exon 19 generates an Rbfox1 mRNA encoding Rbfox1_N, a protein with a nuclear localization signal (NLS) in the C-terminus that is enriched in the nucleus (Hamada et al., 2013; Lee et al., 2009). In contrast, the mRNA including exon 19 encodes Rbfox1_C, a protein lacking the NLS that localizes to the cytoplasm. We examined Rbfox1 protein and mRNA in brain to compare the expression levels of Rbfox1_N and Rbfox1_C isoforms. Immunoblotting of lysates from hippocampus and cortex from P0 and P21 mice with an anti-Rbfox1 antibody revealed six bands ranging from 45 to 55 kDa (Figure 1A). All of the bands were reduced or abolished by an siRNA targeting a constitutive exon present in all Rbfox1 mRNAs (siRF1_E10, Figure 1B), indicating that they represent specific Rbfox1 products. Using an siRNA targeting alternative exon 19, two of the six protein bands were depleted, indicating that these represent Rbfox1_C (red arrows in Figure 1B). In P0 mouse hippocampus and cortex, Rbfox1_C constituted 46% and 49% of Rbfox1 protein (Figure 1A), respectively, and subsequently declined to the 30% from 3 weeks to 6 months of age in adult brain (data not shown). We also examined the splicing of exon 19 by semi-quantitative RT-PCR, and found that 47% and 48% of Rbfox1 mRNA included exon 19 in P0 hippocampus and cortex, respectively (Figure 1C). Rbfox1_C is thus expressed at significant concentrations in mouse brain.

To confirm that endogenous Rbfox1 localizes to the cytoplasm, we performed immunoblotting on subcellular fractions (Figure 1D). We prepared cytosolic fractions by permeabilizing the plasma membrane but not the nucleus of dissociated hippocampal cultures with digitonin (Mackall et al., 1979). After collecting the cytosolic fraction that leaked out of the cells, cultures were further solubilized with RIPA buffer. As shown in Figure 1D, the cytoplasmic protein GAPDH was present in the digitonin-solubilized cytosolic fraction and in the RIPA-solubilized remaining fraction, indicating that the lysis was partial. More importantly, the nuclear marker U1-70K was absent from the cytosolic fraction, indicating that digitonin permeabilization released cytosolic, but not nuclear proteins. Rbfox1 immunoblots of the cytosolic fraction detected both Rbfox1_C and Rbfox1_N isoforms, indicating that both Rbfox1

splice isoforms are present in the cytoplasm. However, the ratio of Rbfox1_C to Rbfox1_N was higher in the cytosolic fraction, with Rbfox1_C representing the dominant isoform in the cytoplasm. Using antibodies specific for Rbfox2, Rbfox3, and Rbfox RRM, we detected Rbfox3, but not Rbfox2, in the cytosolic fraction. Thus, Rbfox1 and Rbfox3 are the major Rbfox paralogs in the cytoplasm of hippocampal neurons.

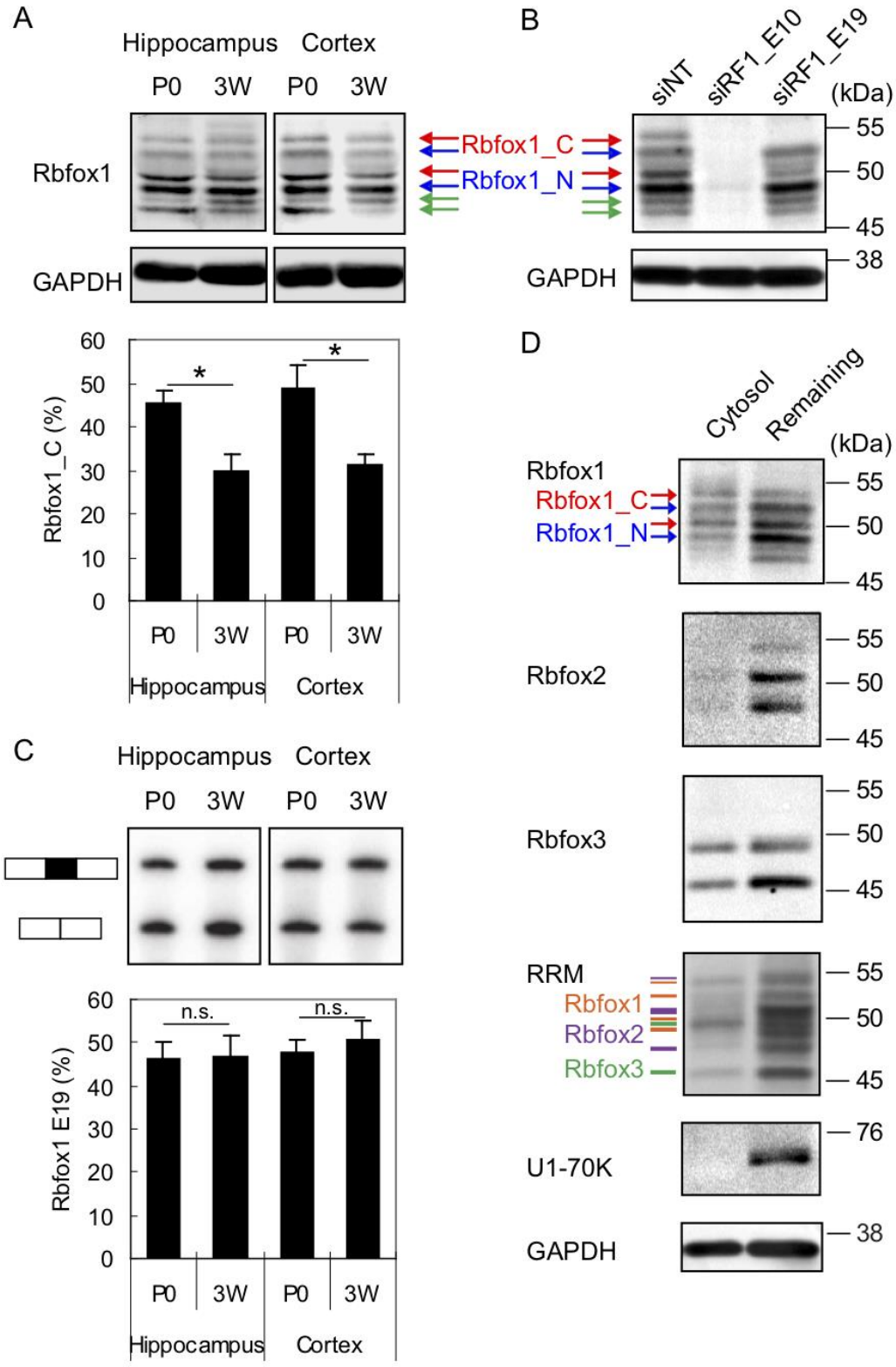

Figure 1. Expression and localization of Rbfox1 isoforms in neurons

(A) Immunoblot of Rbfox1 isoforms during development in mouse hippocampus and cortex at postnatal day 0 (P0), and 3 weeks (3W). Cytoplasmic Rbfox1 isoform (Rbfox1_C) and nuclear Rbfox1 isoform (Rbfox1_N) are indicated by

red and blue arrows, respectively. The green arrow points to a lower molecular weight isoform that is reduced by Rbfox1 siRNA (panel B), but whose provenance is unknown. The percentage of Rbfox1_C in the two dominant bands in the middle is shown in the bar graph below. Error bars indicate SD. N = 3. Statistical significance was determined by student's t-test. * indicates *p* value < 0.05.

(B) Immunoblot of Rbfox1 using an Rbfox1 pan siRNA (siRF1_E10) and an Rbfox1_C specific siRNA (siRF1_E19) in hippocampal neurons (DIV17).

(C) Semi-quantitative PCR analysis showing the splicing of Rbfox1 exon 19 in the same tissue and at the same time points as in (A). The percentage of exon 19 splicing is shown in histogram. Error bars indicate SD. N = 3. The percentage of Rbfox1 exon 19 inclusion was calculated; student's t-test, $p < 0.05$. n.s. = not significant.

(D) Immunoblot showing that Rbfox1 and Rbfox3 but not Rbfox2 are present in a cytosolic fraction purified from mouse hippocampal neurons (DIV14, treated with AraC). In the RRM immunoblots, the orange lines correspond to Rbfox1 proteins, the purple lines correspond to Rbfox2 proteins, and the green lines correspond to Rbfox3 proteins.

Rbfox1 regulation of mRNA expression

Only a few changes in mRNA expression levels were detected in the brain of Rbfox1 KO mice (Gehman et al., 2011; Lovci et al., 2013), which we postulated was due to compensation by Rbfox3. To examine the cytoplasmic function of Rbfox1, we isolated dissociated mouse hippocampal neurons, which express Rbfox1_C at high levels. To obtain a neuron-enriched culture, we added AraC to eliminate glial cells and co-cultured with filter inserts containing glial cells (Figures 2A, S1A, and S1B). We performed double siRNA-mediated knockdown (KD) of Rbfox1 and Rbfox3 (Figure 2B). After acute KD, we used microarray analysis to detect changes in the transcriptome (n = 3 biological replicates). Analyzing for splicing changes, we identified 338 up-regulated and 208 down-regulated alternative cassette exons in the double KD neurons (Figure 2C). Our results recapitulated 11 of the 20 splicing changes identified in the whole brain of Rbfox1 KO mice (Gehman et al., 2011).

In addition to splicing changes, we identified 746 genes exhibiting changes in abundance (expression) in the double KD (Figure 2D and Table S1), and validated a subset of genes by RT-qPCR analysis (20/23 = 87%, Figure S1C). The majority (676 genes, or 91%) were down-regulated in the double KD, indicating that their

abundance is normally increased by Rbfox1 and Rbfox3. We also measured the protein products of several regulated genes by quantitative immunoblotting. As shown in Figure S2, mRNAs of calcium/calmodulin-dependent protein kinase (CaMK) family members, CaMK2A, CaMK2B, and CaMK4, were reduced in double KD cultures with a corresponding decrease in the concentration of CaMK2A and CaMK2B, but not CaMK4 protein. We also observed a slight increase in Rbfox2 mRNA and a 2-fold increase in Rbfox2 protein in the Rbfox1 and 3 knockdown cultures, as was reported in Rbfox1 KO mice (Gehman et al., 2011). These data suggest that Rbfox1 or Rbfox3 may repress Rbfox2 expression at the translational level to form a negative regulatory loop for Rbfox proteins in neurons.

To determine whether the changes in mRNA expression were caused directly or indirectly by the loss of Rbfox1 and Rbfox3, we searched for conserved (U)GCAUG sequence motifs in the 3' UTRs of transcripts as an indicator of direct Rbfox1 regulation. The down-regulated gene set was significantly enriched for genes containing a 3' UTR UGCAUG motif that was conserved across human, mouse, rat, dog, and chicken genomes (12%, $p < 10^{-15}$, hypergeometric test, Figure 2E). Considering only conservation between human and mouse genomes, this enrichment increased to 41% ($p < 10^{-15}$, hypergeometric test, Figure 2E). In contrast, we detected no enrichment of (U)GCAUG motifs in up-regulated genes. Together, these findings indicate that in addition to regulating alternative splicing, Rbfox1 and 3 regulate mRNA and protein abundance, and suggest that this regulation occurs by direct RNA binding to (U)GCAUG sites in the 3' UTR.

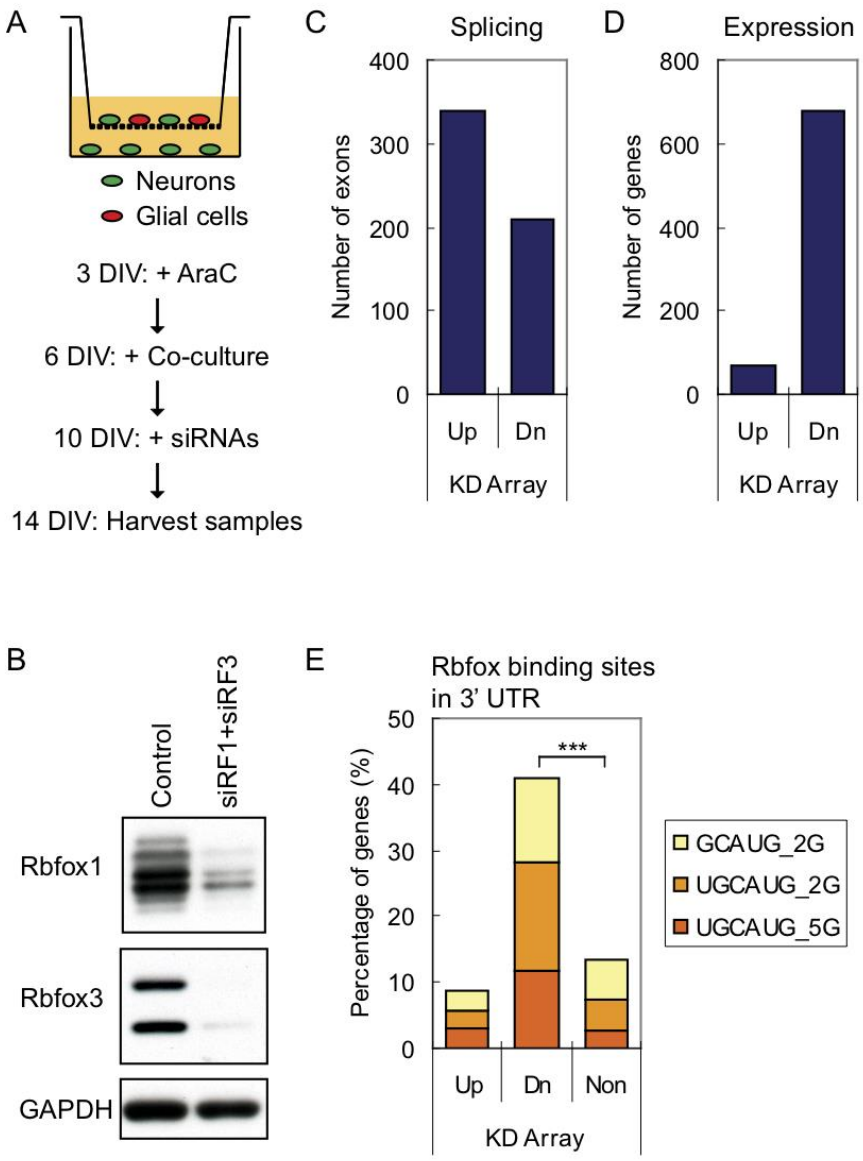

Figure 2. Rbfox1 regulates mRNA expression: knockdown and microarray analysis

(A) Experimental flow chart.

(B) Immunoblot showing the knockdown (KD) of Rbfox1 and Rbfox3 proteins in neurons incubated with Accell siRNAs targeting Rbfox1 (siRF1) and Rbfox3 (siRF3). GAPDH is used as loading control.

(C) Histogram of up-regulated (Up) and down-regulated (Dn) exons in KD experiments. (D) Histogram of up-regulated (Up) and down-regulated (Dn) gene in KD experiments.

(E) Histogram of percentage of genes that contain ≥1 UGCAUG motif conserved in the 3' UTR in human, mouse, rat, dog, and chicken genomes (UGCAUG_5G), ≥1 UGCAUG motif conserved in human and mouse genomes (UGCAUG_2G), or ≥1

GCAUG motif conserved in human and mouse genomes (GCAUG_2G). *** $p < 10^{-15}$ by hypergeometric test.
For additional data, see Figures S1 and S2.

Rbfox1_C but not Rbfox1_N rescues the expression changes induced by double KD of Rbfox1 and 3

To differentiate between the functions of Rbfox1_C and Rbfox1_N, we performed double KD of Rbfox1 and 3 and then rescued with either siRNA resistant Rbfox1_C (Flag-Rbfox1_C_siMt) or Rbfox1_N (Flag-Rbfox1_N_siMt). To facilitate these experiments, we performed them in cultures containing both glia and neurons, rather than in the filter co-culture system (after confirming that selected genes were regulated by double KD in both culture systems, Figure S3). To achieve cell-type specific rescue, we used AAV2/9 vectors with the human synapsin I promoter driving the expression of Flag-Rbfox1_C_siMt and Flag-Rbfox1_N_siMt in neurons (Figures S4A and S4B). The concentrations of virus were adjusted to match the expression of endogenous Rbfox1 and Rbfox3 (Figure S4C). Immunocytochemistry with Flag antibodies revealed that virally expressed Rbfox1_C localized predominantly to the cytoplasm and processes, with low but detectable expression in the nucleus (Figures S4D and S4F), while virally expressed Rbfox1_N localized predominantly in the nucleus, with low levels of detection in the somatic cytoplasm (Figures S4E and S4G). We performed RNAseq on: 1) control cells treated with non-targeting siRNAs and virus expressing EGFP; 2) cells treated with Rbfox1 and 3 siRNAs and virus expressing EGFP; 3) cells treated with Rbfox1 and 3 siRNAs and virus expressing Flag-Rbfox1_C_siMt; and 4) cells treated with Rbfox1 and 3 siRNAs and virus expressing Flag-Rbfox1_N_siMt (Figure S4C).

Strikingly, we found that changes in splicing were induced predominantly by Rbfox1_N while the large majority of changes in mRNA abundance (expression) were regulated by Rbfox1_C. Comparing Rbfox1_N rescue to double KD, we identified 146 up-regulated and 172 down-regulated alternative cassette exons (Figure 3A). Fewer exons were affected by the Rbfox1_C rescue of the double KD: 89 up-regulated and 61 down-regulated alternative cassette exons. Of the exons affected by either Rbox1 isoform, 81% changed in the same direction, and of this set 74% were more strongly affected by Rbfox1_N than by Rbfox1_C (more intense

green and red signal in Figure 3B in the Rbfox1_N column than in the Rbfox1_C column). Exons affected by Rbfox1_C are potentially directly regulated by its low concentrations in the nucleus, or could be indirectly affected by changes in other proteins. An opposite pattern was observed in expression changes: the expression of 275 genes was altered by Rbfox1_C, whereas Rbfox1_N only affected the expression of 49 genes (Figure 3C). Of the genes whose expression was altered by either Rbfox1 isoform, 91% showed the same direction of change, and most of these genes (79%) showed a greater magnitude of change with Rbfox1_C rescue than with Rbfox1_N rescue (more intense green and red signal in Figure 3D in the Rbfox1_C column than in the Rbfox1_N column). These results indicate that Rbfox1_N predominately regulates pre-mRNA splicing, while Rbfox1_C predominately regulates mRNA abundance. We thus focused our subsequent analyses of splicing on the effects of Rbfox1_N and our analyses of overall mRNA abundance on Rbfox1_C.

To define a set of genes whose splicing is regulated by Rbfox1_N for downstream analyses, we selected exons showing opposite changes in splicing between 1) control and double KD and 2) double KD and Rbfox1_N rescue, and filtered for exons whose splicing change reaches statistical significance in either 1) or 2). Using these criteria, we defined 182 Rbfox1 activated exons and 184 Rbfox1 repressed exons in a total of 332 genes as Rbfox1_N splicing targets (Tables S1 and S2). Examining the flanking upstream and downstream introns of these exons, we found that GCAUG motif was the most enriched pentamer in these regions. Consistent with previous studies, the GCAUG motif was particularly enriched in the proximal region of introns downstream of the Rbfox1 activated exons (Underwood et al., 2005; Yeo et al., 2009; Zhang et al., 2008). Next, we examined the frequency of conserved (U)GCAUG motifs in the 3' UTR sequences of transcripts whose expression was altered in double KD compared to control and in Rbfox1_C rescue compared to double KD. Consistent with the results in Figure 2E, genes whose expression was down-regulated by double KD of Rbfox1 and 3 were significantly enriched for conserved (U)GCAUG motifs in their 3' UTRs. Correspondingly, genes whose expression was up-regulated by Rbfox1_C rescue were also enriched for conserved (U)GCAUG motifs in the 3' UTR. This enrichment was not observed in genes whose expression was down-regulated by Rbfox1_C rescue (Figure 3E). We

also compared the transcriptome data obtained by microarray and RNAseq methods. We found that the sets of genes down-regulated by double KD measured by these two methods overlapped significantly (odds-ratio (OR) = 2.97, p = 1.9e-9). There was also significant overlap between the set of down-regulated genes in the KD measured by microarray and the set of genes up-regulated by Rbfox1_C rescue measured by RNAseq (OR = 8.4, p = 1.1e-16). In contrast, we did not observe significant overlap between the up-regulated gene sets in the KD experiments measured by microarray and RNAseq (Figures 2E and 3E). Thus, gene expression changes that positively correlate with Rbfox1_C expression levels are reproducible between assays. These observations support a role for Rbfox1_C in increasing the stability, and thus the abundance of transcripts containing the (U)GCAUG motifs in their 3' UTR.

To define a high confidence set of "expression" targets of Rbfox1_C (those whose mRNA abundance is regulated by Rbfox1_C), as opposed to the set of "splicing" targets of Rbfox1_N defined earlier, we used data from microarray and RNAseq experiments and selected genes that showed opposite changes in expression between 1) control and double KD and 2) double KD and Rbfox1_C rescue, filtering for genes whose change in expression reached statistical significance in either 1) or 2). This identified 613 genes whose mRNA abundance ("expression") was down-regulated by Rbfox KD but up-regulated upon Rbfox1_C rescue and 403 genes whose abundance was up-regulated by Rbfox KD but down-regulated by Rbfox1_C rescue (Table S1). We termed the former "Rbfox1-increased genes" and the latter "Rbfox1-decreased genes" in the set of "expression" targets. A subset of each group was validated by RT-qPCR (Figure S3). We found that Rbfox1-increased transcripts, but not Rbfox1-decreased genes, were significantly enriched for conserved 3'UTR (U)GCAUG motifs (Figure 3E and Table S1, 40% of the Rbfox1-increased genes, $p < 10^{-15}$ by hypergeometric test).

There was no significant overlap between the set of transcripts whose abundance was regulated by Rbfox1_C and the set of transcripts whose splicing was regulated by Rbfox1_N (Figures 3F and S5). The genetic programs controlled by these different Rbfox1 isoforms thus appear to be distinct.

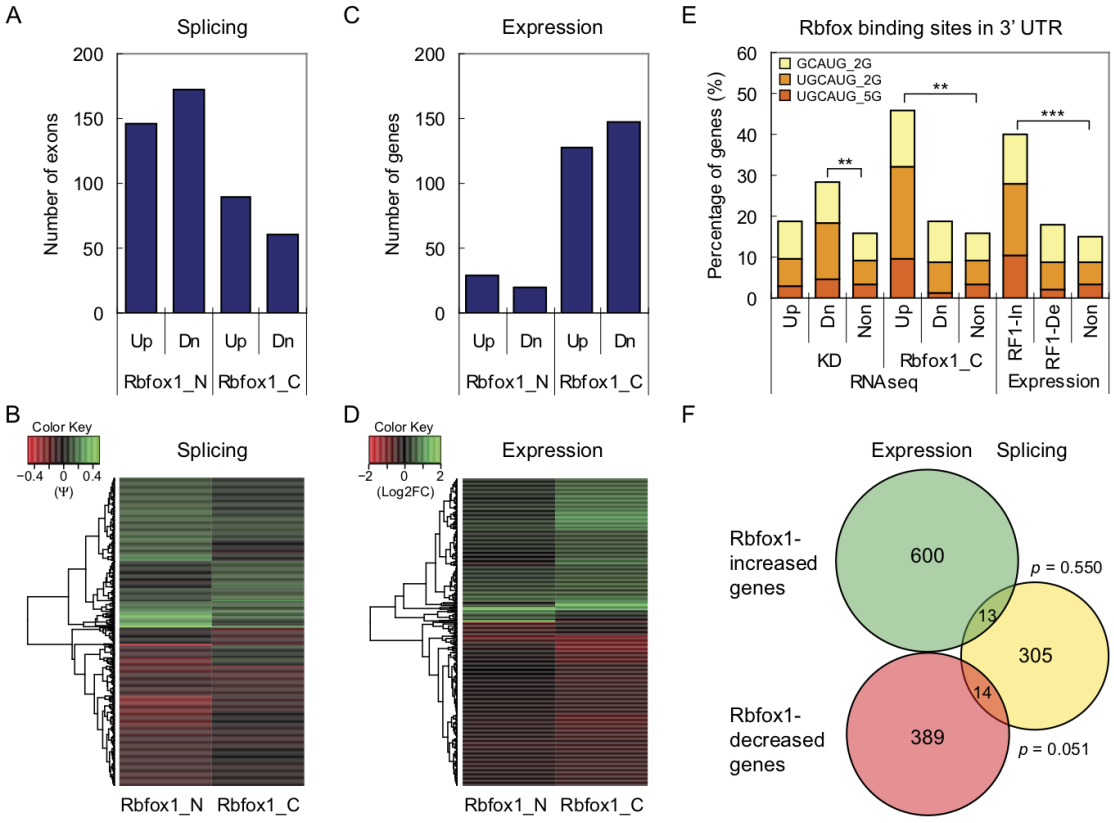

Figure 3. Knockdown and rescue experiments identify distinct functions for Rbfox1_C and Rbfox1_N.

(A) Histogram of up-regulated (Up) and down-regulated (Dn) exons rescued by Rbfox1_N or Rbfox1_C compared to KD. p = 7.74e-15 by Pearson's Chi-squared test with Yates' continuity correction.

(B) Heatmap of the differences in percentage of splicing (□) for the exons in (A).

(C) Histogram of up-regulated (Up) and down-regulated (Dn) genes rescued by Rbfox1_N or Rbfox1_C compared to KD. p = 3.125e-36 by Pearson's Chi-squared test with Yates' continuity correction.

(D) Heatmap of the Log2 fold change (Log2FC) in expression for the genes in (D).

(E) Histogram of the percentage of genes that contain conserved UGCAUG motifs in the 3' UTR. Up = up-regulated, Dn = down-regulated, Non = not changed; In = mRNA concentration increased by Rbfox1, De = mRNA concentration decreased by Rbfox1. * $p < 10^{-5}$, ** $p < 10^{-10}$, and *** $p < 10^{-15}$ by hypergeometric test.

(F) Weighted Venn diagram showing the overlap of genes regulated by Rbfox1 at the level of expression and splicing. *P* values are calculated by hypergeometric test.

For additional data, see Figures S3, S4, and S5.

Rbfox1 proteins bind to the 3' UTR of target mRNAs in the cytoplasm

To identify mRNAs physically bound by Rbfox1, and to assess the location of Rbfox1 binding sites across the transcriptome, we performed iCLIP-seq analysis (Konig et al., 2010). Since our rescue experiments indicated that Rbfox1 has distinct nuclear and cytoplasmic functions (Figures 3A and 3C), we performed subcellular fractionation prior to immunoprecipitation to identify Rbfox1 targets (Figure 4A). We previously found that the majority of unspliced RNA fractionates with chromatin from isolated nuclei (Bhatt et al., 2012; Khodor et al., 2012; Pandya-Jones et al., 2013). To identify the binding of nuclear Rbfox proteins, we generated iCLIP data sets of Rbfox1, 2, and 3 in the high molecular weight (HMW) nuclear fraction containing chromatin, unspliced RNA, and nuclear speckle proteins, and the soluble nucleoplasm (Np) fraction from mouse brains (6 week old male mice). To profile the binding of cytoplasmic Rbfox1 proteins, we performed iCLIP on a cytoplasmic (Cy) fraction of cultured mouse neurons (DIV14). The analyses in this paper focus on the cytoplasmic fraction, and use the soluble Np and HMW fractions for comparison.

Immunoblotting showed that the soluble Np fraction from mouse brain was depleted of the cytoplasmic marker GAPDH and contained the nuclear marker U1-70K (Figure 4B). Both Rbfox1_C and Rbfox1_N isoforms were observed in the HMW and Np fractions. The ER marker protein calnexin was also detected in the soluble Np fraction, suggesting that ribosome-loaded mRNA transcripts associated with the ER copurified with the nuclei (Bhatt et al., 2012). To obtain sufficient material for the Cy fraction, we used forebrain neurons rather than hippocampal neurons. Immunoblot analysis showed that the Cy fraction was enriched for the cytoplasmic protein GAPDH and lacked the nuclear marker U1-70K (Figure 4C).

Following UV crosslinking and cellular fractionation, we immunoprecipitated Rbfox1 with the Rbfox1-specific monoclonal antibody 1D10 and used anti-Flag antibodies as a negative control. We sequenced the RNA fragments crosslinked to immunoprecipitated Rbfox1 and obtained 2.2 and 3.2 million unique Rbfox1 iCLIP tags from the Np fraction and the Cy fraction, respectively (Table S3). These iCLIP tags were mapped to the longest transcript of each gene in the UCSC Known Gene Table (Hsu et al., 2006). In iCLIP, the UV crosslink site is located one nucleotide (nt) upstream of the 5' end of the aligned iCLIP tag. To define reproducible and clustered crosslink sites, the probability of each site was calculated based on the number of

tags mapping to that particular crosslink site compared to random sites. Crosslinked sites with an FDR < 0.01 were selected, and those located within 20 nts of one another were clustered. Clusters with width > 1 nt were used for downstream analyses. With these criteria, significant iCLIP clusters were identified in the Rbfox1 Np and Cy fractions, comprised of 136,483 and 162,916 tags respectively (Table S3).

For the Rbfox1 Cy fraction, 78% of the clustered tags mapped to the 3' UTR and 17% mapped to introns (Figure 4D). The distribution of mapped tags from the Np fraction was similar to that in the Cy fraction. In contrast, 93% of the Rbfox1 clustered tags mapped to introns in the HMW nuclear fraction. By comparison, analysis of Rbfox targets in whole cells in mouse brain reported that about 70% of clustered tags mapped to introns and that 20% to 27% mapped to 3'UTR (Lovci et al., 2013; Weyn-Vanhentenryck et al., 2014).

To evaluate the specificity of the iCLIP data, we examined the enrichment of pentamer motifs in the sequences surrounding Rbfox1 crosslinking sites in 3' UTRs. In the Cy fraction, GCAUG was the most enriched pentamer within the sequence extending 40 nucleotides on either side of the crosslink site. The 50 most-enriched pentamers also included 6 that differed by one nucleotide from GCAUG, suggesting that Rbfox1 can bind to sub-optimal GCAUG motifs *in vivo*, as has been seen by others (Lambert et al., 2014).

As in the Cy fraction, GCAUG was also the most enriched pentamer for Rbfox1 in the Np fraction, and the rankings of pentamers were highly correlated between the Cy and the Np fractions (Figure 4E; $\rho = 0.83$, $p < 2.2 \times 10^{-16}$, Spearman correlation). Interestingly, several U-rich motifs were more enriched in the Np than in the Cy fraction. This could be caused by differences in Rbfox1 interacting proteins in different cellular compartments. The Rbfox1 iCLIP pentamers were also highly correlated with Rbfox2 and Rbfox3 iCLIP pentamers in the Np fraction, as expected from their similar RNA binding properties (data not shown). The extensive overlap of 3' UTR iCLIP clusters from the soluble Np and Cy fractions indicates that Rbfox likely binds fully processed mRNAs in the nucleus and accompanies them to the cytoplasm.

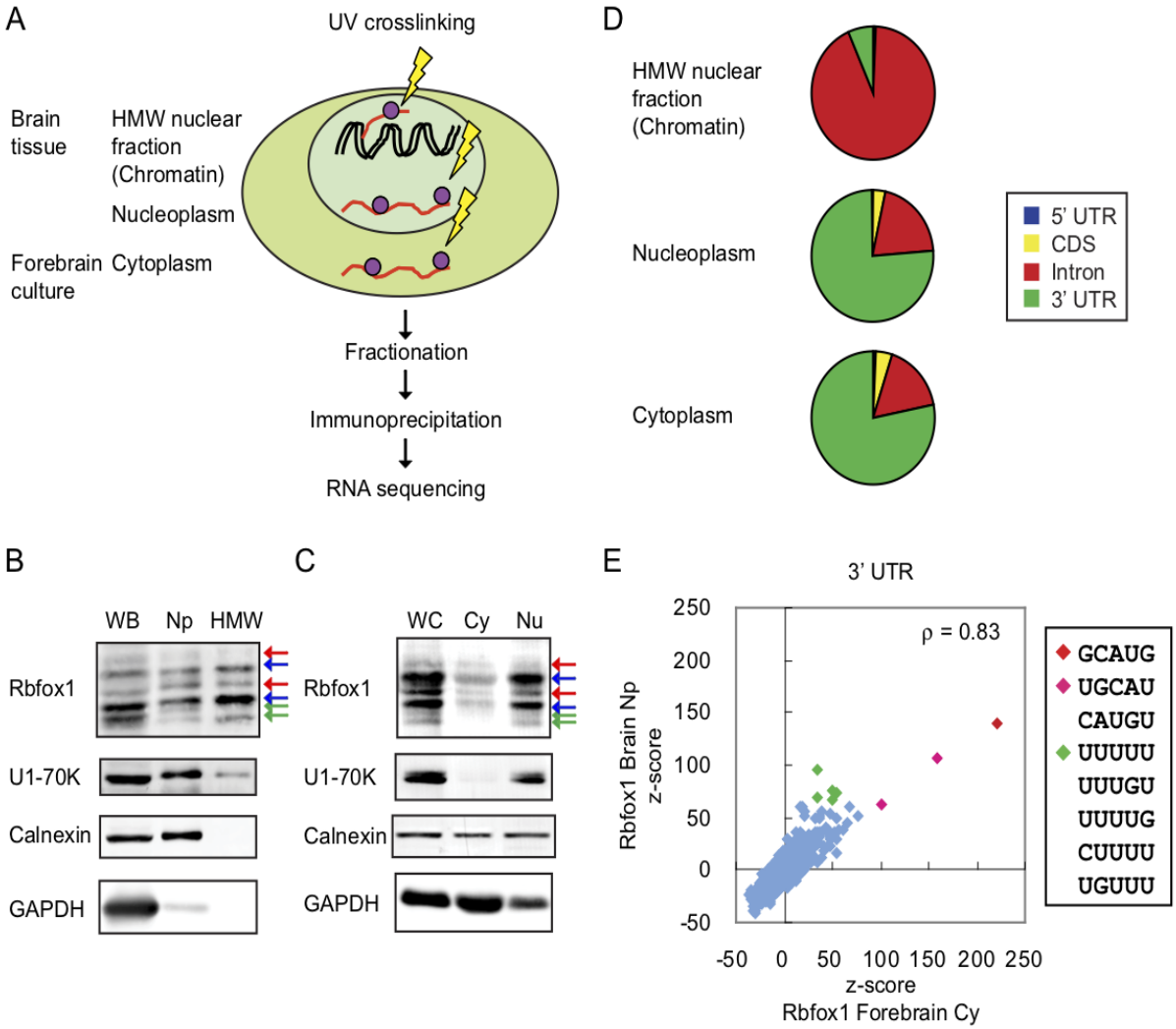

Figure 4. Characterization of Rbfox1 iCLIP tags in the 3' UTR

(A) Illustration of iCLIP experimental workflow. HMW: high molecular weight nuclear fraction that contains chromatin and unspliced RNA.

(B, C) Immunoblot analysis of purity of the fractions. WB: whole brain; Np: nucleoplasm; HMW: high molecular weight nuclear fraction containing chromatin; WC: whole culture; Cy: cytoplasm; Nu: nucleus.

(D) Pie charts of the percentage of Rbfox1 clustered tags mapped to 5' UTR, coding sequence (CDS), intron, and 3' UTR in different iCLIP experiments.

(E) Scatter plots of the z-scores of pentamers around the Rbfox1 crosslink sites in the 3' UTR in the cytoplasm and nucleoplasm.

Cytoplasmic Rbfox1 increases the expression levels of iCLIP target genes

We next characterized the properties of the iCLIP clusters. We defined clusters ("GCAUG clusters") as high confidence Rbfox binding sites *in vivo* if they contained at least one GCAUG motif within 10 nts upstream or downstream of the cluster. Binding of Rbfox1 within a GCAUG cluster is illustrated by the mapped clusters in the Camta1 3' UTR (Figure 5A). Camta1 was identified as an Rbfox1-increased gene in the KD and rescue experiments. Ten cytoplasmic Rbfox1 iCLIP clusters were identified in its 3' UTR and 5 of them overlapped with conserved GCAUG motifs, indicating direct binding of Rbfox1 to these sites (Figure 5A). The first Rbfox1 cluster in the Camta 3'UTR did not overlap with a GCAUG motif, but had a sub-optimal GCAcG motif, suggesting that this cluster also reflected a direct Rbfox1 binding site. Other clusters that did not directly overlap with a GCAUG motif were located within 50 nts of GCAUG motifs, suggesting that crosslinking at these sites might result from an Rbfox1 interaction with a GCAUG motif.

Examining the distribution of GCAUG clusters in cytoplasmic Rbfox1 target transcripts, we found that GCAUG clusters were enriched at the 5' and 3' ends of the 3' UTRs (Figure 5B). Similar 5' and 3' enrichment has been observed for proteins and miRNAs controlling mRNA stability and translation (Bartel, 2009; Boudreau et al., 2014; Chi et al., 2009). The binding of Rbfox1 to these regions is consistent with our observations of cytoplasmic Rbfox1 affecting mRNA abundance. We defined a set of 3' UTR target genes as containing at least one significant iCLIP cluster and a total of 11 tags in their 3' UTRs. Of these 1490 genes identified in the Cy fraction, 788 (53%) contained a cluster with a GCAUG motif (Table S2). In the Np fraction, 915 genes were identified as Rbfox1 3' UTR target genes in brain tissue. Of these genes, 400 (44%) contained GCAUG clusters in 3' UTR (Table S4 and Figures S6A and S6B).

We next asked whether Rbfox1-mediated changes in mRNA abundance correlated with Rbfox1 binding to the 3' UTR. We found that Rbfox1-increased genes were significantly enriched for genes containing 3' UTR clusters compared to non-regulated genes (23%, $p < 10^{-15}$, hypergeometric test, Figure 5C). In contrast, Rbfox1-decreased genes were not enriched for Rbfox1 iCLIP targets. Subdividing iCLIP target genes into those with or without a GCAUG cluster in the 3' UTR, we found those with GCAUG clusters were enriched in Rbfox1-increased genes. These

results indicate that Rbfox1 binding to 3' UTR GCAUG motifs increases the level of the target mRNAs in the cytoplasm. While binding of Rbfox1 to mRNAs lacking 3' UTR GCAUG motifs were identified by iCLIP, these interactions were not correlated with any changes in mRNA abundance. We thus focused on iCLIP targets with GCAUG clusters and used these as high confidence Rbfox1 binding targets for downstream analyses.

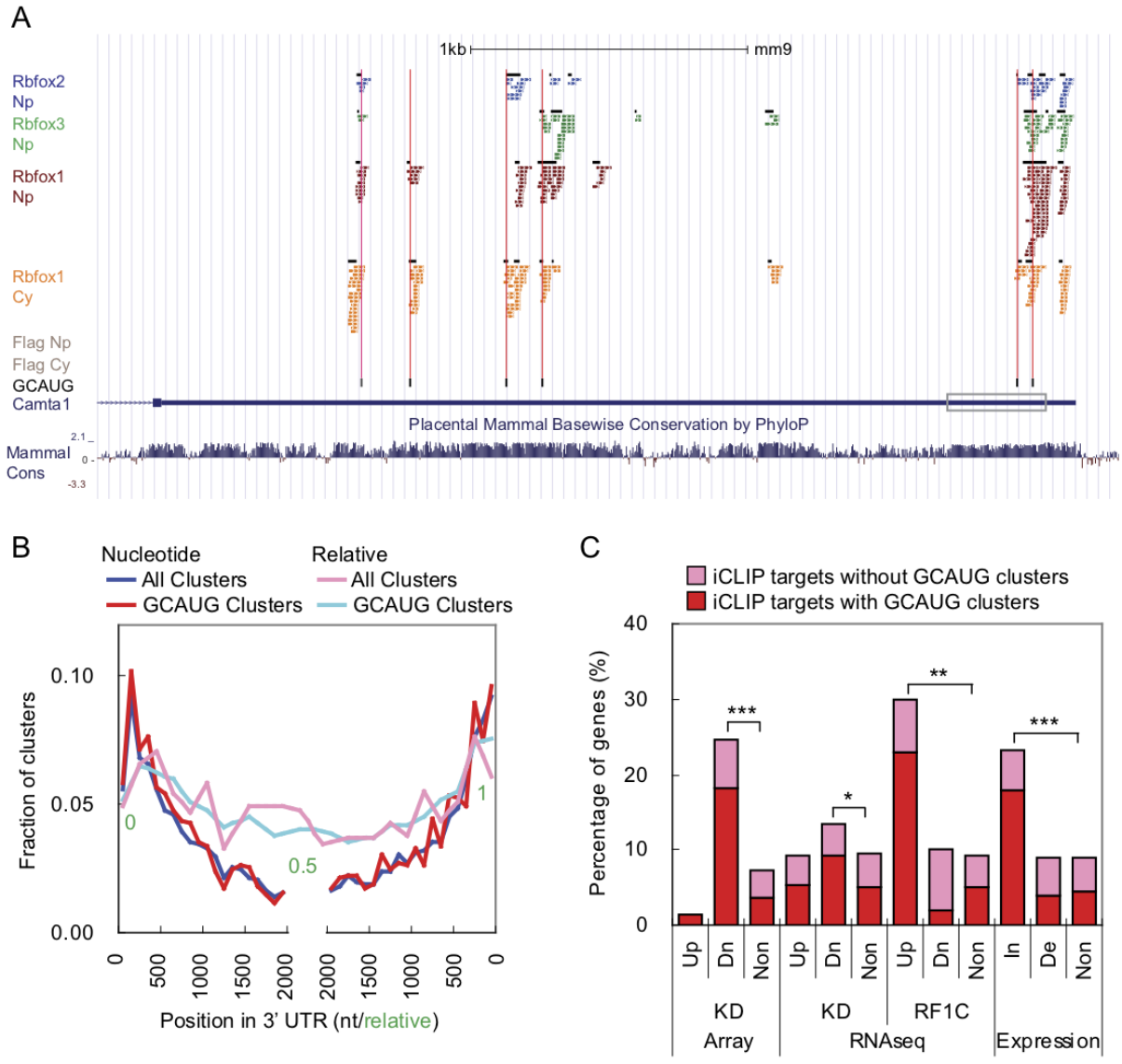

Figure 5. Identification of Rbfox1 iCLIP 3' UTR target genes

(A) Screenshot of UCSC genome browser showing iCLIP tags and clusters (black box) in Camta1 3' UTR. GCAUG motifs are underlined in black and a UGCAcG motif is underlined in gray. The boxed region indicates the part of 3' UTR subcloned to the luciferase reporters in Figure 6A.

(B) The distribution of the clusters within binned 3' UTR locations relative to the 5' and 3' ends shown as nucleotide (nt) and relative positions.
(C) Histogram of the percentage of genes that contain iCLIP clusters in the 3' UTR in different experiments. Up: up-regulated in the experiment; Dn: up-regulated in the experiment; In: mRNA increased by Rbfox1; De: mRNA decreased by Rbfox1. * $p < 10^{-5}$, ** $p < 10^{-10}$, and *** p value $< 10^{-15}$ by hypergeometric test.

For additional data, see Figure S6.

Binding of Rbfox to 3' UTR GCAUG motifs in the cytoplasm increases target mRNA concentration and translation

We next tested whether binding of Rbfox1 to the 3' UTR was sufficient to alter target mRNA concentration and translation. We focused on Camk2a because of its roles in memory and in synaptic plasticity (Lisman et al., 2002). Both Camk2a mRNA and protein were decreased by approximately 40% upon Rbfox1 and 3 KD (Figure S2). The Camk2a 3' UTR is 3372 nt long and contains five GCAUG motifs. Two of the five motifs overlapped with Rbfox1 iCLIP clusters (Figure S6C). We coexpressed a luciferase reporter gene containing the full length Camk2a 3' UTR (Figure 6A) with Rbfox1 in HEKT cells and found that Rbfox1_C but not Rbfox1_N induced a 70% increase in luciferase activity (Figure 6B). To test the role of the Rbfox binding sites, we generated a reporter containing a shorter 1.1 kb fragment of the Camk2a 3' UTR and deleted the 4 (U)GCAUG motifs within this fragment (Figure 6A). When the wildtype Camk2a reporter was coexpressed with Rbfox1_C or Rbfox1_N in HEKT cells, a two-fold increase of luciferase activity was observed with Rbfox1_C but not with Rbfox1_N (Figure 6C). RT-qPCR analysis of the luciferase mRNA revealed a somewhat smaller increase in mRNA, indicating that the change in luciferase expression is at least partially due to changes in mRNA stability. Deletion of the (U)GCAUG motifs abolished the Rbfox1_C-induced increase in luciferase activity and in reporter mRNA levels.

Cell fractionation and overexpression data indicated that a portion of Rbfox1_N is cytoplasmically localized (Figures 1D and S4G). This motivated us to test the activity of Rbfox1_N in the cytoplasm by deleting the NLS peptide sequence FAPY (Rbfox1_NdNLS, Figure 6E). Coexpression of Rbfox1_NdNLS with a luciferase reporter gene containing part of the Camta1 3' UTR (containing iCLIP GCAUG clusters) revealed that the mutant, cytoplasmically localized Rbfox1_NdNLS

significantly increased luciferase activity of the reporter (Figure 6F). Alternative splicing of exon 15 of Rbfox3 also generates a cytoplasmically localized Rbfox3_SC isoform (short cytoplasmic Rbfox3) (Kim et al., 2009b). We found that Rbfox3_SC also increased luciferase activity when expressed with the Camta1 3'UTR luciferase reporter (Figure 6F). Together, these results indicate that multiple isoforms of Rbfox1 or 3 can increase mRNA concentration and promote translation as long as they localize to the cytoplasm.

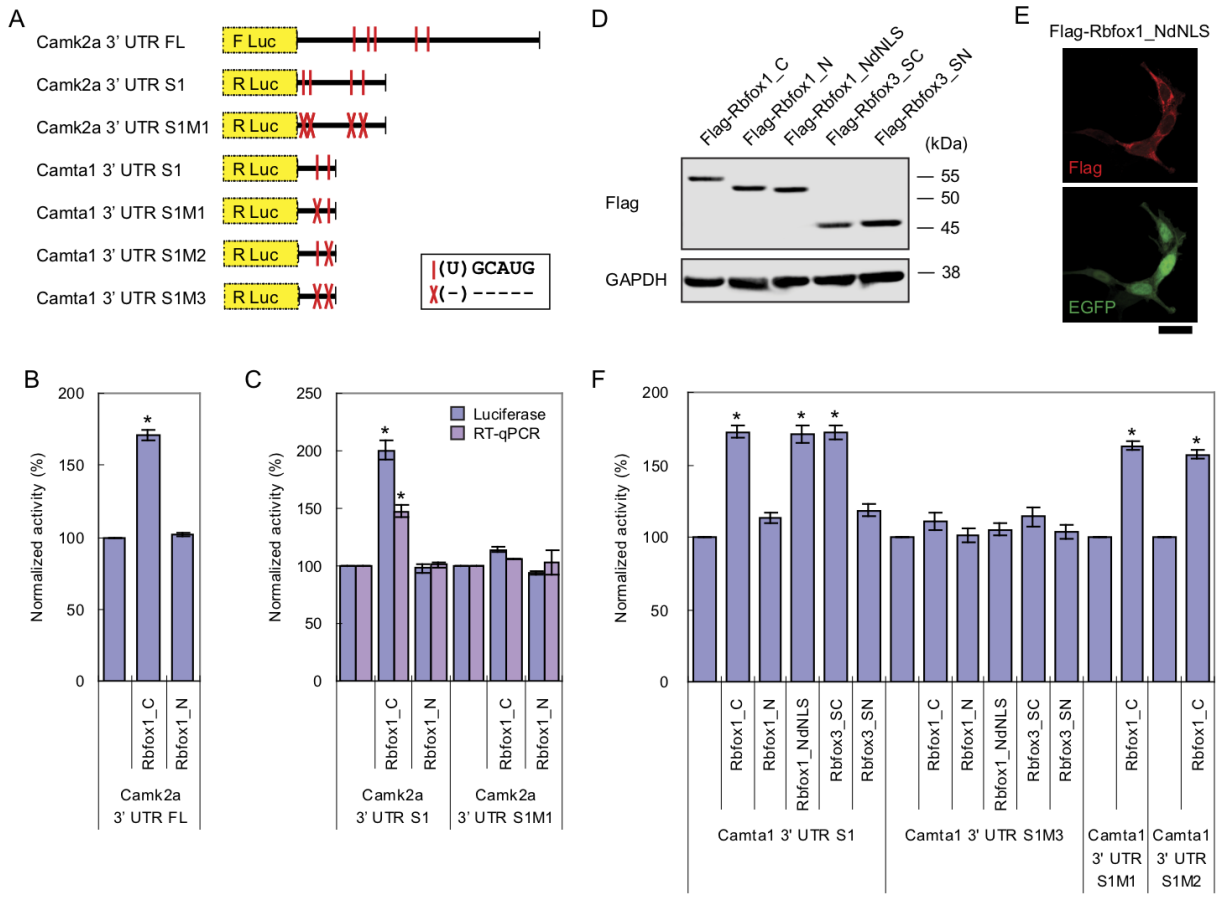

Figure 6. Rbfox1 and Rbfox3 proteins increase gene expression by binding to the 3' UTR

(A) Diagram depicting the luciferase reporters containing part of Camk2a 3' UTR or Camta 3' UTR as labeled in Figures S6 and 5A, respectively. (U)GCAUG motifs are denoted by vertical red lines, with red crosses marking deletion of these motifs.

(B) Histogram of normalized luciferase activity of the reporter containing full length (FL) Camk2a 3' UTR when coexpressed with Rbfox1_C or Rbfox1_N in HEKT cells. Error bars indicate SD. * $p < 0.001$ by student's t-test. N = 3.

(C) Histogram of normalized luciferase activity and mRNA concentration (RT-qPCR) of Camk2a 3' UTR S1 reporters when coexpressed with Rbfox1_C or Rbfox1_N in HEKT cells. Error bars indicate SD. * $p < 0.001$ by student's t-test. N = 3.

(D) Immunoblot showing of Rbfox1 and Rbfox3 splice isoforms and a mutant expressed in HEKT cells. dNLS = delete nuclear localization signal, SC = short cytoplasmic isoform, and SN = short nuclear isoform.
(E) Immunocytochemistry of Flag-Rbfox1_NdNLS detected with anti-Flag antibodies (red) and the whole cell labeled with EGFP (green) in HEKT cells. Scale bar = 20 □m.
(F) Histogram of normalized luciferase activity of Camta1 3' UTR S1 reporters when coexpressed with Rbfox1 or Rbfox3 isoform or mutant in HEKT cells. Error bars indicate SD. * $p < 0.001$ by student's t-test. N = 3.

Rbfox1_C increases the expression of genes affecting synaptic activity and autism

To define a high confidence set of genes whose expression is directly regulated by Rbfox1 in the cytoplasm, we combined our iCLIP data with the transcriptome data to identify genes that had opposite expression changes in the KD and Rbfox1_C rescue experiments and that had cytoplasmic Rbfox1 iCLIP GCAUG clusters in their 3' UTRs. The overlap between Rbfox1-increased genes and iCLIP target genes was highly significant, whereas the overlap between Rbfox1-decreased genes and iCLIP targets was not significant (Figure 7A). These analyses identified a set of 109 directly bound Rbfox1-increased transcripts for downstream functional analyses (Table S5).

Gene ontology (GO) analysis of the Rbfox1 regulated genes shown in Figure 3F and 7A revealed that the Rbfox1-increased genes and iCLIP 3' UTR targets were enriched for terms of transmission of nerve impulse and synaptic transmission (Figure 7B and Table S6). These enrichments were even greater in the high confidence set of 109 direct Rbfox1_C-increased genes. Analyzing the 109 genes using the Kyoto Encyclopedia of Genes and Genomes (KEGG) revealed a significant enrichment for calcium signaling pathways, including 4 CaM kinases (Camk2a, Camk2b, Camk2g, and Camk4) and one calcineurin B (Ppp3r1) (Table S7). Enrichment analysis using Mammalian Phenotype Ontology (Smith and Eppig, 2012) revealed that the 109 direct Rbfox1_C-increased genes were enriched for phenotypes related to seizure (Table S8). Together, these results indicate that Rbfox1_C target mRNAs play an important role in controlling synaptic activity, in particular via the calcium-signaling pathway.

We next compared Rbfox1-regulated genes to modules within a gene co-expression network derived from human cortical gene expression data from fetal brain to 3 years of postnatal development. Three of these coexpression modules, devM13, devM16, and devM17, were enriched for the GO term of synaptic transmission, as well as ASD susceptibility genes (Parikshak et al., 2013). As shown in Figure 7C, we found that the 109 direct Rbfox1_C-increased genes were highly enriched in the same three synaptic modules. To directly examine the correlation with ASD, we compared the direct Rbfox1_C-increased genes to several sets of ASD candidate genes and found that the Rbfox1_C-increased genes were enriched in an ASD coexpression module (asdM12) that is down regulated in post mortem cerebral cortex from patients with ASD (Figure 7C) (Voineagu et al., 2011). Notably, Rbfox1 was characterized as a hub gene in asdM12 and while its putative splicing targets were only modestly enriched, it was subsequently hypothesized to increase the mRNA stability of these ASD genes (Ray et al., 2013). Our finding that genes whose expression was directly increased by Rbfox1_C were significantly enriched for these ASD related genes supports this hypothesis. Rbfox1_C-increased genes also showed high enrichment of Fragile X mental retardation protein (FMRP) targets (Darnell et al., 2011), further connecting post-transcriptional regulation with ASD biology. The substantially stronger correlation of the ASD module with cytoplasmic Rbfox1 regulation than with its nuclear splicing targets underscores the need to understand this portion of the Rbfox1 program.

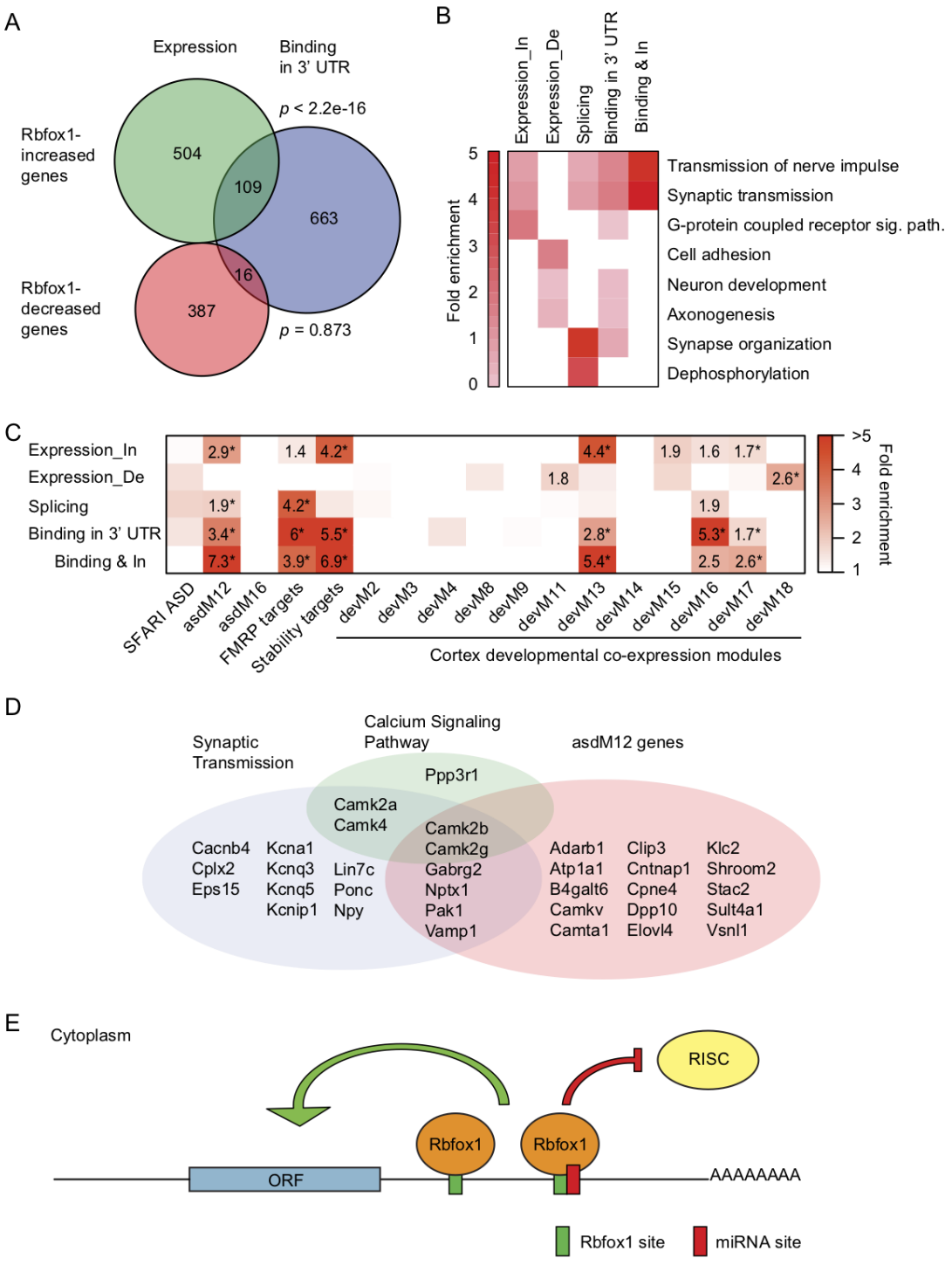

Figure 7. Rbfox1 increases the expression level of autism genes in the cytoplasm

(A) Weighted Venn diagram showing the overlap of genes whose expression is increased or decreased by Rbfox1 and iCLIP target genes with Rbfox1 bound in 3' UTR. *P* values calculated by hypergeometric test.

(B) Heatmap of the fold enrichment of GO terms in different experiments. In = increased. De = decreased. Sig. path. = signaling pathway.
(C) Heatmap of the enrichment of Rbfox1 regulated genes in gene sets of candidate autism genes ,SFARI ASD (Basu et al., 2009), ASD-associated co-expression modules from human cortex ,asdMs (Voineagu et al., 2011), FMRP targets (Darnell et al., 2011), Rbox1 3' UTR stability targets (Ray et al., 2013), and co-expression modules from fetal cortex ,devMs (Parikshak et al., 2013). All enrichment values for overrepresenting sets with odds ratio > 1.5 are shown. * FDR adjusted two-sided Fisher's exact test p value < 0.05.
(D) Venn diagram showing the overlap of direct Rbfox1_C -increased genes in three functional categories.
(E) A model for the cytoplasmic function of Rbfox1 in neurons. Rbfox1 binds to the 3' UTR of target mRNAs and increases their concentration in the cytoplasm of neurons. Rbfox1 binding is predicted to antagonize miRNA binding to a miRNA binding site overlapping or neighboring an Rbfox1 binding site in the 3' UTR. For additional data, see Figure S7.

Rbfox1_C may compete with microRNAs to regulate mRNA stability and translation

Several RBPs have been shown to regulate microRNA (miRNA) activity by binding to the 3' UTRs of target mRNAs (Ciafre and Galardi, 2013; Srikantan et al., 2012; Xue et al., 2013). Since Rbfox1 showed an opposite activity to that of miRNAs, but exhibited similar enriched binding at the 5' and 3' ends of 3' UTR (Boudreau et al., 2014; Chi et al., 2009), we hypothesized that the binding of Rbfox1 may interfere with the binding of miRNAs and thereby antagonize miRNA activity. To test this hypothesis, we compared the Rbfox1 iCLIP data to an Ago CLIP dataset generated from P13 mouse neocortex (Chi et al., 2009). We searched for miRNA binding sites located within 50 nucleotides of the Rbfox1-bound GCAUG motifs (Tables S9). Since one Rbfox1 binding site can be close to multiple miRNA sites and vice versa, the number of single Rbfox1 site and miRNA site pairs with the same 50 nt interval was counted. By this criterion, 196 pairs of Rbfox1 and miRNA sites were identified. This number was significantly higher than the number of pairs identified after randomization of miRNA sites within the same 3' UTR where the miRNA sites were identified, indicating that the proximity of Rbfox1 binding sites to miRNA sites within the 3' UTR was not by chance (Figure S7A, z score = 5.38). These 196 pairs

included 173 miRNA sites and 109 GCAUG motifs in 87 genes (Table S10). We found that Rbfox1-bound GCAUG motifs were more conserved than GCAUG motifs present in the same 3' UTR but not bound by Rbfox1 (Figure S7B). The conservation scores of GCAUG motifs and their flanking sequences were greater for Rbfox1-bound GCAUG motifs that were adjacent to or overlapping a miRNA site, indicating that the colocalization is under high selection pressure, consistent with it playing an important role in the regulation of gene expression. The Ago CLIP data used here identified the binding sites of the 20 most abundant miRNAs (Chi et al., 2009). We found that 14 of these 20 miRNA sites overlapped with a GCAUG motif in at least one 3' UTR (Figure S7C). For example, the Camk2a 3' UTR was found to contain 11 miRNA binding sites, three of which, miR-26, miR-124, and miR-30 binding sites, were located within 50 nucleotides of the most upstream GCAUG motif bound by Rbfox1 (Figures S6C and S7C), with the miR-124 site overlapping with the GCAUG motif. In the context of our data showing that Rbfox1 binding stabilizes mRNAs and promotes translation (Figure 6), this finding suggests that Rbfox1 blocks Ago binding to these three miRNA sites. Within the 50 nts surrounding the GCAUG motif, the number of miRNA seed sites was greatest in regions overlapping the GCAUG motif and gradually decreased with distance from GCAUG motif (Figure S7D), indicating that the miRNA sites were concentrated in regions in which Rbfox1 would be expected to interfere with miRNA binding.

3.1.4. DISCUSSION

A cytoplasmic function for Rbfox proteins

The goal of this study was to delineate the function of cytoplasmic Rbfox. Using KD and rescue approaches together with Rbfox1 iCLIP of subcellular neuronal fractions, we identified 109 genes whose abundance was directly regulated by Rbfox1_C. Our data indicate that cytoplasmically localized Rbfox1 promotes the stability and/or translation of target transcripts by binding to their 3' UTRs (Figure 6). We also show that cytoplasmic Rbfox1 targets are enriched in human cortical development modules affecting synaptic function and ASD (Figure 7C). Our findings highlight the importance of considering the cytoplasmic arm of Rbfox1 regulation in linking Rbfox1 to synaptic function and to neurodevelopmental disorders such as ASD.

We focused on one nuclear and one cytoplasmic Rbfox1 isoform, but there are others. Using a monoclonal antibody 1D10 that targets the N-terminal sequence of Rbfox1 and a polyclonal antibody against Rbfox RRM (Figure 1D), we detected six Rbfox1 bands ranging from 45 and 55 kDa that were all reduced by a pan-Rbfox1 siRNA (Figure 1B), and eliminated in the Rbfox1 KO mouse (data not shown). Two of these bands were eliminated by an siRNA targeting the exon of the cytoplasmic isoforms (Figure 1B). We previously found that the two of the middle bands likely represent N-terminally cleaved Rbfox1 isoforms (Lee et al., 2009). Additional bands of Rbfox1 may represent differentially phosphorylated proteins. The diverse species of Rbfox1 imply many levels of regulation and/or function. It will be interesting to examine whether and how neuronal activity regulates Rbfox1 splicing, proteolysis and/or post-translational modifications, as such modifications could alter Rbfox1 regulation of gene expression.

Over 90% of the changes in mRNA level detected by microarray analysis represented decreases in expression induced by KD of Rbfox1 and 3, reflecting a role for Rbfox in stabilizing mRNAs (Figure 2D and Table S1). In contrast, the RNAseq experiments identified more similar numbers of up and down-regulated genes (Figure 3C), although significantly more down-regulated genes contained (U)GCAUG sequences in their 3'UTRs. One difference that could lead to differences in the gene expression was that the microarray analyses were performed on pure neurons cultured with glial cells in inserts, while the RNAseq analyses were performed on mixed neuronal-glial cultures. Thus, the cell environment and culture conditions may be reflected in the transcriptome analyses. We addressed this variation by considering all of our datasets together – including the KD in both culture conditions, the rescue experiments, and the iCLIP target sets (Table S1) – and focused on genes that showed consistent changes in all of the experiments. Most importantly, we focused on transcripts that underwent opposite directions of regulation in the KD and Rbfox1_C rescue experiments and that were bound by Rbfox1 in iCLIP experiments. The results of these analyses identify a large class of transcripts whose expression was positively regulated by Rbfox1_C (Table S5). There may yet be some transcripts that are negatively regulated by Rbfox1, but these will require additional experiments to identify.

Our data add to a growing literature revealing the multifunctionality of RBPs (Bielli et al., 2011; Heraud-Farlow and Kiebler, 2014; Turner and Hodson, 2012; Vanharanta et al., 2014). The differences in activity between Rbfox1 isoforms are reflected in the iCLIP data. While the majority of the Rbfox1 binding was detected in introns in the HMW fraction, the binding of Rbfox1 shifted to 3' UTR when assayed in the soluble nucleoplasm and the cytoplasm. Although not always specifically localized to the nucleus or cytoplasm, other RNA binding proteins have been found to bind introns to affect splicing, as well as 5' or 3' UTRs to affect translation (Ince-Dunn et al., 2012; Licatalosi et al., 2008; Xue et al., 2009). In many cases, it is not clear how these functions are segregated and whether different isoforms are involved or differently modified. In the case of Rbfox1 and Rbfox3, the nuclear and cytoplasmic functions arise at least in part from differentially spliced isoforms. We note, however, that some Rbfox1_N is constitutively present in the cytoplasm (Figure 1D), and that a low but detectable amount of Rbfox1_C is present in the nucleus. The finding that the NLS deleted Rbfox1_N mutant can regulate stability and translation of target mRNAs (Figure 6F) indicates that the primary determinant of target mRNA regulation in the cytoplasm is simply cytoplasmic localization of Rbfox1 rather than any other feature of the Rbfox1_C or Rbfox1_N.

Several RBPs are known to regulate mRNA stability using different mechanisms. For example, HuR proteins and Ataxin-2 proteins can bind to AU-rich elements (AREs) in the 3' UTR and stabilize target mRNAs (Lebedeva et al., 2011; Mukherjee et al., 2011; Yokoshi et al., 2014), while PTB and hnRNP L compete with miRNA binding in the 3' UTR and stabilize target mRNAs (Rossbach et al., 2014; Xue et al., 2013). HuR can stimulate or inhibit miRNA binding and thus regulate mRNA decay (Kim et al., 2009a; Young et al., 2012). Our results show that Rbfox1 proteins can increase mRNA concentration in the cytoplasm, and suggest that one mechanism for this is to stabilize mRNAs by competing with miRNA binding. However, this mechanism is likely only active on a subset of Rbfox1 target transcripts. For example, we find that Rbfox1 increased expression of the luciferase Camta1 3' UTR reporter (Figure 6F), which lacks identified miRNA binding sites. In *Xenopus Oocytes*, Rbfox2 (XRbm9) is exclusively expressed in the cytoplasm and directly interacts with XGld2 in the cytoplasmic polyadenylation complex to promote translation (Papin et al., 2008). Identification of the cytoplasmic interacting partners of

Rbfox1 may provide insights into the molecular mechanisms of cytoplasmic Rbfox1 regulation.

Rbfox1_C regulates genes involved in synaptic function, calcium signaling, and autism.

Recent studies have focused attention on Rbfox1 as a critical regulator of gene expression in cortical development (Parikshak et al., 2013; Weyn-Vanhentenryck et al., 2014), and as a candidate ASD susceptibility gene (Fogel et al., 2012; Martin et al., 2007; Sebat et al., 2007; Voineagu et al., 2011; Weyn-Vanhentenryck et al., 2014). While these studies focused on Rbfox1's role as a splicing factor, we show that the mRNAs that are regulated by Rbfox1_C are significantly enriched for genes involved in cortical development and autism (Figure 7C) (Parikshak et al., 2013; Voineagu et al., 2011). In a coexpression analysis of the brain transcriptome from patients with autism, RBFOX1, CNTNAP1, CHRM1, APBA2 were identified as 4 hub genes, genes that are defined as being highly connected in the ASD-associated co-expression module, asdM12. These four genes, along with SCAMP5 and KLC2, were ranked highest in this module (Voineagu et al., 2011). Here, we show that Rbfox1 bind the 3'UTRs of CNTNAP1, CHRM1, SCAMP5 and KLC2 transcripts, and that CNTNAP1 and KLC2 mRNA levels are both increased by Rbfox1_C (Table S1). These results suggest that Rbfox1 is upstream of the two hub genes, CNTNAP1 and CHRM1, in a molecular pathway that is altered in autism. Mutations in FMRP are the most common single gene cause of autism (Talkowski et al., 2014), and we find that Rbfox1 3' UTR target genes overlap significantly with FMRP target genes (Darnell et al., 2011). Together, these results link gene expression changes associated with sporadic autism with a single gene cause of autism. Our findings thus add to the emerging recognition that post-transcriptional RNA metabolism plays a critical role in cortical development and neurodevelopmental disorders (Darnell and Richter, 2012).

We find that Rbfox1_N and Rbfox1_C regulate two different sets of genes (Figure 3F). Both sets are enriched for the same GO terms of transmission of nerve impulse and synaptic transmission, but their targets can be quite different. For example, in the CaM kinase family, the splicing of Camk2d is regulated by Rbfox1_N. However, the expression of Camk2a, Camk2b, and Camk4 is regulated by

Rbfox1_C, and Camk2g is regulated both at the level of splicing by Rbfox1_N and at the level of expression by Rbfox1_C (Figure S5). Taken together, our results identify a coherent and intricate gene network regulated by two distinct Rbfox1 splice isoforms and exemplify the functional consequences of alternative splicing for this RNA binding protein. The existence of multiple additional Rbfox1, Rbfox2 and Rbfox3 isoforms and variants indicates that our analysis likely uncovers only a fraction of the total complexity of Rbfox-mediated RNA regulation. Understanding the mechanisms by which RBP mutations give rise to neural circuit abnormalities and disease will require consideration of their multiple functions in RNA metabolism, in the nucleus and in the cytoplasm.

3.1.5. EXPERIMENTAL PROCEDURES

Tissues for Immunoblotting and RT-PCR

All experiments with animals were performed using approaches approved by the UCLA Institutional Animal Care and Use Committee. Hippocampi and cortices at postnatal day 0 (P0) and 3 weeks were dissected from C57BL/6J mice. Protein was purified from half of the tissues for immunoblotting. RNAs were purified from the other half of the tissues for RT-PCR analysis.

Subcellular Fractionation of Neuronal Cultures

Hippocampal cultures used in Figure 1 were prepared from postnatal day 0 C57BL/6J mice (Jackson Laboratory) as previously described (Ho et al., 2014) and incubated with 2 □M Cytosine beta-D-arabinofuranoside (AraC) (Sigma Aldrich, c1768) from postnatal day 3 to day 6. On day 13, the cultures were incubated with 15 □M of digitonin (Sigma Aldrich, D141-100MG) and complete protease inhibitor (Roche #05892791001) in 1X PBS buffer for 3 minutes at room temperature to permeabilize the cells and the eluate was collected as the cytosol fraction. An equal volume of RIPA buffer was then used to completely lyse the cells.

RNAi Knockdown in Neuronal Cultures

Primary mouse hippocampal and cortical cultures were prepared from postnatal day 0 C57BL/6J mice. 160,000 hippocampal cells were plated in one 12-well well and 120,000 cortical cells were plated in a cell culture insert with pore size

of 3 □m (Corning Life Sciences, 353181). On day 3, hippocampal cultures were incubated with 2 □M AraC for 3 days and then co-cultured with the cortical culture from day 6. Two Rbfox1 and two Rbfox3 Accell siRNAs (Dharmacon, sequences in Supplemental Information) were added to the co-culture on day 10 at a total concentration of 1.2 mM and incubated for 4 days prior to RNA and protein extraction.

Microarray

RNA from three biological replicates for each condition was probed for gene expression and alternative splicing changes using Affymetrix MJAY microarrays (Affymetrix). Array analysis was performed using the OmniViewer method (http://metarray.ucsc.edu/omniviewer/) (Sugnet et al., 2006).

Adeno-Associated Virus (AAV) 2/9 Transduction, RNAi, cDNA Library Preparation, and RNA Sequencing

The siRNA target site in the Rbfox1 coding sequence was mutated to generate a silent mutation and the coding sequence of the mutated Flag-tagged Rbfox1_C or Rbfox1_N was then cloned into pAAV-hSyn-eNpHR 3.0-EYFP plasmid (Addgene plasmid # 26972), downstream of the hSynI promoter between AgeI and EcoRI restriction sites to replace eNpHR 3.0-EYFP coding sequence. AAV2/9 vectors containing hSyn.Flag-Rbfox1_C_siMt and hSyn.Flag-Rbfox1_N_siMt were generated at the University of Pennsylvania Vector Core Facility. An AAV2/9 vector expressing hSyn.EGFP was used as a control for transduction (Penn Vector Core, #AV-9-PV1696). Hippocampal neurons (9 DIV) were transduced with AAV2/9 vectors expressing EGFP, Flag-Rbfox1_C_siMt, or Flag-Rbfox1_N_siMt at a concentration of 1.5 X 10^3 genomic copies (GC)/cell for 12 h and then removed. The neurons (10 DIV) were then incubated with non-targeting (Dharmacon #D001910-01 and #D001910-02) or Rbfox1 and Rbfox3 Accell siRNA for 4 days at concentration of 1.2 mM. Total RNA was extracted using RNeasy Micro Kit (Qiagen). Ribosomal RNA was removed using Ribo-Zero™ rRNA Removal Kits (Epicentre), and the cDNA libraries were prepared using TruSeq RNA Sample Preparation Kit (Illumina) and sequenced in HiSeq 2000 (Illumina) (pair end, 50 nt) by the Southern California Genotyping Consortium (SCGC) Gene Expression Core Facility (Los Angeles, California).

Alternative splicing changes were analyzed by SpliceTrap (Wu et al., 2011). Splicing changes where percent spliced in (psi) > 10, and reads of exon 1 > 50, exon 2 > 20, exon 3 > 50, exon 1-exon 2 junction > 5, exon 2-exon 3 junction > 5, and exon 1-exon 3 junctions > 5 in both samples in the comparison were considered significant. Gene expression changes were analyzed by Cufflinks-2.0.2. (Trapnell et al., 2010) and $q < 0.3$ was set to detect significant expression changes. Gene expression changes were validated by RT-qPCR on RNA samples from two independent biological replicates from those used for RNA sequencing. The expression levels of each gene were normalized to Tuj1 (Tubb3) expression for comparison. The means of normalized expression were calculated and the statistical significance was determined using a paired, one-tailed Student's t test with significance set to $p < 0.05$. N = 2 biological replicates.

Criteria for Defining Expression and Splicing Gene Sets

Genes selected for inclusion in the splicing set were required to have exons that showed significant splicing changes in Rbfox1 and 3 double knockdown (KD) or Rbfox1_N rescue experiment as measured by RNA sequencing, and that showed opposite direction of splicing changes in the KD and Rbfox1_N rescue experiments. This identified 366 Rbfox1 regulated alternative exons in 332 genes as shown in Tables S1 and S2.

For the expression set, two sets of genes were selected and combined. The first set of genes was required to have significant expression changes in the KD experiment measured by microarray and showed opposite expression changes in the Rbfox1_C rescue experiment measured by RNA sequencing. The second set of genes was required to have significant expression changes in the knockdown or Rbfox1_C rescue experiment measured by RNA sequencing and showed opposite direction of expression changes in the KD and Rbfox1_C rescue experiments. This identified 613 Rbfox1-increased genes and 403 Rbfox1-decreased genes as shown in Table S1.

iCLIP Data Analyses

A high molecular weight (HMW) nuclear fraction and soluble nucleoplasm fraction were purified from the brains of 6 weeks old male C57BL/6J mice. Briefly,

nuclei were purified as described (Grabowski, 2005) and lysed. Soluble and HMW fractions were separated by centrifugation. A cytoplasmic fraction was purified from mouse forebrain cultures at DIV14. iCLIP was performed according to the original protocol (Konig et al., 2010), with some modifications described in Supplemental Experimental Procedures. iCLIP sequencing results were analyzed as described in Konig et al. (Konig et al., 2010) with a few modifications. In brief, the iCLIP tags generated by PCR duplication were discarded based on the comparisons of the random barcodes in the tags. The unique iCLIP tags were then mapped to mouse genome (mm9/NCBI37) using Bowtie allowing 2 nucleotide mismatches (Langmead et al., 2009). Mapped tags were further mapped to the longest transcripts in Known Gene table (Hsu et al., 2006) and divided into four regions of 5' UTR, CDS, intron, and 3' UTR for downstream analyses. The first nucleotide in the genome upstream of the iCLIP tags was defined as UV-crosslink site and the significance of crosslinking at each crosslink site was evaluated by the false discovery rate (FDR) calculated as described in Konig et al. (Konig et al., 2010). Crosslink sites with FDR ≤ 0.01 were used for clustering. Any two crosslink sites located within 20 nucleotides on the mouse genome were clustered together. The width of a cluster was defined as the distance between the first and the last crosslinked sites and clusters with width > 1 nt were selected for downstream analyses. A cluster was defined as a GCAUG cluster if it overlapped with a GCAUG motif with at least one nucleotide within -10 to 10 nt genomic sequences of the cluster. The iCLIP tags in these clusters were called clustered tags.

Motif Analyses

Crosslink sites with FDR ≤ 0.01 were used for motif analyses. The genomic sequences of the crosslink site plus 40 nucleotides upstream and 40 nucleotides downstream were used for the motif enrichment analyses. The z-scores of each pentamer were calculated by comparing the occurrence of the pentamers around the crosslink sites to the occurrence around randomized sites in the same genomic region (i.e., within the same intron or 3' UTR) to control for the differences in expression of different genes.

Identification of Rbfox 3' UTR Target Genes

To identify 3' UTR target genes for Rbfox1, 2, and 3 in different experiments, the genes were first ranked by the number of clustered tags in 3' UTR. Next, to account for the differences in the number of clustered tags generated in different experiments, genes contained the top 95% of clustered tags were selected as 3' UTR target genes. By this criterion, the top 55% of genes that contained clustered tags in 3' UTR were selected. This set the cutoff as 11 tags/3' UTR for the identification of Rbfox1, 2, and 3 3' UTR target genes in the forebrain cultures and the brain tissues. The cutoffs for Rbfox1 in the forebrain and hindbrain tissues were set higher at 21 tags/3' UTR and 16 tags/3' UTR, respectively, due to the greater numbers of clustered tags generated in these experiments.

Gene Set Enrichment Analysis

Gene set enrichment analysis was performed with candidate gene lists and co-expression networks using a two-tailed Fisher's exact test followed by Benjamini-Hochberg FDR adjustment (Benjamini and Hochberg, 1995). All mouse gene set overlaps were performed using mouse Ensembl IDs, all human lists were converted to their homologous mouse Ensembl IDs using Ensembl 73 (Gencode v18), using only one-to-one orthologs. FDR adjustment took into consideration all gene set overlaps performed. The following gene lists and co-expression modules were used: candidate genes from SFARI with a gene score of S or 1-4 (Basu et al., 2009), two ASD associated co-expression modules from post-mortem human cortex (asdM12 and asdM16; (Voineagu et al., 2011)), FMRP binding targets in mouse brain (Darnell et al., 2011), predicted Rbfox1 3' UTR stability targets (Ray et al., 2013), and 12 co-expression modules reflecting cortical developmental processes (Parikshak et al., 2013) and enriched for protein interactions and GO terms, including cellular proliferation (devM8, and devM11), transcriptional/chromatin regulation (devM2, and devM3), and synaptic development (devM13, devM16, and devM17).

ACCESSION NUMBERS

The microarray, RNAseq, and iCLIP data from cytoplasmic fraction were deposited to the NCBI Gene Expression Omnibus under accession number GSE71917.

AUTHOR CONTRIBUTIONS

J.A.L. and K.C.M. designed the experiments with input from D.L.B.. J.A.L. performed co-culture, RNAi, and rescue experiments for microarray and RNA sequencing experiments, and all biochemical experiments. E.S.A. prepared cDNA for microarray experiments. A.D. and J.A.L. performed iCLIP experiments. J.A.L. and M.F. performed luciferase assays. C.H.L. and J.A.L performed bioinformatic analyses. N.N.P performed gene set enrichment analyses. Figures were prepared by J.A.L., C.H.L., and N.N.P. The manuscript was written by J.A.L and K.C.M with input from the other authors.

ACKNOWLEDGEMENTS

We thank J. König and J. Ule (UCL Institute of Neurology) for the iCLIP protocol; L. Zipursky (UCLA) and members of the Martin and Black labs for helpful discussions; and V. Ho, L. Zipursky and K. Otis (UCLA) for comments on the manuscript. This work was supported by R21 MH101684 to K.C.M., P50-HD-055784 pilot grant to K.C.M., and a NARSAD Young Investigator Award to J.A.L. Work in the Black lab was supported by HHMI, and by NIH grant R01 GM084317. E.S.A. was supported by the UCLA Medical Scientist Training Program, and by NIH Graduate Fellowship 4F30AG033993. D.L.B. is an Investigator of HHMI. N.N.P was supported by NRSA Fellowship F30MH099886. M.F was supported by Fundação para a Ciência e a Tecnologia through the Graduate Program in Areas of Basic and Applied Biology.

3.1.6. REFERENCES

1. Auweter, S.D., Fasan, R., Reymond, L., Underwood, J.G., Black, D.L., Pitsch, S., and Allain, F.H. (2006). Molecular basis of RNA recognition by the human alternative splicing factor Fox-1. The EMBO journal *25*, 163-173.
2. Bartel, D.P. (2009). MicroRNAs: target recognition and regulatory functions. Cell *136*, 215-233.
3. Basu, S.N., Kollu, R., and Banerjee-Basu, S. (2009). AutDB: a gene reference resource for autism research. Nucleic acids research *37*, D832-836.
4. Benjamini, Y., and Hochberg, Y. (1995). Controlling the False Discovery Rate - a Practical and Powerful Approach to Multiple Testing. J Roy Stat Soc B Met *57*, 289-300.
5. Bhalla, K., Phillips, H.A., Crawford, J., McKenzie, O.L., Mulley, J.C., Eyre, H., Gardner, A.E., Kremmidiotis, G., and Callen, D.F. (2004). The de novo chromosome 16 translocations of two patients with abnormal phenotypes (mental retardation and epilepsy) disrupt the A2BP1 gene. Journal of human genetics *49*, 308-311.
6. Bhatt, D.M., Pandya-Jones, A., Tong, A.J., Barozzi, I., Lissner, M.M., Natoli, G., Black, D.L., and Smale, S.T. (2012). Transcript dynamics of proinflammatory genes revealed by sequence analysis of subcellular RNA fractions. Cell *150*, 279-290.
7. Bielli, P., Busa, R., Paronetto, M.P., and Sette, C. (2011). The RNA-binding protein Sam68 is a multifunctional player in human cancer. Endocrine-related cancer *18*, R91-R102.
8. Boudreau, R.L., Jiang, P., Gilmore, B.L., Spengler, R.M., Tirabassi, R., Nelson, J.A., Ross, C.A., Xing, Y., and Davidson, B.L. (2014). Transcriptome-wide discovery of microRNA binding sites in human brain. Neuron *81*, 294-305.
9. Chi, S.W., Zang, J.B., Mele, A., and Darnell, R.B. (2009). Argonaute HITS-CLIP decodes microRNA-mRNA interaction maps. Nature *460*, 479-486.
10. Ciafre, S.A., and Galardi, S. (2013). microRNAs and RNA-binding proteins: a complex network of interactions and reciprocal regulations in cancer. RNA biology *10*, 935-942.
11. Damianov, A., and Black, D.L. (2010). Autoregulation of Fox protein expression to produce dominant negative splicing factors. Rna *16*, 405-416.

12. Darnell, J.C., and Richter, J.D. (2012). Cytoplasmic RNA-binding proteins and the control of complex brain function. Cold Spring Harbor perspectives in biology *4*, a012344.
13. Darnell, J.C., Van Driesche, S.J., Zhang, C., Hung, K.Y., Mele, A., Fraser, C.E., Stone, E.F., Chen, C., Fak, J.J., Chi, S.W.*, et al.* (2011). FMRP stalls ribosomal translocation on mRNAs linked to synaptic function and autism. Cell *146*, 247-261.
14. Fogel, B.L., Wexler, E., Wahnich, A., Friedrich, T., Vijayendran, C., Gao, F., Parikshak, N., Konopka, G., and Geschwind, D.H. (2012). RBFOX1 regulates both splicing and transcriptional networks in human neuronal development. Human molecular genetics *21*, 4171-4186.
15. Gehman, L.T., Stoilov, P., Maguire, J., Damianov, A., Lin, C.H., Shiue, L., Ares, M., Jr., Mody, I., and Black, D.L. (2011). The splicing regulator Rbfox1 (A2BP1) controls neuronal excitation in the mammalian brain. Nature genetics *43*, 706-711.
16. Grabowski, P.J. (2005). Splicing-active nuclear extracts from rat brain. Methods *37*, 323-330.
17. Hamada, N., Ito, H., Iwamoto, I., Mizuno, M., Morishita, R., Inaguma, Y., Kawamoto, S., Tabata, H., and Nagata, K. (2013). Biochemical and morphological characterization of A2BP1 in neuronal tissue. Journal of neuroscience research *91*, 1303-1311.
18. Heraud-Farlow, J.E., and Kiebler, M.A. (2014). The multifunctional Staufen proteins: conserved roles from neurogenesis to synaptic plasticity. Trends in neurosciences *37*, 470-479.
19. Ho, V.M., Dallalzadeh, L.O., Karathanasis, N., Keles, M.F., Vangala, S., Grogan, T., Poirazi, P., and Martin, K.C. (2014). GluA2 mRNA distribution and regulation by miR-124 in hippocampal neurons. Molecular and cellular neurosciences *61*, 1-12.
20. Hsu, F., Kent, W.J., Clawson, H., Kuhn, R.M., Diekhans, M., and Haussler, D. (2006). The UCSC Known Genes. Bioinformatics *22*, 1036-1046.
21. Ince-Dunn, G., Okano, H.J., Jensen, K.B., Park, W.Y., Zhong, R., Ule, J., Mele, A., Fak, J.J., Yang, C., Zhang, C.*, et al.* (2012). Neuronal Elav-like (Hu) proteins

regulate RNA splicing and abundance to control glutamate levels and neuronal excitability. Neuron *75*, 1067-1080.

22. Khodor, Y.L., Menet, J.S., Tolan, M., and Rosbash, M. (2012). Cotranscriptional splicing efficiency differs dramatically between Drosophila and mouse. Rna *18*, 2174-2186.
23. Kim, H.H., Kuwano, Y., Srikantan, S., Lee, E.K., Martindale, J.L., and Gorospe, M. (2009a). HuR recruits let-7/RISC to repress c-Myc expression. Genes & development *23*, 1743-1748.
24. Kim, K.K., Adelstein, R.S., and Kawamoto, S. (2009b). Identification of neuronal nuclei (NeuN) as Fox-3, a new member of the Fox-1 gene family of splicing factors. The Journal of biological chemistry *284*, 31052-31061.
25. Konig, J., Zarnack, K., Rot, G., Curk, T., Kayikci, M., Zupan, B., Turner, D.J., Luscombe, N.M., and Ule, J. (2010). iCLIP reveals the function of hnRNP particles in splicing at individual nucleotide resolution. Nature structural & molecular biology *17*, 909-915.
26. Kuroyanagi, H. (2009). Fox-1 family of RNA-binding proteins. Cellular and molecular life sciences : CMLS *66*, 3895-3907.
27. Lal, D., Reinthaler, E.M., Altmuller, J., Toliat, M.R., Thiele, H., Nurnberg, P., Lerche, H., Hahn, A., Moller, R.S., Muhle, H.*, et al.* (2013a). RBFOX1 and RBFOX3 mutations in rolandic epilepsy. PloS one *8*, e73323.
28. Lal, D., Trucks, H., Moller, R.S., Hjalgrim, H., Koeleman, B.P., de Kovel, C.G., Visscher, F., Weber, Y.G., Lerche, H., Becker, F.*, et al.* (2013b). Rare exonic deletions of the RBFOX1 gene increase risk of idiopathic generalized epilepsy. Epilepsia *54*, 265-271.
29. Lambert, N., Robertson, A., Jangi, M., McGeary, S., Sharp, P.A., and Burge, C.B. (2014). RNA Bind-n-Seq: quantitative assessment of the sequence and structural binding specificity of RNA binding proteins. Molecular cell *54*, 887-900.
30. Langmead, B., Trapnell, C., Pop, M., and Salzberg, S.L. (2009). Ultrafast and memory-efficient alignment of short DNA sequences to the human genome. Genome biology *10*, R25.
31. Lebedeva, S., Jens, M., Theil, K., Schwanhausser, B., Selbach, M., Landthaler, M., and Rajewsky, N. (2011). Transcriptome-wide analysis of regulatory interactions of the RNA-binding protein HuR. Molecular cell *43*, 340-352.

32. Lee, J.A., Tang, Z.Z., and Black, D.L. (2009). An inducible change in Fox-1/A2BP1 splicing modulates the alternative splicing of downstream neuronal target exons. Genes & development *23*, 2284-2293.
33. Licatalosi, D.D., Mele, A., Fak, J.J., Ule, J., Kayikci, M., Chi, S.W., Clark, T.A., Schweitzer, A.C., Blume, J.E., Wang, X.*, et al.* (2008). HITS-CLIP yields genome-wide insights into brain alternative RNA processing. Nature *456*, 464-469.
34. Lisman, J., Schulman, H., and Cline, H. (2002). The molecular basis of CaMKII function in synaptic and behavioural memory. Nature reviews Neuroscience *3*, 175-190.
35. Lovci, M.T., Ghanem, D., Marr, H., Arnold, J., Gee, S., Parra, M., Liang, T.Y., Stark, T.J., Gehman, L.T., Hoon, S.*, et al.* (2013). Rbfox proteins regulate alternative mRNA splicing through evolutionarily conserved RNA bridges. Nature structural & molecular biology *20*, 1434-1442.
36. Lukong, K.E., Chang, K.W., Khandjian, E.W., and Richard, S. (2008). RNA-binding proteins in human genetic disease. Trends in genetics : TIG *24*, 416-425.
37. Mackall, J., Meredith, M., and Lane, M.D. (1979). A mild procedure for the rapid release of cytoplasmic enzymes from cultured animal cells. Analytical biochemistry *95*, 270-274.
38. Martin, C.L., Duvall, J.A., Ilkin, Y., Simon, J.S., Arreaza, M.G., Wilkes, K., Alvarez-Retuerto, A., Whichello, A., Powell, C.M., Rao, K.*, et al.* (2007). Cytogenetic and molecular characterization of A2BP1/FOX1 as a candidate gene for autism. American journal of medical genetics Part B, Neuropsychiatric genetics : the official publication of the International Society of Psychiatric Genetics *144B*, 869-876.
39. Mukherjee, N., Corcoran, D.L., Nusbaum, J.D., Reid, D.W., Georgiev, S., Hafner, M., Ascano, M., Jr., Tuschl, T., Ohler, U., and Keene, J.D. (2011). Integrative regulatory mapping indicates that the RNA-binding protein HuR couples pre-mRNA processing and mRNA stability. Molecular cell *43*, 327-339.
40. Nakahata, S., and Kawamoto, S. (2005). Tissue-dependent isoforms of mammalian Fox-1 homologs are associated with tissue-specific splicing activities. Nucleic acids research *33*, 2078-2089.

41. Pandya-Jones, A., Bhatt, D.M., Lin, C.H., Tong, A.J., Smale, S.T., and Black, D.L. (2013). Splicing kinetics and transcript release from the chromatin compartment limit the rate of Lipid A-induced gene expression. Rna *19*, 811-827.
42. Papin, C., Rouget, C., and Mandart, E. (2008). Xenopus Rbm9 is a novel interactor of XGld2 in the cytoplasmic polyadenylation complex. The FEBS journal *275*, 490-503.
43. Parikshak, N.N., Luo, R., Zhang, A., Won, H., Lowe, J.K., Chandran, V., Horvath, S., and Geschwind, D.H. (2013). Integrative functional genomic analyses implicate specific molecular pathways and circuits in autism. Cell *155*, 1008-1021.
44. Ray, D., Kazan, H., Cook, K.B., Weirauch, M.T., Najafabadi, H.S., Li, X., Gueroussov, S., Albu, M., Zheng, H., Yang, A.*, et al.* (2013). A compendium of RNA-binding motifs for decoding gene regulation. Nature *499*, 172-177.
45. Rossbach, O., Hung, L.H., Khrameeva, E., Schreiner, S., Konig, J., Curk, T., Zupan, B., Ule, J., Gelfand, M.S., and Bindereif, A. (2014). Crosslinking-immunoprecipitation (iCLIP) analysis reveals global regulatory roles of hnRNP L. RNA biology *11*, 146-155.
46. Sebat, J., Lakshmi, B., Malhotra, D., Troge, J., Lese-Martin, C., Walsh, T., Yamrom, B., Yoon, S., Krasnitz, A., Kendall, J.*, et al.* (2007). Strong association of de novo copy number mutations with autism. Science *316*, 445-449.
47. Smith, C.L., and Eppig, J.T. (2012). The Mammalian Phenotype Ontology as a unifying standard for experimental and high-throughput phenotyping data. Mammalian genome : official journal of the International Mammalian Genome Society *23*, 653-668.
48. Srikantan, S., Tominaga, K., and Gorospe, M. (2012). Functional interplay between RNA-binding protein HuR and microRNAs. Current protein & peptide science *13*, 372-379.
49. Sugnet, C.W., Srinivasan, K., Clark, T.A., O'Brien, G., Cline, M.S., Wang, H., Williams, A., Kulp, D., Blume, J.E., Haussler, D.*, et al.* (2006). Unusual intron conservation near tissue-regulated exons found by splicing microarrays. PLoS computational biology *2*, e4.

50. Talkowski, M.E., Minikel, E.V., and Gusella, J.F. (2014). Autism spectrum disorder genetics: diverse genes with diverse clinical outcomes. Harvard review of psychiatry *22*, 65-75.
51. Trapnell, C., Williams, B.A., Pertea, G., Mortazavi, A., Kwan, G., van Baren, M.J., Salzberg, S.L., Wold, B.J., and Pachter, L. (2010). Transcript assembly and quantification by RNA-Seq reveals unannotated transcripts and isoform switching during cell differentiation. Nature biotechnology *28*, 511-515.
52. Turner, M., and Hodson, D.J. (2012). An emerging role of RNA-binding proteins as multifunctional regulators of lymphocyte development and function. Advances in immunology *115*, 161-185.
53. Underwood, J.G., Boutz, P.L., Dougherty, J.D., Stoilov, P., and Black, D.L. (2005). Homologues of the Caenorhabditis elegans Fox-1 protein are neuronal splicing regulators in mammals. Molecular and cellular biology *25*, 10005-10016.
54. Vanharanta, S., Marney, C.B., Shu, W., Valiente, M., Zou, Y., Mele, A., Darnell, R.B., and Massague, J. (2014). Loss of the multifunctional RNA-binding protein RBM47 as a source of selectable metastatic traits in breast cancer. eLife *3*.
55. Voineagu, I., Wang, X., Johnston, P., Lowe, J.K., Tian, Y., Horvath, S., Mill, J., Cantor, R.M., Blencowe, B.J., and Geschwind, D.H. (2011). Transcriptomic analysis of autistic brain reveals convergent molecular pathology. Nature *474*, 380-384.
56. Weyn-Vanhentenryck, S.M., Mele, A., Yan, Q., Sun, S., Farny, N., Zhang, Z., Xue, C., Herre, M., Silver, P.A., Zhang, M.Q.*, et al.* (2014). HITS-CLIP and integrative modeling define the Rbfox splicing-regulatory network linked to brain development and autism. Cell reports *6*, 1139-1152.
57. Wu, J., Akerman, M., Sun, S., McCombie, W.R., Krainer, A.R., and Zhang, M.Q. (2011). SpliceTrap: a method to quantify alternative splicing under single cellular conditions. Bioinformatics *27*, 3010-3016.
58. Xie, X., Lu, J., Kulbokas, E.J., Golub, T.R., Mootha, V., Lindblad-Toh, K., Lander, E.S., and Kellis, M. (2005). Systematic discovery of regulatory motifs in human promoters and 3' UTRs by comparison of several mammals. Nature *434*, 338-345.

59. Xue, Y., Ouyang, K., Huang, J., Zhou, Y., Ouyang, H., Li, H., Wang, G., Wu, Q., Wei, C., Bi, Y.*, et al.* (2013). Direct conversion of fibroblasts to neurons by reprogramming PTB-regulated microRNA circuits. Cell *152*, 82-96.
60. Xue, Y., Zhou, Y., Wu, T., Zhu, T., Ji, X., Kwon, Y.S., Zhang, C., Yeo, G., Black, D.L., Sun, H.*, et al.* (2009). Genome-wide analysis of PTB-RNA interactions reveals a strategy used by the general splicing repressor to modulate exon inclusion or skipping. Molecular cell *36*, 996-1006.
61. Yeo, G.W., Coufal, N.G., Liang, T.Y., Peng, G.E., Fu, X.D., and Gage, F.H. (2009). An RNA code for the FOX2 splicing regulator revealed by mapping RNA-protein interactions in stem cells. Nature structural & molecular biology *16*, 130-137.
62. Yokoshi, M., Li, Q., Yamamoto, M., Okada, H., Suzuki, Y., and Kawahara, Y. (2014). Direct binding of Ataxin-2 to distinct elements in 3' UTRs promotes mRNA stability and protein expression. Molecular cell *55*, 186-198.
63. Young, L.E., Moore, A.E., Sokol, L., Meisner-Kober, N., and Dixon, D.A. (2012). The mRNA stability factor HuR inhibits microRNA-16 targeting of COX-2. Molecular cancer research : MCR *10*, 167-180.
64. 64.Zhang, C., Zhang, Z., Castle, J., Sun, S., Johnson, J., Krainer, A.R., and Zhang, M.Q. (2008). Defining the regulatory network of the tissue-specific splicing factors Fox-1 and Fox-2. Genes & development *22*, 2550-2563.

3.1.7. SUPPLEMENTAL FIGURES

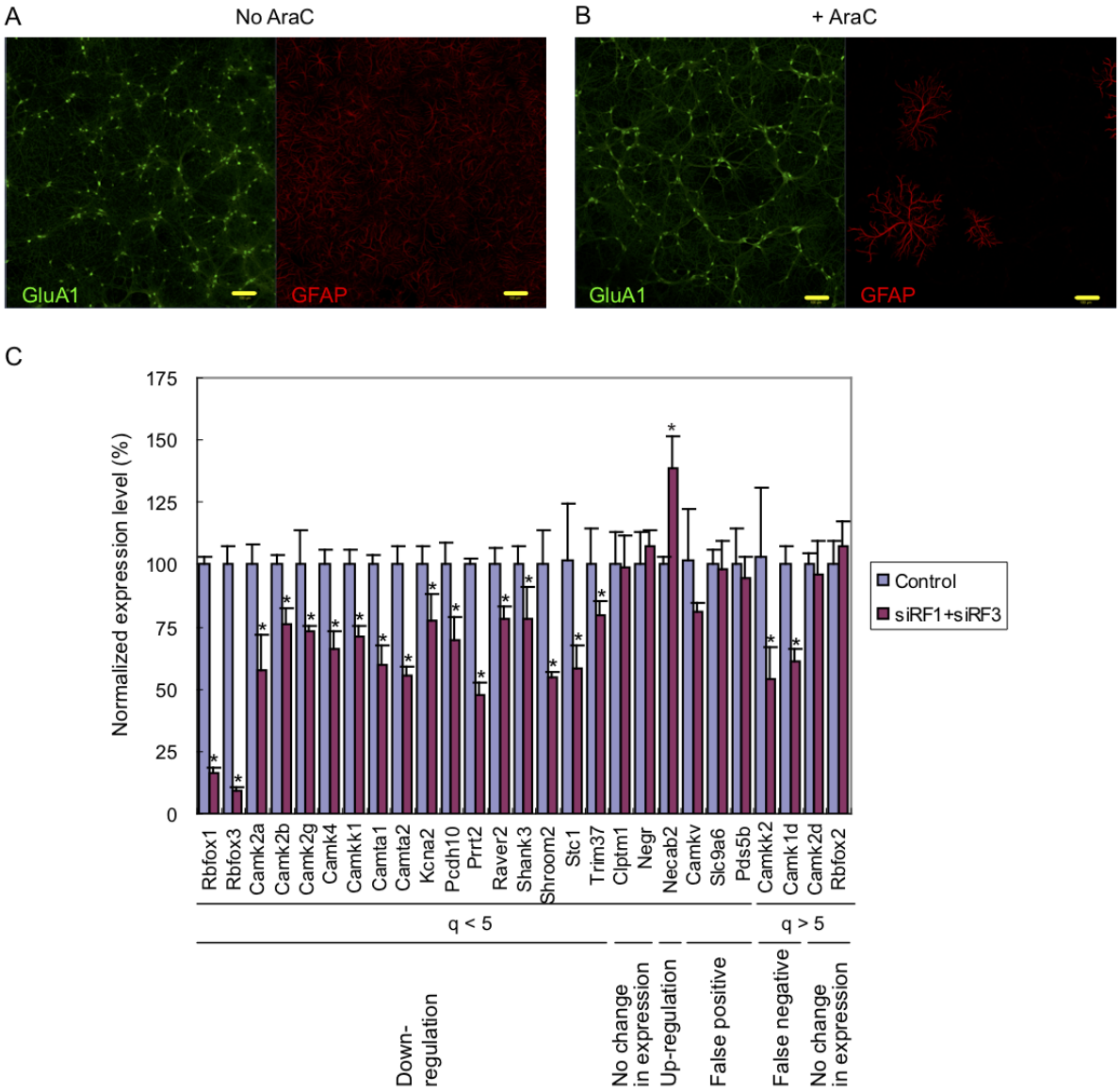

Figure S1, Related to Figure 2. Co-culture system and RT-qPCR validation (A, B) Images reveal the elimination of glial cells after incubation with AraC. Neurons were immunostained with anti-GluA1 antibodies (green) and glial cells with anti-GFAP antibodies (red). Scale bar = 100 μm. (C) Bar graph of the validation of microarray data by RT-qPCR. Error bars indicate standard deviation. * $p < 0.05$ by student's t-test. n = 3. siRF1 = Rbfox1 siRNA; siRF3 = Rbfox3 siRNA.

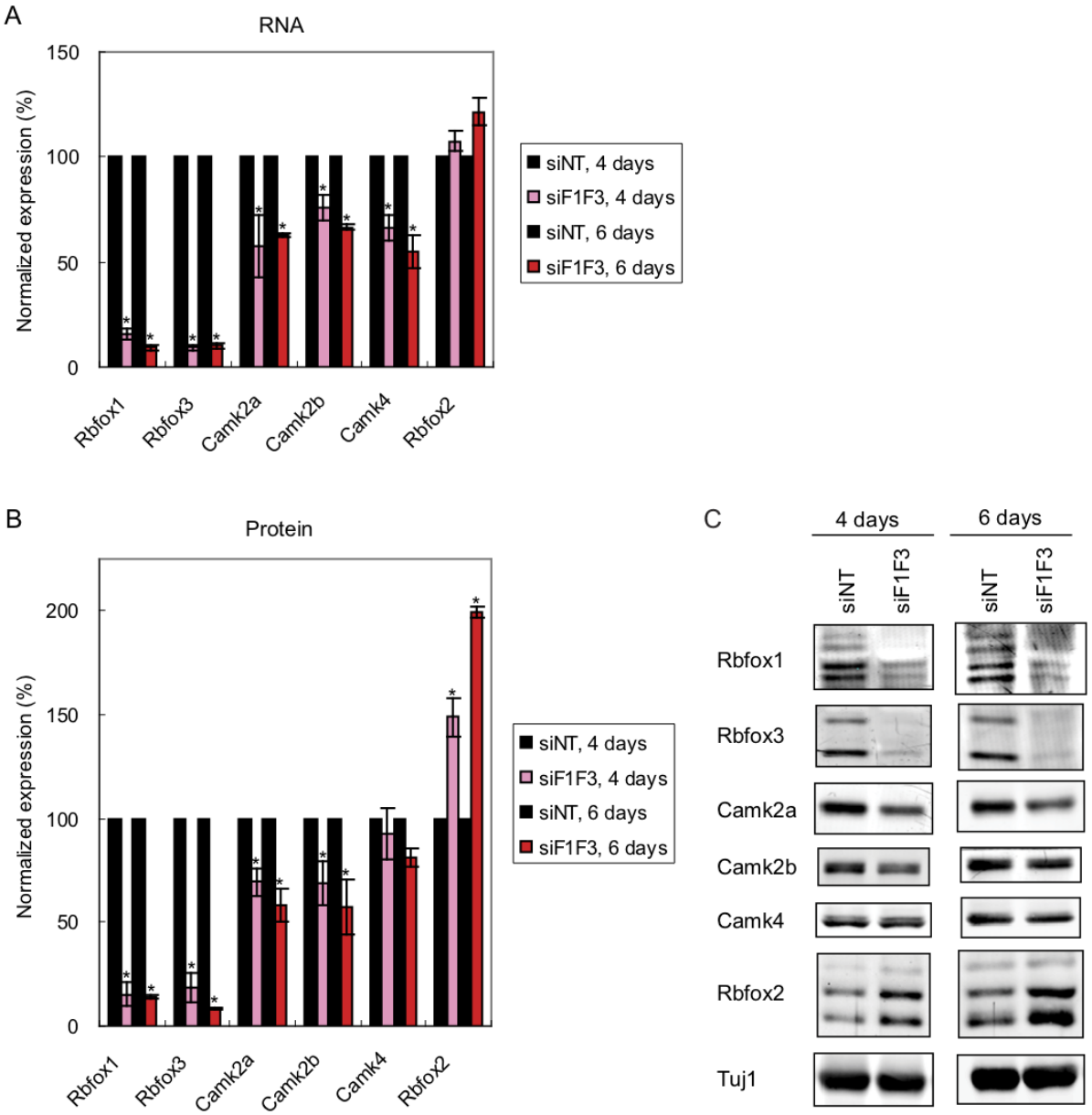

Figure S2, Related to Figure 2. Validation of microarray results (A) Bar graph showing the RT-qPCR analysis of Rbfox1 regulated mRNAs from neurons incubated with Rbfox1 and Rbfox3 siRNAs (siF1F3) for 4 or 6 days. siNT = Non-Targeting siRNAs. Error bars indicate standard deviation. * $p < 0.05$ by student's t-test. n = 2.
(B, C) Immunoblot analysis of proteins encoded by Rbfox1 regulated genes from neurons incubated with Rbfox1 and Rbfox3 siRNAs for 4 or 6 days. Tuj1 is used as a loading control. Bar graph showing the quantification of the protein bands in (C). Error bars indicate standard deviation. * $p < 0.05$ by student's t-test. n = 2.

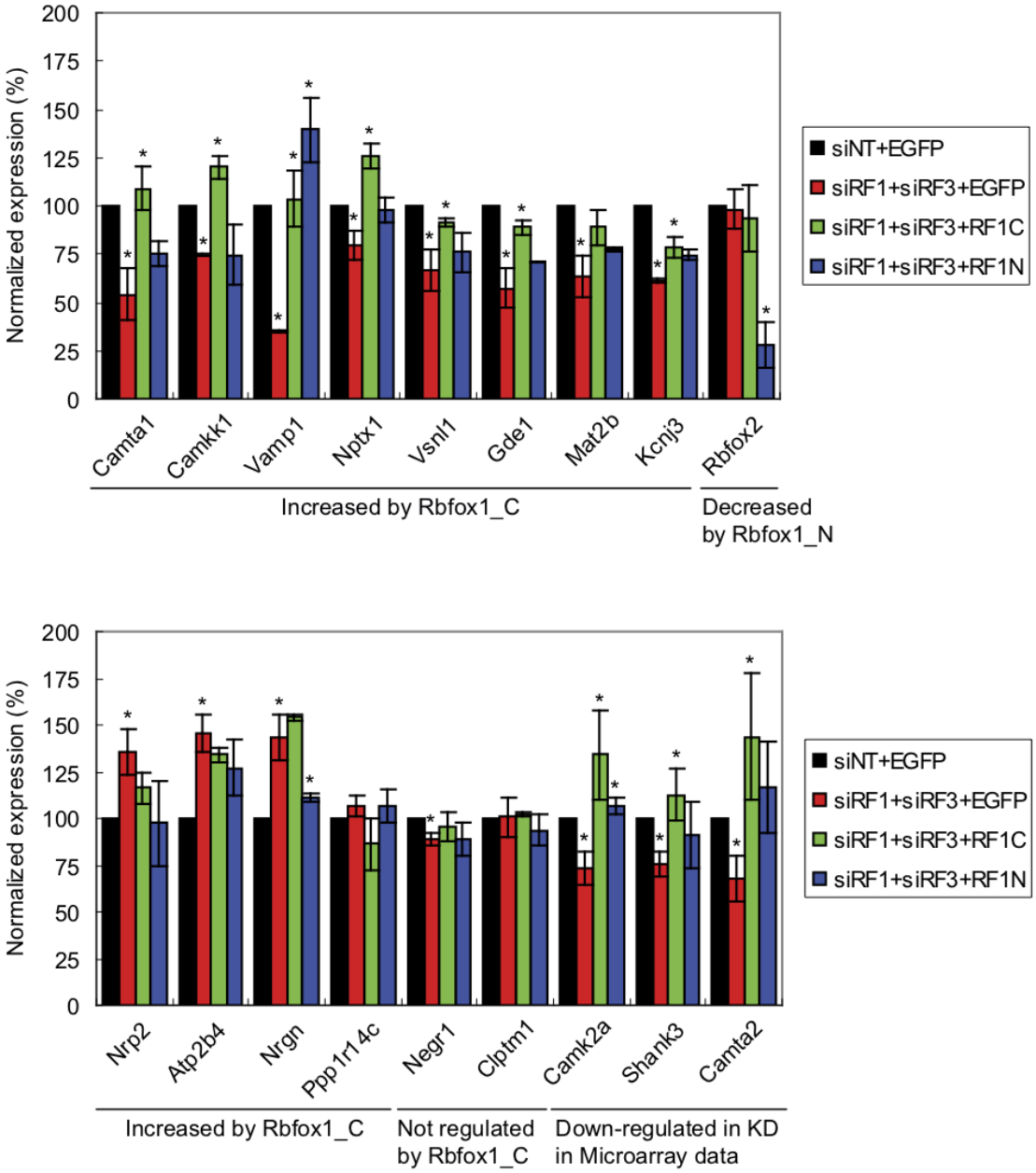

Figure S3, Related to Figure 3. Validation of RNAseq results by RT-qPCR
Bar graph showing qPCR analysis of candidate Rbfox-regulated genes identified by RNAseq analysis (Figure 3). Changes were normalized to Tuj1 (Tubb3) expression. Error bars indicate the standard deviation. * $p < 0.05$ by student's t-test. n = 2.

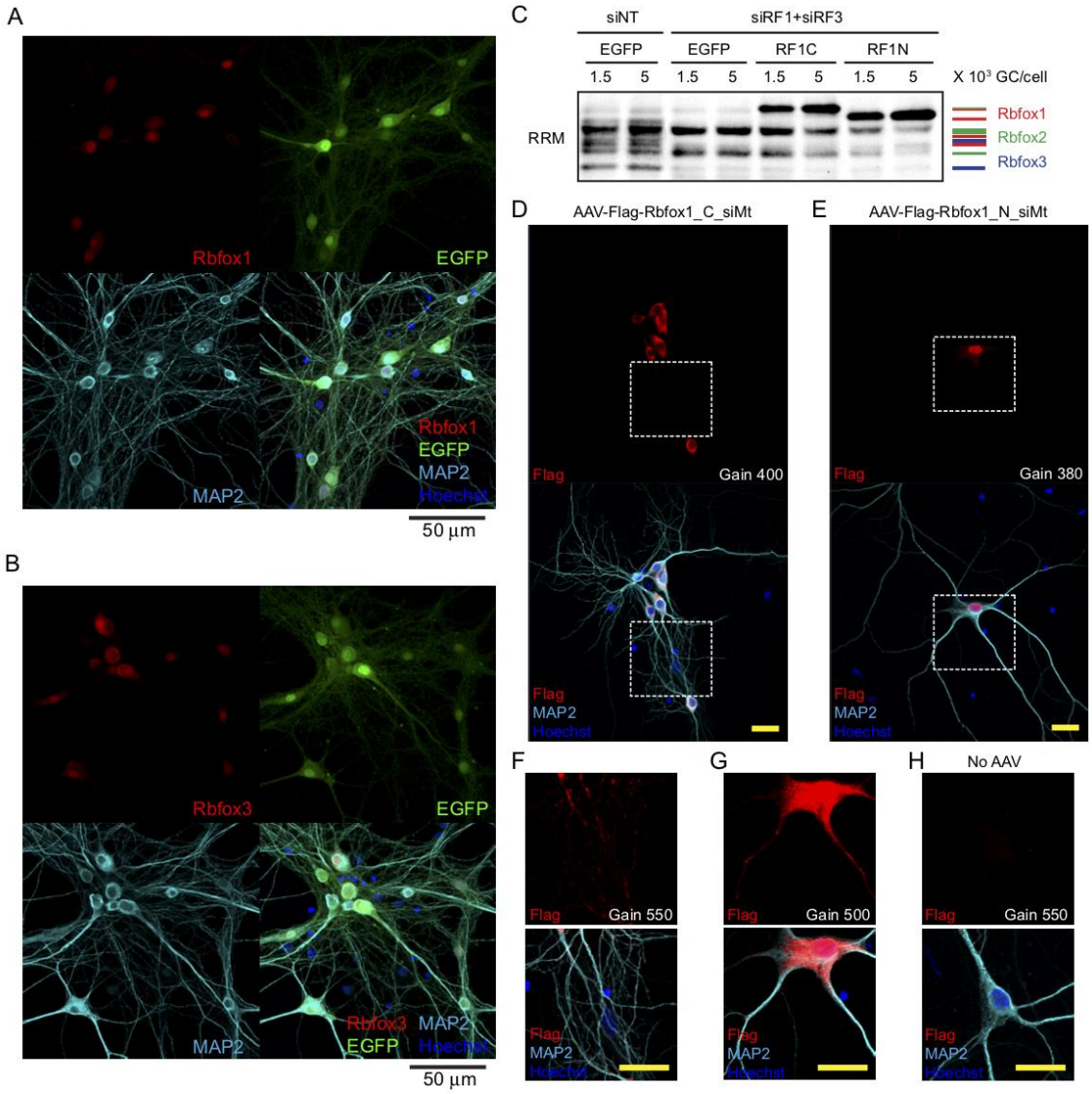

Figure S4, Related to Figure 3. The expression and localization of virally expressed Rbfox1 splice isoforms in neurons. (A) Human synapsin I promotor is only active in neurons. AAV2/9-hSyn.EGFP is expressed in Rbfox1 positive neurons. (B) AAV2/9-hSyn.EGFP is expressed in Rbfox3 positive neurons. (C) Immunoblot analysis showing the amount of Rbfox1 and Rbfox3 double knockdown (siRF1+siRF3) and the amount of Flag-Rbfox1_C_siMt (RF1C) and Flag-Rbfox1_N_siMt (RF1N) expression using two AAV concentrations. GC: genomic copies. (D, E) Photomicrographs showing the subcellular localization of Flag-Rbfox1_C_siMt (red) and Flag-Rbfox1_N_siMt (red) expressed in neurons. The cytoplasm of the neurons is labeled with MAP2 staining (cyan) and the nucleus is stained with Hoechst (blue). The values of the gain used in image acquisition are shown. Scale bar = 20 µm in (D) to (H). (F, G) Images of Flag-Rbfox1_C (red) and Flag-Rbfox1_N (red) shown in higher gain from the boxed areas in (D) and (E). (H) Image of a representative control neuron that is not transduced with AAV.

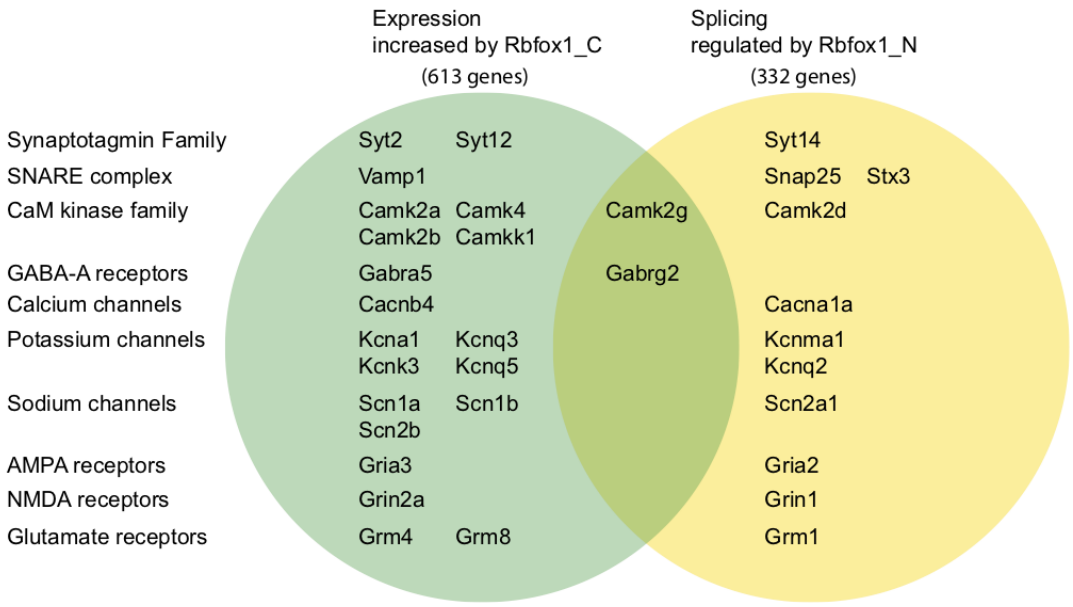

Figure S5, Related to Figure 3. Examples of genes in the same family regulated by different Rbfox1 splice isoforms. Venn diagram showing the overlap of selected genes whose expression is increased by Rbfox1_C and genes whose splicing is regulated by Rbfox1_N.

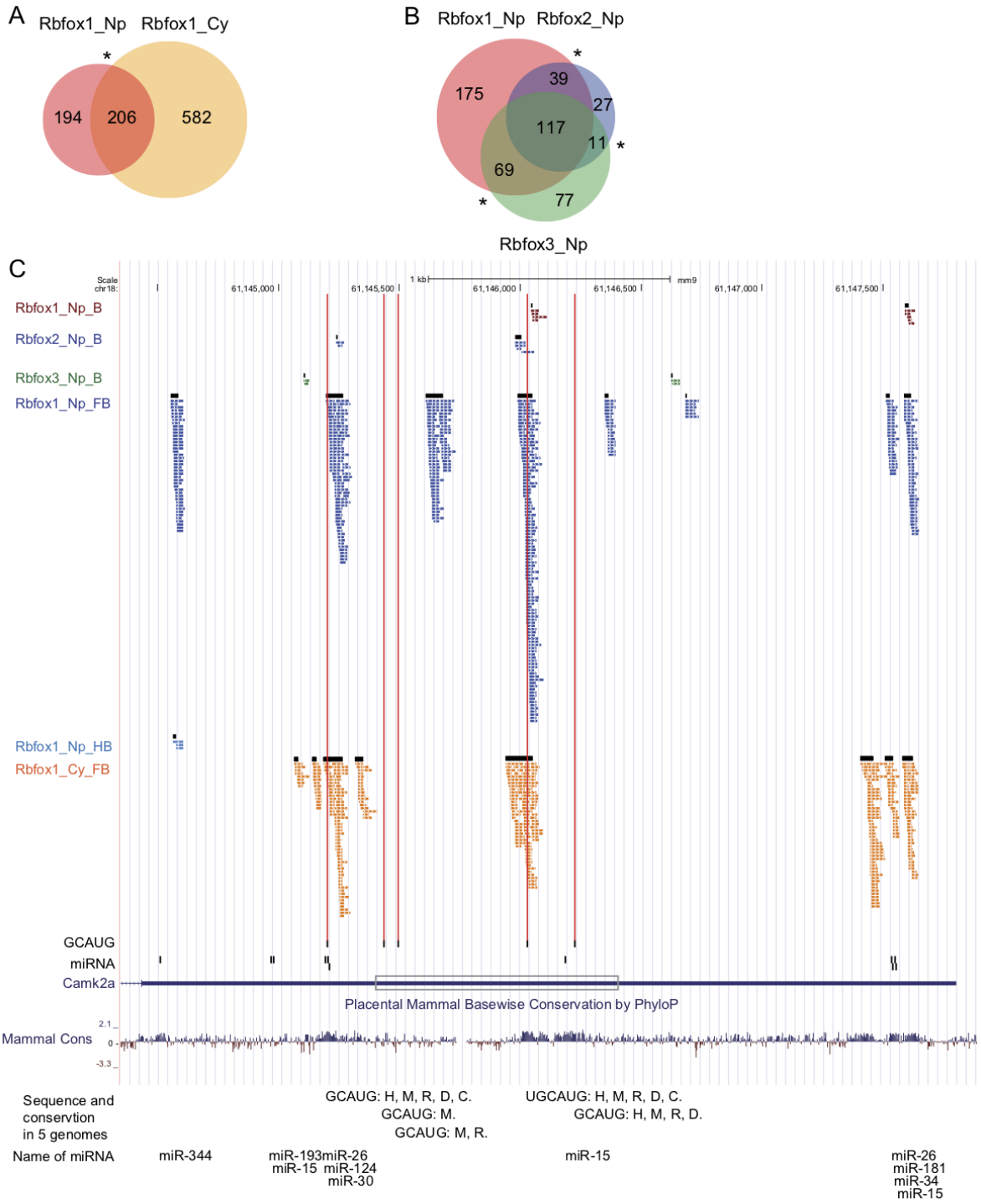

Figure S6, Related to Figure 5. Overlap of iCLIP 3' UTR target genes and tags. (A) A weighted Venn diagram showing

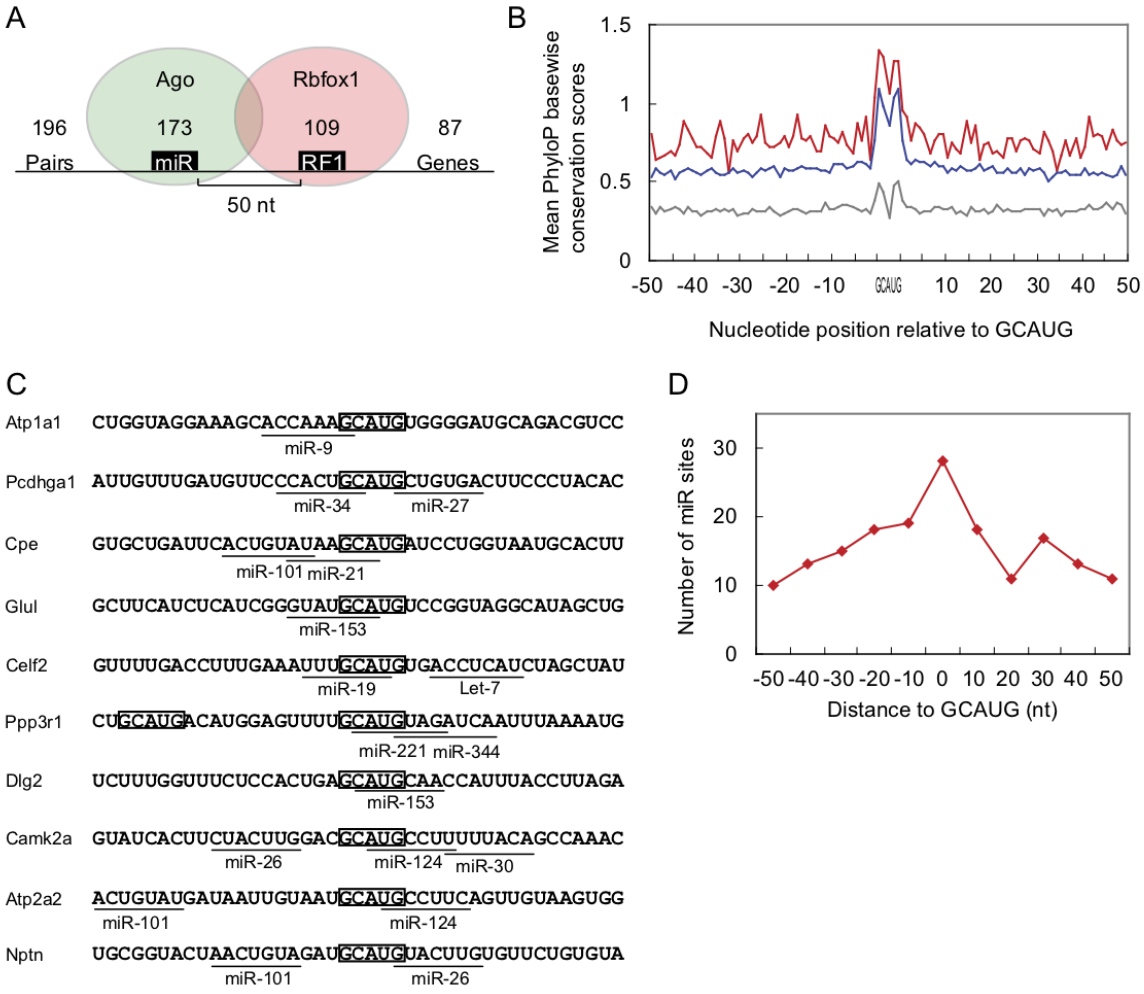

Figure S7, Related to Figure 7. Competition between Rbfox1 and miRNA binding in the 3' UTR of target mRNAs. (A) Diagram showing competition between miRNAs and Rbfox1 binding to target mRNAs. miR indicates a miRNA binding site and RF1 indicates an Rbfox1 binding site, GCAUG. The number of pairs of miRNA and Rbfox1 binding sites located within 50 nucleotides are shown. The number of unique miRNA binding sites, Rbfox1 binding sites, and genes are indicated. (B) Mean PhyloP basewise conservation scores (for placental mammals) of 3' UTR sequences containing a GCAUG motif bound by Rbfox1 and located within 50 nucleotides to a miRNA site (red line), or containing a GCAUG motif bound by Rbfox1 but not close to a miRNA site within flanking 50 nucleotides (blue line), or containing a GCAUG motif within the same 3' UTRs of bound GCAUG but not bound by Rbfox1 (grey line). (C) Examples of RNA sequences with overlapping Rbfox1 binding sites (boxed) and miRNA binding sites (underlined). The names of the miRNAs are labeled under the binding sites. (D) Diagram showing the distribution of the numbers of miRNA sites in binned regions around Rbfox1 binding sites.

3.1.8. SUPPLEMENTAL EXPERIMENTAL PROCEDURES

Immunoblotting and RT-PCR

Protein was purified from tissues using RIPA buffer (Sigma R0278) and quantified by BCA protein assay kit (Pierce, #23225), and 20 □g of protein samples were used for SDS-PAGE. The following primary antibodies were used for Immunoblotting: Rbfox1 (clone 1D10), Rbfox2 (Bethyl, A300-864A), Rbfox3 (Millipore, MAB377), Rbfox RRM (Damianov and Black, 2010), GAPDH (Fitzgerald, 10R-G109a), U1-70K (Sharma et al., 2005), CaMK2A (Millipore #05-532), CaMK2B (LifeSpan #LS-C21191), CaMK4 (LifeSpan #LS-C77627), □-Tubulin (Millipore #AB15708), and Flag (Sigma-Aldrich #F1804). The secondary antibodies were IRDye 800CW Goat anti-Mouse IgG (H + L) (LI-COR #926-32210) and IRDye 680LT Goat anti-Rabbit IgG (H + L) (LI-COR # 926-68021). Immunoblots were scanned using an Odyssey scanner (LI-COR) and the images were analyzed using Image Studio Software (LI-COR). RNAs were purified from the tissues using RNeasy Mini kit (Qiagen) and 1 □g of RNA was reversed transcribed with random hexamers using Superscript III (Invitrogen). One tenth of the reaction was then amplified in 24 PCR cycles with Rbfox1 specific primers (Table S1), one of which was ^{32}P-labeled. PCR products were resolved on 8% polyacrylamide, 7.5 M urea denaturing gels. Gels were dried, exposed and scanned using a Typhoon 9400 PhosphorImager scanner (GE Healthcare). Images were analyzed with ImageQuant TL Software (GE Healthcare).

Primers for Detecting Alternative Splicing Changes of Rbfox1 Exon 19

Primer name	Primer sequence	Length of exon included amplicon (bp)	Length of exon excluded amplicon (bp)
A2bp1_E19_F	GTGGTTATGCTGCGTACCG	269	216
A2bp1_E19_R	GCAATGAAGAAAGAACGAGACC	269	216

Immunocytochemistry

Neurons and HEKT cells grown on coverslips were fixed in 4% paraformaldehyde for 10 min, permeabilized in 0.1% Triton-X for 5 min, blocked in 10% goat serum for 30 min, and incubated with primary antibody for 16–24 hr at 4

°C. Primary antibodies were GluA1 (Millipore #MAB2263), GFAP (Millipore #MAB360), Rbfox1 (clone 1D10), Rbfox3/NeuN (Millipore #MAB377), Flag (Sigma-Aldrich #F1804), and MAP2 (PhosphoSolutions #1100-MAP2). The cells were incubated with secondary Alexa Fluor conjugated antibodies (Invitrogen #11008, #A21422, and #A21103) and Hoechst (Invitrogen #H3570) for 1 hr in the dark at room temperature. Coverslips were mounted on microscope slides using Aqua-Poly/Mount (Polysciences #18606) and allowed to dry overnight before imaging. Images were acquired on a Zeiss LSM700 microscope and processed using the ZEN 2009 software (Carl Zeiss).

Microarray Hybridization, Data Analyses, and RT-qPCR

Total RNA was extracted by RNeasy Mini Kit (Qiagen) and assayed for integrity by Bioanalyzer (Agilent). Samples were prepared from 100 ng total RNA using the WT Expression Kit (Ambion) and GeneChip Terminal Labeling Kit (Affymetrix). The samples were hybridized to the MJAY arrays (Affymetrix) and scanned in the UCLA Microarray Core. Microarray analysis was performed using the OmniViewer method (http://metarray.ucsc.edu/omniviewer/) (Sugnet et al., 2006). For splicing, the OmniViewer method generates a sepscore for changes in specific alternative exons that is a composite representation of probes that detect specific splice isoforms and those that detect general expression level of the transcript. Alternative cassette exons with p = 0 and absolute sepscore value >= 0.3 were set to detect significant splicing changes. For expression, genes with q < 5, intensity >=100, and absolute log2 fold change >= 0.2 were set to detect significant expression changes. Gene expression changes were validated by RT-qPCR. cRNA generated from the WT Expression Kit was primed with random hexamers and reverse transcribed with SuperScript III (Invitrogen). The resulting cDNA was then

used for qPCR with gene specific primers and the expression levels of each gene were normalized to Tuj1 (Tubb3) expression for comparison. The means of normalized expression were calculated and statistical significance was determined using a paired, one-tailed student's t test with significance set to $p < 0.05$. N = 3.

Primer Sequences for qPCR

Primer name	Primer sequence	Length of amplicon (bp)
Rbfox1_QF2	CCAGACCTCCGACAAATGTT	233
Rbfox1_QR2	CCATTGGTGTAGGGGTTGAC	233
Rbfox2_QF1	CAGAAGGTGGAGCACAGACA	243
Rbfox2_QR1	CCCTGTCTGCATCAGCACTA	243
Rbfox3_QF1	AGCAGCCCAAACGACTACAT	239
Rbfox3_QR1	GGCTGTGGCATTATTGACCT	239
Camk2A_F1	GCTTTCAGCCAGAGATCACC	234
Camk2A_R1	CAGTGTAGCACAGCCTCCAA	234
Camk2b_F1	GGGACACCGTTACTCCTGAA	238
Camk2b_R1	CCCACTGAGAAATTCCGTGT	238
Camk2g_F1	GGTCCGGAGGTGTGTAAAGA	207
Camk2g_R1	CCTCCGGTAACAAGGTCAAA	207
Camk4_F1	AGCTGGTCACAGGAGGAGAA	174
Camk4_R1	GGGCTGGAGTTGCATAAAGA	174
Camkk1_F1	ATTTGGTGTTCGACCTCCTG	246
Camkk1_R1	TGGACAGCTGAGCATCATTC	246
Camta1_F1	GAACCAATGAGCGTCCTGAT	178
Camta1_R1	TCTCCTGCTTGATTCGGTCT	178
Camta2_F1	CCTCTCTGCCTCTGTGCTCT	202
Camta2_R1	CTGAATTGGAGGAGCCTCTG	202
Kcna2_F1	AGAAGATGTGACGGGGACTG	178
Kcna2_R1	CCCAGGAAACACAGAAGCAT	178
Pcdh10_F1	ACGGAAGCATTTTGTCCAAC	239

Pcdh10_F1	GTGGCCCAGTGCTTTACATT	239
Prrt2_F2	ACATTGTGGCCTTCGCTTAT	142
Prrt2_R2	GAGGCGATGATGATGAGGAC	142
Raver2_F1	CCCCAGTGACTACAGCGATT	181
Raver2_R1	CTTGATGGTGATGCCATCTG	181
Shank3_F1	CAACATGGGTGCTCAGAATG	172
Shank3_R1	AAGCTCAAAGTTCCCTGCAA	172
Shroom2_F1	TCCTTGGCCACCAATTCTAC	162
Shroom2_R1	CTTGCGGCTGATACTGTCAA	162
Stc1_F1	ACAGCTGCCCAATCACTTCT	198
Stc1_R1	CGCCTCCTATTGAAGTCAGC	198
Trim37_F1	GACTACCTGTGGACCCGAAA	151
Trim37_R1	TGACAGACTGCCTGCTATGG	151
Clptm1_F1	GGTCATCAAAGGCGTTCTGT	200
Clptm1_R1	TGGCGTTGAAGTCTGTGAAG	200
Negr1_F1	ACCCTCGAGTTTCCATTTCC	224
Negr1_R1	GGCCAAACAAGTAAGGGTGA	224
Necab2_F1	AGCAAGACCCTCTCGTTTGA	238
Necab2_R1	CCTCTGTCTCCCAGAACTCG	238
Camkv_F1	GCTCAAGATTGTGCACAGGA	204
Camkv_R1	ATGGCCCAACAGTCTACAGG	204
Slc9a6_F1	CTGGAGCACCTTTCTTCTGG	187
Slc9a6_R1	CAGCCCCATGTAGGAAAAGA	187
Pds5b_F1	TCCAAGAGCACCACGTACAG	203
Pds5b_R1	GACTGTTTGCCTGCTGATGA	203
Camkk2_F1	TGTCAAGCTGGCCTACAATG	205
Camkk2_R1	GGGATGATCCAGCTTTTTGA	205
Camk1d_F1	GGGCAAAGGAGATGTGATGT	246
Camk1d_R1	TCTTTGGCAGAGTCGGAGAT	246

Camk2d_F1	GGGACCATCAGAAACTGGAA	187
Camk2d_R1	TGACTGGCATCAGCTTCACT	187
Vamp1_F1	TTAGAGTTCCGGGTGTTTCG	218
Vamp1_R1	ACTGGTCATGTTGGGAGGAG	218
Nptx1_F1	TGCAGAGCAAGATCGATGAC	245
Nptx1_R1	CAGGCTCTTCTTCACCTTGG	245
Vsnl1_F1	GTGGTACAAGGGCTTCCTCA	225
Vsnl1_R1	GCCCAGTTCAGTTTCTGCTC	225
Gde1_F1	CATTCTTGCCGGAAGTCATC	248
Gde1_R1	CAAATAGTCCGGGGAGACAA	248
Mat2b_F1	TTCCCCACACATGTGAAAGA	235
Mat2b_R1	AGCAATCGAGCTGAGCATTT	235
Kcnj3_F1	GTCATCCTGGAAGGCATTGT	197
Kcnj3_R1	TCCTGCTCTTTCACGCTGTA	197
Nrp2_F1	ACCCACCGTGAAGAGTGAAG	160
Nrp2_R1	CACCCAACCACAGGTCTCTT	160
Atp2b4_F1	TCCGAAATGAGAAGGGTGAG	216
Atp2b4_R1	CCATAGCAAACCCGACATCT	216
Nrgn_F1	AGAGAGGCTGGTTCTGCAAG	184
Nrgn_R1	AATATCGTCGTCTGGCTTGG	184
Ppp1r14c_F1	GTGCTGGAAGAATGGATCGT	217
Ppp1r14c_R1	TCAGCTTCCTCATGCCTCTT	217
Tubb3_F1	TGAGGCCTCCTCTCACAAGT	207
Tubb3_R1	CGCACGACATCTAGGACTGA	207

Determination the Cutoff Q Value for the RNA Sequencing Data

In the KD_Microarray experiments, 748 genes were found to have gene expression changes upon Rbfox1 and Rbfox3 knockdown. These changes were validated by RT-qPCR at validation rate of 86.9% (Figure S1C). However, in the

KD_RNAseq experiments, only 365 genes were found to have gene expression changes when we used q value of 0.05 as the cutoff. This was a smaller number than expected and therefore we looked for a bigger q value as the new cutoff. The new cutoff value was first evaluated by examining the percent of genes that show opposite expression changes in KD and Rbfox1_C rescue experiments using different q values. When the q value was set at 0.05, 418 genes were found to have significant expression changes under KD, Rbfox1_C rescue, or both conditions. Among these genes, 340 genes (81.3%) showed opposite changes in opposite conditions. When the q value was increased to 0.3, the percentage of genes with opposite changes remain similar at 79% while this percentage was lower (64.8%) for genes with q values between 0.3 and 0.99. Thus a q value of 0.3 was used as cutoff for analysis. The expression changes in these genes were further validated by RT-qPCR at validation rate of 86.7% (Figure S3).

Comparison of Rbfox1_N Regulated Exons to Rbfox Regulated Exon Identified in Rbfox1 KO Mice and by Bayesian Network Analysis

The alternative cassette exons identified in Rbfox1 KO mice (Lovci et al., 2013) and by Bayesian network analysis (Weyn-Vanhentenryck et al., 2014) were compared to the Rbfox1_N regulated exons in the splicing set in this study. The coordinates of the Bayesian network exons were converted from mm10 to mm9 using UCSC LiftOver (https://genome.ucsc.edu/cgi-bin/hgLiftOver). The common exons were identified using BEDTools (Quinlan and Hall, 2010) and indicated in Table S2. Statistical significance was assessed by hypergeometric test.

iCLIP, Cellular Fractionation, and RNA Sequencing,

iCLIP was performed according to the original protocol (Konig et al., 2010), with some modifications. In brief, mouse forebrain cultures (DIV14) were irradiated with UV (254 nm) at 500 mJ/cm^2 on ice in Stratalinker 1800 (Statagene) and then partially lysed in lysis buffer (20 mM HEPES [pH 7.0], 150 mM NaCl, and 0.1% Triton X-100) for 1 minute on ice. The eluate was collected as the cytoplasmic fraction and the purity was assessed by immunoblotting. The Rbfox1 target RNA was then immunoprecipitated with Rbfox1 antibodies (clone 1D10) or anti-Flag antibodies (Sigma Aldrich #F3165). The crosslinked RNA was partially fragmented by

Micrococcal Nuclease (NEB # M0247S), dephosphorylated by Fast Alkaline Phosphatase (Thermo Scientific # EF0651), ligated to L3 linker by T4 RNA Ligase1 (NEB # M0204S), and labeled with ^{32}P at the 5' end by T4 Polynucleotide Kinase (NEB # M0201S). Protein-RNA complexes were then resolved by electrophoresis on 10% NuPAGE Bis-Tris Gel (Life Technologies # NP0307), electrotransferred to Protran BA-85 Nitrocellulose Membrane (0.45 μM pore size, Whatman #10104594), and bands that corresponded to Rbfox1 crosslinked to RNA fragments were excised. RNA fragments were eluted by Proteinase K digestion and reverse transcribed with RT primer by Superscript III (Life Technologies). The resulting cDNAs were separated on 5.5% polyacrylamide, 50% urea denaturing gels and the bands corresponding to size of 70 to 120 nt were excised. Purified cDNAs were circularized by CircLigase II ssDNA Ligase (Epicentre #CL9021K), hybridized to Cut_oligo, and linearized by FastDigest BamHI (Thermo Scientific # FD0054). Linearized cDNAs were amplified by PCR with P5 solexa and P3 solexa primers and the PCR products of sizes 150 to 210 bp were purified and sequenced in HiSeq 2000 (Illumina) (single end, 100 nt) by the UCLA Broad Stem Cell Center High Throughput Sequencing Facility.

Distribution of Clusters within the 3' UTR

The distance of the middle position of a cluster to either the start position or end position of a 3' UTR was calculated. The fraction of clusters in a 100 nt segment w

Cytoplasmic RbFox1 regulates the expression of synaptic and autism-related genes
p

and GCAUG clusters were calculated.

Gene Ontology Analysis

The Gene Ontology (GO) analyses were performed using GOMiner (Zeeberg et al., 2003). Enriched GO terms in biological process with FDR < 0.05 were used for comparison between gene sets of Rbfox1 regulated genes and 3' UTR target genes.

KEGG Pathway Analysis and Mammalian Phenotype Ontology Analysis

The enrichment analyses for KEGG pathways (Kanehisa et al., 2014) and Mammalian Phenotype Ontology (Smith and Eppig, 2012) were performed using

WebGestalt (Wang et al., 2013). Enriched terms with FDR < 0.05 were used for comparison between gene sets of Rbfox1 regulated genes and 3' UTR target genes.

Luciferase Assays

The Camk2a luciferase reporter containing full length 3' UTR was purchased from GeneCopoeia (MmiT028785-MT01, NM_009792.3). In this construct, the Camk2a 3' UTR was cloned downstream of a firefly luciferase coding region and a Renilla luciferase gene was also present on the same plasmid for normalization purposes. A mixture of 1 □g of DNA (0.2 □g of Camk2a reporter, 0.4 □g of pcDNA3.1-Flag-Rbfox1 expression plasmid, and pcDNA3.1(+) to 1 □g) was transfected into HEKT cells using Lipofectamine 2000 (Invitrogen). 24 hr later, luciferase expression was assayed with Luc-Pair miR Luciferase Assay Kit (GeneCopoeia # LPFR-M010). Part of the 3' UTR of Camk2a (mm9, chr18:61,145,404-61,146,404 (+)) or Camta1 (mm9, chr4:150,433,733-150,434,095 (-)) were cloned downstream of a Renillia luciferase coding region in plasmid pRL-TK (Promega). To facilitate directional cloning in pRL-TK, four restriction sites of NdeI, KpnI, EcoRV, and XhoI from the multiple cloning site in pcDNA3.1(+) (Invitrogen) were cloned into the XbaI site in the 3' UTR of Renillia luciferase gene before cloning of the Camta1 and Camk2a 3' UTRs. Deletion of Rbfox1 binding sites, the (U)GCAUG sequence, was performed by PCR-based cloning. A mixture of 1 □g of DNA (0.2 □g of Camk2a or Camta1 pRL-TK Renilla luciferase reporter, 0.2 □g of pGL3C firefly luciferase reporter (Promega # E2920), 0.1 □g of pcDNA3.1-Flag-Rbfox1 expression plasmid or 0.05 □g of pcDNA3.1-Flag-Rbfox3 expression plasmid, and pcDNA3.1(+) plasmid to 1 □g) was transfected into HEKT cells in one well of 24-well format using Lipofectamine 2000 (Invitrogen). At 24 hr after transfection, luciferase expression was assayed with Dual-Glo Luciferase Reporter Assay System (Promega) according to manufacturer's instruction and measured on a Molecular Devices Analyst AD microplate reader (Analyst AD 96-384). Renilla luciferase signals were first normalized to firefly luciferase signals, and then normalized to the control samples of each construct. The assays were performed three times in duplicate.

MicroRNA Analysis

Mouse brain Ago CLIP data was downloaded from http://ago.rockefeller.edu/ (Chi et al., 2009). MiRNA target sites located within 50 nt of a GCAUG motif that has Rbfox1 iCLIP tags in the cytoplasm were identified using BEDTools (Quinlan and Hall, 2010).

To evaluate significance, 100 random sets of miRNA target sites were generated by randomizing the positions of miRNA sites in the 3' UTR. The number of miRNA sites in each 3' UTR was not changed. The distribution of the numbers of overlapping pairs of miRNA site and Rbfox1 binding sites was used to calculate the

Description	Catalog number	RNA sequence	Final concentration	Target region	Name used in the paper
Accell Non-targeting siRNA #1	D001910-01	N/A	0.6 mM	N/A	
Accell Non-targeting siRNA #2	D001910-02	N/A	0.6 mM	N/A	
Accell Rbfox1 siRNA #1	A-41929-13	TGCTCCATATTAAATGATA	0.3 mM	ORF-3' UTR	siRF1_E10
Accell Rbfox1 siRNA #2	A-41929-14	GTAAAATATTAGATGTTGA	0.3 mM	ORF	
Accell Rbfox1 siRNA #3	Custom order	GCAACAGAUGAAAUUUCUU	1.2 mM	ORF	siRF1_E19
Accell Rbfox3 siRNA #1	A-065754-09	GTGTGACCATTCAAATTAA	0.3 mM	3' UTR	
Accell Rbfox3 siRNA #2	A-065754-10	GCATCAGCCACAGAAGCTA	0.3 mM	3' UTR	

3.1.9. SUPPLEMENTAL REFERENCES

Chi, S.W., Zang, J.B., Mele, A., and Darnell, R.B. (2009). Argonaute HITS-CLIP decodes microRNA-mRNA interaction maps. Nature *460*, 479-486.

Damianov, A., and Black, D.L. (2010). Autoregulation of Fox protein expression to produce dominant negative splicing factors. Rna *16*, 405-416.

Kanehisa, M., Goto, S., Sato, Y., Kawashima, M., Furumichi, M., and Tanabe, M. (2014). Data, information, knowledge and principle: back to metabolism in KEGG. Nucleic acids research *42*, D199-205.

Konig, J., Zarnack, K., Rot, G., Curk, T., Kayikci, M., Zupan, B., Turner, D.J., Luscombe, N.M., and Ule, J. (2010). iCLIP reveals the function of hnRNP particles in splicing at individual nucleotide resolution. Nature structural & molecular biology *17*, 909-915.

Lovci, M.T., Ghanem, D., Marr, H., Arnold, J., Gee, S., Parra, M., Liang, T.Y., Stark, T.J., Gehman, L.T., Hoon, S.*, et al.* (2013). Rbfox proteins regulate alternative mRNA splicing through evolutionarily conserved RNA bridges. Nature structural & molecular biology *20*, 1434-1442.

Quinlan, A.R., and Hall, I.M. (2010). BEDTools: a flexible suite of utilities for comparing genomic features. Bioinformatics *26*, 841-842.

Sharma, S., Falick, A.M., and Black, D.L. (2005). Polypyrimidine tract binding protein blocks the 5' splice site-dependent assembly of U2AF and the prespliceosomal E complex. Molecular cell *19*, 485-496.

Smith, C.L., and Eppig, J.T. (2012). The Mammalian Phenotype Ontology as a unifying standard for experimental and high-throughput phenotyping data. Mammalian genome : official journal of the International Mammalian Genome Society *23*, 653-668.

Sugnet, C.W., Srinivasan, K., Clark, T.A., O'Brien, G., Cline, M.S., Wang, H., Williams, A., Kulp, D., Blume, J.E., Haussler, D.*, et al.* (2006). Unusual intron conservation near tissue-regulated exons found by splicing microarrays. PLoS computational biology *2*, e4.

Wang, J., Duncan, D., Shi, Z., and Zhang, B. (2013). WEB-based GEne SeT AnaLysis Toolkit (WebGestalt): update 2013. Nucleic acids research *41*, W77-83.

Weyn-Vanhentenryck, S.M., Mele, A., Yan, Q., Sun, S., Farny, N., Zhang, Z., Xue, C., Herre, M., Silver, P.A., Zhang, M.Q.*, et al.* (2014). HITS-CLIP and integrative modeling define the Rbfox splicing-regulatory network linked to brain development and autism. Cell reports *6*, 1139-1152.

Zeeberg, B.R., Feng, W., Wang, G., Wang, M.D., Fojo, A.T., Sunshine, M., Narasimhan, S., Kane, D.W., Reinhold, W.C., Lababidi, S.*, et al.* (2003). GoMiner: a

resource for biological interpretation of genomic and proteomic data. Genome biology *4*, R28.

4. Chapter IV – General discussion

4.1. Main findings

The complexity of neuronal morphologies and neural circuits that enable complex behaviors requires a tight regulation of gene expression at the post-transcriptional level. Importantly, abnormalities in RNA processing and translation within neurons contribute to autism spectrum disorders (ASD). Our studies aimed to advance the understanding of the post-transcriptional mechanisms regulating brain development and plasticity by addressing two fundamental questions.

We asked *whether and how changes in the patterns of alternative cleavage and polyadenylation (APA) are associated with long-lasting forms of long-term potentiation (LTP) that underlie learning and memory.* We found that the induction of chemical LTP in the Schaffer collateral pathway of the hippocampus triggers global changes in APA that lead to an increased use of proximal 3'UTR polyadenylation sites (PASs) and intronic PASs. The resulting differentially regulated APA isoforms have an overall shorter size and display shorter 3'UTRs. We postulate that transcripts with truncated 3'UTRs can be functionally impacted by lacking key regulatory elements such as miRNA and RNA-binding protein (RBP) binding sites commonly contained within 3'UTRs.

RBPs are known to play critical roles in neuronal post-transcriptional regulation controlling the localization of mRNAs to synapses and their translation in an activity-dependent manner. This allows gene expression to be regulated at the level of individual synapses within a single neuron. The RBP RbFox1 was previously identified as a candidate ASD gene and its alternatively spliced nuclear isoform was well characterized as a splicing regulator. *In this study we decided to investigate the function of Rbfox1 in cytoplasmic RNA regulation in mouse hippocampal neurons.* We found that the cytoplasmic isoform of RbFox1 binds to the 3'UTR of its target mRNAs increasing transcripts stability and translation. Moreover, RbFox1 targets in the cytoplasm are enriched for genes involved in cortical development and associated with autism spectrum disorders.

4.2. Future directions

The results from the 3'READS studies presented in Chapter 2 uncovered a dynamic and highly regulated 3'end processing landscape during LTP and opened avenues for future research.

We identified dozens of activity-dependent changes in APA and validated a few by qPCR. Further functional studies on individual differentially expressed APA isoforms should improve our understanding of the role of these changes in long-term memory. Relevant follow-up experiments include studying the differential localization of altered mRNA isoforms, measuring the impact of activity-dependent APA on protein production, and the effect of these changes on protein-protein interaction and function. Moreover, changing the balance of 3'UTR and intronic APA isoforms through overexpression and knockdown experiments could provide insights into the functional role of APA regulation to neuronal plasticity.

In our study we examined APA in hippocampal mini-slices composed of many neuronal (e.g. excitatory, inhibitory, interneurons) and non-neuronal cell types (e.g. glial cells). Previous studies have shown that different hippocampal cell types display unique patterns of gene expression (Zeisel et al., 2015), and that cell-type diversity is critical for synaptic plasticity at the individual and intercellular interaction level (e.g. interaction between neurons and astrocytes, (Allen and Eroglu, 2017). Comparable to a recent profiling study of LTP-induced changes in ribosome-associated transcripts in excitatory neurons (Chen et al., 2017b), cell type specificity could be achieved by crossing a ribotag mouse line (with floxed HA-tagged ribosomal protein L22 in cells expressing Cre recombinase) with transgenic mouse lines expressing cre under cell-type specific promoters (e.g. camk2a, gad1, gfap). Immunoprecipitation followed by 3'READS of the ribosome-associated population of RNAs purified from specific cell types of cLTP stimulated hippocampal mini-slices would allow us to further understand APA regulation in the hippocampus (Sanz et al., 2009). Recently, the activity-dependent response of 30 different cell-types of the visual cortex was characterized using single-cell sequencing (Hrvatin et al., 2018). Similar cell-type specific approaches would help uncover individual contributions of the different cell types to APA during synaptic plasticity.

Local translation is a widely used mechanism in neurons to control gene expression in a time- and synapse-specific manner. Our study lacks intracellular resolution to profile the population of APA isoforms localized to synapses during LTP. APA profiling of cLTP-stimulated hippocampal synaptosome preparations - containing presynaptic terminals attached to post-synaptic dendritic spines - or cellular fractionation of neurons grown on porous membranes followed by sequencing of isolated neuronal processes would start to uncover the distribution of APA isoforms at synapses (Prieto et al., 2015; Taliaferro et al., 2016). Alternatively, dissection of the stratum radiatum region of the hippocampus - mainly composed of CA1 dendrites and

CA3 axons - following cLTP stimulation would enrich the detection of dendritically-localized APA isoforms (Zhong et al., 2006).

The analysis from chapters II and III suggest that miRNA regulation might contribute to APA regulation during hippocampal plasticity and the control of neuronal gene expression modulated by the cytoplasmic form of RbFox1. Profiling the population of miRNAs following LTP induction in acute mouse hippocampal slices would provide an accurate baseline for comparative studies. An overlap between miRNA expression changes and previously identified changes in the number of complimentary miRNA-binding sites in activity-dependent APA isoforms would suggest a miRNA-dependent process of APA in plasticity. To examine the population of functionally active miRNAs and obtain cell-type specificity, high-throughput sequencing of RNA isolated by crosslinking immunoprecipitation (HITS-CLIP) could be used to identify miRNAs and their targets in cLTP-stimulated hippocampal slices of a knock-in mouse line expressing GFP-cmyc-Ago2 specifically in excitatory neurons (He et al., 2012). Using this strategy, only miRNAs loaded into the RISC complex (of which Ago2 is the main catalytic component) would be purified and sequenced. The results of these studies will elucidate networks of alternative 3'UTR isoforms and miRNA-regulatory mechanisms implicated in long-term memory formation and thereby contribute to a deeper understanding of the function of post-transcriptional regulation in the CNS.

New tools developed to analyze post-transcriptional gene regulation at genome-wide and cell type-specific manner promise to uncover new ways in which activity can change the structure and function of individual synapses to store memories in the brain. Elucidation of these regulatory mechanisms, in turn, are likely to reveal important new therapeutic targets for the many diseases in which synaptic plasticity is altered to produced cognitive disorders.

5. References for general introduction and discussion

Alberi, L., Liu, S., Wang, Y., Badie, R., Smith-Hicks, C., Wu, J., et al. (2011). Activity-Induced Notch Signaling in Neurons Requires Arc/Arg3.1 and Is Essential for Synaptic Plasticity in Hippocampal Networks. *Neuron* 69, 437–444. doi:10.1016/j.neuron.2011.01.004.

Alberini, C. M. (2009). Transcription Factors in Long-Term M emory and Synaptic Plasticity. *Physiol. Rev*, 121–145. doi:10.1152/physrev.00017.2008.

Allen, N. J., and Eroglu, C. (2017). Cell Biology of Astrocyte-Synapse Interactions. *Neuron* 96, 697–708. doi:10.1016/j.neuron.2017.09.056.

An, J. J., Gharami, K., Liao, G.-Y., Woo, N. H., Lau, A. G., Vanevski, F., et al. (2008). Distinct Role of Long 3′ UTR BDNF mRNA in Spine Morphology and Synaptic Plasticity in Hippocampal Neurons. *Cell* 134, 175–187. doi:10.1016/j.cell.2008.05.045.

Anders, S., and Huber, W. (2010). Differential expression analysis for sequence count data. *Genome Biol.* 11, R106. doi:10.1186/gb-2010-11-10-r106.

Anders, S., Reyes, A., and Huber, W. (2012). Detecting differential usage of exons from RNA-seq data. *Genome Res.* 22, 2008–2017. doi:10.1101/gr.133744.111.

Ashraf, S. I., McLoon, A. L., Sclarsic, S. M., and Kunes, S. (2006). Synaptic protein synthesis associated with memory is regulated by the RISC pathway in Drosophila. *Cell* 124, 191–205. doi:10.1016/j.cell.2005.12.017.

Banerjee, S., Neveu, P., and Kosik, K. S. (2009). A Coordinated Local Translational Control Point at the Synapse Involving Relief from Silencing and MOV10 Degradation. *Neuron* 64, 871–884. doi:10.1016/j.neuron.2009.11.023.

Barco, A., Alarcon, J. M., and Kandel, E. R. (2002). Expression of constitutively active CREB protein facilitates the late phase of long-term potentiation by enhancing synaptic capture. *Cell* 108, 689–703. doi:10.1016/S0092-8674(02)00657-8.

Bartel, D. P. (2009). MicroRNAs: Target Recognition and Regulatory Functions. *Cell* 136, 215–233. doi:10.1016/j.cell.2009.01.002.

Benito, E., and Barco, A. (2010). CREB's control of intrinsic and synaptic plasticity: implications for CREB-dependent memory models. *Trends Neurosci.* 33, 230–240. doi:10.1016/j.tins.2010.02.001.

Berg, M. G., Singh, L. N., Younis, I., Liu, Q., Pinto, A. M., Kaida, D., et al. (2012). U1 snRNP determines mRNA length and regulates isoform expression. *Cell* 150, 53–64. doi:10.1016/j.cell.2012.05.029.

Berlucchi, G., and Buchtel, H. A. (2009). Neuronal plasticity: Historical roots and evolution of meaning. *Exp. Brain Res.* 192, 307–319. doi:10.1007/s00221-008-

1611-6.

Bhalla, K., Phillips, H., Crawford, J., McKenzie, O. D., Mulley, J., Eyre, H., et al. (2004). The de novo chromosome 16 translocations of two patients with abnormal phenotypes (mental retardation and epilepsy) disrupt the A2BP1 gene. *J. Hum. Genet.* 49. doi:10.1007/s10038-004-0145-4.

Bliss, T. V, and Collingridge, G. L. (1993). A synaptic model of memory: long-term potentiation in the hippocampus. *Nature* 361, 31–39. doi:10.1038/361031a0.

Boudreau, R. L., Jiang, P., Gilmore, B. L., Spengler, R. M., Tirabassi, R., Nelson, J. A., et al. (2014). Transcriptome-wide discovery of microRNA binding sites in Human Brain. *Neuron* 81, 294–305. doi:10.1016/j.neuron.2013.10.062.

Bourne, J. N., Sorra, K. E., Hurlburt, J., and Harris, K. M. (2007). Polyribosomes are increased in spines of CA1 dendrites 2 h after the induction of LTP in mature rat hippocampal slices. *Hippocampus* 17, 1–4. doi:10.1002/hipo.20238.

Boutet, S. C., Cheung, T. H., Quach, N. L., Liu, L., Prescott, S. L., Edalati, A., et al. (2012). Alternative polyadenylation mediates microRNA regulation of muscle stem cell function. *Cell Stem Cell* 10, 327–336. doi:10.1016/j.stem.2012.01.017.

Brai, E., Marathe, S., Astori, S., Fredj, N. Ben, Perry, E., Lamy, C., et al. (2015). Notch1 Regulates Hippocampal Plasticity Through Interaction with the Reelin Pathway, Glutamatergic Transmission and CREB Signaling. *Front. Cell. Neurosci.* 9. doi:10.3389/fncel.2015.00447.

Bresson, S. M., and Conrad, N. K. (2013). The Human Nuclear Poly(A)-Binding Protein Promotes RNA Hyperadenylation and Decay. *PLoS Genet.* 9. doi:10.1371/journal.pgen.1003893.

Buxbaum, A. R., Yoon, Y. J., Singer, R. H., and Park, H. Y. (2015). Single-molecule insights into mRNA dynamics in neurons. *Trends Cell Biol.* 25, 468–475. doi:10.1016/j.tcb.2015.05.005.

Cajal, S. R. Y. (1894). The Croonian Lecture: La Fine Structure des Centres Nerveux. *Proc. R. Soc. London* 55, 444–468. doi:10.1098/rspl.1894.0063.

Cajigas, I. J., Tushev, G., Will, T. J., Tom Dieck, S., Fuerst, N., and Schuman, E. M. (2012). The Local Transcriptome in the Synaptic Neuropil Revealed by Deep Sequencing and High-Resolution Imaging. *Neuron* 74, 453–466. doi:10.1016/j.neuron.2012.02.036.

Chahrour, M., and Zoghbi, H. Y. (2007). The Story of Rett Syndrome: From Clinic to Neurobiology. *Neuron* 56, 422–437. doi:10.1016/j.neuron.2007.10.001.

Chang, S. P., Gong, R., Stuart, J., and Tang, S. J. (2006). Molecular network and chromosomal clustering of genes involved in synaptic plasticity in the hippocampus. *J. Biol. Chem.* 281, 30195–30211. doi:10.1074/jbc.M605876200.

Chen, F. X., Xie, P., Collings, C. K., Cao, K., Aoi, Y., Marshall, S. A., et al. (2017a). PAF1 regulation of promoter-proximal pause release via enhancer activation. *Science (80-.).*, eaan3269. doi:10.1126/science.aan3269.

Chen, P. B., Kawaguchi, R., Blum, C., Achiro, J. M., Coppola, G., O'Dell, T. J., et al. (2017b). Mapping Gene Expression in Excitatory Neurons during Hippocampal Late-Phase Long-Term Potentiation. *Front. Mol. Neurosci.* 10, 1–16. doi:10.3389/fnmol.2017.00039.

Chi, S. W., Zang, J. B., Mele, A., and Darnell, R. B. (2009). Argonaute HITS-CLIP decodes microRNA-mRNA interaction maps. *Nature* 460, 479–86. doi:10.1038/nature08170.

Chotiner, J. K., Khorasani, H., Nairn, A. C., O'Dell, T. J., and Watson, J. B. (2003). Adenylyl cyclase-dependent form of chemical long-term potentiation triggers translational regulation at the elongation step. *Neuroscience* 116, 743–752. doi:10.1016/S0306-4522(02)00797-2.

Cohen, J. E., Lee, P. R., and Fields, R. D. (2014). Systematic identification of 3'-UTR regulatory elements in activity-dependent mRNA stability in hippocampal neurons. *Philos. Trans. R. Soc. B Biol. Sci.* 369, 20130509–20130509. doi:10.1098/rstb.2013.0509.

Colgan, D. F., and Manley, J. L. (1997). Mechanism and regulation of mRNA polyadenylation. *Genes Dev.* 11, 2755–2766. doi:10.1101/gad.11.21.2755.

Davis, T. H., Cuellar, T. L., Koch, S. M., Barker, A. J., Harfe, B. D., McManus, M. T., et al. (2008). Conditional loss of Dicer disrupts cellular and tissue morphogenesis in the cortex and hippocampus. *J. Neurosci.* 28, 4322–4330. doi:10.1523/JNEUROSCI.4815-07.2008.

Derti, A., Garrett-Engele, P., MacIsaac, K. D., Stevens, R. C., Sriram, S., Chen, R., et al. (2012). A quantitative atlas of polyadenylation in five mammals. *Genome Res.* 22, 1173–1183. doi:10.1101/gr.132563.111.

Di Giammartino, D. C., Nishida, K., and Manley, J. L. (2011). Mechanisms and Consequences of Alternative Polyadenylation. *Mol. Cell* 43, 853–866. doi:10.1016/j.molcel.2011.08.017.

Dobin, A., Davis, C. A., Schlesinger, F., Drenkow, J., Zaleski, C., Jha, S., et al. (2013). STAR: Ultrafast universal RNA-seq aligner. *Bioinformatics* 29, 15–21. doi:10.1093/bioinformatics/bts635.

Eacker, S. M., Keuss, M. J., Berezikov, E., Dawson, V. L., and Dawson, T. M. (2011). Neuronal activity regulates hippocampal miRNA expression. *PLoS One* 6. doi:10.1371/journal.pone.0025068.

Eberwine, J., Belt, B., Kacharmina, J. E., and Miyashiro, K. (2002). Analysis of

subcellularly localized mRNAs using in situ hybridization, mRNA amplification, and expression profiling. *Neurochem. Res.* 27, 1065–1077. doi:10.1023/A:1020956805307.

Ehlers, M. D. (2003). Activity level controls postsynaptic composition and signaling via the ubiquitin-proteasome system. *Nat. Neurosci.* 6, 231–242. doi:10.1038/nn1013.

Elkon, R., Ugalde, A. P., and Agami, R. (2013). Alternative cleavage and polyadenylation: extent, regulation and function. *Nat. Rev. Genet.* 14, 496–506. doi:10.1038/nrg3482.

Fiore, R., Khudayberdiev, S., Christensen, M., Siegel, G., Flavell, S. W., Kim, T. K., et al. (2009). Mef2-mediated transcription of the miR379-410 cluster regulates activity-dependent dendritogenesis by fine-tuning Pumilio2 protein levels. *Embo J* 28, 697–710. doi:10.1038/emboj.2009.10.

Fischl, H., Howe, F. S., Furger, A., and Mellor, J. (2017). Paf1 Has Distinct Roles in Transcription Elongation and Differential Transcript Fate. *Mol. Cell* 65, 685–698.e8. doi:10.1016/j.molcel.2017.01.006.

Flavell, S. W., Kim, T., Gray, J. M., Harmin, D. A., Hemberg, M., Hong, E. J., et al. (2008). Genome-Wide Analysis of MEF2 Transcriptional Program Reveals Synaptic Target Genes and Neuronal Activity-Dependent Polyadenylation Site Selection. *Neuron* 60, 1022–1038. doi:10.1016/j.neuron.2008.11.029.

Flexner, J. B., Flexner, L. B., and Stellar, E. (1963). Memory in Mice as Affected by Intracerebral Puromycin. *Science (80-.).* 141, 57–59. doi:10.1126/science.141.3575.57.

Frey, U., Krug, M., Reymann, K. G., and Matthies, H. (1988). Anisomycin, an inhibitor of protein synthesis, blocks late phases of LTP phenomena in the hippocampal CA1 region in vitro. *Brain Res.* 452, 57–65. doi:10.1016/0006-8993(88)90008-X.

Gao, F.-B., and Taylor, J. P. (2014). RNA metabolism in neurological disease. *Brain Res.* 1584, 1–2. doi:10.1016/j.brainres.2014.09.011.

Gehman, L. T., Stoilov, P., Maguire, J., Damianov, A., Lin, C. H., Shiue, L., et al. (2011). The splicing regulator Rbfox1 (A2BP1) controls neuronal excitation in the mammalian brain. in *Nature Genetics*, 706–711. doi:10.1038/ng.841.

Glock, C., Heumüller, M., and Schuman, E. M. (2017). mRNA transport & local translation in neurons. *Curr. Opin. Neurobiol.* 45, 169–177. doi:10.1016/j.conb.2017.05.005.

Gu, Q.-H., Yu, D., Hu, Z., Liu, X., Yang, Y., Luo, Y., et al. (2015). miR-26a and miR-384-5p are required for LTP maintenance and spine enlargement. *Nat. Commun.* 6, 6789. doi:10.1038/ncomms7789.

Han, K., Gennarino, V. A., Lee, Y., Pang, K., Hashimoto-Torii, K., Choufani, S., et al.

(2013). Human-specific regulation of MeCP2 levels in fetal brains by microRNA miR-483-5p. *Genes Dev.* 27, 485–490. doi:10.1101/gad.207456.112.

Hansen, K. F., Sakamoto, K., Wayman, G. A., Impey, S., and Obrietan, K. (2010). Transgenic miR132 alters neuronal spine density and impairs novel object recognition memory. *PLoS One* 5. doi:10.1371/journal.pone.0015497.

Håvik, B., Røkke, H., Dagyte, G., Stavrum, A. K., Bramham, C. R., and Steen, V. M. (2007). Synaptic activity-induced global gene expression patterns in the dentate gyrus of adult behaving rats: Induction of immunity-linked genes. *Neuroscience* 148, 925–936. doi:10.1016/j.neuroscience.2007.07.024.

He, M., Liu, Y., Wang, X., Zhang, M. Q., Hannon, G. J., and Huang, Z. J. (2012). Cell-type-based analysis of microRNA profiles in the mouse brain. *Neuron* 73, 35–48. doi:10.1016/j.neuron.2011.11.010.

Hebb, D. O. (1949). *The Organization of Behavior*.

Hebert, S. S., Papadopoulou, A. S., Smith, P., Galas, M. C., Planel, E., Silahtaroglu, A. N., et al. (2010). Genetic ablation of dicer in adult forebrain neurons results in abnormal tau hyperphosphorylation and neurodegeneration. *Hum. Mol. Genet.* 19, 3959–3969. doi:10.1093/hmg/ddq311.

Hermey, G., Mahlke, C., Gutzmann, J. J., Schreiber, J., Blüthgen, N., and Kuhl, D. (2013). Genome-Wide Profiling of the Activity-Dependent Hippocampal Transcriptome. *PLoS One* 8. doi:10.1371/journal.pone.0076903.

Hilgers, V., Perry, M. W., Hendrix, D., Stark, A., Levine, M., and Haley, B. (2011). Neural-specific elongation of 3' UTRs during Drosophila development. *Proc. Natl. Acad. Sci. U. S. A.* 108, 15864–9. doi:10.1073/pnas.1112672108.

Ho, V. M., Lee, J.-A., and Martin, K. C. (2011). The cell biology of synaptic plasticity. *Science* 334, 623–8. doi:10.1126/science.1209236.

Holt, C. E., and Schuman, E. M. (2013). The central dogma decentralized: New perspectives on RNA function and local translation in neurons. *Neuron* 80, 648–657. doi:10.1016/j.neuron.2013.10.036.

Holtmaat, A., and Svoboda, K. (2009). Experience-dependent structural synaptic plasticity in the mammalian brain. *Nat. Rev. Neurosci.* 10, 647–658. doi:10.1038/nrn2699.

Hoque, M., Ji, Z., Zheng, D., Luo, W., Li, W., You, B., et al. (2013). Analysis of alternative cleavage and polyadenylation by 3' region extraction and deep sequencing. *Nat. Methods* 10, 133–9. doi:10.1038/nmeth.2288.

Hrvatin, S., Hochbaum, D. R., Nagy, M. A., Cicconet, M., Robertson, K., Cheadle, L., et al. (2018). Single-cell analysis of experience-dependent transcriptomic states in the mouse visual cortex. *Nat. Neurosci.* 21, 120–129. doi:10.1038/s41593-017-

0029-5.

Huber, K. M., Kayser, M. S., and Bear, M. F. (2000). Role for rapid dendritic protein synthesis in hippocampal mGluR- dependent long-term depression. *Science (80-.).* 288, 1254–1256. doi:10.1126/science.288.5469.1254.

Huntzinger, E., and Izaurralde, E. (2011). Gene silencing by microRNAs: contributions of translational repression and mRNA decay. *Nat. Rev. Genet.* 12, 99–110. doi:10.1038/nrg2936.

James, W. (1890). *The principles of psychology (Vols. 1 & 2)*. doi:10.1037/10538-000.

Ji, Z., Lee, J. Y., Pan, Z., Jiang, B., and Tian, B. (2009). Progressive lengthening of 3' untranslated regions of mRNAs by alternative polyadenylation during mouse embryonic development. *Proc. Natl. Acad. Sci. U. S. A.* 106, 7028–33. doi:10.1073/pnas.0900028106.

Ji, Z., and Tian, B. (2009). Reprogramming of 3' untranslated regions of mRNAs by alternative polyadenylation in generation of pluripotent stem cells from different cell types. *PLoS One* 4, e8419. doi:10.1371/journal.pone.0008419.

Jin, Y., Suzuki, H., Maegawa, S., Endo, H., Sugano, S., Hashimoto, K., et al. (2003). A vertebrate RNA-binding protein Fox-1 regulates tissue-specific splicing via the pentanucleotide GCAUG. *EMBO J.* 22, 905–912. doi:10.1093/emboj/cdg089.

Job, C., and Eberwine, J. (2001). Localization and translation of mRNA in dendrites and axons. *Nat. Rev. Neurosci.* 2, 889–898. doi:10.1038/35104069.

Kandel, E. R. (2001). The Molecular Biology of Memory Storage: A Dialogue between Genes and Synapses. *Science (80-.).* 294, 1030–1038. doi:10.1126/science.1067020.

Kandel, E. R., Schwartz, J. H., and Jessell, T. M. (2013). *Principles of Neural Science*. doi:10.1036/0838577016.

Kang, H., and Schuman, E. M. (1996). A Requirement for Local Protein Synthesis in Neurotrophin-Induced Hippocampal Synaptic Plasticity. *Science (80-.).* 273, 1402–1406. doi:10.1126/science.273.5280.1402.

Kelleher, R. J., Govindarajan, A., Jung, H.-Y., Kang, H., and Tonegawa, S. (2004). Translational Control by MAPK Signaling in Long-Term Synaptic Plasticity and Memory. *Cell* 116, 467–479. doi:10.1016/S0092-8674(04)00115-1.

Kiebler, M. A., and Bassell, G. J. (2006). Neuronal RNA Granules: Movers and Makers. *Neuron* 51, 685–690. doi:10.1016/j.neuron.2006.08.021.

Konopka, W., Kiryk, A., Novak, M., Herwerth, M., Parkitna, J. R., Wawrzyniak, M., et al. (2010). MicroRNA loss enhances learning and memory in mice. *J. Neurosci.* 30, 14835–42. doi:10.1523/JNEUROSCI.3030-10.2010.

Kye, M.-J., Liu, T., Levy, S. F., Xu, N. L., Groves, B. B., Bonneau, R., et al. (2007).

Somatodendritic microRNAs identified by laser capture and multiplex RT-PCR. *RNA* 13, 1224–1234. doi:10.1261/rna.480407.

Lagos-Quintana, M., Rauhut, R., Yalcin, A., Meyer, J., Lendeckel, W., and Tuschl, T. (2002). Identification of tissue-specific MicroRNAs from mouse. *Curr. Biol.* 12, 735–739. doi:10.1016/S0960-9822(02)00809-6.

Landgraf, P., Rusu, M., Sheridan, R., Sewer, A., Iovino, N., Aravin, A., et al. (2007). A Mammalian microRNA Expression Atlas Based on Small RNA Library Sequencing. *Cell* 129, 1401–1414. doi:10.1016/j.cell.2007.04.040.

Langmead, B., and Salzberg, S. L. (2012). Fast gapped-read alignment with Bowtie 2. *Nat Methods* 9, 357–359. doi:10.1038/nmeth.1923.

Lau, A. G., Irier, H. a, Gu, J., Tian, D., Ku, L., Liu, G., et al. (2010). Distinct 3'UTRs differentially regulate activity-dependent translation of brain-derived neurotrophic factor (BDNF). *Proc. Natl. Acad. Sci. U. S. A.* 107, 15945–50. doi:10.1073/pnas.1002929107.

Lawrence, M., Huber, W., Pagès, H., Aboyoun, P., Carlson, M., Gentleman, R., et al. (2013). Software for Computing and Annotating Genomic Ranges. *PLoS Comput. Biol.* 9. doi:10.1371/journal.pcbi.1003118.

Leach, P. T., Poplawski, S. G., Kenney, J. W., Hoffman, B., Liebermann, D. a, Abel, T., et al. (2012). Gadd45b knockout mice exhibit selective deficits in hippocampus-dependent long-term memory. *Learn. Mem.* 19, 319–24. doi:10.1101/lm.024984.111.

Lee, J. A., Tang, Z. Z., and Black, D. L. (2009). An inducible change in Fox-1/A2BP1 splicing modulates the alternative splicing of downstream neuronal target exons. *Genes Dev.* 23, 2284–2293. doi:10.1101/gad.1837009.

Li, W., You, B., Hoque, M., Zheng, D., Luo, W., Ji, Z., et al. (2015). Systematic profiling of poly(a)+ transcripts modulated by core 3' end processing and splicing factors reveals regulatory rules of alternative cleavage and polyadenylation. *PLoS Genet.* 11, e1005166. doi:10.1371/journal.pgen.1005166.

Lianoglou, S., Garg, V., Yang, J. L., Leslie, C. S., and Mayr, C. (2013). Ubiquitously transcribed genes use alternative polyadenylation to achieve tissue-specific expression. *Genes Dev.* 27, 2380–2396. doi:10.1101/gad.229328.113.

Litman, P., Barg, J., Rindzoonski, L., and Ginzburg, I. (1993). Subcellular localization of tau mRNA in differentiating neuronal cell culture: Implications for neuronal polarity. *Neuron* 10, 627–638. doi:10.1016/0896-6273(93)90165-N.

Liu-Yesucevitz, L., Bassell, G. J., Gitler, A. D., Hart, A. C., Klann, E., Richter, J. D., et al. (2011). Local RNA Translation at the Synapse and in Disease. *J. Neurosci.* 31, 16086–16093. doi:10.1523/JNEUROSCI.4105-11.2011.

Lonze, B. E., and Ginty, D. D. (2002). Function and Regulation of CREB Family Transcription Factors in the Nervous System CREB and its close relatives are now widely accepted. *Neuron* 35, 605–623. doi:10.1016/S0896-6273(02)00828-0.

Love, M. I., Huber, W., and Anders, S. (2014). Moderated estimation of fold change and dispersion for RNA-seq data with DESeq2. *Genome Biol.* 15, 1–34. doi:Artn 550\rDoi 10.1186/S13059-014-0550-8.

Lugli, G., Torvik, V. I., Larson, J., and Smalheiser, N. R. (2008). Expression of microRNAs and their precursors in synaptic fractions of adult mouse forebrain. *J. Neurochem.* 106, 650–661. doi:10.1111/j.1471-4159.2008.05413.x.

Lukong, K. E., Chang, K. wei, Khandjian, E. W., and Richard, S. (2008). RNA-binding proteins in human genetic disease. *Trends Genet.* 24, 416–425. doi:10.1016/j.tig.2008.05.004.

Luo, W., Ji, Z., Pan, Z., You, B., Hoque, M., Li, W., et al. (2013). The Conserved Intronic Cleavage and Polyadenylation Site of CstF-77 Gene Imparts Control of 3′ End Processing Activity through Feedback Autoregulation and by U1 snRNP. *PLoS Genet.* 9. doi:10.1371/journal.pgen.1003613.

Lutz, C. S., and Moreira, A. (2011). Alternative mRNA polyadenylation in eukaryotes: An effective regulator of gene expression. *Wiley Interdiscip. Rev. RNA* 2, 22–31. doi:10.1002/wrna.47.

Maag, J. L. V, Panja, D., Sporild, I., Patil, S., Kaczorowski, D. C., Bramham, C. R., et al. (2015). Dynamic expression of long noncoding RNAs and repeat elements in synaptic plasticity. *Front. Neurosci.* 9, 1–16. doi:10.3389/fnins.2015.00351.

Majdan, M., and Shatz, C. J. (2006). Effects of visual experience on activity-dependent gene regulation in cortex. *Nat. Neurosci.* 9, 650–9. doi:10.1038/nn1674.

Makhinson, M., Chotiner, J. K., Watson, J. B., and O'Dell, T. J. (1999). Adenylyl cyclase activation modulates activity-dependent changes in synaptic strength and Ca2+/calmodulin-dependent kinase II autophosphorylation. *J. Neurosci.* 19, 2500–2510.

Malmevik, J., Petri, R., Klussendorf, T., Knauff, P., Åkerblom, M., Johansson, J., et al. (2015). Identification of the miRNA targetome in hippocampal neurons using RIP-seq. *Nat. Publ. Gr.* 5, 12609. doi:10.1038/srep12609.

Mansuy, I. M., Mayford, M., Jacob, B., Kandel, E. R., and Bach, M. E. (1998). Restricted and regulated overexpression reveals calcineurin as a key component in the transition from short-term to long-term memory. *Cell* 92, 39–49. doi:10.1016/S0092-8674(00)80897-1.

Martin, C. L., Duvall, J. A., Ilkin, Y., Simon, J. S., Arreaza, M. G., Wilkes, K., et al. (2007). Cytogenetic and molecular characterization of A2BP1/FOX1 as a

candidate gene for autism. *Am. J. Med. Genet. Part B Neuropsychiatr. Genet.* 144, 869–876. doi:10.1002/ajmg.b.30530.

Martin, K. C., Casadio, A., Zhu, H., Yaping, E., Rose, J. C., Chen, M., et al. (1997a). Synapse-specific, long-term facilitation of aplysia sensory to motor synapses: A function for local protein synthesis in memory storage. *Cell* 91, 927–938. doi:10.1016/S0092-8674(00)80484-5.

Martin, K. C., and Ephrussi, A. (2009). mRNA Localization: Gene Expression in the Spatial Dimension. *Cell* 136, 719–730. doi:10.1016/j.cell.2009.01.044.

Martin, K. C., Michael, D., Rose, J. C., Barad, M., Casadio, A., Zhu, H., et al. (1997b). MAP kinase translocates into the nucleus of the presynaptic cell and is required for long-term facilitation in Aplysia. *Neuron* 18, 899–912. doi:10.1016/S0896-6273(00)80330-X.

Martin, K. C., and Zukin, R. S. (2006). RNA Trafficking and Local Protein Synthesis in Dendrites: An Overview. *J. Neurosci.* 26, 7131–7134. doi:10.1523/JNEUROSCI.1801-06.2006.

Mayford, M., Baranes, D., Podsypanina, K., and Kandel, E. R. (1996). The 3'-untranslated region of CaMKII is a cis-acting signal for the localization and translation of mRNA in dendrites. *Proc. Natl. Acad. Sci.* 93, 13250–13255. doi:10.1073/pnas.93.23.13250.

Mayford, M., Siegelbaum, S. A., and Kandel, E. R. (2012). Synapses and memory storage. *Cold Spring Harb. Perspect. Biol.* 4, 1–18. doi:10.1101/cshperspect.a005751.

Mayr, C. (2016). Evolution and Biological Roles of Alternative 3'UTRs. *Trends Cell Biol.*, 227–37. doi:10.1016/j.tcb.2015.10.012.

Mayr, C., and Bartel, D. P. (2009). Widespread shortening of 3'UTRs by alternative cleavage and polyadenylation activates oncogenes in cancer cells. *Cell* 138, 673–84. doi:10.1016/j.cell.2009.06.016.

McNair, K., Davies, C. H., and Cobb, S. R. (2006). Plasticity-related regulation of the hippocampal proteome. *Eur. J. Neurosci.* 23, 575–580. doi:10.1111/j.1460-9568.2005.04542.x.

McNeill, E., and Van Vactor, D. (2012). MicroRNAs Shape the Neuronal Landscape. *Neuron* 75, 363–379. doi:10.1016/j.neuron.2012.07.005.

Miller, S., Yasuda, M., Coats, J. K., Jones, Y., Martone, M. E., and Mayford, M. (2002). Disruption of dendritic translation of CaMKIIα impairs stabilization of synaptic plasticity and memory consolidation. *Neuron* 36, 507–519. doi:10.1016/S0896-6273(02)00978-9.

Miura, P., Sanfilippo, P., Shenker, S., and Lai, E. C. (2014). Alternative polyadenylation

in the nervous system: To what lengths will 3' UTR extensions take us? *BioEssays* 36, 766–777. doi:10.1002/bies.201300174.

Miura, P., Shenker, S., Andreu-agullo, C., Miura, P., Shenker, S., Andreu-agullo, C., et al. (2013). Widespread and extensive lengthening of 3 ′ UTRs in the mammalian brain. *Genome Res.*, 812–825. doi:10.1101/gr.146886.112.

Nam, J. W., Rissland, O. S., Koppstein, D., Abreu-Goodger, C., Jan, C., Agarwal, V., et al. (2014). Global analyses of the effect of different cellular contexts on microRNA targeting. *Mol. Cell* 53, 1031–1043. doi:10.1016/j.molcel.2014.02.013.

Nguyen, P. V, Abel, T., and Kandel, E. R. (1994). Requirement of a critical period of transcription for induction of a late phase of LTP. *Science* 265, 1104–7. doi:10.1126/science.8066450.

O'Leary, T., van Rossum, M. C. W., and Wyllie, D. J. A. (2010). Homeostasis of intrinsic excitability in hippocampal neurones: dynamics and mechanism of the response to chronic depolarization. *J. Physiol.* 588, 157–70. doi:10.1113/jphysiol.2009.181024.

Ostroff, L. E., Fiala, J. C., Allwardt, B., and Harris, K. M. (2002). Polyribosomes redistribute from dendritic shafts into spines with enlarged synapses during LTP in developing rat hippocampal slices. *Neuron* 35, 535–545. doi:10.1016/S0896-6273(02)00785-7.

Pattabiraman, P. P., Tropea, D., Chiaruttini, C., Tongiorgi, E., Cattaneo, A., and Domenici, L. (2005). Neuronal activity regulates the developmental expression and subcellular localization of cortical BDNF mRNA isoforms in vivo. *Mol. Cell. Neurosci.* 28, 556–70. doi:10.1016/j.mcn.2004.11.010.

Peter J Russel (2009). *iGenetics: A molecular approach*. 3rd ed. Pearson.

Poon, M. M., Choi, S.-H., Jamieson, C. a M., Geschwind, D. H., and Martin, K. C. (2006). Identification of process-localized mRNAs from cultured rodent hippocampal neurons. *J. Neurosci.* 26, 13390–9. doi:10.1523/JNEUROSCI.3432-06.2006.

Prieto, G. A., Snigdha, S., Baglietto-Vargas, D., Smith, E. D., Berchtold, N. C., Tong, L., et al. (2015). Synapse-specific IL-1 receptor subunit reconfiguration augments vulnerability to IL-1β in the aged hippocampus. *Proc. Natl. Acad. Sci.* 112, E5078–E5087. doi:10.1073/pnas.1514486112.

Raj, B., and Blencowe, B. J. (2015). Alternative Splicing in the Mammalian Nervous System: Recent Insights into Mechanisms and Functional Roles. *Neuron* 87, 14–27. doi:10.1016/j.neuron.2015.05.004.

Rajasethupathy, P., Fiumara, F., Sheridan, R., Betel, D., Puthanveettil, S. V, Russo, J. J., et al. (2009). Characterization of small RNAs in Aplysia reveals a role for miR-

124 in constraining synaptic plasticity through CREB. *Neuron* 63, 803–17. doi:10.1016/j.neuron.2009.05.029.

Ray, D., Kazan, H., Cook, K. B., Weirauch, M. T., Najafabadi, H. S., Li, X., et al. (2013). A compendium of RNA-binding motifs for decoding gene regulation. *Nature* 499, 172–7. doi:10.1038/nature12311.

Ryan, M. M., Ryan, B., Kyrke-Smith, M., Logan, B., Tate, W. P., Abraham, W. C., et al. (2012). Temporal profiling of gene networks associated with the late phase of long-term potentiation in vivo. *PLoS One* 7, 1–14. doi:10.1371/journal.pone.0040538.

Rybak-Wolf, A., Jens, M., Murakawa, Y., Herzog, M., Landthaler, M., and Rajewsky, N. (2014). A variety of dicer substrates in human and C. elegans. *Cell* 159, 1153–1167. doi:10.1016/j.cell.2014.10.040.

Sala, C., Futai, K., Yamamoto, K., Worley, P. F., Hayashi, Y., and Sheng, M. (2003). Inhibition of dendritic spine morphogenesis and synaptic transmission by activity-inducible protein Homer1a. *J. Neurosci.* 23, 6327–37. doi:23/15/6327 [pii].

Sandberg, R., Neilson, J. R., Sarma, A., Sharp, P. A., and Burge, C. B. (2008). Proliferating Cells Express mRNAs with shortened 3' untranslated regions and fewer microRNA target sites. *Science (80-.).* 320, 1643–1648. Available at: http://science.sciencemag.org/content/320/5883/1643.full-text.pdf+html.

Santos, A. R. A., and Duarte, C. B. (2008). Validation of internal control genes for expression studies: Effects of the neurotrophin BDNF on hippocampal neurons. *J. Neurosci. Res.* 86, 3684–3692. doi:10.1002/jnr.21796.

Sanz, E., Yang, L., Su, T., Morris, D. R., McKnight, G. S., and Amieux, P. S. (2009). Cell-type-specific isolation of ribosome-associated mRNA from complex tissues. *Proc. Natl. Acad. Sci. U. S. A.* 106, 13939–44. doi:10.1073/pnas.0907143106.

Schratt, G. M., Tuebing, F., Nigh, E. a, Kane, C. G., Sabatini, M. E., Kiebler, M., et al. (2006). A brain-specific microRNA regulates dendritic spine development. *Nature* 439, 283–9. doi:10.1038/nature04367.

Scoville, W. B., and Milner, B. (1957). LOSS OF RECENT MEMORY AFTER BILATERAL HIPPOCAMPAL LESIONS. *J. Neurol. Neurosurg. Psychiatry* 20, 11–21. doi:10.1136/jnnp.20.1.11.

Sebat, J., Lakshmi, B., Malhotra, D., Troge, J., Lese-Martin, C., Walsh, T., et al. (2007). Strong association of de novo copy number mutations with autism. *Science (80-.).* 316, 445–449. doi:10.1126/science.1138659.

Sempere, L. F., Freemantle, S., Pitha-Rowe, I., Moss, E., Dmitrovsky, E., and Ambros, V. (2004). Expression profiling of mammalian microRNAs uncovers a subset of brain-expressed microRNAs with possible roles in murine and human neuronal

differentiation. *Genome Biol.* 5, R13. doi:10.1186/gb-2004-5-3-r13.

Shaywitz, A. J., and Greenberg, M. E. (1999). CREB: A Stimulus-Induced Transcription Factor Activated by A Diverse Array of Extracellular Signals. *Annu. Rev. Biochem.* 68, 821–861. doi:10.1146/annurev.biochem.68.1.821.

Shepard, P. J., Choi, E.-A., Lu, J., Flanagan, L. a, Hertel, K. J., and Shi, Y. (2011). Complex and dynamic landscape of RNA polyadenylation revealed by PAS-Seq. *RNA* 17, 761–772. doi:10.1261/rna.2581711.

Shi, Y., Di Giammartino, D. C., Taylor, D., Sarkeshik, A., Rice, W. J., Yates, J. R., et al. (2009). Molecular Architecture of the Human Pre-mRNA 3′ Processing Complex. *Mol. Cell* 33, 365–376. doi:10.1016/j.molcel.2008.12.028.

Shi, Y., and Manley, J. L. (2015). The end of the message: Multiple protein:RNA interactions define the mRNA polyadenylation site. *Genes Dev.* 29, 889–897. doi:10.1101/gad.261974.115.

Siegel, G., Obernosterer, G., Fiore, R., Oehmen, M., Bicker, S., Christensen, M., et al. (2009). A functional screen implicates microRNA-138-dependent regulation of the depalmitoylation enzyme APT1 in dendritic spine morphogenesis. *Nat. Cell Biol.* 11, 705–16. doi:10.1038/ncb1876.

Silva, A. J., Kogan, J. H., Frankland, P. W., and Kida, S. (1998). CREB AND MEMORY. *Annu. Rev. Neurosci.* 21, 127–148. doi:10.1146/annurev.neuro.21.1.127.

Silva, a J., Paylor, R., Wehner, J. M., and Tonegawa, S. (1992). Impaired spatial learning in alpha-calcium-calmodulin kinase II mutant mice. *Science* 257, 206–211. doi:10.1126/science.1321493.

Smibert, P., Miura, P., Westholm, J. O., Shenker, S., May, G., Duff, M. O., et al. (2012). Global patterns of tissue-specific alternative polyadenylation in Drosophila. *Cell Rep.* 1, 277–289. doi:10.1016/j.celrep.2012.01.001.Global.

Squire, L., and Wixted, J. T. (2011). The Cognitive Neuroscience of Human Memory Since H.M. *Annu. Rev. Neurosci.* 34, 259–88. doi:10.1146/annurev-neuro-061010-113720.

Steward, O., and Levy, W. B. (1982). Preferential localization of polyribosomes under the base of dendritic spines in granule cells of the dentate gyrus. *J Neurosci* 2, 284–291. doi:0270-6474/82/0203-0284.

Sutton, M. A., and Schuman, E. M. (2006). Dendritic Protein Synthesis, Synaptic Plasticity, and Memory. *Cell* 127, 49–58. doi:10.1016/j.cell.2006.09.014.

Taliaferro, J. M., Vidaki, M., Oliveira, R., Gertler, F. B., Swanson, M. S., Burge, C. B., et al. (2016). Distal Alternative Last Exons Localize mRNAs to Neural Projections. *Mol. Cell*, 1–13. doi:10.1016/j.molcel.2016.01.020.

Tan, C. L., Plotkin, J. L., Venø, M. T., von Schimmelmann, M., Feinberg, P., Mann, S., et al. (2013). MicroRNA-128 governs neuronal excitability and motor behavior in mice. *Science* 342, 1254–8. doi:10.1126/science.1244193.

Tang, S. J., Reis, G., Kang, H., Gingras, A.-C., Sonenberg, N., and Schuman, E. M. (2002). A rapamycin-sensitive signaling pathway contributes to long-term synaptic plasticity in the hippocampus. *Proc. Natl. Acad. Sci. U. S. A.* 99, 467–72. doi:10.1073/pnas.012605299.

Tanzi, E. (1893). I fatti e le induzioni dell'odierna istologia del sistema nervoso. *Riv Sper Fren Med Leg*, 419–472.

Tian, B., and Graber, J. H. (2012). Signals for pre-mRNA cleavage and polyadenylation. *Wiley Interdiscip. Rev. RNA* 3, 385–396. doi:10.1002/wrna.116.

Tian, B., Hu, J., Zhang, H., and Lutz, C. S. (2005). A large-scale analysis of mRNA polyadenylation of human and mouse genes. *Nucleic Acids Res.* 33, 201–212. doi:10.1093/nar/gki158.

Tian, B., and Manley, J. L. (2013). Alternative cleavage and polyadenylation: The long and short of it. *Trends Biochem. Sci.* 38, 312–320. doi:10.1016/j.tibs.2013.03.005.

Tian, B., and Manley, J. L. (2017). Alternative polyadenylation of mRNA precursors. *Nat. Rev. Mol. Cell Biol.* 18, 18–30. doi:10.1038/nrm.2016.116.

Vo, N., Klein, M. E., Varlamova, O., Keller, D. M., Yamamoto, T., Goodman, R. H., et al. (2005). A cAMP-response element binding protein-induced microRNA regulates neuronal morphogenesis. *Proc. Natl. Acad. Sci. U. S. A.* 102, 16426–31. doi:10.1073/pnas.0508448102.

Voineagu, I., Wang, X., Johnston, P., Lowe, J. K., Tian, Y., Horvath, S., et al. (2011). Transcriptomic analysis of autistic brain reveals convergent molecular pathology. *Nature* 474, 380–386. doi:10.1038/nature10110.

Wang, D. O., Kim, S. M., Zhao, Y., Hwang, H., Miura, S. K., Sossin, W. S., et al. (2009). Synapse- and stimulus-specific local translation during long-term neuronal plasticity. *Science* 324, 1536–1540. doi:10.1126/science.1173205.

Wang, D. O., Martin, K. C., and Zukin, R. S. (2010a). Spatially restricting gene expression by local translation at synapses. *Trends Neurosci.* 33, 173–82. doi:10.1016/j.tins.2010.01.005.

Wang, E. T., Sandberg, R., Luo, S., Khrebtukova, I., Zhang, L., Mayr, C., et al. (2008). Alternative isoform regulation in human tissue transcriptomes. *Nature* 456, 470–476. doi:10.1038/nature07509.

Wang, E. T., Taliaferro, J. M., Lee, J.-A., Sudhakaran, I. P., Rossoll, W., Gross, C., et al. (2016). Dysregulation of mRNA Localization and Translation in Genetic Disease. *J. Neurosci.* 36, 11418–11426. doi:10.1523/JNEUROSCI.2352-16.2016.

Wang, W.-X., Wilfred, B. R., Hu, Y., Stromberg, A. J., and Nelson, P. T. (2010b). Anti-Argonaute RIP-Chip shows that miRNA transfections alter global patterns of mRNA recruitment to microribonucleoprotein complexes. *RNA* 16, 394–404. doi:10.1261/rna.1905910.

Wayman, G. A., Davare, M., Ando, H., Fortin, D., Varlamova, O., Cheng, H.-Y. M., et al. (2008). An activity-regulated microRNA controls dendritic plasticity by down-regulating p250GAP. *Proc. Natl. Acad. Sci.* 105, 9093–9098. doi:10.1073/pnas.0803072105.

Weyn-Vanhentenryck, S. M., Mele, A., Yan, Q., Sun, S., Farny, N., Zhang, Z., et al. (2014). HITS-CLIP and Integrative Modeling Define the Rbfox Splicing-Regulatory Network Linked to Brain Development and Autism. *Cell Rep.* 6, 1139–1152. doi:10.1016/j.celrep.2014.02.005.

Winder, D. G., Mansuy, I. M., Osman, M., Moallem, T. M., and Kandel, E. R. (1998). Genetic and pharmacological evidence for a novel, intermediate phase of long-term potentiation suppressed by calcineurin. *Cell* 92, 25–37. doi:10.1016/S0092-8674(00)80896-X.

Yang, Y., Li, W., Hoque, M., Hou, L., Shen, S., Tian, B., et al. (2016). PAF Complex Plays Novel Subunit-Specific Roles in Alternative Cleavage and Polyadenylation. *PLoS Genet.* 12. doi:10.1371/journal.pgen.1005794.

Zeisel, a., Manchado, a. B. M., Codeluppi, S., Lonnerberg, P., La Manno, G., Jureus, a., et al. (2015). Cell types in the mouse cortex and hippocampus revealed by single-cell RNA-seq. *Science (80-.).* 347, 1138–42. doi:10.1126/science.aaa1934.

Zhang, H., Hu, J., Recce, M., and Tian, B. (2005a). PolyA_DB: A database for mammalian mRNA polyadenylation. *Nucleic Acids Res.* 33, 116–120. doi:10.1093/nar/gki055.

Zhang, H., Lee, J. Y., and Tian, B. (2005b). Biased alternative polyadenylation in human tissues. *Genome Biol* 6, R100. doi:10.1186/gb-2005-6-12-r100.

Zheng, D., Liu, X., and Tian, B. I. N. (2016). 3′ READS+ , a sensitive and accurate method for 3′ end sequencing of polyadenylated RNA. *Rna*, 1–9. doi:10.1261/rna.057075.116.forms.

Zheng, D., and Tian, B. (2014). RNA-binding proteins in regulation of alternative cleavage and polyadenylation. *Adv. Exp. Med. Biol.* 825, 97–127. doi:10.1007/978-1-4939-1221-6_3.

Zhong, J., Zhang, T., and Bloch, L. M. (2006). Dendritic mRNAs encode diversified functionalities in hippocampal pyramidal neurons. *BMC Neurosci.* 7, 17. doi:10.1186/1471-2202-7-17.

Appendix

Appendix 1 – Publication: Activity-Dependent Regulation of Alternative Cleavage and Polyadenylation During Hippocampal Long-Term Potentiation

SCIENTIFIC REPORTS

OPEN

Activity-Dependent Regulation of Alternative Cleavage and Polyadenylation During Hippocampal Long-Term Potentiation

Received: 5 July 2017
Accepted: 21 November 2017
Published online: 12 December 2017

Mariana M. Fontes[1,2], Aysegul Guvenek[3], Riki Kawaguchi[4], Dinghai Zheng[3], Alden Huang[4], Victoria M. Ho[1,5], Patrick B. Chen[1,5], Xiaochuan Liu[3], Thomas J. O'Dell[6], Giovanni Coppola[4], Bin Tian[3] & Kelsey C. Martin[1,4]

Long-lasting forms of synaptic plasticity that underlie learning and memory require new transcription and translation for their persistence. The remarkable polarity and compartmentalization of neurons raises questions about the spatial and temporal regulation of gene expression within neurons. Alternative cleavage and polyadenylation (APA) generates mRNA isoforms with different 3′ untranslated regions (3′UTRs) and/or coding sequences. Changes in the 3′UTR composition of mRNAs can alter gene expression by regulating transcript localization, stability and/or translation, while changes in the coding sequences lead to mRNAs encoding distinct proteins. Using specialized 3′ end deep sequencing methods, we undertook a comprehensive analysis of APA following induction of long-term potentiation (LTP) of mouse hippocampal CA3-CA1 synapses. We identified extensive LTP-induced APA changes, including a general trend of 3′UTR shortening and activation of intronic APA isoforms. Comparison with transcriptome profiling indicated that most APA regulatory events were uncoupled from changes in transcript abundance. We further show that specific APA regulatory events can impact expression of two molecules with known functions during LTP, including 3′UTR APA of *Notch1* and intronic APA of *Creb1*. Together, our results reveal that activity-dependent APA provides an important layer of gene regulation during learning and memory.

Long-term potentiation (LTP) is a form of synaptic plasticity that corresponds to a long-lasting increase in synaptic transmission in response to specific patterns of neuronal firing or activity, and underlies learning and memory[1,2]. The early-phase of LTP (E-LTP) is independent of new gene expression while the late-phase of LTP (L-LTP), which lasts several hours to days, requires new transcription and translation[3–6].

Pre-mRNA cleavage and polyadenylation (C/P) is a nearly universal 3′ end processing mechanism for protein-coding genes in eukaryotes, and is coupled to transcription termination[7]. C/P consists of an endonucleolytic cleavage of pre-mRNAs followed by the synthesis of a polyadenosine tail, and is carried out by the C/P complex, which contains over 20 factors and many associated factors[8]. The site for C/P, known as polyA site (PAS), is defined by upstream and downstream cis regulatory elements, the most prominent of which is the A[A/U]UAAA element located upstream of the PAS[9–11].

[1]Department of Biological Chemistry, David Geffen School of Medicine, University of California, Los Angeles, Los Angeles, CA, USA. [2]Graduate Program in Areas of Basic and Applied Biology, University of Porto, Porto, Portugal. [3]Department of Microbiology, Biochemistry and Molecular Genetics, Rutgers New Jersey Medical School, Newark, NJ, USA. [4]Department of Psychiatry and Biobehavioral Sciences, Semel Institute for Neuroscience, David Geffen School of Medicine, University of California, Los Angeles, Los Angeles, CA, USA. [5]Interdepartmental Graduate Program in Neuroscience, University of California, Los Angeles, Los Angeles, CA, USA. [6]Department of Physiology, David Geffen School of Medicine, University of California, Los Angeles, Los Angeles, CA, USA. Mariana M. Fontes and Aysegul Guvenek contributed equally to this work. Correspondence and requests for materials should be addressed to B.T. (email: btian@rutgers.edu) or K.C.M. (email: kcmartin@mednet.ucla.edu)

Most mammalian genes contain multiple PASs that yield multiple mRNA isoforms[12–14]. While the majority of alternative PASs are located within the 3′-most exon and lead to changes in 3′UTR lengths, a sizable fraction of PASs are located in introns and control the selection of alternative terminal exons, affecting both coding sequences (CDSs) and 3′UTRs[12]. A growing number of mechanisms have been found to regulate APA, including core C/P factors[15,16], splicing factors[15,17], and RNA-binding proteins that interact with sequence motifs near the PAS[18].

Several tissues exhibit unique patterns of APA regulation[19–21]. For example, distal PASs tend to be selected in the brain, leading to preferential expression of mRNAs with long 3′UTRs[22–26]. Since the 3′UTR contains binding motifs for RNA-binding proteins and miRNA target sites, alteration of 3′UTR length offers an effective means to modulate gene expression by controlling aspects of mRNA metabolism, such as stability and translation[10,27–29].

In keeping with the preferential expression of distal PAS isoforms in neurons, 3′UTRs play a particularly important role in compartmentalized gene expression by directing the localization and regulated translation of mRNAs within dendrites and axons and at synapses[30–33]. RNA sequencing of the synaptic neuropil in mouse hippocampus identified over 2,000 axonally and dendritically localized mRNAs[34]. Localization of mRNAs in neurons often depends on specific cis-acting elements within the 3′UTR[35,36]. Interestingly, Taliaferro *et al.* found that transcripts using distal alternative last exons tended to be localized to neurites[37]. In addition, several studies have reported APA regulation following neuronal activation. An early microarray analysis found that a set of genes expressed truncated mRNAs through APA in cultured rat neuronal hippocampal cells following chronic potassium chloride depolarization[38]. It was suggested that the APA events may couple with transcriptional regulation through MEF2[38]. Using Rat PC12 and mouse MN-1 neurons, Berg *et al.* showed that activity-induced APA changes were recapitulated by functional inhibition of U1 snRNP[17], a complex that is involved not only in 5′ splice site recognition but also in the inhibition of premature usage of PAS[15,17,39]. The authors suggested that shortage of U1 snRNP during transcriptional upregulation following neuronal activation may lead to activation of proximal PAS.

Here, using deep sequencing of 3′ ends of transcripts, we systematically characterized APA regulation following LTP induction in acute mouse hippocampal slices. We examined both 3′UTR APA and intronic APA events at different time points post LTP, and analyzed the interplay between APA and gene expression regulation. Our study reveals global shortening of 3′UTR and activation of intronic APA, in line with previous reports. However, APA events are largely uncoupled from gene expression changes, and constitute a distinct layer of gene regulation during LTP.

Results

We were interested in understanding whether and how APA, a widespread pre-mRNA processing mechanism, plays a role in LTP. To this end, we perfused acute hippocampal mini-slices with forskolin and high concentrations of calcium and potassium to induce chemical LTP (cLTP). This form of LTP depends on bursting of CA3 neurons and produces a long-lasting, NMDAR-dependent plasticity that requires new transcription and translation[40,41]. We extracted RNA from hippocampal mini-slices 1 (1 hr) and 3 hours (3 hr) post LTP induction (Fig. 1a), collecting time-matched controls from the same animals (Fig. 1a, see Materials and Methods[40,41]. Reverse transcription-quantitative PCR (RT-qPCR) analysis of the immediate early gene *Arc* as well as the short and long intronic APA *Homer1* isoforms confirmed their regulation after LTP induction, as previously reported[42,43].

To determine APA profiles after LTP induction, we subjected RNA samples to 3′READS, a method we previously developed to specifically study the 3′ end of transcripts[44] (see Materials and Methods). After exclusion of outlier samples (Fig. S1), we obtained >10 million (M) PAS-containing reads per sample and identified 24,908 PASs in 13,445 genes, including 294 non-coding RNA genes. About 55% of identified PASs were associated with AAUAAA, 17% with AUUAAA, 20% with other close variants, and ~8% with no identifiable A[A/U]UAAA or their close variants in the −40 to −1 nt region of the PAS (Fig. 1b). These values were comparable at 1 hr and 3 hr, for both control and LTP samples. We note that a higher percentage of PASs were associated with the AAUAAA hexamer in our RNA samples than the 42% previously reported in the mouse genome[12], presumably because APA transcripts in brain preferentially use distal PASs[4,22,24–26], which are more frequently associated with AAUAAA than proximal PASs[13].

Approximately half of all detected protein-coding genes used 2 or more PASs, with no significant difference in the number of PASs per gene between control and LTP samples (Fig. 1c). As shown in Fig. 1e, most PASs (>85%) were found in the 3′UTR of the 3′-most exon, with less than 15% of PASs located in introns. Notably, we observed a small but significant (3,432 vs. 2,911, $P = 5.3 \times 10^{-16}$, Binomial test) global increase in the number of detected intronic PASs 3 hr post LTP, suggesting upregulation of intronic PAS usage following LTP induction (see below for more analysis). By contrast, no significant difference was detected 1 hr post LTP.

LTP induces global shortening of 3′UTRs. We next focused on 3′UTR APA events and asked whether there was a global change in 3′UTR length after LTP induction. To simplify our analysis, we focused on the two most abundant 3′UTR APA isoforms, named proximal and distal PASs based on their relative positions in the 3′UTR (Fig. 2a), and compared their relative expression changes in LTP-induced vs. control samples. While similar numbers of genes displayed 3′UTR shortening and lengthening after 1 hr of LTP induction (72 vs. 88, Fig. 2b), a bias toward 3′UTR shortening was detected 3 hr post LTP induction (203 vs. 77, Fig. 2c). Notably, the genes that displayed 3′UTR changes 3 hr after LTP induction were largely distinct from those with 3′UTR changes 1 hr after LTP induction (Fig. 2d).

To measure the extent of 3′UTR length change elicited by LTP, we divided genes into groups with lengthened 3′UTRs, unchanged 3′UTRs or shortened 3′UTRs, and calculated their average difference in 3′UTR length. At 1 hr, both lengthened and shortened 3′UTR genes underwent mild changes in 3′UTR length (median = 64

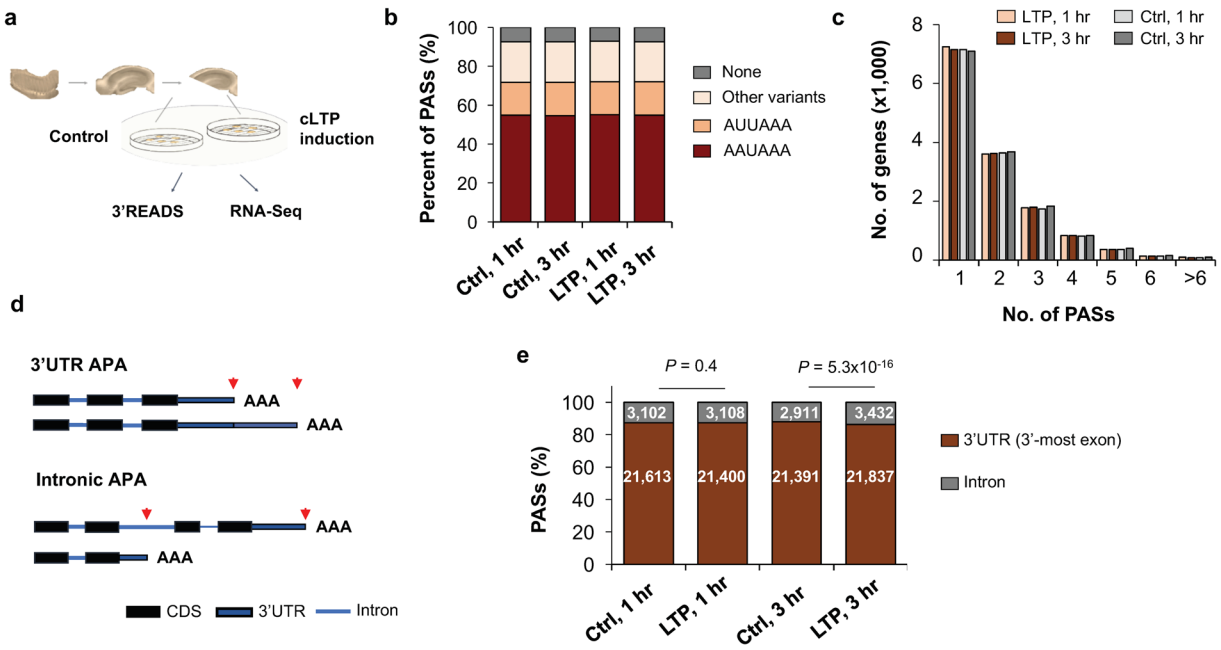

Figure 1. Analysis of APA in LTP. (**a**) Experimental design. RNAs from chemical LTP (cLTP)-induced and time-matched control hippocampal slices were subjected to 3′READS+ analysis to examine APA, or RNA-seq for gene expression. (**b**) Distribution of the A[A/U]UAA element in identified poly(A) sites (PASs). Percentage of PASs associated with either AAUAAA, AUUAAA, other variants of A[A/U]UAAA, or not associated with any A[A/U]UAAA element are shown for each sample group. (**c**) Number of PASs identified per gene. Genes with only one PAS have the highest frequency and the majority of genes displayed APA in the hippocampal samples analyzed. (**d**) Diagram showing 3′UTR APA (top) and intronic APA (bottom). 3′UTR APA isoforms have alternative 3′ UTRs resulting from the choice of different PASs in the 3′UTR. Two PASs are shown, i.e., proximal PAS and distal PAS. Intronic APA isoforms have different 3′UTRs as well as coding sequences (CDS). (**e**) Distribution of PASs in different regions of the mRNA: 3′UTR (in 3′-most exon only) vs. upstream intron. Change of PAS distribution during LTP is observed 3 hr post LTP induction. Number of PAS in each region is specified in each bar. P-values (Binomial test) indicate difference in fractions of 3′UTR PASs and intronic PASs in LTP vs. control samples.

nucleotides (nt) and 55 nt, respectively, Fig. 2e). By contrast, at 3 hr, while genes with lengthened 3′UTRs displayed a mild change of 3′UTR length (median = 43 nt), genes with shortened 3′UTRs showed a more pronounced 3′UTR length change (median = 81 nt) (Fig. 2f).

3′UTR length changes have previously been shown to alter miRNA targeting[45,46]. We next set out to globally identify miRNA target sites that would be affected by 3′ UTR shortening 3 hr after LTP induction. Of the 164 genes that displayed both 3′UTR shortening and contained miRNA target sites (based on the TargetScan database), 117 had their miRNA target sites (882 sites in total) removed by 3′UTR shortening (Fig. 2g). Thus, 3′UTR shortening could potentially play an important role in modulating miRNA regulation following LTP induction. An example gene, *Notch1*, is shown in Fig. 2h, displayed significant 3′UTR shortening in the 3 hr samples ($P = 4 \times 10^{-4}$, Fig. 2e), but not in the 1 hr samples. The Notch1 protein has been reported to be critical for hippocampal synaptic plasticity and memory formation[47,48]. Interestingly, we found a target site for miR-384-5p between the proximal and distal PASs of *Notch1* (Fig. 2h), a miRNA whose downregulation was shown to be required for the maintenance of LTP[49]. Thus, shortening of *Notch1* 3′UTR after LTP induction could help de-repress *Notch1* expression by miR-384-5p, contributing to LTP maintenance. RT-qPCR analysis using primer sets targeting a common coding region and a region that exists only in the long 3′UTR isoform confirmed increased *Notch1* gene expression and relatively higher expression of short 3′UTR isoform compared to long 3′UTR isoform (Fig. 2j).

Previous studies in other systems have indicated that the distance between two 3′UTR PASs, also known as alternative 3′UTR (aUTR) size (Fig. 2a), often correlates with the extent of 3′UTR APA[15], a phenomenon likely attributable to competition between the two adjacent PASs for usage. We thus divided genes with 3′UTR-APA regulation at 1 hr or 3 hr post-LTP into five groups based on their aUTR sizes (aUTR bins 1–5) and asked whether the difference in the relative expression of two APA isoforms between LTP and control samples (relative expression difference, RED) was a function of aUTR size. The mean RED values shown in Fig. 2i revealed that genes with longer aUTRs underwent significantly greater 3′UTR shortening 3 hr post-LTP as compared to 1 hr (gene bin 1 vs gene bin 5 comparison at 3 hr: p-value = 2.2×10^{-11}, Wilcoxon rank sum test). Together, these results indicate that LTP drives a general shortening of 3′UTR 3 hr post LTP induction, especially in transcripts with long aUTRs.

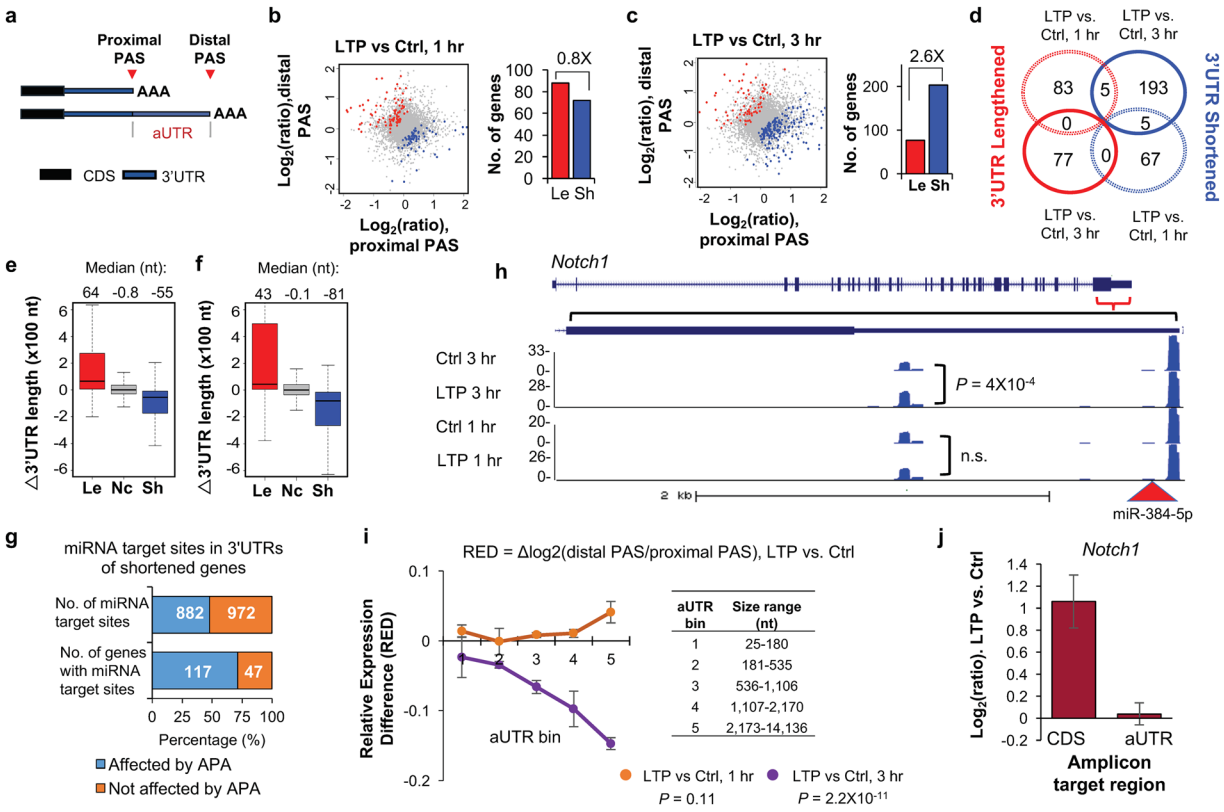

Figure 2. Regulation of 3′UTR APA after LTP induction. (**a**) Schematic of 3′UTR APA. (**b**) 3′UTR APA regulation after 1 hr LTP induction. Left, Scatterplot comparing expression changes of proximal and distal PASs after 1 hr LTP induction. Genes that significantly switched to proximal PAS usage are in blue and those that switched to distal PAS usage are in red ($P < 0.05$, DEXSeq, and relative abundance change >5%). Grey dots are genes without significant APA regulation. Right, bar graph comparing the number of genes with lengthened or shortened 3′UTRs (Le and Sh, respectively). (**c**) As in (**b**), 3 hr post LTP induction. (**d**) Venn diagram comparing genes with significant 3′UTR regulation 1 hr post LTP induction and 3 hr post LTP induction. (**e**) 3′UTR length change in 1 hr post LTP induction. Genes with 3′UTRs significantly shortened (blue), lengthened (red), or unchanged (grey) are shown. 3′UTR size was based on weighted mean of all 3′UTR isoforms. Median values are indicated on the top. (**f**) As in (**e**), except that data are based on 3 hr post LTP induction. (**g**) Effect of 3′UTR shortening on miRNA targeting. Number of miRNA target sites that are removed (882) or not removed (972) by 3′UTR shortening is indicated in the upper bar, and number of genes that contain removed (117) or not removed (47) miRNA target sites by 3′UTR shortening are indicated in lower bar. (**h**) An example gene *Notch1*, which displayed 3′UTR shortening after LTP. UCSC genome browser tracks of 3′READS data are shown. Gene structure and 3′UTR sequence are indicated on top. Peaks from two polyA sites indicate reads for corresponding APA isoforms. miR-384-5p target site is indicated. Reads are based on combined samples. (**i**) Relationship between aUTR size and 3′UTR-APA regulation at 1 hr or 3 hr post LTP induction. Relative expression difference (RED) was calculated for all genes with APA sites. The formula of RED is indicated above the graph. Genes were divided into five groups (aUTR bins, listed on the right) based on aUTR size, with approximately equal number of genes in each bin. For each bin, mean RED was calculated. Error bars are standard error of mean (SEM). P-value (Wilcoxon rank sum test) indicates the difference between bin 1 and bin 5. (**j**) RT-qPCR validation of *Notch1* APA regulation. Two different primer sets were used to detect the expression of a common coding region (left bar) and a region in the alternative 3′UTR (right bar). Error bars are SEM of 4 replicates.

3′UTR regulation and changes in transcript abundance. Gene ontology analysis of genes with 3′UTR shortening indicated that genes with diverse functions are affected by this mechanism (Table S3). We next asked whether there was any correlation between LTP-induced 3′UTR changes and LTP-induced changes in transcript abundance. To obtain high resolution gene expression data, we performed RNA-seq from a separate set of acute mouse hippocampal mini-slices 1 hr or 3 hr after LTP induction, with time-matched controls from the same animals. To prevent 3′UTR changes from influencing gene expression analysis, we used only RNA-seq reads mapping to the coding region of genes (see Materials and Methods for details). We identified 79 and 1,029 genes that were significantly differentially expressed at 1 hr and 3 hr time points (fold change >1.2, FDR <0.1, DEseq) (Fig. 3a and b). At both time points, upregulated genes outnumbered downregulated ones (77 vs. 2 at 1 hr; 907 vs. 122 at 3 hr, Fig. 3c), indicating that LTP primarily elicits activation of gene expression[42]. Notably, most genes regulated at 1 hr were also regulated at 3 hr (Fig. 3d), indicating continuous activation of expression. The top

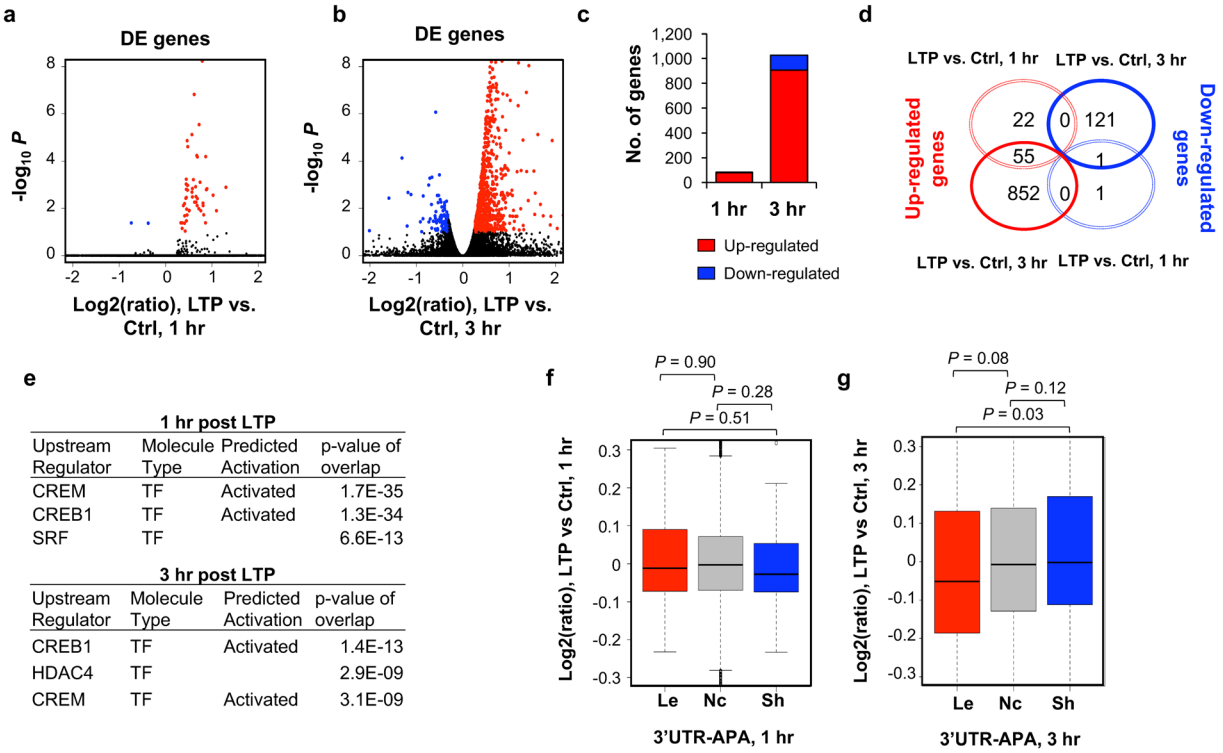

1 hr post LTP

Upstream Regulator	Molecule Type	Predicted Activation	p-value of overlap
CREM	TF	Activated	1.7E-35
CREB1	TF	Activated	1.3E-34
SRF	TF		6.6E-13

3 hr post LTP

Upstream Regulator	Molecule Type	Predicted Activation	p-value of overlap
CREB1	TF	Activated	1.4E-13
HDAC4	TF		2.9E-09
CREM	TF	Activated	3.1E-09

Figure 3. Regulation of gene expression after LTP induction. Differentially expressed (DE) genes 1 hr (**a**) or 3 hr (**b**) post LTP induction, as determined by RNA-seq. X-axis, log2(ratio) of gene expression (LTP vs Control); Y- axis, $-\log_{10}P$ (DESeq). DE genes were selected based on expression change >20% and FDR <0.1. Genes with upregulated expression are highlighted in red and those with downregulated expression in blue. Black dots represent genes without significant regulation. (**c**) Bar graph summarizing DE genes shown in (**a**) and (**b**). (**d**) Venn diagram comparing DE genes at 1 hr LTP and 3 hr LTP. (**e**) IPA upstream regulator analysis for significantly regulated genes. This data is generated through the use of Ingenuity Pathways Analysis, a web-delivered application (www.Ingenuity.com). (**f**) and (**g**) Gene expression regulation vs. LTP-induced 3′UTR-APA regulation. Box plots showing the log2(ratio) of gene expression, LTP vs. Ctrl, for genes with 3′UTR lengthened (Le), shortened (Sh) or no change (Nc) at 1 hr (**f**) or 3 hr (**g**) post LTP induction. Only genes with significant 3′UTR APA regulation (those from Fig. 2) were included. P-values (Wilcoxon rank sum test) indicate difference between gene groups.

differentially expressed (DE) genes we identified are consistent with previous studies[50–52], including upregulation of *Gadd45g*, *Egr2*, *c-Fos*, *Arc* and *Npas4* (Table 1). Notably, gene expression changes based on RNA-seq were well correlated with those based on 3′READS (r = 0.81 and r = 0.78 for significantly regulated genes at 1 hr and 3 hr, respectively, Figure S2), attesting to the quality of our sequencing data.

GO analysis of DE genes after LTP induction revealed several shared terms at 1 hr and 3 hr, including those related to signaling ("signal transduction" and "single organism signaling"), metabolic process ("positive regulation of metabolic process" and "negative regulation of macromolecule metabolic process", "nucleic acid metabolic process"), and nucleus ("nucleus", Table 2). Additionally, DE genes at 1 hr were enriched in "tissue development" and "transcription factor complex" (Table 2). At 3 hr, DE genes were also enriched in "neuron projection development" and "excitatory synapse" (Table 2). Thus, GO terms do not appear to overlap with those associated with genes showing 3′UTR shortening (Table S3). In addition, Ingenuity Pathway Analysis (IPA) identified a set of transcription factors (TFs) that are predicted to regulate genes with expression changes post LTP (Fig. 3e), including CREM, CREB1, and HDAC4, which is consistent with the notion that CREB proteins play key roles in memory and synaptic plasticity, and facilitate the late phase of LTP[53–55]. By contrast, no significant TFs were predicted to be associated with genes showing 3′UTR shortening (data not shown). Taken together, both GO and IPA analysis results indicate that transcriptional regulation and APA may target different sets of genes.

To specifically address the interplay between 3′UTR-APA change and gene expression regulation, we analyzed the mRNA expression fold change of genes with significantly shortened and lengthened 3′UTR isoforms (P < 0.05, DEXSeq and relative abundance change of APA isoform >5%). There was no discernable correlation between gene expression change and 3′UTR-APA regulation at 1 hr post LTP (Fig. 3f). At 3 hr post LTP, while genes with lengthened 3′UTRs appeared to be modestly downregulated as compared to genes with shortened or unchanged 3′UTRs (P = 0.03 or P = 0.08, respectively, Wilcoxon test, Fig. 3g), there was no discernable difference between genes without 3′UTR APA changes and those with shortened 3′UTRs (P = 0.12, Wilcoxon test, Fig. 3g). Therefore, alteration of 3′UTR length is largely uncoupled from gene expression changes.

DE genes 1 hr post LTP			DE genes 3 hr post LTP		
Gene	**Log2(ratio)**	**FDR**	**Gene**	**Log2(ratio)**	**FDR**
Btg2	2.4	2.5E-99	*Rasl11a*	2	2.7E-86
Egr2	2.3	2.1E-80	*Fos*	1.5	2.4E-64
Fos	1.9	3.5E-70	*Tinf2*	1.6	1.1E-51
Nr4a1	1.6	8.8E-66	*Arc*	1.2	2.1E-42
Arc	1.8	1.3E-47	*Cyr61*	1.8	1.4E-41
Dusp6	1.0	3.9E-27	*Txndc11*	1.1	2.9E-32
Gadd45g	1.3	1.4E-26	*Sik1*	1.3	7.7E-32
Npas4	2.6	2.7E-22	*Thbs1*	1.8	2.3E-31
Dusp1	1.3	3.3E-19	*Gem*	1.1	4.9E-26
Trib1	1.3	2.2E-18	*Btg2*	1.2	3.7E-25
Ppp1r15a	1.0	1.0E-17	*Pax6*	1.1	1.3E-22
Errfi1	0.8	2.6E-17	*Gadd45g*	1.0	1.3E-21
Egr1	1.3	7.7E-16	*Il6*	1.2	8.1E-20
Nr4a2	0.9	1.0E-15	*Kmt2d*	0.8	2.0E-19
Arl4d	1.1	4.3E-15	*Trh*	2.1	3.4E-19
Sik1	1.0	3.9E-14	*Rtl1*	0.8	1.6E-17
Fosb	1.4	1.0E-13	*Ppp1r3g*	1.4	7.7E-16
Rgs4	0.7	1.8E-13	*Grin2b*	0.7	1.3E-15
Egr4	2.1	7.8E-13	*Rnf217*	0.9	6.2E-14
Ciart	0.9	3.4E-12	*Ccnl1*	0.7	7.1E-13
Cyr61	0.8	4.3E-10	*Nfkb1*	0.7	1.1E-12
Csrnp1	0.7	4.3E-10	*Nfil3*	0.8	1.1E-12
Thbs1	0.9	7.7E-10	*Sipa1l3*	0.9	2.2E-12
Junb	1.7	9.0E-10	*Nr4a2*	1.0	8.0E-12
Ptgs2	0.9	1.7E-09	*Iqsec2*	0.7	8.0E-12

Table 1. Top 25 differentially expressed (DE) genes at 1 hr and 3 hr post LTP induction. Log_2(ratio) and FDR (DESeq). FDR was based on multiple testing adjustment using the Benjamini-Hochberg method.

GO term	Category	$-Log_{10}P$
Enriched for DE genes, 1 hr post LTP		
positive regulation of metabolic process	BP	16.3
negative regulation of macromolecule metabolic process	BP	12.1
tissue development	BP	10.6
signal transduction	BP	8.8
nucleic acid metabolic process	BP	8.6
nucleus	CC	8.4
transcription factor complex	CC	4.0
protein phosphatase type 1 complex	CC	3.0
Enriched for DE genes, 3 hr post LTP		
neuron projection development	BP	7.5
single organism signaling	BP	7.3
regulation of nucleic acid-templated transcription	BP	5.9
negative regulation of macromolecule metabolic process	BP	5.5
positive regulation of metabolic process	BP	5.5
neuron part	CC	8.6
excitatory synapse	CC	4.6
nucleus	CC	3.9

Table 2. GO terms enriched for upregulated and downregulated genes 1 hr or 3 hr post LTP induction. BP, biological process; CC, cellular component. *P* is based on the Fisher's exact test.

Widespread activation of intronic APA during LTP. About 12% of APA sites identified in our samples were located in introns (Fig. 1e), which can impact coding sequence usage. We next tested the significance of the LTP-induced regulation of intronic APA usage. We combined all isoforms using PASs in RefSeq-supported introns and compared their expression with all transcripts using PASs in the 3′-most exon (Fig. 4a). We detected a modest

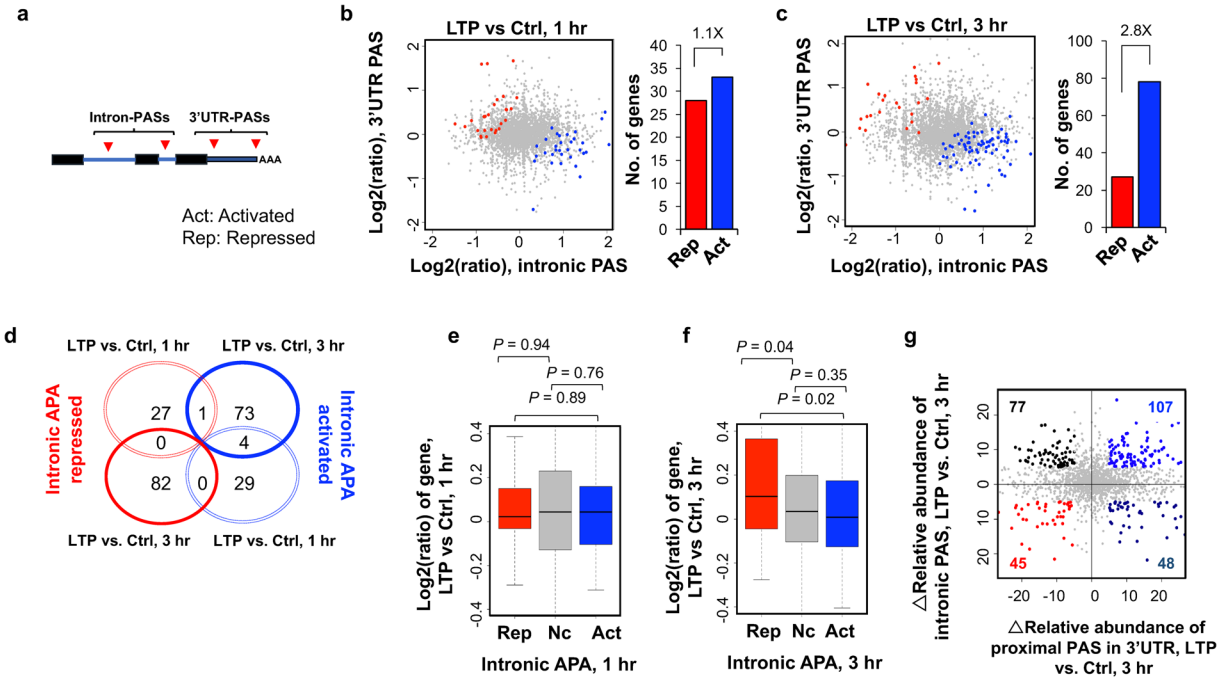

Figure 4. Regulation of intronic APA after LTP induction. (**a**) Schematic of intronic APA analysis. Intronic PASs were compared with 3′UTR-PASs. (**b**) and (**c**) Left, scatterplot comparing expression change (LTP vs. control) of intronic PASs (x-axis) and 3′UTR PASs (y-axis). Genes with significantly activated intronic PAS usage are shown in blue (Act) and those with significantly repressed intronic PAS usage in red (Rep) ($p < 0.05$, DEXSeq and relative abundance change >5%). Grey dots represent genes without significant regulation (Nc). Right, bar graph showing the number of genes with activated or repressed intronic APA. (**d**) Venn diagram comparing genes with CDS-APA regulation at 1 hr post LTP and 3 hr post LTP. Genes correspond to those in (**b**) and (**c**). (**e**) and (**f**), Box plot showing the $\log_2$ratio (LTP/Ctrl) of genes with intronic PAS activation or intronic PAS repression, 1 hr (**e**) or 3 hr (**f**) post LTP induction. Genes with significant intronic APA regulation are those from (**b**) or (**c**). P-values (Wilcoxon rank sum test) indicate the difference between groups. (**g**) Scatterplot comparing 3′UTR APA regulation (x-axis) and intronic APA regulation (y-axis) at 3 hr post LTP induction. Δ relative abundance for 3′UTR APA is based on the two 3′UTR PASs with most reads, as in Fig. 2, and Δ relative abundance for intronic APA is based on all intronic PAS reads vs. all 3′UTR PAS reads. Genes with intronic APA and/or 3′UTR APA change (>5% relative abundance) are highlighted with different colors based on the type of change.

difference at 1 hr between genes with activated intronic APA and genes with repressed intronic APA (33 vs. 28, Fig. 4b). However, at 3 hr post LTP, genes with activated intronic APA significantly outnumbered those with repressed intronic PAS by 2.8-fold (78 vs. 27, Fig. 4c). These data indicate that LTP induces not only a general shortening of 3′UTR but also triggers an overall transcript truncation through increased usage of intronic PASs. In addition, the genes with intronic APA regulation at 1 hr differed from those with intronic APA regulation at 3 hr (Fig. 4d).

We then asked whether intronic APA is related to gene expression level changes. At the 1 hr post LTP time-point, gene expression changes appeared to be unrelated to intronic APA regulation (Fig. 4e). By contrast, at 3 hr post LTP, genes with repressed intronic APA tended to be upregulated relative to genes without APA regulation or with activated intronic APA ($P = 0.04$ or 0.02, respectively, Wilcoxon rank sum test, Fig. 4f). However, genes with activated intronic APA, which accounted for most of the APA events, did not show significant difference in expression compared to genes without intronic APA changes ($P = 0.35$, Wilcoxon rank sum test). Therefore, intronic activation of APA is not coupled with activation of gene expression. GO analysis did not reveal any terms highly significantly enriched for genes with activated intronic APA (Table S4), indicating that intronic APA regulation, unlike transcriptional control, is not specific for genes with certain functions.

We next examined how intronic APA was related to 3′UTR-APA. Using the 3 hr post-LTP data, we identified 107 genes with both shortened 3′UTRs and activated intronic APA, a number greater than genes with shortened 3′UTRs and repressed intronic APA (48), lengthened 3′UTRs and activated intronic APA (77) or lengthened 3′UTRs and repressed intronic APA (45) (Fig. 4g). This result indicates that, for a group of genes, 3′UTR shortening is coupled with activation of intronic APA. Presumably, for those genes, proximal PASs are generally preferred regardless of the location, in the 3′-most exon or in an intron.

Previous studies have shown that intronic APA events regulated by certain factors, such as U1 snRNP (U1)[17] and RNA polymerase II associated factor (PAF) complex[56], display a 5′ to 3′ polarity, i.e., more regulation at the 5′ end than the 3′ end. By dividing intronic PAS isoforms into 5 groups based on the intron locations of their PASs, i.e., first intron (+1), second (+2), last (−1), second to last (−2), and middle (between +2 and −2 introns), we found that PASs located in the 5′-most intron (+1) indeed had the highest increase in usage as compared to those

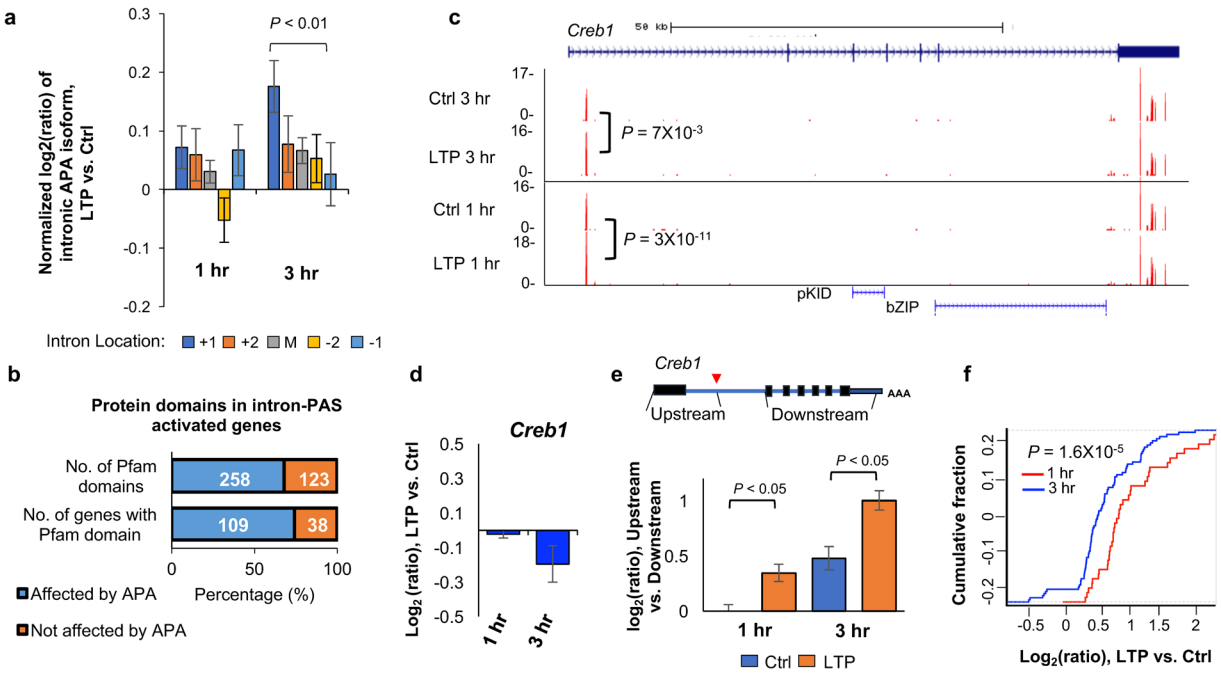

Figure 5. Characteristics of intronic APA after LTP induction. (**a**) Normalized expression changes of intronic PAS isoforms. Intronic PAS isoforms were divided into five groups based on the intron location where PAS resides, i.e., first (+1), second (+2), last (−1), second to last (−2), and middle (between +2 and −2 introns). Expression changes are expressed as log2(ratio), LTP vs. Ctrl. Only genes with ≥4 introns and only PAS isoforms with ≥2 reads were used for analysis. Values for five intron groups were normalized by mean-centering. Error bars are standard error of mean. P-value (Wilcoxon rank sum test) indicating difference between first and last intron values is shown. (**b**) Protein domains that can potentially be removed or truncated by intronic PAS activation. Number of pfam domains that can be removed or not removed by intronic APA is indicated in the upper bar, and number of genes that contain domains removed or not removed by intronic PAS activation is indicated in the lower bar. (**c**) An example gene *Creb1*, which displayed significant intronic PAS activation. Gene structure is shown on top and peaks for PASs are shown in UCSC genome browser tracks. P-values based on comparison of intronic PAS and 3′UTR PAS (DEXSeq) are indicated. Pfam domains are indicated. Reads are acquired by combining samples. (**d**) Gene expression change of *Creb1* after LTP. (**e**) Expression changes based on RNA-seq reads mapped to different regions of *Creb1*. Schematic of *Creb1* is shown on the top, and log2(ratio) from indicated region is shown in a bar plot. Two regions were analyzed, including the region from transcription start site to the intronic PAS, and the region from the second to the last exons. (**f**) Gene expression changes (LTP vs. Ctrl) of CREB1 target genes obtained from the IPA database. The blue curve corresponds to 81 target genes in the 3 hr post LTP samples, whereas the red corresponds to 37 target genes in the 1 hr post LTP samples.

in the 3′-most intron 3 hr post LTP ($P = 0.008$, Wilcoxon rank sum test). By contrast, no such trend was discernable with the 1 hr APA events (Fig. 5a). This result suggests that a regulatory mechanism similar to U1 and PAF complex, which specifically impacts 5′ intronic PASs, takes place 3 hr post LTP (see Discussion).

To further explore the consequences of intronic APA activation following LTP induction, we examined protein domains that could be removed or truncated through shortening of coding regions. Of the 147 genes that showed significant intronic PAS activation and contained Pfam-annotated domains, 109 could lose their protein domains (258 domains in total) as a result of intronic APA activation (Fig. 5b). One of the most significantly regulated genes by intronic APA was *Creb1*, whose intronic PAS increased both 1 hr and 3 hr post LTP inductions (Fig. 5c). The regulated intronic PAS is located at the 5′ end of the first intron (Fig. 5c), usage of which could remove much of the protein sequence of *Creb1*, including two key domains—the phosphorylated kinase-inducible-domain (pKID) and basic leucine zipper domain (bZIP) (Fig. 5c). Since *Creb1* plays a central role in transcriptional activation of many genes during LTP, as previously shown[57,58] and predicted by our IPA analysis in this study (Fig. 3e), we hypothesized that activation of its intronic APA may function to inhibit *Creb1* expression, blunting its role in transcriptional activation. Indeed, using the RNA-seq data, we found that while *Creb1* mRNA appeared unchanged 1 hr post LTP, it was slightly downregulated 3 hr post LTP (Fig. 5d). Importantly, downregulation of *Creb1* mRNA mainly occurred to exons downstream of the intronic PAS but not to the first exon (Fig. 5e), suggesting that downregulation of *Creb1* mRNA level occurred through the usage of intronic PAS. Consistent with repressed *Creb1* expression, upregulation of *Creb1* target genes was decreased 3 hr post LTP as compared to 1 hr post LTP ($P = 1.6 \times 10^{-5}$, Fig. 5f). Notably, the intronic PAS of *Creb1* is conserved in human and rat based on PolyA_DB[59], highlighting its functional importance. Taken together, intronic APA of Creb1 may play an important role in downregulation of its gene expression, controlling the extent and/or timing of the Creb1-mediated gene expression program.

Discussion

Regulation of transcription and protein synthesis is critical during L-LTP[49,60–64], and post-transcriptional gene regulation is key to the development and function of neural circuits[35,65,66]. mRNA isoform changes through APA represent a widespread, although poorly understood, mechanism in eukaryotes. APA may play a special regulatory role in the nervous system, because neuronal transcripts generally have long 3′UTRs[21,24] and sequence motifs in 3′UTRs contribute to both spatial and temporal control of gene expression during neuronal plasticity[36]. Inspired by studies indicating activity-dependent regulation of APA in neurons[17,38], we undertook a genome-wide approach to systematically examine activity-dependent APA regulation following LTP induction in mouse hippocampal slices. With a specialized 3′ end-based sequencing method, 3′READS, we uncovered a global trend of 3′UTR shortening and activation of intronic APA 3 hr post LTP, a time point that also involves substantial transcriptional changes. By contrast, the global APA regulation was not discernable 1hr post LTP, when only a small number of genes have expression changes. Thus, it is possible that regulation of PAS usage, a co-transcriptional process, is globally coupled with transcriptional regulation. On the other hand, for individual genes, we did not observe coupling between 3′UTR shortening or activation of intronic PASs with regulation of gene expression.

Comparison with previous studies. The APA regulation following LTP induction detected in our study is consistent with a previous microarray study done in cultured rat hippocampal neurons that reported significant transcript truncation following KCl depolarization[38]. Of note, our stimulation protocol induced Hebbian synaptic plasticity[41], while the 1 hr or 6 hr of continuous KCl depolarization in cultured neurons likely produced homeostatic plasticity[67]. Despite this difference, 10 of the 29 genes undergoing APA regulation (34.5%, 30 predicted-only genes from Flavell *et al*., 2008 were excluded) following KCl depolarization also underwent APA regulation after LTP induction in hippocampal slices, suggesting a common mechanism of APA regulation during homeostatic and Hebbian plasticity. Our high-resolution genome-wide approach provides additional insights into APA regulation during plasticity by expanding the catalog of genes with activity-dependent APA changes from a total of 59 in Flavell *et al*. (2008) to over 1,100 genes (Fig. 1f). Our study further provides a comprehensive characterization of the two different types of APA regulation, 3′UTR APA and intronic APA, which could not be dissected using microarrays or traditional RNA-seq. Notably, we also performed the same experiments using PAS-Seq, another 3′ end-based sequencing method[68]. However, due to high variance of read counts across samples and within genes, we could not identify significantly regulated APA isoforms following LTP induction (data not shown), attesting to the technical advantage of using 3′READS in analysis of APA.

Potential mechanisms. The molecular mechanism(s) underlying activity-dependent APA regulation during LTP remain largely unclear. Global shortening of 3′UTRs and activation of intronic APA sites have been observed in proliferating cells compared to quiescent ones[45]. Cancer cells, undifferentiated cells and cells at early developmental stages display similar patterns[46,68,69]. The mechanisms underlying proliferation-based APA are largely unknown, although higher expression levels of C/P factors and thus increased general C/P activity have been suggested to be responsible for more efficient 3′ end processing at proximal PASs[69,70]. While we did not observe increased expression of C/P factors at the RNA level post LTP (Fig. S3a), the C/P factor gene *Wdr33* did appear to be regulated by APA (Fig. S3b), raising the possibility that regulation of certain C/P factors may lead to the global APA changes observed in this study. In addition, we cannot rule out the possibility that some of the C/P factors might be regulated post-translationally and have altered activities post LTP.

The Dreyfuss lab reported that a shortage of U1 snRNP (U1) relative to the pre-mRNA abundance caused subdued inhibition of cleavage/polyadenylation by U1[17] and, consequently, activation of proximal PASs in introns and 3′UTRs. Indeed, using our previous 3′READS data from mouse C2C12 myoblast cells[15], we found that the expression of intronic APA isoform of *Creb1* increased by 3.7-fold when U1 was functionally inhibited by an antisense oligo to U1 snRNA (Fig. S5a). Global activation of proximal PASs in 3′UTRs and introns has also been reported in cells with reduced expression of the PAF complex[56], which plays a role in promoter-proximal pausing and transcriptional elongation[71,72]. We also re-analyzed our previous data of knockdown of Paf1, one of the subunits of PAF complex, in C2C12 cells. Interestingly, intronic APA of *Creb1* increased by 7.8-fold when Paf1 was knocked down (Fig. S5b). Although we did not detect a global correlation in intronic APA regulation between U1 inhibition or Paf1 knockdown and LTP activation, there were modest correlations between these conditions for PAS regulation in the first intron ($r = 0.21$ and 0.31 for Paf1 knockdown vs. LTP and for U1 inhibition vs. LTP, respectively, Pearson correlation, Fig. S5d and Fig. S5e). This result suggests that PASs in the first intron, as in the case of *Creb1*, might be regulated by U1 and/or PAF mechanisms in cells activated for LTP. Future studies need to determine mechanistic details concerning these potential connections.

Intriguingly, we also found from our previous data that knockdown of PABPN1 expression by siRNA (siPABPN1) in C2C12 cells substantially upregulated the expression of the intronic APA isoform of *Creb1* by 16-fold in C2C12 cells[15]. Because of PABPN1′s role in nuclear RNA surveillance[15,73], it is possible that the intronic PAS isoform of *Creb1* is rapidly degraded after usage. This further supports the model that intronic polyadenylation of *Creb1* serves to inhibit the expression of full-length isoform. Moreover, similar to U1 inhibition and Paf1 knockdown, regulation of PASs in the first introns of genes by LTP was modestly correlated with those by siPABPN1 ($r = 0.34$, Pearson correlation, Fig. S5f), suggesting a general pattern similar to that of the intronic PAS of *Creb1*.

Functional implications. APA generates mRNA isoforms with different 3′UTR lengths and/or coding sequences. mRNA isoforms resulting from LTP induction may localize to distinct subcellular compartments, and produce different protein levels[23,28,74]. The functional consequences of 3′UTR-APA events emerge from differences in cis-regulatory elements contained within the alternative 3′UTRs, including motifs recognized by

miRNAs and RBPs. Shorter 3′UTR isoforms can escape miRNA-mediated destabilization and translation repression through the loss of miRNA binding sites, a strategy that is used to achieve both cell type specificity and correct developmental timing[75–77]. Indeed, we found that genes with lengthened 3′UTRs tended to be downregulated, implying a role for 3′UTR in gene regulation during hippocampal plasticity. A case in point is the *Notch1* gene, which plays important roles in LTP and whose 3′UTR shortening removes a target site of miR-384–5p, an important miRNA for LTP maintenance[47–49]. Future studies are needed to examine the detailed mechanisms and consequences behind APA of *Notch1* and explore other similar cases.

Intronic APA events can impact protein functions by generating alternative C-termini. For example, intronic APA was previously shown to affect the molecular functions of *Homer1*, a gene that undergoes differential APA 3 hr post LTP induction. Our data is consistent with this finding (Fig. S5). The shorter *Homer1* CDS isoform that is inducible by neuronal activity acts in dominant negative fashion to inhibit the function of the full-length *Homer1* isoform[43] by preventing dimerization. Here we revealed significant regulation of intronic APA in *Creb1*, which plays a key role in LTP[78]. Activation of intronic PAS of *Creb1* leads to a significantly truncated transcript that is likely to be rapidly degraded (see above). This mechanism may function to limit *Creb1*'s function in gene activation during LTP. Notably, activation of PAS in the first intron, as in the case of *Creb1*, is a widespread phenomenon during LTP. Further proteomic studies will provide insights into whether there is a surge of short peptides during LTP induction as a result of intronic APA activation, and, if so, whether they play functional roles in learning and memory.

Methods

Preparation of hippocampal acute slices. Hippocampal slices were prepared from isoflurane-anesthetized 2–3 month old male C57BL/6 mice (Charles River, Wilmington, MA, USA). Hippocampi were quickly isolated on ice, and 400-micron thick transverse slices were cut using a manual tissue chopper. The dentate gyrus was trimmed with a single incision, and the slices were placed in interface chambers at 30 °C to recover for 2 hr with continuous ACSF perfusion. From a single animal we collected ~10 hippocampal slices. Half of the mini-slices were used for cLTP induction and the remaining treated with a DMSO vehicle solution as time-matched controls. cLTP was induced by perfusing ACSF containing 50 uM forskolin for 5 min followed by 5 min of 50 uM forskolin, 30 mM KCl and 10 mM Ca^{2+} ACSF. Control slices were treated in parallel with ACSF containing 0.2% DMSO for 10 min. Slices were collected 1 hr or 3 hr post stimulation by freezing in dry ice. Use of mice in this study followed the recommendations of and protocol approved by the UCLA Institutional Animal Care and Use Committee. To validate successful LTP induction, we monitored expression of candidate transcripts by qPCR, and prepared sequencing libraries from samples that exhibited LTP-induced upregulation of *Arc* mRNA and increases in *Homer1* short isoform and unaltered concentrations of *Homer1* long isoform and *Hprt*. We obtained triplicates for all controls and cLTP samples for 3′READS+, RNA-seq and PAS-seq experiments.

RNA extraction and RT-qPCR. To extract RNA, frozen slices were homogenized using a pestle in TRIzol for 5 min. 200 uL of chloroform per 1 mL of TRIzol were added to the homogenate and after centrifugation the top aqueous phase was collected. To precipitate and elute total RNA containing both mRNA and small RNAs we then used the Qiagen microRNeasy kit. We obtained ~2.5 ug of total RNA from 5 hippocampal slices. For RT-qPCRs we used 200 ng of total RNA and performed reverse transcription with random hexamers and SuperScript III in a total volume of 20 uL. The cDNA was then quantified by qPCR using SYBR green (primer sequences available upon request). The mRNA levels of *Hprt* were used as internal controls since its expression is activity-independent[79].

RNA-seq and Differential Expression Analysis. Three biological replicates of each condition (control and LTP-induced) at two different time-points (1 hr and 3 hr) after LTP were collected. For each replicate, hippocampal slices from the same animal were used to generate both LTP-induced samples and matched controls. The minimum RIN of all samples was 7.5, as determined by the 4200 Tapestation Instrument (Agilent). All RNA-seq libraries were prepared using the TruSeq Stranded Total RNA sample prep kit with Ribo-Zero according to manufacturer's specified protocol (Illumina). Samples were multiplexed and sequenced across multiple HiSeq 2500 high-output lanes using 100 bp paired-end reads to achieve a minimum depth of ~75 M reads per sample. Transcriptome alignment was performed using STAR v. 2.4.1c[80] with default settings, and GRCm38/mm10 (Data statistics, Table S2). Raw counts were quantified using R GenomicFeatures and GenomicAlignments and RSamtools packages[81]. Differential expression analysis was performed for each time-point separately in DESeq[82]. We excluded outlier samples, as determined by sample clustering (Fig. S1b). We applied an FDR cutoff of <0.1 and fold change >1.2 as the threshold for significance. GO analysis was carried out based on Fisher's exact test.

3′READS+ and its analysis. The 3′ region extraction and deep sequencing (3′READS+) method was previously described in[44]. Briefly, 1 μg of input RNA was used for each sample, and poly(A) + RNA was selected using oligo d(T)25 magnetic beads (NEB), followed by on-bead fragmentation using RNase III (NEB). Poly(A) + RNA fragments were then selected using a chimeric oligo containing 15 regular dTs and five locked nucleic acid dTs conjugated on streptavidin beads, followed by RNase H (NEB) digestion. Eluted RNA fragments were ligated with 5′ and 3′ adapters, followed by RT and PCR (15x) to obtain cDNA libraries for sequencing on the Illumina platform. Processing of 3′READS+ data was carried out as previously described[12]. Briefly, reads were mapped to the mouse genome using bowtie 2[83]. Reads with $\geq$2 unaligned Ts at the 5′ end were used to identify PASs. PASs located within 24 nt from each other were clustered together (Table S1).

APA analysis. Differential expression of APA isoforms are carried out with DEXSeq.[84]. Significant events were those with $p < 0.05$ and relative abundance difference >5%. Outlier samples were excluded as determined by sample clustering (Fig. S1a). Relative expression (RE) of two most abundant 3′UTR APA isoforms, e.g., proximal and distal PASs, was calculated by log2 (distal PAS/proximal PAS). Relative Expression Difference (RED) of two

isoforms in two samples was based on difference in RE between the two isoforms in the two samples. For intronic APA analysis, RE was based on comparison of all intronic APA isoforms combined (intronic PAS set) with all 3′UTR PAS isoforms combined (3′UTR PAS set), and RED was also based on the two sets.

The weighted mean of 3′UTR size for each gene was based on 3′UTR sizes of all APA isoforms, weighted by the expression level of each isoform based on the number of PAS-containing reads.

Analysis of introns. The intron location was based on the RefSeq database, considering all RefSeq-supported splicing isoforms. Introns were divided into five groups; first, second, last, second last and middle (contains all the introns between +2 and −2). Only genes with at least four introns were analyzed. Relative expression was calculated by intronic PAS read number divided by that of 3′UTR PASs of the same gene.

Data access. The sequencing data from this study has been submitted to the NCBI Gene Expression Omnibus under SuperSeries accession number GSE84644 (RNA-seq, GSE84503; 3′READS+, GSE84643). RNA-seq and 3′READS data can also be accessed through a web based expression browser at https://coppolalab.ucla.edu/gclabapps/3readsbrowser/home.

Reviewer link: https://www.ncbi.nlm.nih.gov/geo/query/acc.cgi?token=efmjesqabfetlef&acc=GSE84644.

References

1. Bliss, T. V. & Collingridge, G. L. A synaptic model of memory: long-term potentiation in the hippocampus. *Nature* **361**, 31–39 (1993).
2. Silva, A. J., Paylor, R., Wehner, J. M. & Tonegawa, S. Impaired spatial learning in alpha-calcium-calmodulin kinase II mutant mice. *Science* **257**, 206–211 (1992).
3. Frey, U., Krug, M., Reymann, K. G. & Matthies, H. Anisomycin, an inhibitor of protein synthesis, blocks late phases of LTP phenomena in the hippocampal CA1 region *in vitro*. *Brain Res.* **452**, 57–65 (1988).
4. Ho, V. M., Lee, J.-A. & Martin, K. C. The cell biology of synaptic plasticity. *Science* **334**, 623–8 (2011).
5. Kandel, E. R. The molecular biology of memory storage: a dialogue between genes and synapses. *Science* **294**, 1030–8 (2001).
6. Nguyen, P. V., Abel, T. & Kandel, E. R. Requirement of a critical period of transcription for induction of a late phase of LTP. *Science* **265**, 1104–7 (1994).
7. Colgan, D. F. & Manley, J. L. Mechanism and regulation of mRNA polyadenylation. *Genes Dev.* **11**, 2755–2766 (1997).
8. Shi, Y. *et al*. Molecular Architecture of the Human Pre-mRNA 3′ Processing Complex. *Mol. Cell* **33**, 365–376 (2009).
9. Di Giammartino, D. C., Nishida, K. & Manley, J. L. Mechanisms and Consequences of Alternative Polyadenylation. *Mol. Cell* **43**, 853–866 (2011).
10. Elkon, R., Ugalde, A. P. & Agami, R. Alternative cleavage and polyadenylation: extent, regulation and function. *Nat. Rev. Genet.* **14**, 496–506 (2013).
11. Tian, B. & Graber, J. H. Signals for pre-mRNA cleavage and polyadenylation. *Wiley Interdisciplinary Reviews: RNA* **3**, 385–396 (2012).
12. Hoque, M. *et al*. Analysis of alternative cleavage and polyadenylation by 3′ region extraction and deep sequencing. *Nat. Methods* **10**, 133–9 (2013).
13. Tian, B., Hu, J., Zhang, H. & Lutz, C. S. A large-scale analysis of mRNA polyadenylation of human and mouse genes. *Nucleic Acids Res.* **33**, 201–212 (2005).
14. Derti, A. *et al*. A quantitative atlas of polyadenylation in five mammals. *Genome Res.* **22**, 1173–1183 (2012).
15. Li, W. *et al*. Systematic profiling of poly(a)+ transcripts modulated by core 3′ end processing and splicing factors reveals regulatory rules of alternative cleavage and polyadenylation. *PLoS Genet.* **11**, e1005166 (2015).
16. Shi, Y. & Manley, J. L. The end of the message: Multiple protein:RNA interactions define the mRNA polyadenylation site. *Genes Dev.* **29**, 889–897 (2015).
17. Berg, M. G. *et al*. U1 snRNP determines mRNA length and regulates isoform expression. *Cell* **150**, 53–64 (2012).
18. Zheng, D. & Tian, B. RNA-binding proteins in regulation of alternative cleavage and polyadenylation. *Adv. Exp. Med. Biol.* **825**, 97–127 (2014).
19. Lianoglou, S., Garg, V., Yang, J. L., Leslie, C. S. & Mayr, C. Ubiquitously transcribed genes use alternative polyadenylation to achieve tissue-specific expression. *Genes Dev.* **27**, 2380–2396 (2013).
20. Wang, E. T. *et al*. Alternative isoform regulation in human tissue transcriptomes. *Nature* **456**, 470–476 (2008).
21. Zhang, H., Lee, J. Y. & Tian, B. Biased alternative polyadenylation in human tissues. *Genome Biol.* **6**, R100 (2005).
22. Hilgers, V. *et al*. Neural-specific elongation of 3′ UTRs during Drosophila development. *Proc. Natl. Acad. Sci. USA* **108**, 15864–9 (2011).
23. Miura, P., Sanfilippo, P., Shenker, S. & Lai, E. C. Alternative polyadenylation in the nervous system: To what lengths will 3′ UTR extensions take us? *BioEssays* **36**, 766–777 (2014).
24. Miura, P., Shenker, S., Andreu-Agullo, C., Westholm, J. O. & Lai, E. C. Widespread and extensive lengthening of 3′ UTRs in the mammalian brain. *Genome Res.* **23**, 812–25 (2013).
25. Smibert, P. *et al*. Global patterns of tissue-specific alternative polyadenylation in Drosophila. *Cell Rep.* **1**, 277–289 (2012).
26. Zhang, H., Hu, J., Recce, M. & Tian, B. PolyA_DB: A database for mammalian mRNA polyadenylation. *Nucleic Acids Res.* **33**, 116–120 (2005).
27. Lutz, C. S. & Moreira, A. Alternative mRNA polyadenylation in eukaryotes: An effective regulator of gene expression. *Wiley Interdisciplinary Reviews: RNA* **2**, 22–31 (2011).
28. Mayr, C. Evolution and Biological Roles of Alternative 3′UTRs. *Trends Cell Biol.* **26**, 227–37 (2016).
29. Tian, B. & Manley, J. L. Alternative polyadenylation of mRNA precursors. *Nat. Rev. Mol. Cell Biol.* **18**, 18–30 (2017).
30. Job, C. & Eberwine, J. Localization and translation of mRNA in dendrites and axons. *Nat. Rev. Neurosci.* **2**, 889–898 (2001).
31. Martin, K. C. *et al*. Synapse-specific, long-term facilitation of aplysia sensory to motor synapses: A function for local protein synthesis in memory storage. *Cell* **91**, 927–938 (1997).
32. Sutton, M. A. & Schuman, E. M. Dendritic Protein Synthesis, Synaptic Plasticity, and Memory. *Cell* **127**, 49–58 (2006).
33. Wang, W.-X., Wilfred, B. R., Hu, Y., Stromberg, A. J. & Nelson, P. T. Anti-Argonaute RIP-Chip shows that miRNA transfections alter global patterns of mRNA recruitment to microribonucleoprotein complexes. *RNA* **16**, 394–404 (2010).
34. Cajigas, I. J. *et al*. The Local Transcriptome in the Synaptic Neuropil Revealed by Deep Sequencing and High-Resolution Imaging. *Neuron* **74**, 453–466 (2012).
35. Holt, C. E. & Schuman, E. M. The central dogma decentralized: New perspectives on RNA function and local translation in neurons. *Neuron* **80**, 648–657 (2013).
36. Martin, K. C. & Ephrussi, A. mRNA Localization: Gene Expression in the Spatial Dimension. *Cell* **136**, 719–730 (2009).
37. Taliaferro, J. M. *et al*. Distal Alternative Last Exons Localize mRNAs to Neural Projections. *Mol. Cell* **61**, 821–33 (2016).

38. Flavell, S. W. *et al*. Genome-Wide Analysis of MEF2 Transcriptional Program Reveals Synaptic Target Genes and Neuronal Activity-Dependent Polyadenylation Site Selection. *Neuron* **60**, 1022–1038 (2008).
39. Luo, W. *et al*. The Conserved Intronic Cleavage and Polyadenylation Site of CstF-77 Gene Imparts Control of 3′ End Processing Activity through Feedback Autoregulation and by U1 snRNP. *PLoS Genet*. **9**, (2013).
40. Makhinson, M., Chotiner, J. K., Watson, J. B. & O'Dell, T. J. Adenylyl cyclase activation modulates activity-dependent changes in synaptic strength and Ca2+/calmodulin-dependent kinase II autophosphorylation. *J. Neurosci.* **19**, 2500–2510 (1999).
41. Chotiner, J. K., Khorasani, H., Nairn, A. C., O'Dell, T. J. & Watson, J. B. Adenylyl cyclase-dependent form of chemical long-term potentiation triggers translational regulation at the elongation step. *Neuroscience* **116**, 743–752 (2003).
42. Chen, P. B. *et al*. Mapping Gene Expression in Excitatory Neurons during Hippocampal Late-Phase Long-Term Potentiation. *Front. Mol. Neurosci.* **10**, 1–16 (2017).
43. Sala, C. *et al*. Inhibition of dendritic spine morphogenesis and synaptic transmission by activity-inducible protein Homer1a. *J. Neurosci.* **23**, 6327–37 (2003).
44. Zheng, D., Liu, X. & Tian, B. 3′READS+, a sensitive and accurate method for 3′ end sequencing of polyadenylated RNA. *RNA* **22**, 1631–9 (2016).
45. Sandberg, R., Neilson, J. R., Sarma, A., Sharp, P. A. & Burge, C. B. Proliferating cells express mRNAs with shortened 3′ untranslated regions and fewer microRNA target sites. *Science* **320**, 1643–7 (2008).
46. Mayr, C. & Bartel, D. P. Widespread shortening of 3′UTRs by alternative cleavage and polyadenylation activates oncogenes in cancer cells. *Cell* **138**, 673–84 (2009).
47. Alberi, L. *et al*. Activity-Induced Notch Signaling in Neurons Requires Arc/Arg3.1 and Is Essential for Synaptic Plasticity in Hippocampal Networks. *Neuron* **69**, 437–444 (2011).
48. Brai, E. *et al.* Notch1 Regulates Hippocampal Plasticity Through Interaction with the Reelin Pathway, Glutamatergic Transmission and CREB Signaling. *Front. Cell. Neurosci.* **9**, 447 (2015).
49. Gu, Q.-H. *et al*. miR-26a and miR-384-5p are required for LTP maintenance and spine enlargement. *Nat. Commun.* **6**, 6789 (2015).
50. Hermey, G. *et al*. Genome-Wide Profiling of the Activity-Dependent Hippocampal Transcriptome. *PLoS One* **8**, (2013).
51. Majdan, M. & Shatz, C. J. Effects of visual experience on activity-dependent gene regulation in cortex. *Nat. Neurosci.* **9**, 650–9 (2006).
52. Leach, P. T. *et al*. Gadd45b knockout mice exhibit selective deficits in hippocampus-dependent long-term memory. *Learn. Mem.* **19**, 319–24 (2012).
53. Barco, A., Alarcon, J. M. & Kandel, E. R. Expression of constitutively active CREB protein facilitates the late phase of long-term potentiation by enhancing synaptic capture. *Cell* **108**, 689–703 (2002).
54. Benito, E. & Barco, A. CREB's control of intrinsic and synaptic plasticity: implications for CREB-dependent memory models. *Trends in Neurosciences* **33**, 230–240 (2010).
55. Silva, A. J., Kogan, J. H., Frankland, P. W. & Kida, S. CREB and memory. *Annu. Rev. Neurosci.* **21**, 127–48 (1998).
56. Yang, Y. *et al.* PAF Complex Plays Novel Subunit-Specific Roles in Alternative Cleavage and Polyadenylation. *PLoS Genet*. **12**, (2016).
57. Alberini, C. M. Transcription factors in long-term memory and synaptic plasticity. *Physiol. Rev.* **89**, 121–45 (2009).
58. Lonze, B. E. & Ginty, D. D. Function and Regulation of CREB Family Transcription Factors in the Nervous System CREB and its close relatives are now widely accepted. *Neuron* **35**, 605–623 (2002).
59. Wang, R., Nambiar, R., Zheng, D. & Tian, B. PolyA_DB 3 catalogs cleavage and polyadenylation sites identified by deep sequencing in multiple genomes. *Nucleic Acids Res* (2017).
60. Håvik, B. *et al*. Synaptic activity-induced global gene expression patterns in the dentate gyrus of adult behaving rats: Induction of immunity-linked genes. *Neuroscience* **148**, 925–936 (2007).
61. Maag, J. L. V. *et al*. Dynamic expression of long noncoding RNAs and repeat elements in synaptic plasticity. *Front. Neurosci.* **9**, 1–16 (2015).
62. McNair, K., Davies, C. H. & Cobb, S. R. Plasticity-related regulation of the hippocampal proteome. *Eur. J. Neurosci.* **23**, 575–580 (2006).
63. Chang, S. P., Gong, R., Stuart, J. & Tang, S. J. Molecular network and chromosomal clustering of genes involved in synaptic plasticity in the hippocampus. *J. Biol. Chem.* **281**, 30195–30211 (2006).
64. Ryan, M. M. *et al*. Temporal profiling of gene networks associated with the late phase of long-term potentiation *in vivo*. *PLoS One* **7**, 1–14 (2012).
65. Buxbaum, A. R., Yoon, Y. J., Singer, R. H. & Park, H. Y. Single-molecule insights into mRNA dynamics in neurons. *Trends in Cell Biology* **25**, 468–475 (2015).
66. Raj, B. & Blencowe, B. J. Alternative Splicing in the Mammalian Nervous System: Recent Insights into Mechanisms and Functional Roles. *Neuron* **87**, 14–27 (2015).
67. O'Leary, T., van Rossum, M. C. W. & Wyllie, D. J. A. Homeostasis of intrinsic excitability in hippocampal neurones: dynamics and mechanism of the response to chronic depolarization. *J. Physiol.* **588**, 157–70 (2010).
68. Shepard, P. J. *et al*. Complex and dynamic landscape of RNA polyadenylation revealed by PAS-Seq. *RNA* **17**, 761–772 (2011).
69. Ji, Z., Lee, J. Y., Pan, Z., Jiang, B. & Tian, B. Progressive lengthening of 3′ untranslated regions of mRNAs by alternative polyadenylation during mouse embryonic development. *Proc. Natl. Acad. Sci. USA* **106**, 7028–33 (2009).
70. Ji, Z. & Tian, B. Reprogramming of 3′ untranslated regions of mRNAs by alternative polyadenylation in generation of pluripotent stem cells from different cell types. *PLoS One* **4**, e8419 (2009).
71. Chen, F. X. *et al*. PAF1 regulation of promoter-proximal pause release via enhancer activation. *Science* **357**, 1294–1298 (2017).
72. Fischl, H., Howe, F. S., Furger, A. & Mellor, J. Paf1 Has Distinct Roles in Transcription Elongation and Differential Transcript Fate. *Mol. Cell* **65**, 685–698.e8 (2017).
73. Bresson, S. M. & Conrad, N. K. The human nuclear poly(a)-binding protein promotes RNA hyperadenylation and decay. *PLoS Genet.* **9**, e1003893 (2013).
74. Cohen, J. E., Lee, P. R. & Fields, R. D. Systematic identification of 3′-UTR regulatory elements in activity-dependent mRNA stability in hippocampal neurons. *Philos. Trans. R. Soc. B Biol. Sci.* **369**, 20130509–20130509 (2014).
75. Boutet, S. C. *et al*. Alternative polyadenylation mediates microRNA regulation of muscle stem cell function. *Cell Stem Cell* **10**, 327–336 (2012).
76. Han, K. *et al*. Human-specific regulation of MeCP2 levels in fetal brains by microRNA miR-483-5p. *Genes Dev.* **27**, 485–490 (2013).
77. Nam, J. W. *et al*. Global analyses of the effect of different cellular contexts on microRNA targeting. *Mol. Cell* **53**, 1031–1043 (2014).
78. Frank, D. A. & Greenberg, M. E. CREB: a mediator of long-term memory from mollusks to mammals. *Cell* **79**, 5–8 (1994).
79. Santos, A. R. A. & Duarte, C. B. Validation of internal control genes for expression studies: Effects of the neurotrophin BDNF on hippocampal neurons. *J. Neurosci. Res.* **86**, 3684–3692 (2008).
80. Dobin, A. *et al*. STAR: ultrafast universal RNA-seq aligner. *Bioinformatics* **29**, 15–21 (2013).
81. Lawrence, M. *et al*. Software for computing and annotating genomic ranges. *PLoS Comput. Biol.* **9**, e1003118 (2013).
82. Anders, S. & Huber, W. Differential expression analysis for sequence count data. *Genome Biol.* **11**, R106 (2010).
83. Langmead, B. & Salzberg, S. L. Fast gapped-read alignment with Bowtie 2. *Nat. Methods* **9**, 357–359 (2012).
84. Anders, S., Reyes, A. & Huber, W. Detecting differential usage of exons from RNA-seq data. *Genome Res.* **22**, 2008–2017 (2012).

Acknowledgements

We thank S. L. Zipursky for comments on the manuscript, members of BT and KCM labs for helpful discussions, and S. Deverasetty for development of the 3′READS+ and RNA-seq web browser. We thank Q. Wang for assistance with PAS-Seq library preparation and protocol optimization. This work was supported by NIH R01GM084089 (to BT), NIH R01NS045324 (to KCM), NIH R01MH060919 (to TJO), Graduate Program in Areas of Basic and Applied Biology and Fundação para a Ciência e a Tecnologia SFRH/BD/51289/2010 (to MMF). We acknowledge the support of the NINDS Informatics Center for Neurogenetics and Neurogenomics (P30 NS062691).

Author Contributions

M.M.F., B.T., and K.C.M. conceived of and designed the experiments. M.M.F., D.Z., A.H., V.M.H., and P.B.C. performed the experiments. A.G., R.K., X.L., G.C., and B.T. analyzed the data. T.J.O. contributed reagents and materials. M.M.F., A.G., B.T., and K.C.M. wrote the paper.

Additional Information

Supplementary information accompanies this paper at https://doi.org/10.1038/s41598-017-17407-w.

Competing Interests: The authors declare that they have no competing interests.

Publisher's note: Springer Nature remains neutral with regard to jurisdictional claims in published maps and institutional affiliations.

Appendix 2 – Publication: Cytoplasmic Rbfox1 Regulates the Expression of Synaptic and Autism-Related Genes

Article

Neuron

Cytoplasmic Rbfox1 Regulates the Expression of Synaptic and Autism-Related Genes

Highlights

- Nuclear and cytoplasmic Rbfox1 isoforms regulate distinct neuronal mRNAs
- Cytoplasmic Rbfox1 regulates the stability and translation of its target mRNAs
- Rbfox1 and miRNA binding sites overlap significantly in target mRNA 3′ UTRs
- Cytoplasmic Rbfox1 targets are enriched in cortical development and autism genes

Authors

Ji-Ann Lee, Andrey Damianov, Chia-Ho Lin, ..., Daniel H. Geschwind, Douglas L. Black, Kelsey C. Martin

Correspondence

kcmartin@mednet.ucla.edu

In Brief

Rbfox1 regulates the splicing of many exons in the nucleus of neurons. Lee at al. demonstrate that Rbfox1 also binds to the 3′ UTR of target mRNAs in the cytoplasm to upregulate the expression of synaptic and autism-related genes.

Accession Numbers

GSE71917

Lee et al., 2016, Neuron *89*, 113–128
January 6, 2016
http://dx.doi.org/10.1016/j.neuron.2015.11.025

CellPress

Neuron
Article

Cytoplasmic Rbfox1 Regulates the Expression of Synaptic and Autism-Related Genes

Ji-Ann Lee,[1] Andrey Damianov,[2] Chia-Ho Lin,[2] Mariana Fontes,[1] Neelroop N. Parikshak,[3] Erik S. Anderson,[2] Daniel H. Geschwind,[3] Douglas L. Black,[2,4] and Kelsey C. Martin[1,*]
[1]Department of Biological Chemistry
[2]Department of Microbiology, Immunology, and Molecular Genetics
[3]Program in Neurobehavioral Genetics, Semel Institute, David Geffen School of Medicine
[4]Howard Hughes Medical Institute
University of California, Los Angeles, Los Angeles, CA 90095, USA
*Correspondence: kcmartin@mednet.ucla.edu
http://dx.doi.org/10.1016/j.neuron.2015.11.025

SUMMARY

Human genetic studies have identified the neuronal RNA binding protein, Rbfox1, as a candidate gene for autism spectrum disorders. While Rbfox1 functions as a splicing regulator in the nucleus, it is also alternatively spliced to produce cytoplasmic isoforms. To investigate the function of cytoplasmic Rbfox1, we knocked down Rbfox proteins in mouse neurons and rescued with cytoplasmic or nuclear Rbfox1. Transcriptome profiling showed that nuclear Rbfox1 rescued splicing changes, whereas cytoplasmic Rbfox1 rescued changes in mRNA levels. iCLIP-seq of subcellular fractions revealed that Rbfox1 bound predominantly to introns in nascent RNA, while cytoplasmic Rbox1 bound to 3′ UTRs. Cytoplasmic Rbfox1 binding increased target mRNA stability and translation, and Rbfox1 and miRNA binding sites overlapped significantly. Cytoplasmic Rbfox1 target mRNAs were enriched in genes involved in cortical development and autism. Our results uncover a new Rbfox1 regulatory network and highlight the importance of cytoplasmic RNA metabolism to cortical development and disease.

INTRODUCTION

Post-transcriptional regulation of RNA within neurons provides temporal and spatial control of gene expression during brain development and plasticity. RNA binding proteins (RBPs) play central roles in regulating each step of RNA processing. Mutations in RBPs have been found to cause and/or contribute to many human neurodevelopmental and neurologic disorders (Darnell and Richter, 2012; Lukong et al., 2008). Human genetic studies have focused attention on *RBFOX1*, a vertebrate homolog of the *Caenorhabditis elegans Feminizing gene 1 on X* (also known as Ataxin-2 Binding Protein 1 [*A2BP1*]) by associating chromosomal translocations and copy number variations in *RBFOX1* with autism-spectrum disorders (ASDs) (Martin et al., 2007; Sebat et al., 2007). A gene co-expression network analysis of post mortem cerebral cortex from individuals with ASD identified *RBFOX1* as a hub gene in a module of co-expressed transcripts involved in neuronal function and downregulated in ASD (Voineagu et al., 2011). Other studies found *RBFOX1* mutations associated with human epilepsy syndromes (Bhalla et al., 2004; Lal et al., 2013a, 2013b; Martin et al., 2007), which is often co-morbid with ASD.

Mammals express three Rbfox paralogs: Rbfox1 expressed in neurons, heart, and muscle; Rbfox2 expressed in these three tissues as well as in stem cells, hematopoietic cells, and other cells; and Rbfox3 (also known as NeuN) expressed only in neurons (Kim et al., 2009b; Kuroyanagi, 2009). All Rbfox proteins contain a single RNA recognition motif (RRM)-type RNA binding domain that binds the hexanucleotide (U)GCAUG with great specificity (Auweter et al., 2006). When this sequence is present in regulated exons or flanking introns, Rbfox functions as a splicing regulator to promote or repress exon inclusion (Kuroyanagi, 2009). Studies in knockout (KO) mice revealed a role for Rbfox1 in regulating neuronal splicing networks involved in neurodevelopmental disorders and in controlling neuronal excitability (Gehman et al., 2011). A subsequent study identified several hundred additional Rbfox1-dependent splicing changes during neuronal differentiation of human fetal primary neural progenitor cells (Fogel et al., 2012). Crosslinking-immunoprecipitation and RNA-seq (CLIP-seq) identified additional Rbfox1 splicing targets in mouse brain, including many ASD-related genes (Lovci et al., 2013; Weyn-Vanhentenryck et al., 2014).

Rbfox1 is itself alternatively spliced to produce nuclear and cytoplasmic isoforms, referred to as Rbfox1_N and Rbfox1_C, respectively (Lee et al., 2009; Nakahata and Kawamoto, 2005). While the function of Rbfox1_N in splicing has been well studied, the function of Rbfox1_C is largely unexplored. The conservation of Rbfox binding sites in the 3′ UTRs of many neuronal transcripts suggests that Rbfox1 plays a role in regulating mRNAs in the cytoplasm (Ray et al., 2013; Xie et al., 2005). Ray et al. (2013) correlated the expression of Rbfox1 in different tissues with the presence of Rbfox1 binding sites in 3′ UTRs and proposed that Rbfox1 stabilizes target mRNAs. Although they confirmed this by luciferase assay for one target using Rbfox1_N, it was not clear whether this stabilization arose from Rbfox1 actions in the nucleus or the cytoplasm. Other studies identifying Rbfox1

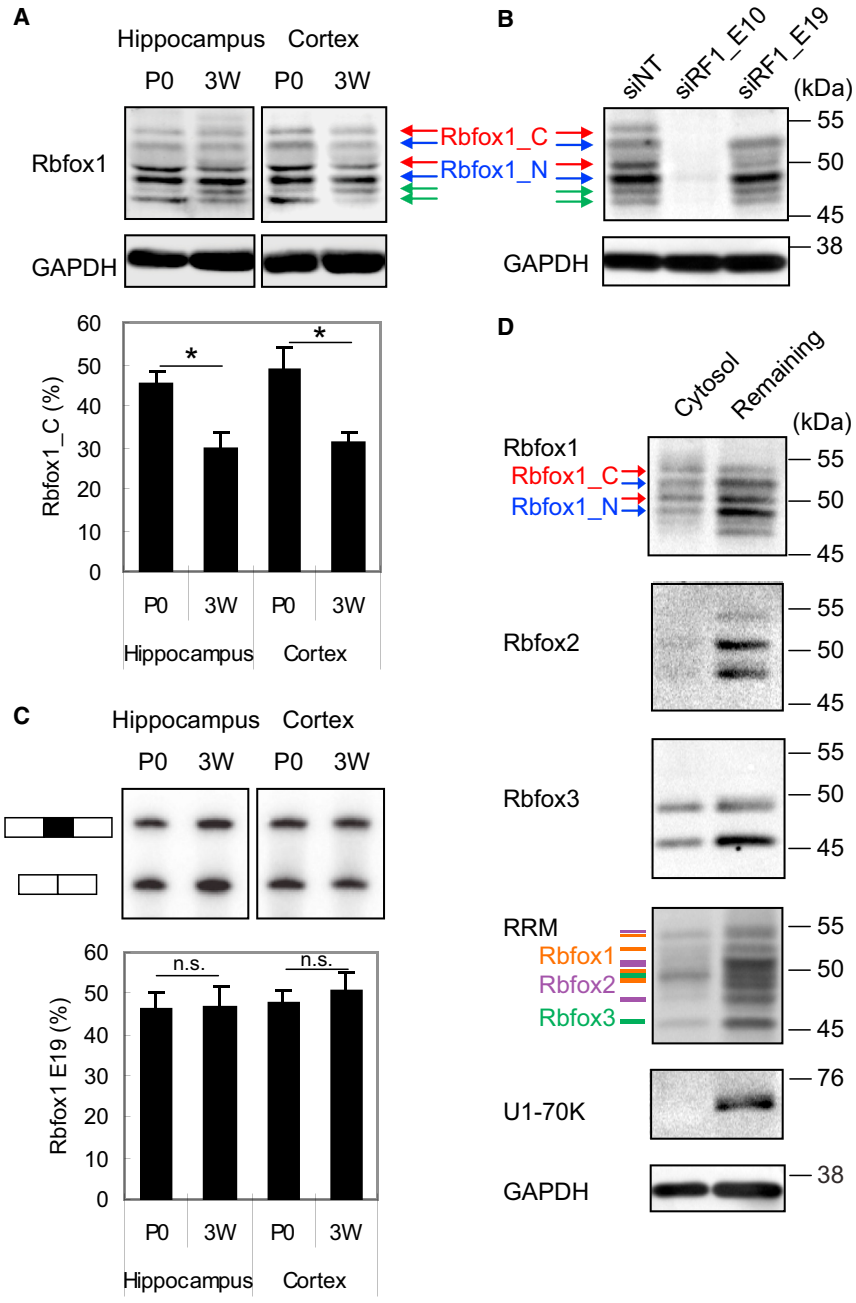

Figure 1. Expression and localization of Rbfox1 isoforms in neurons

(A) Immunoblot of Rbfox1 isoforms during development in mouse hippocampus and cortex at postnatal day 0 (P0), and 3 weeks (3W). Cytoplasmic Rbfox1 isoform (Rbfox1_C) and nuclear Rbfox1 isoform (Rbfox1_N) are indicated by red and blue arrows, respectively. The green arrow points to a lower molecular weight isoform that is reduced by Rbfox1 siRNA (panel B), but whose provenance is unknown. The percentage of Rbfox1_C in the two dominant bands in the middle is shown in the bar graph below. Error bars indicate SD. n = 3. Statistical significance was determined by Student's t test. *p value < 0.05.

(B) Immunoblot of Rbfox1 using an Rbfox1 pan siRNA (siRF1_E10) and an Rbfox1_C specific siRNA (siRF1_E19) in hippocampal neurons (DIV17).

(C) Semiquantitative PCR analysis showing the splicing of Rbfox1 exon 19 in the same tissue and at the same time points as in (A). The percentage of exon 19 splicing is shown in histogram. Error bars indicate SD. n = 3. The percentage of Rbfox1 exon 19 inclusion was calculated; Student's t test, $p < 0.05$. n.s. = not significant.

(D) Immunoblot showing that Rbfox1 and Rbfox3 but not Rbfox2 are present in a cytosolic fraction purified from mouse hippocampal neurons (DIV14, treated with AraC). In the RRM immunoblots, the orange lines correspond to Rbfox1 proteins, the purple lines correspond to Rbfox2 proteins, and the green lines correspond to Rbfox3 proteins.

targets using CLIP-seq were done in whole tissue and thus could not differentiate between nuclear and cytoplasmic targets of Rbfox1 (Lovci et al., 2013; Weyn-Vanhentenryck et al., 2014).

To dissect the functions of Rbfox1 in the cytoplasm and nucleus, we profiled the transcriptome of neurons expressing either Rbfox1_C or Rbfox1_N. We complemented these experiments with Rbfox1 individual-nucleotide resolution CLIP (iCLIP) from subcellular fractions of neurons to identify the specific transcripts bound by Rbfox1 in the cytoplasm. Together, these findings identify a large number of transcripts regulated by cytoplasmically localized Rbfox1, independent of its effect on splicing. Our results indicate that the cytoplasmic portion of the Rbfox1 regulatory network controls many essential neuronal functions and further show that these cytoplasmic targets overlap extensively with regulatory modules involved in cortical development and ASD.

RESULTS

Rbfox1_C Is Expressed at Significant Levels in Mouse Brain

The *Rbfox1* gene contains several promoters and alternatively spliced exons, which generate multiple protein isoforms (Damianov and Black, 2010). The skipping of mouse exon 19 generates an Rbfox1 mRNA encoding Rbfox1_N, a protein with a nuclear localization signal (NLS) in the C terminus that is enriched in the nucleus (Hamada et al., 2013; Lee et al., 2009). In contrast, the mRNA including exon 19 encodes Rbfox1_C, a protein lacking the NLS that localizes to the cytoplasm. We examined Rbfox1 protein and mRNA in brain to compare the expression levels of Rbfox1_N and Rbfox1_C isoforms. Immunoblotting of lysates from hippocampus and cortex from P0 and P21 mice with an anti-Rbfox1 antibody revealed six bands ranging from 45 to 55 kDa (Figure 1A). All of the bands were

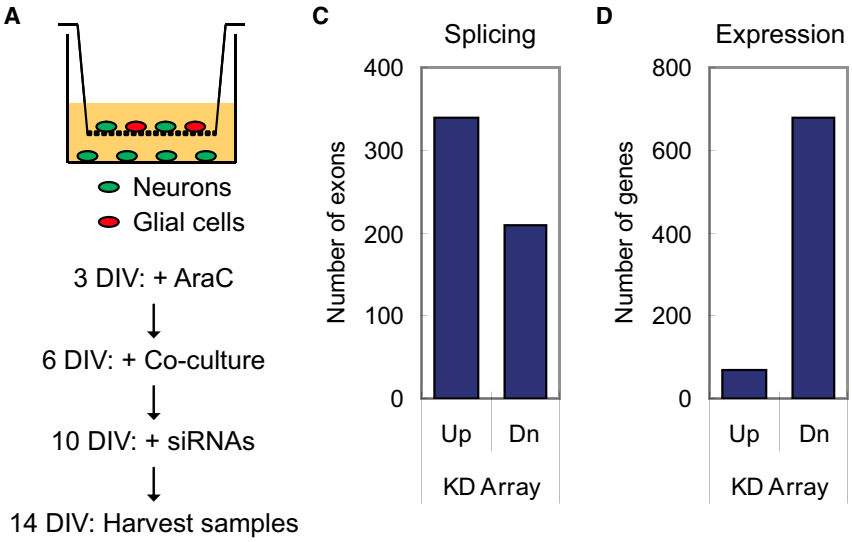

Figure 2. Rbfox1 Regulates mRNA Expression: Knockdown and Microarray Analysis

(A) Experimental flow chart.

(B) Immunoblot showing the knockdown (KD) of Rbfox1 and Rbfox3 proteins in neurons incubated with Accell siRNAs targeting Rbfox1 (siRF1) and Rbfox3 (siRF3). GAPDH is used as loading control.

(C) Histogram of upregulated (Up) and downregulated (Dn) exons in KD experiments.

(D) Histogram of upregulated (Up) and downregulated (Dn) genes in KD experiments.

(E) Histogram of percentage of genes that contain ≥1 UGCAUG motif conserved in the 3′ UTR in human, mouse, rat, dog, and chicken genomes (UGCAUG_5G), ≥1 UGCAUG motif conserved in human and mouse genomes (UGCAUG_2G), or ≥1 GCAUG motif conserved in human and mouse genomes (GCAUG_2G). ***$p < 10^{-15}$ by hypergeometric test. Non, not changed.

For additional data, see Figures S1 and S2.

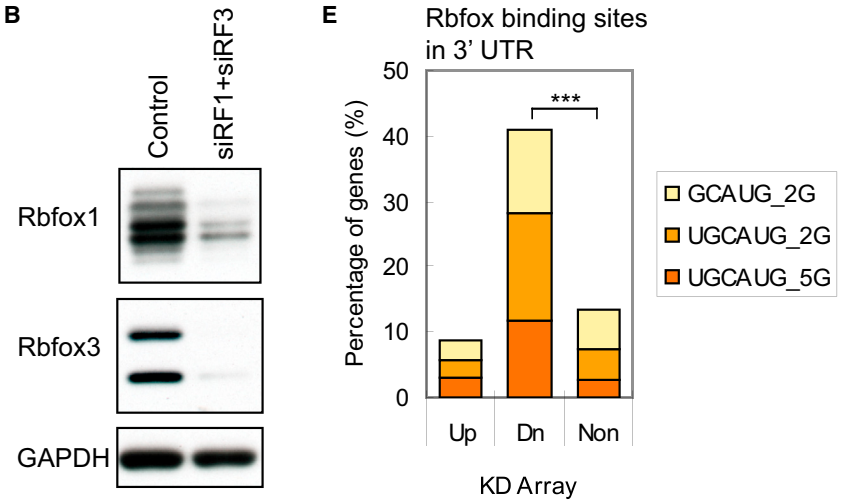

reduced or abolished by an siRNA targeting a constitutive exon present in all Rbfox1 mRNAs (siRF1_E10, Figure 1B), indicating that they represent specific Rbfox1 products. Using an siRNA targeting alternative exon 19, two of the six protein bands were depleted, indicating that these represent Rbfox1_C (red arrows in Figure 1B). In P0 mouse hippocampus and cortex, Rbfox1_C constituted 46% and 49% of Rbfox1 protein (Figure 1A), respectively, and subsequently declined to the 30% from 3 weeks to 6 months of age in adult brain (data not shown). We also examined the splicing of exon 19 by semiquantitative RT-PCR and found that 47% and 48% of Rbfox1 mRNA included exon 19 in P0 hippocampus and cortex, respectively (Figure 1C). Rbfox1_C is thus expressed at significant concentrations in mouse brain.

To confirm that endogenous Rbfox1 localizes to the cytoplasm, we performed immunoblotting on subcellular fractions (Figure 1D). We prepared cytosolic fractions by permeabilizing the plasma membrane but not the nucleus of dissociated hippocampal cultures with digitonin (Mackall et al., 1979). After collecting the cytosolic fraction that leaked out of the cells, cultures were further solubilized with RIPA buffer. As shown in Figure 1D, the cytoplasmic protein GAPDH was present in the digitonin-solubilized cytosolic fraction and in the RIPA-solubilized remaining fraction, indicating that the lysis was partial. More importantly, the nuclear marker U1-70K was absent from the cytosolic fraction, indicating that digitonin permeabilization released cytosolic, but not nuclear proteins. Rbfox1 immunoblots of the cytosolic fraction detected both Rbfox1_C and Rbfox1_N isoforms, indicating that both Rbfox1 splice isoforms are present in the cytoplasm. However, the ratio of Rbfox1_C to Rbfox1_N was higher in the cytosolic fraction, with Rbfox1_C representing the dominant isoform in the cytoplasm. Using antibodies specific for Rbfox2, Rbfox3, and Rbfox RRM, we detected Rbfox3, but not Rbfox2, in the cytosolic fraction. Thus, Rbfox1 and Rbfox3 are the major Rbfox paralogs in the cytoplasm of hippocampal neurons.

Rbfox1 Regulation of mRNA Expression

Only a few changes in mRNA expression levels were detected in the brain of *Rbfox1* KO mice (Gehman et al., 2011; Lovci et al., 2013), which we postulated was due to compensation by Rbfox3. To examine the cytoplasmic function of Rbfox1, we isolated dissociated mouse hippocampal neurons, which express Rbfox1_C at high levels. To obtain a neuron-enriched culture, we added AraC to eliminate glial cells and co-cultured with filter inserts containing glial cells (Figures 2A, S1A, and S1B). We performed double siRNA-mediated knockdown (KD) of Rbfox1 and

Rbfox3 (Figure 2B). After acute KD, we used microarray analysis to detect changes in the transcriptome (n = 3 biological replicates). Analyzing for splicing changes, we identified 338 upregulated and 208 downregulated alternative cassette exons in the double KD neurons (Figure 2C). Our results recapitulated 11 of the 20 splicing changes identified in the whole brain of *Rbfox1* KO mice (Gehman et al., 2011).

In addition to splicing changes, we identified 746 genes exhibiting changes in abundance (expression) in the double KD (Figure 2D and Table S1) and validated a subset of genes by RT-qPCR analysis (20/23 = 87%, Figure S1C). The majority (676 genes, or 91%) were downregulated in the double KD, indicating that their abundance is normally increased by Rbfox1 and Rbfox3. We also measured the protein products of several regulated genes by quantitative immunoblotting. As shown in Figure S2, mRNAs of calcium/calmodulin-dependent protein kinase (CaMK) family members, CaMK2A, CaMK2B, and CaMK4, were reduced in double KD cultures with a corresponding decrease in the concentration of CaMK2A and CaMK2B, but not CaMK4 protein. We also observed a slight increase in Rbfox2 mRNA and a 2-fold increase in Rbfox2 protein in the Rbfox1 and Rbfox3 knockdown cultures, as was reported in *Rbfox1* KO mice (Gehman et al., 2011). These data suggest that Rbfox1 or Rbfox3 may repress Rbfox2 expression at the translational level to form a negative regulatory loop for Rbfox proteins in neurons.

To determine whether the changes in mRNA expression were caused directly or indirectly by the loss of Rbfox1 and Rbfox3, we searched for conserved (U)GCAUG sequence motifs in the 3′ UTRs of transcripts as an indicator of direct Rbfox1 regulation. The downregulated gene set was significantly enriched for genes containing a 3′ UTR UGCAUG motif that was conserved across human, mouse, rat, dog, and chicken genomes (12%, $p < 10^{-15}$, hypergeometric test, Figure 2E). Considering only conservation between human and mouse genomes, this enrichment increased to 41% ($p < 10^{-15}$, hypergeometric test, Figure 2E). In contrast, we detected no enrichment of (U)GCAUG motifs in upregulated genes. Together, these findings indicate that in addition to regulating alternative splicing, Rbfox1 and 3 regulate mRNA and protein abundance and suggest that this regulation occurs by direct RNA binding to (U)GCAUG sites in the 3′ UTR.

Rbfox1_C but Not Rbfox1_N Rescues the Expression Changes Induced by Double KD of Rbfox1 and 3

To differentiate between the functions of Rbfox1_C and Rbfox1_N, we performed double KD of Rbfox1 and 3 and then rescued with either siRNA resistant Rbfox1_C (Flag-Rbfox1_C_siMt) or Rbfox1_N (Flag-Rbfox1_N_siMt). To facilitate these experiments, we performed them in cultures containing both glia and neurons, rather than in the filter co-culture system (after confirming that selected genes were regulated by double KD in both culture systems, Figure S3). To achieve cell-type-specific rescue, we used AAV2/9 vectors with the human synapsin I promoter driving the expression of Flag-Rbfox1_C_siMt and Flag-Rbfox1_N_siMt in neurons (Figures S4A and S4B). The concentrations of virus were adjusted to match the expression of endogenous Rbfox1 and Rbfox3 (Figure S4C). Immunocytochemistry with Flag antibodies revealed that virally expressed Rbfox1_C localized predominantly to the cytoplasm and processes, with low but detectable expression in the nucleus (Figures S4D and S4F), while virally expressed Rbfox1_N localized predominantly in the nucleus, with low levels of detection in the somatic cytoplasm (Figures S4E and S4G). We performed RNA-seq on: (1) control cells treated with non-targeting siRNAs and virus expressing EGFP; (2) cells treated with Rbfox1 and 3 siRNAs and virus expressing EGFP; (3) cells treated with Rbfox1 and 3 siRNAs and virus expressing Flag-Rbfox1_C_siMt; and (4) cells treated with Rbfox1 and 3 siRNAs and virus expressing Flag-Rbfox1_N_siMt (Figure S4C).

Strikingly, we found that changes in splicing were induced predominantly by Rbfox1_N, while the large majority of changes in mRNA abundance (expression) were regulated by Rbfox1_C. Comparing Rbfox1_N rescue to double KD, we identified 146 upregulated and 172 downregulated alternative cassette exons (Figure 3A). Fewer exons were affected by the Rbfox1_C rescue of the double KD: 89 upregulated and 61 downregulated alternative cassette exons. Of the exons affected by either Rbox1 isoform, 81% changed in the same direction, and of this set 74% were more strongly affected by Rbfox1_N than by Rbfox1_C (more intense green and red signal in Figure 3B in the Rbfox1_N column than in the Rbfox1_C column). Exons affected by Rbfox1_C are potentially directly regulated by its low concentrations in the nucleus, or could be indirectly affected by changes in other proteins. An opposite pattern was observed in expression changes: the expression of 275 genes was altered by Rbfox1_C, whereas Rbfox1_N only affected the expression of 49 genes (Figure 3C). Of the genes whose expression was altered by either Rbfox1 isoform, 91% showed the same direction of change, and most of these genes (79%) showed a greater magnitude of change with Rbfox1_C rescue than with Rbfox1_N rescue (more intense green and red signal in Figure 3D in the Rbfox1_C column than in the Rbfox1_N column). These results indicate that Rbfox1_N predominately regulates pre-mRNA splicing, while Rbfox1_C predominately regulates mRNA abundance. We thus focused our subsequent analyses of splicing on the effects of Rbfox1_N and our analyses of overall mRNA abundance on Rbfox1_C.

To define a set of genes whose splicing is regulated by Rbfox1_N for downstream analyses, we selected exons showing opposite changes in splicing between (1) control and double KD and (2) double KD and Rbfox1_N rescue and filtered for exons whose splicing change reaches statistical significance in either (1) or (2). Using these criteria, we defined 182 Rbfox1 activated exons and 184 Rbfox1 repressed exons in a total of 332 genes as Rbfox1_N splicing targets (Tables S1 and S2). Examining the flanking upstream and downstream introns of these exons, we found that GCAUG motif was the most enriched pentamer in these regions. Consistent with previous studies, the GCAUG motif was particularly enriched in the proximal region of introns downstream of the Rbfox1 activated exons (Underwood et al., 2005; Yeo et al., 2009; Zhang et al., 2008). Next, we examined the frequency of conserved (U)GCAUG motifs in the 3′ UTR sequences of transcripts whose expression was altered in double KD compared to control and in Rbfox1_C rescue compared to double KD. Consistent with the results in Figure 2E, genes whose expression was downregulated by double KD of Rbfox1 and 3

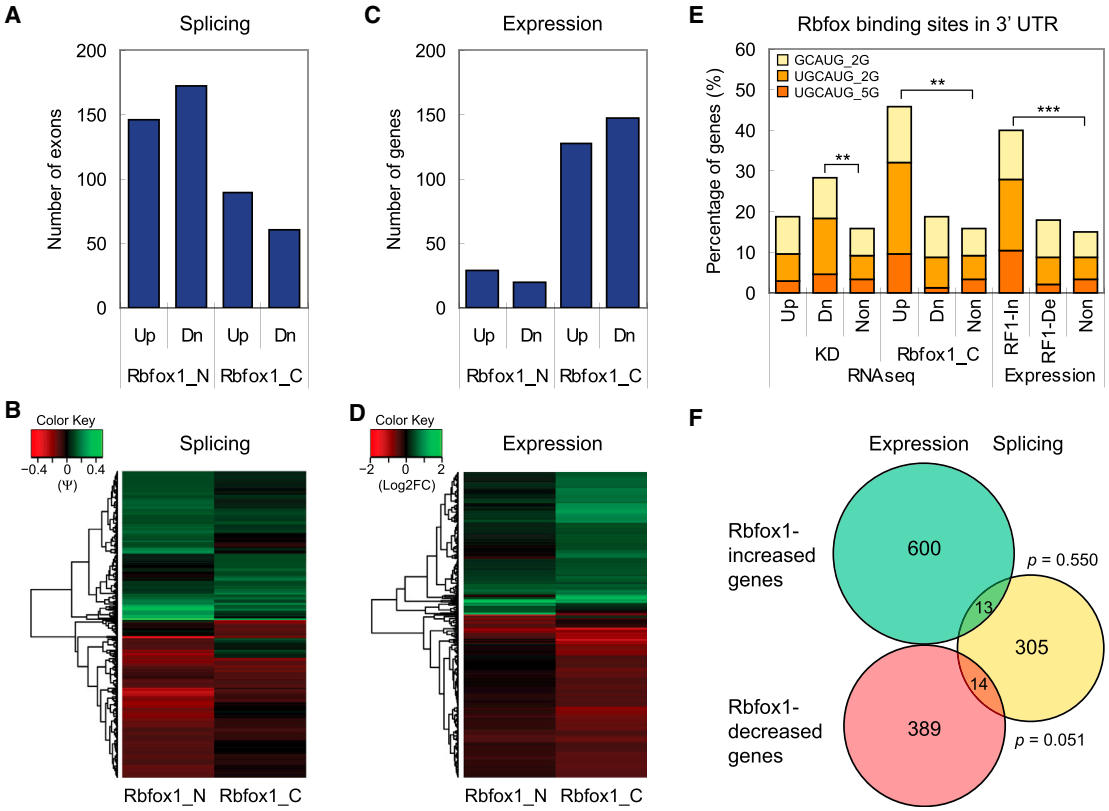

Figure 3. Knockdown and Rescue Experiments Identify Distinct Functions for Rbfox1_C and Rbfox1_N

(A) Histogram of upregulated (Up) and downregulated (Dn) exons rescued by Rbfox1_N or Rbfox1_C compared to KD. p = 7.74e-15 by Pearson's chi-square test with Yates' continuity correction.

(B) Heatmap of the differences in percentage of splicing (Ψ) for the exons in (A).

(C) Histogram of upregulated (Up) and downregulated (Dn) genes rescued by Rbfox1_N or Rbfox1_C compared to KD. p = 3.125e-36 by Pearson's chi-square test with Yates' continuity correction.

(D) Heatmap of the Log2 fold change (Log2FC) in expression for the genes in (D).

(E) Histogram of the percentage of genes that contain conserved UGCAUG motifs in the 3′ UTR. Up, upregulated; Dn, downregulated; Non, not changed; In, mRNA concentration increased by Rbfox1; De, mRNA concentration decreased by Rbfox1. *$p < 10^{-5}$, **$p < 10^{-10}$, and ***$p < 10^{-15}$ by hypergeometric test.

(F) Weighted Venn diagram showing the overlap of genes regulated by Rbfox1 at the level of expression and splicing. p values are calculated by hypergeometric test.

For additional data, see Figures S3, S4, and S5.

were significantly enriched for conserved (U)GCAUG motifs in their 3′ UTRs. Correspondingly, genes whose expression was upregulated by Rbfox1_C rescue were also enriched for conserved (U)GCAUG motifs in the 3′ UTR. This enrichment was not observed in genes whose expression was downregulated by Rbfox1_C rescue (Figure 3E). We also compared the transcriptome data obtained by microarray and RNA-seq methods. We found that the sets of genes downregulated by double KD measured by these two methods overlapped significantly (odds-ratio (OR) = 2.97, p = 1.9e-9). There was also significant overlap between the set of downregulated genes in the KD measured by microarray and the set of genes upregulated by Rbfox1_C rescue measured by RNA-seq (OR = 8.4, p = 1.1e-16). In contrast, we did not observe significant overlap between the upregulated gene sets in the KD experiments measured by microarray and RNA-seq (Figures 2E and 3E). Thus, gene expression changes that positively correlate with Rbfox1_C expression levels are reproducible between assays. These observations support a role for Rbfox1_C in increasing the stability and thus the abundance of transcripts containing the (U)GCAUG motifs in their 3′ UTR.

To define a high confidence set of "expression" targets of Rbfox1_C (those whose mRNA abundance is regulated by Rbfox1_C), as opposed to the set of "splicing" targets of Rbfox1_N defined earlier, we used data from microarray and RNA-seq experiments and selected genes that showed opposite changes in expression between (1) control and double KD and (2) double KD and Rbfox1_C rescue, filtering for genes whose change in expression reached statistical significance in either (1) or (2). This identified 613 genes whose mRNA abundance ("expression") was downregulated by Rbfox KD but upregulated upon Rbfox1_C rescue and 403 genes whose abundance was upregulated by Rbfox KD but downregulated by Rbfox1_C rescue (Table S1). We termed the former "Rbfox1-increased

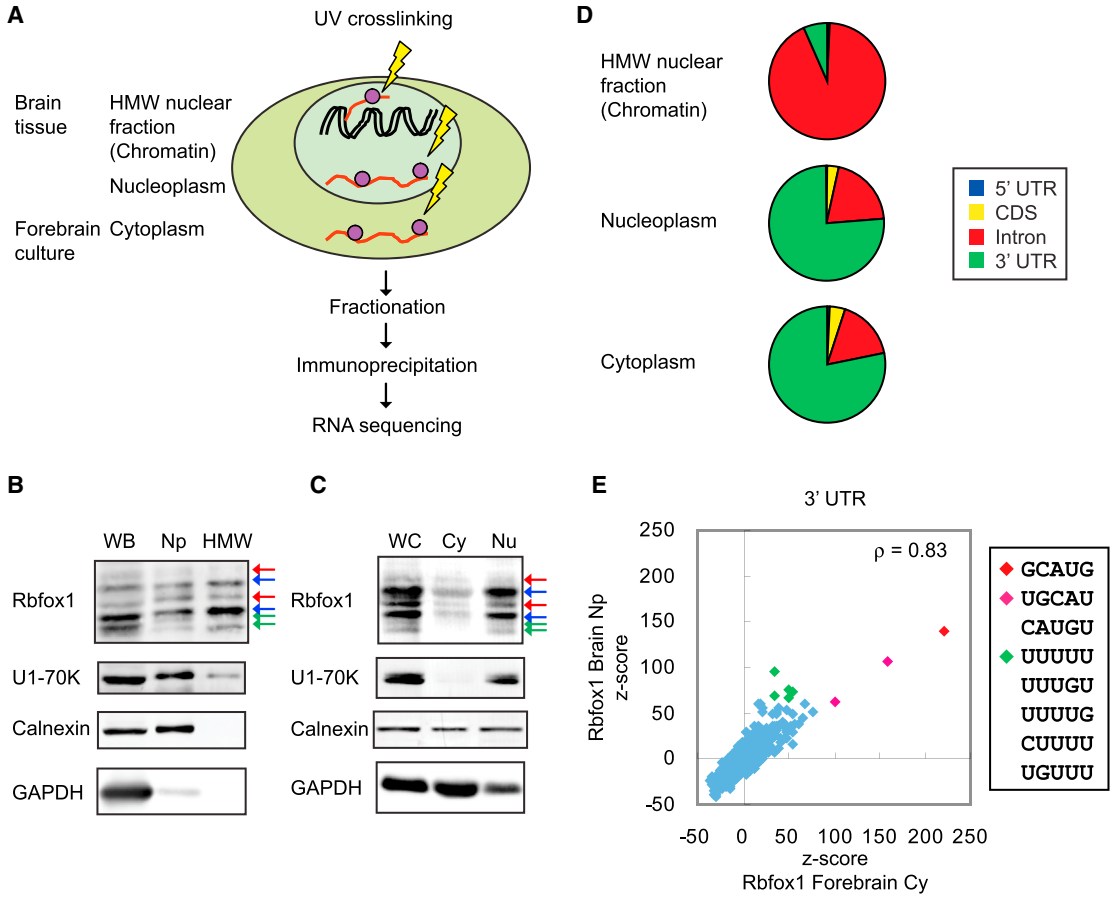

Figure 4. Characterization of Rbfox1 iCLIP Tags in the 3′ UTR

(A) Illustration of iCLIP experimental workflow. HMW, high molecular weight nuclear fraction that contains chromatin and unspliced RNA.

(B and C) Immunoblot analysis of purity of the fractions. WB, whole brain; Np, nucleoplasm; HMW, high molecular weight nuclear fraction containing chromatin; WC, whole culture; Cy, cytoplasm; Nu, nucleus.

(D) Pie charts of the percentage of Rbfox1 clustered tags mapped to 5′ UTR, coding sequence (CDS), intron, and 3′ UTR in different iCLIP experiments.

(E) Scatter plots of the *Z* scores of pentamers around the Rbfox1 crosslink sites in the 3′ UTR in the cytoplasm and nucleoplasm.

genes'' and the latter ''Rbfox1-decreased genes'' in the set of ''expression'' targets. A subset of each group was validated by RT-qPCR (Figure S3). We found that Rbfox1-increased transcripts, but not Rbfox1-decreased genes, were significantly enriched for conserved 3′ UTR (U)GCAUG motifs (Figure 3E and Table S1, 40% of the Rbfox1-increased genes, $p < 10^{-15}$ by hypergeometric test).

There was no significant overlap between the set of transcripts whose abundance was regulated by Rbfox1_C and the set of transcripts whose splicing was regulated by Rbfox1_N (Figures 3F and S5). The genetic programs controlled by these different Rbfox1 isoforms thus appear to be distinct.

Rbfox1 Proteins Bind to the 3′ UTR of Target mRNAs in the Cytoplasm

To identify mRNAs physically bound by Rbfox1, and to assess the location of Rbfox1 binding sites across the transcriptome, we performed iCLIP-seq analysis (König et al., 2010). Since our rescue experiments indicated that Rbfox1 has distinct nuclear and cytoplasmic functions (Figures 3A and 3C), we performed subcellular fractionation prior to immunoprecipitation to identify Rbfox1 targets (Figure 4A). We previously found that the majority of unspliced RNA fractionates with chromatin from isolated nuclei (Bhatt et al., 2012; Khodor et al., 2012; Pandya-Jones et al., 2013). To identify the binding of nuclear Rbfox proteins, we generated iCLIP datasets of Rbfox1, 2, and 3 in the high molecular weight (HMW) nuclear fraction containing chromatin, unspliced RNA, and nuclear speckle proteins, and the soluble nucleoplasm (Np) fraction from mouse brains (6-week-old male mice). To profile the binding of cytoplasmic Rbfox1 proteins, we performed iCLIP on a cytoplasmic (Cy) fraction of cultured mouse neurons (14 days in vitro [DIV14]). The analyses in this paper focus on the cytoplasmic fraction and use the soluble Np and HMW fractions for comparison.

Immunoblotting showed that the soluble Np fraction from mouse brain was depleted of the cytoplasmic marker GAPDH and contained the nuclear marker U1-70K (Figure 4B). Both Rbfox1_C and Rbfox1_N isoforms were observed in the HMW

and Np fractions. The ER marker protein calnexin was also detected in the soluble Np fraction, suggesting that ribosome-loaded mRNA transcripts associated with the ER copurified with the nuclei (Bhatt et al., 2012). To obtain sufficient material for the Cy fraction, we used forebrain neurons rather than hippocampal neurons. Immunoblot analysis showed that the Cy fraction was enriched for the cytoplasmic protein GAPDH and lacked the nuclear marker U1-70K (Figure 4C).

Following UV crosslinking and cellular fractionation, we immunoprecipitated Rbfox1 with the Rbfox1-specific monoclonal antibody 1D10 and used anti-Flag antibodies as a negative control. We sequenced the RNA fragments crosslinked to immunoprecipitated Rbfox1 and obtained 2.2 and 3.2 million unique Rbfox1 iCLIP tags from the Np fraction and the Cy fraction, respectively (Table S3). These iCLIP tags were mapped to the longest transcript of each gene in the UCSC Known Gene Table (Hsu et al., 2006). In iCLIP, the UV crosslink site is located 1 nucleotide (nt) upstream of the 5′ end of the aligned iCLIP tag. To define reproducible and clustered crosslink sites, we calculated the probability of each site based on the number of tags mapping to that particular crosslink site compared to random sites. Crosslinked sites with an FDR < 0.01 were selected, and those located within 20 nt of one another were clustered. Clusters with width > 1 nt were used for downstream analyses. With these criteria, significant iCLIP clusters were identified in the Rbfox1 Np and Cy fractions, comprised of 136,483 and 162,916 tags, respectively (Table S3).

For the Rbfox1 Cy fraction, 78% of the clustered tags mapped to the 3′ UTR and 17% mapped to introns (Figure 4D). The distribution of mapped tags from the Np fraction was similar to that in the Cy fraction. In contrast, 93% of the Rbfox1 clustered tags mapped to introns in the HMW nuclear fraction. By comparison, analysis of Rbfox targets in whole cells in mouse brain reported that about 70% of clustered tags mapped to introns and that 20% to 27% mapped to 3′ UTR (Lovci et al., 2013; Weyn-Vanhentenryck et al., 2014).

To evaluate the specificity of the iCLIP data, we examined the enrichment of pentamer motifs in the sequences surrounding Rbfox1 crosslinking sites in 3′ UTRs. In the Cy fraction, GCAUG was the most enriched pentamer within the sequence extending 40 nt on either side of the crosslink site. The 50 most-enriched pentamers also included six that differed by 1 nt from GCAUG, suggesting that Rbfox1 can bind to sub-optimal GCAUG motifs in vivo, as has been seen by others (Lambert et al., 2014).

As in the Cy fraction, GCAUG was also the most enriched pentamer for Rbfox1 in the Np fraction, and the rankings of pentamers were highly correlated between the Cy and the Np fractions (Figure 4E; $\rho = 0.83$, $p < 2.2 \times 10^{-16}$, Spearman correlation). Interestingly, several U-rich motifs were more enriched in the Np than in the Cy fraction. This could be caused by differences in Rbfox1 interacting proteins in different cellular compartments. The Rbfox1 iCLIP pentamers were also highly correlated with Rbfox2 and Rbfox3 iCLIP pentamers in the Np fraction, as expected from their similar RNA binding properties (data not shown). The extensive overlap of 3′ UTR iCLIP clusters from the soluble Np and Cy fractions indicates that Rbfox probably binds fully processed mRNAs in the nucleus and accompanies them to the cytoplasm.

Cytoplasmic Rbfox1 Increases the Expression Levels of iCLIP Target Genes

We next characterized the properties of the iCLIP clusters. We defined clusters (“GCAUG clusters”) as high confidence Rbfox binding sites in vivo if they contained at least one GCAUG motif within 10 nt upstream or downstream of the cluster. Binding of Rbfox1 within a GCAUG cluster is illustrated by the mapped clusters in the Camta1 3′ UTR (Figure 5A). *Camta1* was identified as an Rbfox1-increased gene in the KD and rescue experiments. Ten cytoplasmic Rbfox1 iCLIP clusters were identified in its 3′ UTR and five of them overlapped with conserved GCAUG motifs, indicating direct binding of Rbfox1 to these sites (Figure 5A). The first Rbfox1 cluster in the Camta1 3′ UTR did not overlap with a GCAUG motif but had a sub-optimal GCACG motif, suggesting that this cluster also reflected a direct Rbfox1 binding site. Other clusters that did not directly overlap with a GCAUG motif were located within 50 nt of GCAUG motifs, suggesting that crosslinking at these sites might result from an Rbfox1 interaction with a GCAUG motif.

Examining the distribution of GCAUG clusters in cytoplasmic Rbfox1 target transcripts, we found that GCAUG clusters were enriched at the 5′ and 3′ ends of the 3′ UTRs (Figure 5B). Similar 5′ and 3′ enrichment has been observed for proteins and miRNAs controlling mRNA stability and translation (Bartel, 2009; Boudreau et al., 2014; Chi et al., 2009). The binding of Rbfox1 to these regions is consistent with our observations of cytoplasmic Rbfox1 affecting mRNA abundance. We defined a set of 3′ UTR target genes as containing at least one significant iCLIP cluster and a total of 11 tags in their 3′ UTRs. Of these 1,490 genes identified in the Cy fraction, 788 (53%) contained a cluster with a GCAUG motif (Table S2). In the Np fraction, 915 genes were identified as Rbfox1 3′ UTR target genes in brain tissue. Of these genes, 400 (44%) contained GCAUG clusters in 3′ UTR (Table S4 and Figures S6A and S6B).

We next asked whether Rbfox1-mediated changes in mRNA abundance correlated with Rbfox1 binding to the 3′ UTR. We found that Rbfox1-increased genes were significantly enriched for genes containing 3′ UTR clusters compared to non-regulated genes (23%, $p < 10^{-15}$, hypergeometric test, Figure 5C). In contrast, Rbfox1-decreased genes were not enriched for Rbfox1 iCLIP targets. Subdividing iCLIP target genes into those with or without a GCAUG cluster in the 3′ UTR, we found that those with GCAUG clusters were enriched in Rbfox1-increased genes. These results indicate that Rbfox1 binding to 3′ UTR GCAUG motifs increases the level of the target mRNAs in the cytoplasm. While binding of Rbfox1 to mRNAs lacking 3′ UTR GCAUG motifs were identified by iCLIP, these interactions were not correlated with any changes in mRNA abundance. We thus focused on iCLIP targets with GCAUG clusters and used these as high confidence Rbfox1 binding targets for downstream analyses.

Binding of Rbfox to 3′ UTR GCAUG Motifs in the Cytoplasm Increases Target mRNA Concentration and Translation

We next tested whether binding of Rbfox1 to the 3′ UTR was sufficient to alter target mRNA concentration and translation. We focused on *Camk2a* because of its roles in memory and in synaptic plasticity (Lisman et al., 2002). Both Camk2a mRNA

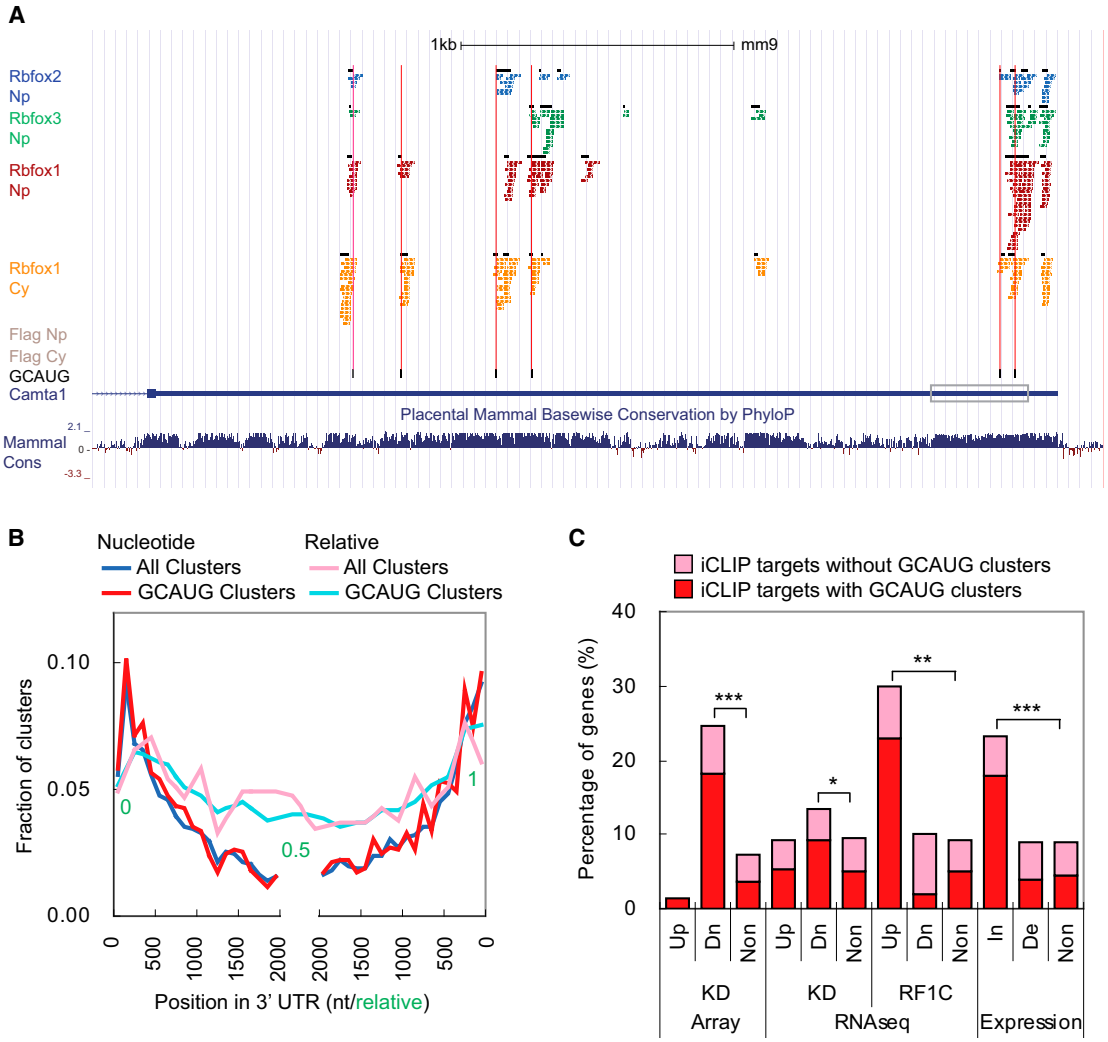

Figure 5. Identification of Rbfox1 iCLIP 3′ UTR Target Genes

(A) Screenshot of UCSC genome browser showing iCLIP tags and clusters (black box) in Camta1 3′ UTR. GCAUG motifs are underlined in black and a UGCACG motif is underlined in gray. The boxed region indicates the part of 3′ UTR subcloned to the luciferase reporters in Figure 6A.

(B) The distribution of the clusters within binned 3′ UTR locations relative to the 5′ and 3′ ends shown as nucleotide (nt) and relative positions.

(C) Histogram of the percentage of genes that contain iCLIP clusters in the 3′ UTR in different experiments. Up, upregulated in the experiment; Dn, downregulated in the experiment; In, mRNA increased by Rbfox1; De, mRNA decreased by Rbfox1. *$p < 10^{-5}$, **$p < 10^{-10}$, and ***$p < 10^{-15}$ by hypergeometric test.

For additional data, see Figure S6.

and protein were decreased by approximately 40% upon Rbfox1 and 3 KD (Figure S2). The Camk2a 3′ UTR is 3,372 nt long and contains five GCAUG motifs. Two of the five motifs overlapped with Rbfox1 iCLIP clusters (Figure S6C). We coexpressed a luciferase reporter gene containing the full-length Camk2a 3′ UTR (Figure 6A) with Rbfox1 in HEKT cells and found that Rbfox1_C but not Rbfox1_N induced a 70% increase in luciferase activity (Figure 6B). To test the role of the Rbfox binding sites, we generated a reporter containing a shorter 1.1 kb fragment of the Camk2a 3′ UTR and deleted the four (U)GCAUG motifs within this fragment (Figure 6A). When the wild-type Camk2a reporter was coexpressed with Rbfox1_C or Rbfox1_N in HEKT cells, a 2-fold increase of luciferase activity was observed with Rbfox1_C but not with Rbfox1_N (Figure 6C). RT-qPCR analysis of the luciferase mRNA revealed a somewhat smaller increase in mRNA, indicating that the change in luciferase expression is at least partially due to changes in mRNA stability. Deletion of the (U)GCAUG motifs abolished the Rbfox1_C-induced increase in luciferase activity and in reporter mRNA levels.

Cell fractionation and overexpression data indicated that a portion of Rbfox1_N is cytoplasmically localized (Figures 1D and S4G). This motivated us to test the activity of Rbfox1_N in the cytoplasm by deleting the NLS peptide sequence FAPY (Rbfox1_NdNLS; Figure 6E). Coexpression of Rbfox1_NdNLS with a luciferase reporter gene containing part of the Camta1 3′ UTR (containing iCLIP GCAUG clusters) revealed that the

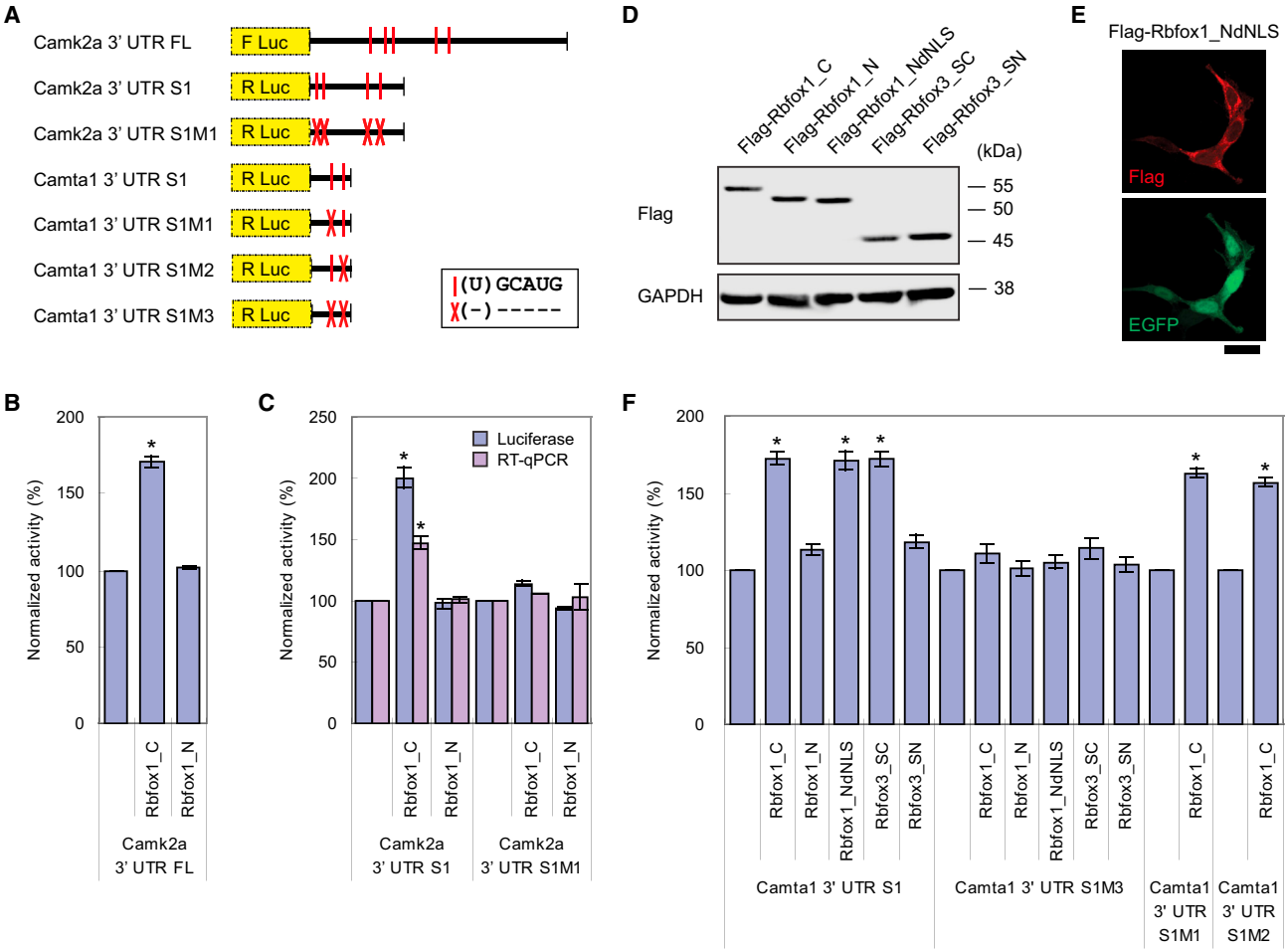

Figure 6. Rbfox1 and Rbfox3 Proteins Increase Gene Expression by Binding to the 3′ UTR

(A) Diagram depicting the luciferase reporters containing part of Camk2a 3′ UTR or Camta 3′ UTR as labeled in Figures S6 and 5A, respectively. (U)GCAUG motifs are denoted by vertical red lines, with red crosses marking deletion of these motifs.

(B) Histogram of normalized luciferase activity of the reporter containing full-length (FL) Camk2a 3′ UTR when coexpressed with Rbfox1_C or Rbfox1_N in HEKT cells. Error bars indicate SD. *$p < 0.001$ by Student's t test. n = 3.

(C) Histogram of normalized luciferase activity and mRNA concentration (RT-qPCR) of Camk2a 3′ UTR S1 reporters when coexpressed with Rbfox1_C or Rbfox1_N in HEKT cells. Error bars indicate SD. *$p < 0.001$ by Student's t test. n = 3.

(D) Immunoblot showing of Rbfox1 and Rbfox3 splice isoforms and a mutant expressed in HEKT cells. dNLS, delete nuclear localization signal; SC, short cytoplasmic isoform; SN, short nuclear isoform.

(E) Immunocytochemistry of Flag-Rbfox1_NdNLS detected with anti-Flag antibodies (red) and the whole cell labeled with EGFP (green) in HEKT cells. Scale bar = 20 μm.

(F) Histogram of normalized luciferase activity of Camta1 3′ UTR S1 reporters when coexpressed with Rbfox1 or Rbfox3 isoform or mutant in HEKT cells. Error bars indicate SD. *$p < 0.001$ by Student's t test. n = 3.

mutant, cytoplasmically localized Rbfox1_NdNLS significantly increased luciferase activity of the reporter (Figure 6F). Alternative splicing of exon 15 of Rbfox3 also generates a cytoplasmically localized Rbfox3_SC isoform (short cytoplasmic Rbfox3) (Kim et al., 2009b). We found that Rbfox3_SC also increased luciferase activity when expressed with the Camta1 3′ UTR luciferase reporter (Figure 6F). Together, these results indicate that multiple isoforms of Rbfox1 or 3 can increase mRNA concentration and promote translation as long as they localize to the cytoplasm.

Rbfox1_C Increases the Expression of Genes Affecting Synaptic Activity and Autism

To define a high confidence set of genes whose expression is directly regulated by Rbfox1 in the cytoplasm, we combined our iCLIP data with the transcriptome data to identify genes that had opposite expression changes in the KD and Rbfox1_C rescue experiments and that had cytoplasmic Rbfox1 iCLIP GCAUG clusters in their 3′ UTRs. The overlap between Rbfox1-increased genes and iCLIP target genes was highly significant, whereas the overlap between Rbfox1-decreased genes

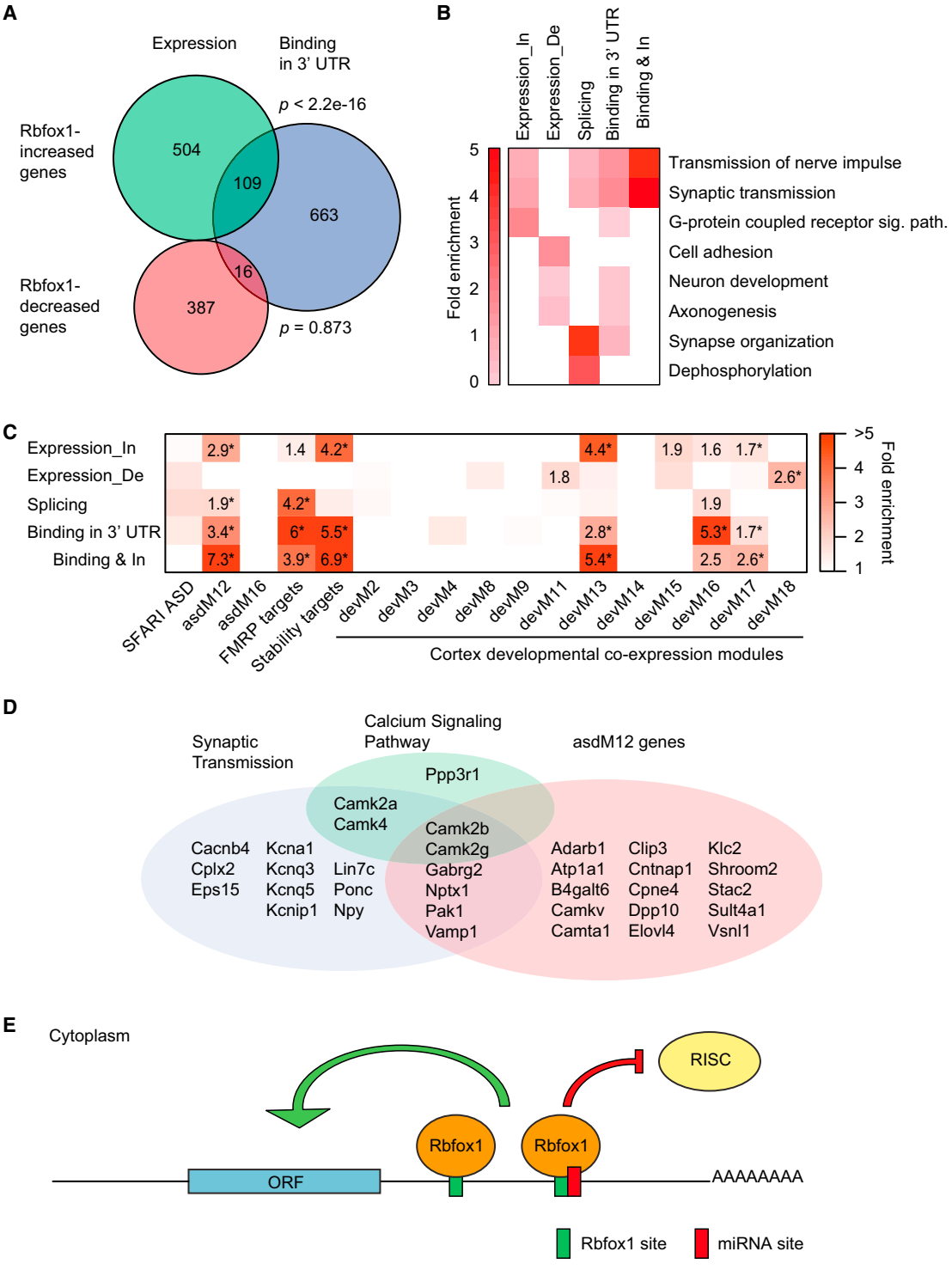

Figure 7. Rbfox1 Increases the Expression Level of Autism Genes in the Cytoplasm

(A) Weighted Venn diagram showing the overlap of genes whose expression is increased or decreased by Rbfox1 and iCLIP target genes with Rbfox1 bound in 3′ UTR. p values calculated by hypergeometric test.

(B) Heatmap of the fold enrichment of GO terms in different experiments. In, increased; De, decreased; Sig. path., signaling pathway.

(legend continued on next page)

and iCLIP targets was not significant (Figure 7A). These analyses identified a set of 109 directly bound Rbfox1-increased transcripts for downstream functional analyses (Table S5).

Gene ontology (GO) analysis of the Rbfox1-regulated genes shown in Figures 3F and 7A revealed that the Rbfox1-increased genes and iCLIP 3′ UTR targets were enriched for terms of transmission of nerve impulse and synaptic transmission (Figure 7B and Table S6). These enrichments were even greater in the high confidence set of 109 direct Rbfox1_C-increased genes. Analyzing the 109 genes using the Kyoto Encyclopedia of Genes and Genomes (KEGG) revealed a significant enrichment for calcium signaling pathways, including 4 CaM kinases (*Camk2a*, *Camk2b*, *Camk2g*, and *Camk4*) and one calcineurin B (*Ppp3r1*) (Table S7). Enrichment analysis using Mammalian Phenotype Ontology (Smith and Eppig, 2012) revealed that the 109 direct Rbfox1_C-increased genes were enriched for phenotypes related to seizure (Table S8). Together, these results indicate that Rbfox1_C target mRNAs play an important role in controlling synaptic activity, in particular via the calcium signaling pathway.

We next compared Rbfox1-regulated genes to modules within a gene co-expression network derived from human cortical gene expression data from fetal brain to 3 years of postnatal development. Three of these coexpression modules, devM13, devM16, and devM17, were enriched for the GO term of synaptic transmission, as well as ASD susceptibility genes (Parikshak et al., 2013). As shown in Figure 7C, we found that the 109 direct Rbfox1_C-increased genes were highly enriched in the same three synaptic modules. To directly examine the correlation with ASD, we compared the direct Rbfox1_C-increased genes to several sets of ASD candidate genes and found that the Rbfox1_C-increased genes were enriched in an ASD coexpression module (asdM12) that is downregulated in post mortem cerebral cortex from patients with ASD (Figure 7C) (Voineagu et al., 2011). Notably, *RBFOX1* was characterized as a hub gene in asdM12 and while its putative splicing targets were only modestly enriched, it was subsequently hypothesized to increase the mRNA stability of these ASD genes (Ray et al., 2013). Our finding that genes whose expression was directly increased by Rbfox1_C were significantly enriched for these ASD-related genes supports this hypothesis. Rbfox1_C-increased genes also showed high enrichment of Fragile X mental retardation protein (FMRP) targets (Darnell et al., 2011), further connecting post-transcriptional regulation with ASD biology. The substantially stronger correlation of the ASD module with cytoplasmic Rbfox1 regulation than with its nuclear splicing targets underscores the need to understand this portion of the Rbfox1 program.

Rbfox1_C May Compete with MicroRNAs to Regulate mRNA Stability and Translation

Several RBPs have been shown to regulate microRNA (miRNA) activity by binding to the 3′ UTRs of target mRNAs (Ciafrè and Galardi, 2013; Srikantan et al., 2012; Xue et al., 2013). Since Rbfox1 showed an opposite activity to that of miRNAs, but exhibited similar enriched binding at the 5′ and 3′ ends of 3′ UTR (Boudreau et al., 2014; Chi et al., 2009), we hypothesized that the binding of Rbfox1 may interfere with the binding of miRNAs and thereby antagonize miRNA activity. To test this hypothesis, we compared the Rbfox1 iCLIP data to an Ago CLIP dataset generated from P13 mouse neocortex (Chi et al., 2009). We searched for miRNA binding sites located within 50 nt of the Rbfox1-bound GCAUG motifs (Table S9). Since one Rbfox1 binding site can be close to multiple miRNA sites and vice versa, the number of single Rbfox1 site and miRNA site pairs with the same 50 nt interval was counted. By this criterion, 196 pairs of Rbfox1 and miRNA sites were identified. This number was significantly higher than the number of pairs identified after randomization of miRNA sites within the same 3′ UTR where the miRNA sites were identified, indicating that the proximity of Rbfox1 binding sites to miRNA sites within the 3′ UTR was not by chance (Figure S7A, Z score = 5.38). These 196 pairs included 173 miRNA sites and 109 GCAUG motifs in 87 genes (Table S10). We found that Rbfox1-bound GCAUG motifs were more conserved than GCAUG motifs present in the same 3′ UTR but not bound by Rbfox1 (Figure S7B). The conservation scores of GCAUG motifs and their flanking sequences were greater for Rbfox1-bound GCAUG motifs that were adjacent to or overlapping a miRNA site, indicating that the colocalization is under high selection pressure, consistent with it playing an important role in the regulation of gene expression. The Ago CLIP data used here identified the binding sites of the 20 most abundant miRNAs (Chi et al., 2009). We found that 14 of these 20 miRNA sites overlapped with a GCAUG motif in at least one 3′ UTR (Figure S7C). For example, the Camk2a 3′ UTR was found to contain 11 miRNA binding sites, three of which, miR-26, miR-124, and miR-30 binding sites, were located within 50 nt of the most upstream GCAUG motif bound by Rbfox1 (Figures S6C and S7C), with the miR-124 site overlapping with the GCAUG motif. In the context of our data showing that Rbfox1 binding stabilizes mRNAs and promotes translation (Figure 6), this finding suggests that Rbfox1 blocks Ago binding to these three miRNA sites. Within the 50 nt surrounding the GCAUG motif, the number of miRNA seed sites was greatest in regions overlapping the GCAUG motif and gradually decreased with distance from GCAUG motif (Figure S7D), indicating that the miRNA sites

(C) Heatmap of the enrichment of Rbfox1 regulated genes in gene sets of candidate autism genes, SFARI ASD (Basu et al., 2009), ASD-associated co-expression modules from human cortex, asdMs (Voineagu et al., 2011), FMRP targets (Darnell et al., 2011), Rbox1 3′ UTR stability targets (Ray et al., 2013), and co-expression modules from fetal cortex, devMs (Parikshak et al., 2013). All enrichment values for overrepresenting sets with odds ratio >1.5 are shown. *FDR adjusted two-sided Fisher's exact test p value < 0.05.

(D) Venn diagram showing the overlap of direct Rbfox1_C -increased genes in three functional categories.

(E) A model for the cytoplasmic function of Rbfox1 in neurons. Rbfox1 binds to the 3′ UTR of target mRNAs and increases their concentration in the cytoplasm of neurons. Rbfox1 binding is predicted to antagonize miRNA binding to a miRNA binding site overlapping or neighboring an Rbfox1 binding site in the 3′ UTR. For additional data, see Figure S7.

were concentrated in regions in which Rbfox1 would be expected to interfere with miRNA binding.

DISCUSSION

A Cytoplasmic Function for Rbfox Proteins

The goal of this study was to delineate the function of cytoplasmic Rbfox. Using KD and rescue approaches together with Rbfox1 iCLIP of subcellular neuronal fractions, we identified 109 genes whose abundance was directly regulated by Rbfox1_C. Our data indicate that cytoplasmically localized Rbfox1 promotes the stability and/or translation of target transcripts by binding to their 3′ UTRs (Figure 6). We also show that cytoplasmic Rbfox1 targets are enriched in human cortical development modules affecting synaptic function and ASD (Figure 7C). Our findings highlight the importance of considering the cytoplasmic arm of Rbfox1 regulation in linking Rbfox1 to synaptic function and to neurodevelopmental disorders such as ASD.

We focused on one nuclear and one cytoplasmic Rbfox1 isoform, but there are others. Using a monoclonal antibody 1D10 that targets the N-terminal sequence of Rbfox1 and a polyclonal antibody against Rbfox RRM (Figure 1D), we detected six Rbfox1 bands ranging from 45 and 55 kDa that were all reduced by a pan-Rbfox1 siRNA (Figure 1B) and eliminated in the *Rbfox1* KO mouse (data not shown). Two of these bands were eliminated by an siRNA targeting the exon of the cytoplasmic isoforms (Figure 1B). We previously found that the two of the middle bands probably represent N-terminally cleaved Rbfox1 isoforms (Lee et al., 2009). Additional bands of Rbfox1 may represent differentially phosphorylated proteins. The diverse species of Rbfox1 imply many levels of regulation and/or function. It will be interesting to examine whether and how neuronal activity regulates Rbfox1 splicing, proteolysis, and/or post-translational modifications, as such modifications could alter Rbfox1 regulation of gene expression.

Over 90% of the changes in mRNA level detected by microarray analysis represented decreases in expression induced by KD of Rbfox1 and 3, reflecting a role for Rbfox in stabilizing mRNAs (Figure 2D and Table S1). In contrast, the RNA-seq experiments identified more similar numbers of up- and downregulated genes (Figure 3C), although significantly more downregulated genes contained (U)GCAUG sequences in their 3′ UTRs. One difference that could lead to differences in the gene expression was that the microarray analyses were performed on pure neurons cultured with glial cells in inserts, while the RNA-seq analyses were performed on mixed neuronal-glial cultures. Thus, the cell environment and culture conditions may be reflected in the transcriptome analyses. We addressed this variation by considering all of our datasets together—including the KD in both culture conditions, the rescue experiments, and the iCLIP target sets (Table S1)—and focused on genes that showed consistent changes in all of the experiments. Most importantly, we focused on transcripts that underwent opposite directions of regulation in the KD and Rbfox1_C rescue experiments and that were bound by Rbfox1 in iCLIP experiments. The results of these analyses identify a large class of transcripts whose expression was positively regulated by Rbfox1_C (Table S5). There may yet be some transcripts that are negatively regulated by Rbfox1, but these will require additional experiments to identify.

Our data add to a growing literature revealing the multifunctionality of RBPs (Bielli et al., 2011; Heraud-Farlow and Kiebler, 2014; Turner and Hodson, 2012; Vanharanta et al., 2014). The differences in activity between Rbfox1 isoforms are reflected in the iCLIP data. While the majority of the Rbfox1 binding was detected in introns in the HMW fraction, the binding of Rbfox1 shifted to 3′ UTR when assayed in the soluble nucleoplasm and the cytoplasm. Although not always specifically localized to the nucleus or cytoplasm, other RNA binding proteins have been found to bind introns to affect splicing, as well as 5′ or 3′ UTRs to affect translation (Ince-Dunn et al., 2012; Licatalosi et al., 2008; Xue et al., 2009). In many cases, it is not clear how these functions are segregated and whether different isoforms are involved or differently modified. In the case of Rbfox1 and Rbfox3, the nuclear and cytoplasmic functions arise at least in part from differentially spliced isoforms. We note, however, that some Rbfox1_N is constitutively present in the cytoplasm (Figure 1D) and that a low but detectable amount of Rbfox1_C is present in the nucleus. The finding that the NLS deleted Rbfox1_N mutant can regulate stability and translation of target mRNAs (Figure 6F) indicates that the primary determinant of target mRNA regulation in the cytoplasm is simply cytoplasmic localization of Rbfox1 rather than any other feature of the Rbfox1_C or Rbfox1_N.

Several RBPs are known to regulate mRNA stability using different mechanisms. For example, HuR proteins and Ataxin-2 proteins can bind to AU-rich elements (AREs) in the 3′ UTR and stabilize target mRNAs (Lebedeva et al., 2011; Mukherjee et al., 2011; Yokoshi et al., 2014), while PTB and hnRNP L compete with miRNA binding in the 3′ UTR and stabilize target mRNAs (Rossbach et al., 2014; Xue et al., 2013). HuR can stimulate or inhibit miRNA binding and thus regulate mRNA decay (Kim et al., 2009a; Young et al., 2012). Our results show that Rbfox1 proteins can increase mRNA concentration in the cytoplasm and suggest that one mechanism for this is to stabilize mRNAs by competing with miRNA binding. However, this mechanism is likely only active on a subset of Rbfox1 target transcripts. For example, we find that Rbfox1 increased expression of the luciferase Camta1 3′ UTR reporter (Figure 6F), which lacks identified miRNA binding sites. In *Xenopus Oocytes*, Rbfox2 (XRbm9) is exclusively expressed in the cytoplasm and directly interacts with XGld2 in the cytoplasmic polyadenylation complex to promote translation (Papin et al., 2008). Identification of the cytoplasmic interacting partners of Rbfox1 may provide insights into the molecular mechanisms of cytoplasmic Rbfox1 regulation.

Rbfox1_C Regulates Genes Involved in Synaptic Function, Calcium Signaling, and Autism

Recent studies have focused attention on Rbfox1 as a critical regulator of gene expression in cortical development (Parikshak et al., 2013; Weyn-Vanhentenryck et al., 2014), and as a candidate ASD susceptibility gene (Fogel et al., 2012; Martin et al., 2007; Sebat et al., 2007; Voineagu et al., 2011; Weyn-Vanhentenryck et al., 2014). While these studies focused on Rbfox1's role as a splicing factor, we show that the mRNAs that are

regulated by Rbfox1_C are significantly enriched for genes involved in cortical development and autism (Figure 7C) (Parikshak et al., 2013; Voineagu et al., 2011). In a coexpression analysis of the brain transcriptome from patients with autism, *RBFOX1*, *CNTNAP1*, *CHRM1*, and *APBA2* were identified as four hub genes, genes that are defined as being highly connected in the ASD-associated co-expression module, asdM12. These four genes, along with *SCAMP5* and *KLC2*, were ranked highest in this module (Voineagu et al., 2011). Here, we show that Rbfox1 binds the 3′ UTRs of *CNTNAP1*, *CHRM1*, *SCAMP5*, and *KLC2* transcripts and that *CNTNAP1* and *KLC2* mRNA levels are both increased by Rbfox1_C (Table S1). These results suggest that *RBFOX1* is upstream of the two hub genes, *CNTNAP1* and *CHRM1*, in a molecular pathway that is altered in autism. Mutations in FMRP are the most common single gene cause of autism (Talkowski et al., 2014), and we find that Rbfox1 3′ UTR target genes overlap significantly with FMRP target genes (Darnell et al., 2011). Together, these results link gene expression changes associated with sporadic autism with a single gene cause of autism. Our findings thus add to the emerging recognition that post-transcriptional RNA metabolism plays a critical role in cortical development and neurodevelopmental disorders (Darnell and Richter, 2012).

We find that Rbfox1_N and Rbfox1_C regulate two different sets of genes (Figure 3F). Both sets are enriched for the same GO terms of transmission of nerve impulse and synaptic transmission, but their targets can be quite different. For example, in the CaM kinase family, the splicing of *Camk2d* is regulated by Rbfox1_N. However, the expression of *Camk2a*, *Camk2b*, and *Camk4* is regulated by Rbfox1_C, and *Camk2g* is regulated both at the level of splicing by Rbfox1_N and at the level of expression by Rbfox1_C (Figure S5). Taken together, our results identify a coherent and intricate gene network regulated by two distinct Rbfox1 splice isoforms and exemplify the functional consequences of alternative splicing for this RNA binding protein. The existence of multiple additional Rbfox1, Rbfox2, and Rbfox3 isoforms and variants indicates that our analysis probably uncovers only a fraction of the total complexity of Rbfox-mediated RNA regulation. Understanding the mechanisms by which RBP mutations give rise to neural circuit abnormalities and disease will require consideration of their multiple functions in RNA metabolism, in the nucleus, and in the cytoplasm.

EXPERIMENTAL PROCEDURES

Tissues for Immunoblotting and RT-PCR

All experiments with animals were performed using approaches approved by the UCLA Institutional Animal Care and Use Committee. Hippocampi and cortices at postnatal day 0 (P0) and 3 weeks were dissected from C57BL/6J mice. Protein was purified from half of the tissues for immunoblotting. RNAs were purified from the other half of the tissues for RT-PCR analysis.

Subcellular Fractionation of Neuronal Cultures

Hippocampal cultures used in Figure 1 were prepared from postnatal day 0 C57BL/6J mice (Jackson Laboratory) as previously described (Ho et al., 2014) and incubated with 2 μM Cytosine beta-D-arabinofuranoside (AraC) (Sigma Aldrich, c1768) from postnatal day 3 to day 6. On day 13, the cultures were incubated with 15 μM of digitonin (Sigma Aldrich, D141-100MG) and complete protease inhibitor (Roche #05892791001) in 1× PBS buffer for 3 min at room temperature to permeabilize the cells and the eluate was collected as the cytosol fraction. An equal volume of RIPA buffer was then used to completely lyse the cells.

RNAi Knockdown in Neuronal Cultures

Primary mouse hippocampal and cortical cultures were prepared from postnatal day 0 C57BL/6J mice. 160,000 hippocampal cells were plated in one 12-well well and 120,000 cortical cells were plated in a cell culture insert with pore size of 3 μm (Corning Life Sciences, 353181). On day 3, hippocampal cultures were incubated with 2 μM AraC for 3 days and then co-cultured with the cortical culture from day 6. Two Rbfox1 and two Rbfox3 Accell siRNAs (Dharmacon, sequences in Supplemental Experimental Procedures) were added to the co-culture on day 10 at a total concentration of 1.2 mM and incubated for 4 days prior to RNA and protein extraction.

Microarray

RNA from three biological replicates for each condition was probed for gene expression and alternative splicing changes using Affymetrix MJAY microarrays (Affymetrix). Array analysis was performed using the OmniViewer method (http://metarray.ucsc.edu/omniviewer/) (Sugnet et al., 2006).

Adeno-Associated Virus 2/9 Transduction, RNAi, cDNA Library Preparation, and RNA Sequencing

The siRNA target site in the Rbfox1 coding sequence was mutated to generate a silent mutation and the coding sequence of the mutated Flag-tagged Rbfox1_C or Rbfox1_N was then cloned into pAAV-hSyn-eNpHR 3.0-EYFP plasmid (Addgene plasmid # 26972), downstream of the hSynI promoter between AgeI and EcoRI restriction sites to replace eNpHR 3.0-EYFP coding sequence. AAV2/9 vectors containing hSyn.Flag-Rbfox1_C_siMt and hSyn.Flag-Rbfox1_N_siMt were generated at the University of Pennsylvania Vector Core Facility. An AAV2/9 vector expressing hSyn.EGFP was used as a control for transduction (Penn Vector Core, #AV-9-PV1696). Hippocampal neurons (DIV9) were transduced with AAV2/9 vectors expressing EGFP, Flag-Rbfox1_C_siMt, or Flag-Rbfox1_N_siMt at a concentration of 1.5×10^3 genomic copies (GC)/cell for 12 hr and then removed. The neurons (DIV10) were then incubated with non-targeting (Dharmacon #D001910-01 and #D001910-02) or Rbfox1 and Rbfox3 Accell siRNA for 4 days at concentration of 1.2 mM. Total RNA was extracted using RNeasy Micro Kit (QIAGEN). Ribosomal RNA was removed using Ribo-Zero rRNA Removal Kits (Epicenter), and the cDNA libraries were prepared using TruSeq RNA Sample Preparation Kit (Illumina) and sequenced in HiSeq 2000 (Illumina) (pair end, 50 nt) by the Southern California Genotyping Consortium (SCGC) Gene Expression Core Facility (Los Angeles, California). Alternative splicing changes were analyzed by SpliceTrap (Wu et al., 2011). Splicing changes where percent spliced in (psi) > 10, and reads of exon 1 > 50, exon 2 > 20, exon 3 > 50, exon 1-exon 2 junction > 5, exon 2-exon 3 junction > 5, and exon 1-exon 3 junctions > 5 in both samples in the comparison were considered significant. Gene expression changes were analyzed by Cufflinks-2.0.2. (Trapnell et al., 2010) and $q < 0.3$ was set to detect significant expression changes. Gene expression changes were validated by RT-qPCR on RNA samples from two independent biological replicates from those used for RNA sequencing. The expression levels of each gene were normalized to Tuj1 (*Tubb3*) expression for comparison. The means of normalized expression were calculated and the statistical significance was determined using a paired, one-tailed Student's t test with significance set to $p < 0.05$. $n = 2$ biological replicates.

Criteria for Defining Expression and Splicing Gene Sets

Genes selected for inclusion in the splicing set were required to have exons that showed significant splicing changes in Rbfox1 and 3 double knockdown (KD) or Rbfox1_N rescue experiment as measured by RNA sequencing and that showed opposite direction of splicing changes in the KD and Rbfox1_N rescue experiments. This identified 366 Rbfox1-regulated alternative exons in 332 genes as shown in Tables S1 and S2.

For the expression set, two sets of genes were selected and combined. The first set of genes was required to have significant expression changes in the KD experiment measured by microarray and showed opposite expression changes in the Rbfox1_C rescue experiment measured by RNA sequencing. The second set of genes was required to have significant expression changes

in the knockdown or Rbfox1_C rescue experiment measured by RNA sequencing and showed opposite direction of expression changes in the KD and Rbfox1_C rescue experiments. This identified 613 Rbfox1-increased genes and 403 Rbfox1-decreased genes as shown in Table S1.

iCLIP Data Analyses

A high molecular weight (HMW) nuclear fraction and soluble nucleoplasm fraction were purified from the brains of 6-week-old male C57BL/6J mice. Briefly, nuclei were purified as described (Grabowski, 2005) and lysed. Soluble and HMW fractions were separated by centrifugation. A cytoplasmic fraction was purified from mouse forebrain cultures at DIV14. iCLIP was performed according to the original protocol (König et al., 2010), with some modifications described in Supplemental Experimental Procedures. iCLIP sequencing results were analyzed as described in König et al. (König et al., 2010) with a few modifications. In brief, the iCLIP tags generated by PCR duplication were discarded based on the comparisons of the random barcodes in the tags. The unique iCLIP tags were then mapped to mouse genome (mm9/NCBI37) using Bowtie allowing 2 nucleotide mismatches (Langmead et al., 2009). Mapped tags were further mapped to the longest transcripts in Known Gene table (Hsu et al., 2006) and divided into four regions of 5′ UTR, CDS, intron, and 3′ UTR for downstream analyses. The first nucleotide in the genome upstream of the iCLIP tags was defined as UV-crosslink site and the significance of crosslinking at each crosslink site was evaluated by the false discovery rate (FDR) calculated as described in König et al. (König et al., 2010). Crosslink sites with FDR $\leq$ 0.01 were used for clustering. Any two crosslink sites located within 20 nt on the mouse genome were clustered together. The width of a cluster was defined as the distance between the first and the last crosslinked sites and clusters with width > 1 nt were selected for downstream analyses. A cluster was defined as a GCAUG cluster if it overlapped with a GCAUG motif with at least 1 nt within –10 to 10 nt genomic sequences of the cluster. The iCLIP tags in these clusters were called clustered tags.

Motif Analyses

Crosslink sites with FDR $\leq$ 0.01 were used for motif analyses. The genomic sequences of the crosslink site plus 40 nt upstream and 40 nt downstream were used for the motif enrichment analyses. The *Z* scores of each pentamer were calculated by comparing the occurrence of the pentamers around the crosslink sites to the occurrence around randomized sites in the same genomic region (i.e., within the same intron or 3′ UTR) to control for the differences in expression of different genes.

Identification of Rbfox 3′ UTR Target Genes

To identify 3′ UTR target genes for Rbfox1, 2, and 3 in different experiments, we first ranked the genes by the number of clustered tags in 3′ UTR. Next, to account for the differences in the number of clustered tags generated in different experiments, were selected genes that contained the top 95% of clustered tags as 3′ UTR target genes. By this criterion, the top 55% of genes that contained clustered tags in 3′ UTR were selected. This set the cutoff as 11 tags/3′ UTR for the identification of Rbfox1, 2, and 3 3′ UTR target genes in the forebrain cultures and the brain tissues. The cutoffs for Rbfox1 in the forebrain and hindbrain tissues were set higher at 21 tags/3′ UTR and 16 tags/3′ UTR, respectively, due to the greater numbers of clustered tags generated in these experiments.

Gene Set Enrichment Analysis

Gene set enrichment analysis was performed with candidate gene lists and co-expression networks using a two-tailed Fisher's exact test followed by Benjamini-Hochberg FDR adjustment (Benjamini and Hochberg, 1995). All mouse gene set overlaps were performed using mouse Ensembl IDs, all human lists were converted to their homologous mouse Ensembl IDs using Ensembl 73 (Gencode v18), using only one-to-one orthologs. FDR adjustment took into consideration all gene set overlaps performed. The following gene lists and co-expression modules were used: candidate genes from SFARI with a gene score of S or 1-4 (Basu et al., 2009), two ASD associated co-expression modules from post mortem human cortex (asdM12 and asdM16; [Voineagu et al., 2011]), FMRP binding targets in mouse brain (Darnell et al., 2011), predicted Rbfox1 3′ UTR stability targets (Ray et al., 2013), and 12 co-expression modules reflecting cortical developmental processes (Parikshak et al., 2013) and enriched for protein interactions and GO terms, including cellular proliferation (devM8 and devM11), transcriptional/chromatin regulation (devM2 and devM3), and synaptic development (devM13, devM16, and devM17).

ACCESSION NUMBERS

The accession number for the microarray, RNA-seq, and iCLIP data from cytoplasmic fraction reported in this paper is GEO: GSE71917.

SUPPLEMENTAL INFORMATION

Supplemental Information includes Supplemental Experimental Procedures, seven figures, and ten tables and can be found with this article online at http://dx.doi.org/10.1016/j.neuron.2015.11.025.

AUTHOR CONTRIBUTIONS

J.-A.L. and K.C.M. designed the experiments with input from D.L.B.. J.-A.L. performed co-culture, RNAi, and rescue experiments for microarray and RNA sequencing experiments, and all biochemical experiments. E.S.A. prepared cDNA for microarray experiments. A.D. and J.-A.L. performed iCLIP experiments. J.-A.L. and M.F. performed luciferase assays. C.-H.L. and J.-A.L performed bioinformatic analyses. N.N.P performed gene set enrichment analyses. Figures were prepared by J.-A.L., C.-H.L., and N.N.P.. The manuscript was written by J.-A.L and K.C.M with input from D.L.B., D.H.G., and the other authors.

ACKNOWLEDGMENTS

We thank J. König and J. Ule (UCL Institute of Neurology) for the iCLIP protocol; L. Zipursky (UCLA) and members of the K.C.M. and D.L.B. labs for helpful discussions; and V. Ho, L. Zipursky and K. Otis (UCLA) for comments on the manuscript. This work was supported by R21 MH101684 to K.C.M., P50-HD-055784 pilot grant to K.C.M., and a NARSAD Young Investigator Award to J.-A.L. Work in the D.L.B. lab was supported by HHMI, and by NIH grant R01 GM084317. E.S.A. was supported by the UCLA Medical Scientist Training Program, and by NIH Graduate Fellowship 4F30AG033993. D.L.B. is an Investigator of HHMI. N.N.P. was supported by NRSA Fellowship F30MH099886. M.F. was supported by Fundação para a Ciência e a Tecnologia through the Graduate Program in Areas of Basic and Applied Biology.

Received: July 1, 2015
Revised: September 3, 2015
Accepted: November 6, 2015
Published: December 10, 2015

REFERENCES

Auweter, S.D., Fasan, R., Reymond, L., Underwood, J.G., Black, D.L., Pitsch, S., and Allain, F.H. (2006). Molecular basis of RNA recognition by the human alternative splicing factor Fox-1. EMBO J. *25*, 163–173.

Bartel, D.P. (2009). MicroRNAs: target recognition and regulatory functions. Cell *136*, 215–233.

Basu, S.N., Kollu, R., and Banerjee-Basu, S. (2009). AutDB: a gene reference resource for autism research. Nucleic Acids Res. *37*, D832–D836.

Benjamini, Y., and Hochberg, Y. (1995). Controlling the false discovery rate - a practical and powerful approach to multiple testing. J. Roy. Stat. Soc. B Met. *57*, 289–300.

Bhalla, K., Phillips, H.A., Crawford, J., McKenzie, O.L., Mulley, J.C., Eyre, H., Gardner, A.E., Kremmidiotis, G., and Callen, D.F. (2004). The de novo chromosome 16 translocations of two patients with abnormal phenotypes (mental retardation and epilepsy) disrupt the A2BP1 gene. J. Hum. Genet. *49*, 308–311.

Bhatt, D.M., Pandya-Jones, A., Tong, A.J., Barozzi, I., Lissner, M.M., Natoli, G., Black, D.L., and Smale, S.T. (2012). Transcript dynamics of proinflammatory genes revealed by sequence analysis of subcellular RNA fractions. Cell *150*, 279–290.

Bielli, P., Busà, R., Paronetto, M.P., and Sette, C. (2011). The RNA-binding protein Sam68 is a multifunctional player in human cancer. Endocr. Relat. Cancer *18*, R91–R102.

Boudreau, R.L., Jiang, P., Gilmore, B.L., Spengler, R.M., Tirabassi, R., Nelson, J.A., Ross, C.A., Xing, Y., and Davidson, B.L. (2014). Transcriptome-wide discovery of microRNA binding sites in human brain. Neuron *81*, 294–305.

Chi, S.W., Zang, J.B., Mele, A., and Darnell, R.B. (2009). Argonaute HITS-CLIP decodes microRNA-mRNA interaction maps. Nature *460*, 479–486.

Ciafrè, S.A., and Galardi, S. (2013). microRNAs and RNA-binding proteins: a complex network of interactions and reciprocal regulations in cancer. RNA Biol. *10*, 935–942.

Damianov, A., and Black, D.L. (2010). Autoregulation of Fox protein expression to produce dominant negative splicing factors. RNA *16*, 405–416.

Darnell, J.C., and Richter, J.D. (2012). Cytoplasmic RNA-binding proteins and the control of complex brain function. Cold Spring Harb. Perspect. Biol. *4*, a012344.

Darnell, J.C., Van Driesche, S.J., Zhang, C., Hung, K.Y., Mele, A., Fraser, C.E., Stone, E.F., Chen, C., Fak, J.J., Chi, S.W., et al. (2011). FMRP stalls ribosomal translocation on mRNAs linked to synaptic function and autism. Cell *146*, 247–261.

Fogel, B.L., Wexler, E., Wahnich, A., Friedrich, T., Vijayendran, C., Gao, F., Parikshak, N., Konopka, G., and Geschwind, D.H. (2012). RBFOX1 regulates both splicing and transcriptional networks in human neuronal development. Hum. Mol. Genet. *21*, 4171–4186.

Gehman, L.T., Stoilov, P., Maguire, J., Damianov, A., Lin, C.H., Shiue, L., Ares, M., Jr., Mody, I., and Black, D.L. (2011). The splicing regulator Rbfox1 (A2BP1) controls neuronal excitation in the mammalian brain. Nat. Genet. *43*, 706–711.

Grabowski, P.J. (2005). Splicing-active nuclear extracts from rat brain. Methods *37*, 323–330.

Hamada, N., Ito, H., Iwamoto, I., Mizuno, M., Morishita, R., Inaguma, Y., Kawamoto, S., Tabata, H., and Nagata, K. (2013). Biochemical and morphological characterization of A2BP1 in neuronal tissue. J. Neurosci. Res. *91*, 1303–1311.

Heraud-Farlow, J.E., and Kiebler, M.A. (2014). The multifunctional Staufen proteins: conserved roles from neurogenesis to synaptic plasticity. Trends Neurosci. *37*, 470–479.

Ho, V.M., Dallalzadeh, L.O., Karathanasis, N., Keles, M.F., Vangala, S., Grogan, T., Poirazi, P., and Martin, K.C. (2014). GluA2 mRNA distribution and regulation by miR-124 in hippocampal neurons. Mol. Cell. Neurosci. *61*, 1–12.

Hsu, F., Kent, W.J., Clawson, H., Kuhn, R.M., Diekhans, M., and Haussler, D. (2006). The UCSC Known Genes. Bioinformatics *22*, 1036–1046.

Ince-Dunn, G., Okano, H.J., Jensen, K.B., Park, W.Y., Zhong, R., Ule, J., Mele, A., Fak, J.J., Yang, C., Zhang, C., et al. (2012). Neuronal Elav-like (Hu) proteins regulate RNA splicing and abundance to control glutamate levels and neuronal excitability. Neuron *75*, 1067–1080.

Khodor, Y.L., Menet, J.S., Tolan, M., and Rosbash, M. (2012). Cotranscriptional splicing efficiency differs dramatically between Drosophila and mouse. RNA *18*, 2174–2186.

Kim, H.H., Kuwano, Y., Srikantan, S., Lee, E.K., Martindale, J.L., and Gorospe, M. (2009a). HuR recruits let-7/RISC to repress c-Myc expression. Genes Dev. *23*, 1743–1748.

Kim, K.K., Adelstein, R.S., and Kawamoto, S. (2009b). Identification of neuronal nuclei (NeuN) as Fox-3, a new member of the Fox-1 gene family of splicing factors. J. Biol. Chem. *284*, 31052–31061.

König, J., Zarnack, K., Rot, G., Curk, T., Kayikci, M., Zupan, B., Turner, D.J., Luscombe, N.M., and Ule, J. (2010). iCLIP reveals the function of hnRNP particles in splicing at individual nucleotide resolution. Nat. Struct. Mol. Biol. *17*, 909–915.

Kuroyanagi, H. (2009). Fox-1 family of RNA-binding proteins. Cell. Mol. Life Sci. *66*, 3895–3907.

Lal, D., Reinthaler, E.M., Altmüller, J., Toliat, M.R., Thiele, H., Nürnberg, P., Lerche, H., Hahn, A., Møller, R.S., Muhle, H., et al. (2013a). RBFOX1 and RBFOX3 mutations in rolandic epilepsy. PLoS ONE *8*, e73323.

Lal, D., Trucks, H., Møller, R.S., Hjalgrim, H., Koeleman, B.P., de Kovel, C.G., Visscher, F., Weber, Y.G., Lerche, H., Becker, F., et al.; EMINet Consortium; EPICURE Consortium (2013b). Rare exonic deletions of the RBFOX1 gene increase risk of idiopathic generalized epilepsy. Epilepsia *54*, 265–271.

Lambert, N., Robertson, A., Jangi, M., McGeary, S., Sharp, P.A., and Burge, C.B. (2014). RNA Bind-n-Seq: quantitative assessment of the sequence and structural binding specificity of RNA binding proteins. Mol. Cell *54*, 887–900.

Langmead, B., Trapnell, C., Pop, M., and Salzberg, S.L. (2009). Ultrafast and memory-efficient alignment of short DNA sequences to the human genome. Genome Biol. *10*, R25.

Lebedeva, S., Jens, M., Theil, K., Schwanhäusser, B., Selbach, M., Landthaler, M., and Rajewsky, N. (2011). Transcriptome-wide analysis of regulatory interactions of the RNA-binding protein HuR. Mol. Cell *43*, 340–352.

Lee, J.A., Tang, Z.Z., and Black, D.L. (2009). An inducible change in Fox-1/A2BP1 splicing modulates the alternative splicing of downstream neuronal target exons. Genes Dev. *23*, 2284–2293.

Licatalosi, D.D., Mele, A., Fak, J.J., Ule, J., Kayikci, M., Chi, S.W., Clark, T.A., Schweitzer, A.C., Blume, J.E., Wang, X., et al. (2008). HITS-CLIP yields genome-wide insights into brain alternative RNA processing. Nature *456*, 464–469.

Lisman, J., Schulman, H., and Cline, H. (2002). The molecular basis of CaMKII function in synaptic and behavioural memory. Nat. Rev. Neurosci. *3*, 175–190.

Lovci, M.T., Ghanem, D., Marr, H., Arnold, J., Gee, S., Parra, M., Liang, T.Y., Stark, T.J., Gehman, L.T., Hoon, S., et al. (2013). Rbfox proteins regulate alternative mRNA splicing through evolutionarily conserved RNA bridges. Nat. Struct. Mol. Biol. *20*, 1434–1442.

Lukong, K.E., Chang, K.W., Khandjian, E.W., and Richard, S. (2008). RNA-binding proteins in human genetic disease. Trends Genet. *24*, 416–425.

Mackall, J., Meredith, M., and Lane, M.D. (1979). A mild procedure for the rapid release of cytoplasmic enzymes from cultured animal cells. Anal. Biochem. *95*, 270–274.

Martin, C.L., Duvall, J.A., Ilkin, Y., Simon, J.S., Arreaza, M.G., Wilkes, K., Alvarez-Retuerto, A., Whichello, A., Powell, C.M., Rao, K., et al. (2007). Cytogenetic and molecular characterization of A2BP1/FOX1 as a candidate gene for autism. Am. J. Med. Genet. B Neuropsychiatr. Genet. *144B*, 869–876.

Mukherjee, N., Corcoran, D.L., Nusbaum, J.D., Reid, D.W., Georgiev, S., Hafner, M., Ascano, M., Jr., Tuschl, T., Ohler, U., and Keene, J.D. (2011). Integrative regulatory mapping indicates that the RNA-binding protein HuR couples pre-mRNA processing and mRNA stability. Mol. Cell *43*, 327–339.

Nakahata, S., and Kawamoto, S. (2005). Tissue-dependent isoforms of mammalian Fox-1 homologs are associated with tissue-specific splicing activities. Nucleic Acids Res. *33*, 2078–2089.

Pandya-Jones, A., Bhatt, D.M., Lin, C.H., Tong, A.J., Smale, S.T., and Black, D.L. (2013). Splicing kinetics and transcript release from the chromatin compartment limit the rate of Lipid A-induced gene expression. RNA *19*, 811–827.

Papin, C., Rouget, C., and Mandart, E. (2008). Xenopus Rbm9 is a novel interactor of XGld2 in the cytoplasmic polyadenylation complex. FEBS J. *275*, 490–503.

Parikshak, N.N., Luo, R., Zhang, A., Won, H., Lowe, J.K., Chandran, V., Horvath, S., and Geschwind, D.H. (2013). Integrative functional genomic analyses implicate specific molecular pathways and circuits in autism. Cell *155*, 1008–1021.

Ray, D., Kazan, H., Cook, K.B., Weirauch, M.T., Najafabadi, H.S., Li, X., Gueroussov, S., Albu, M., Zheng, H., Yang, A., et al. (2013). A compendium of RNA-binding motifs for decoding gene regulation. Nature *499*, 172–177.

Rossbach, O., Hung, L.H., Khrameeva, E., Schreiner, S., König, J., Curk, T., Zupan, B., Ule, J., Gelfand, M.S., and Bindereif, A. (2014). Crosslinking-

immunoprecipitation (iCLIP) analysis reveals global regulatory roles of hnRNP L. RNA Biol. *11*, 146–155.

Sebat, J., Lakshmi, B., Malhotra, D., Troge, J., Lese-Martin, C., Walsh, T., Yamrom, B., Yoon, S., Krasnitz, A., Kendall, J., et al. (2007). Strong association of de novo copy number mutations with autism. Science *316*, 445–449.

Smith, C.L., and Eppig, J.T. (2012). The Mammalian Phenotype Ontology as a unifying standard for experimental and high-throughput phenotyping data. Mamm. Genome *23*, 653–668.

Srikantan, S., Tominaga, K., and Gorospe, M. (2012). Functional interplay between RNA-binding protein HuR and microRNAs. Curr. Protein Pept. Sci. *13*, 372–379.

Sugnet, C.W., Srinivasan, K., Clark, T.A., O'Brien, G., Cline, M.S., Wang, H., Williams, A., Kulp, D., Blume, J.E., Haussler, D., and Ares, M., Jr. (2006). Unusual intron conservation near tissue-regulated exons found by splicing microarrays. PLoS Comput. Biol. *2*, e4.

Talkowski, M.E., Minikel, E.V., and Gusella, J.F. (2014). Autism spectrum disorder genetics: diverse genes with diverse clinical outcomes. Harv. Rev. Psychiatry *22*, 65–75.

Trapnell, C., Williams, B.A., Pertea, G., Mortazavi, A., Kwan, G., van Baren, M.J., Salzberg, S.L., Wold, B.J., and Pachter, L. (2010). Transcript assembly and quantification by RNA-Seq reveals unannotated transcripts and isoform switching during cell differentiation. Nat. Biotechnol. *28*, 511–515.

Turner, M., and Hodson, D.J. (2012). An emerging role of RNA-binding proteins as multifunctional regulators of lymphocyte development and function. Adv. Immunol. *115*, 161–185.

Underwood, J.G., Boutz, P.L., Dougherty, J.D., Stoilov, P., and Black, D.L. (2005). Homologues of the Caenorhabditis elegans Fox-1 protein are neuronal splicing regulators in mammals. Mol. Cell. Biol. *25*, 10005–10016.

Vanharanta, S., Marney, C.B., Shu, W., Valiente, M., Zou, Y., Mele, A., Darnell, R.B., and Massagué, J. (2014). Loss of the multifunctional RNA-binding protein RBM47 as a source of selectable metastatic traits in breast cancer. eLife *3*, 3.

Voineagu, I., Wang, X., Johnston, P., Lowe, J.K., Tian, Y., Horvath, S., Mill, J., Cantor, R.M., Blencowe, B.J., and Geschwind, D.H. (2011). Transcriptomic analysis of autistic brain reveals convergent molecular pathology. Nature *474*, 380–384.

Weyn-Vanhentenryck, S.M., Mele, A., Yan, Q., Sun, S., Farny, N., Zhang, Z., Xue, C., Herre, M., Silver, P.A., Zhang, M.Q., et al. (2014). HITS-CLIP and integrative modeling define the Rbfox splicing-regulatory network linked to brain development and autism. Cell Rep. *6*, 1139–1152.

Wu, J., Akerman, M., Sun, S., McCombie, W.R., Krainer, A.R., and Zhang, M.Q. (2011). SpliceTrap: a method to quantify alternative splicing under single cellular conditions. Bioinformatics *27*, 3010–3016.

Xie, X., Lu, J., Kulbokas, E.J., Golub, T.R., Mootha, V., Lindblad-Toh, K., Lander, E.S., and Kellis, M. (2005). Systematic discovery of regulatory motifs in human promoters and 3′ UTRs by comparison of several mammals. Nature *434*, 338–345.

Xue, Y., Zhou, Y., Wu, T., Zhu, T., Ji, X., Kwon, Y.S., Zhang, C., Yeo, G., Black, D.L., Sun, H., et al. (2009). Genome-wide analysis of PTB-RNA interactions reveals a strategy used by the general splicing repressor to modulate exon inclusion or skipping. Mol. Cell *36*, 996–1006.

Xue, Y., Ouyang, K., Huang, J., Zhou, Y., Ouyang, H., Li, H., Wang, G., Wu, Q., Wei, C., Bi, Y., et al. (2013). Direct conversion of fibroblasts to neurons by reprogramming PTB-regulated microRNA circuits. Cell *152*, 82–96.

Yeo, G.W., Coufal, N.G., Liang, T.Y., Peng, G.E., Fu, X.D., and Gage, F.H. (2009). An RNA code for the FOX2 splicing regulator revealed by mapping RNA-protein interactions in stem cells. Nat. Struct. Mol. Biol. *16*, 130–137.

Yokoshi, M., Li, Q., Yamamoto, M., Okada, H., Suzuki, Y., and Kawahara, Y. (2014). Direct binding of Ataxin-2 to distinct elements in 3′ UTRs promotes mRNA stability and protein expression. Mol. Cell *55*, 186–198.

Young, L.E., Moore, A.E., Sokol, L., Meisner-Kober, N., and Dixon, D.A. (2012). The mRNA stability factor HuR inhibits microRNA-16 targeting of COX-2. Mol. Cancer Res. *10*, 167–180.

Zhang, C., Zhang, Z., Castle, J., Sun, S., Johnson, J., Krainer, A.R., and Zhang, M.Q. (2008). Defining the regulatory network of the tissue-specific splicing factors Fox-1 and Fox-2. Genes Dev. *22*, 2550–2563.